Imperial College London

National Centre for the Replacement Refinement & Reduction of Animals in Research

Further Development and Refinement of Hematopoietic Cell Transplantation in Zebrafish

Dorottya Ilona Pólos

Imperial College London

Department of Life Sciences

Thesis submitted for the degree of
Doctor of Philosophy (PhD)

2021

Statement of originality

I declare that all work presented in this thesis is my own, and that all ideas, information, data, results and figures from other sources have been appropriately referenced. Contributions from others have been clearly specified and acknowledged as appropriate.

Dorottya Pólos

March 2021

Copyright declaration

Funding

This PhD project was funded by the National Centre for the Replacement, Refinement and Reduction of Animals in Research, grant reference number NC/N003446/1

Abstract

Hematopoietic stem cells are a rare but crucial population of cells that are responsible for maintaining hematopoiesis throughout vertebrate life. Clinically, hematopoietic stem cells have been utilised for treatment of hematological disease, autoimmune disorders and cancer through the application of hematopoietic cell transplants. A detailed understanding of the behaviour of hematopoietic stem cells and their post-transplant interaction with the niche can lead to improved transplant outcomes. However, there are many challenges in studying hematopoietic stem cell transplantation in mammalian systems owing to the difficulty of observing transplanted cells *in vivo*. This thesis aims to refine hematopoietic cell transplantation protocols described in adult zebrafish (*Danio rerio*). To this end, fluorescent hematopoietic stem and precursor populations were further characterised in transgenic donor fish using a combination of flow cytometry and microscopy techniques. Furthermore, *Runx*:mCherry positive populations were assessed for stem cell functionality through transplantation. The utility of bloodless *cmyb*^{t25127} mutant fish to investigate hematopoietic cell transplantation by longitudinal imaging was evaluated. In addition, the stimulatory effects of viral mimetics were assessed in transgenic and *cmyb*^{t25127} mutant fish. Finally, the effect of antibiotic treatment was investigated in transgenic fish.

These experiments revealed two fluorescent cell populations in *Tg(Runx:mCherry)* transgenic zebrafish kidney marrow. Hematopoietic cell transplant studies and transcript analysis indicated that the *Runx*:mCherry ^{low} population could be enriched for hematopoietic stem cells. Furthermore, experiments revealed that homozygous *cmyb*^{t25127} mutant fish are capable of regenerating their tail fin following amputation and of initiating a partial anti-viral response to resiquimod stimulation. Finally, a post-transplant scoring system was devised in homozygous *cmyb*^{t25127} mutant fish and used to assess functional differences between *Runx*:mCherry^{high} and ^{low} populations. Overall, this thesis has further developed hematopoietic cell transplantation in zebrafish and demonstrated that *in vivo* imaging can be used to track the transplant outcome and behaviour of transplanted cells.

Acknowledgements

They say it takes a village to raise a thesis. Ultimately, this thesis and the work presented within would not have been possible without the support of many people. First of all, I would like to thank Maggie and Laurence for the opportunity to work on this project, giving me valuable guidance and feedback throughout, encouraging me, and for challenging me to become a more independent and confident scientist. I am grateful for the scientific rigor you have taught me. I would also like to thank Marie who laid down the foundations for this project, mentored me during my undergraduate project and helped me prepare for this endeavor. Thank you also to Clare Lloyd and Cristina Lo Celso for being on my Progress Review Panel and providing constructive and helpful feedback throughout my PhD.

I would like to thank members of the Dallman lab past and present for generating such a welcoming, kind and fun environment to work in and making not one but two fish room moves manageable. In particular, I am grateful to: Ralf, for his insights and the many conversations by our desks, Marie-Christine for sharing valuable expertise and for her kindness, Natalie for her support and guidance when I started this project, Anna for her infectious laughter and for taking on responsibilities, and Håkon and Hannah for generating a fun environment. Special thanks to Madina for her support and friendship over these years. I would not have had anywhere near as enjoyable a time if it were not for our cake breaks, dance sessions and shared fish room duties. Thank you also for being there to listen to my exciting breakthroughs, as well as my frustrations and struggles.

I must also thank my undergraduate and Masters' students who have taught me as much as I have taught them and who have helped me realize my passion for teaching and science outreach. Particular thanks to Chloe, Alice and Yuan, whose work is also included in this thesis.

I am also grateful to the many friends who have made these past 3-4 years so wonderful and fun- you know who you are! Whether through joining a dance society with me, through departmental drinks, dinners out, movie nights, lunch breaks or brunches, you have made these past few years special.

I am also immensely grateful to the Schuck lab in Heidelberg, who nurtured my love of science and opened my eyes up to the beauty and excitement of microscopy. I thank Sebastian for his mentorship, patience and for all that he has taught me.

I am also grateful to the staff of the Flow Cytometry Facility and Facility for Imaging by Light Microscopy for providing me with excellent training and support throughout the project. Particular thanks to Jane Srivastava and Jess Rowley for countless FACS sessions and for making much of this work possible, and to Stephen Rothery, David Gaboriau and Andreas Bruckbauer for your imaging expertise.

I am also grateful to Oundle School for providing me with the opportunity to follow my passion for outreach and for the many amazing colleagues I have met here. Particular thanks to my friends in the Cedars who have given me cake and support when I struggled the most with writing.

Special thanks to my partner Andonis, who has helped me immeasurably throughout the thesis and beyond, and has been an incredible source of support, comfort, kindness and laughter. Words cannot express how grateful I am to you for all the ways you have been there for me.

Finally, I would like to thank my whole family who have always been incredibly supportive. My siblings Áron, Bálint and Márton, as well as my cousins and aunt, for listening to my fish stories, encouraging me and sharing their passion for science with me. Those members of my family who are no longer with us but have nonetheless inspired me to pursue my passion for science, my aunt Kati and my grandparents. And finally, my mum and dad for their unconditional support and belief in me. You have always been in my corner. Thank you.

List of Abbreviations

5-FU	5-Fluorouracil
ABC	ATP-binding cassette
ACP	Acid phosphatase
AGM	Aorta gonad mesonephros
AKP	Alkaline phosphatase
ALPM	Anterior lateral-plate mesoderm
ANOVA	Analysis of variance
BF	Brightfield
BM	Bone marrow
BrdU	5-bromo-2-deoxyuridine
CBFβ	Core binding factor β
CD	Cluster of differentiation
cDNA	Complementary DNA
Cebp1	CCAAT enhancer binding protein 1
CHT	Caudal hematopoietic tissue
cKit	Stem cell factor receptor
CLP	Common lymphoid progenitor
CMP	Common myeloid progenitor
CNS	Central nervous system
CRISPR	Clustered regularly interspaced short palindromic repeats
Ct	Cycle threshold
DAMP	Damage-associated molecular pattern
DAPI	4’,6-diamino-2-phenylindole dihydrochloride
dpa	Days post amputation
dpf	Days post fertilisation
dpi	Days post injury
dpt	Days post transplant
dsRNA	Double-stranded RNA
EHT	Endothelial-to-hematopoietic transition
EMH	Extramedullary hematopoiesis

EMP	Erythromyeloid progenitor
ENU	N-ethyl-N-nitrosourea
Egr1	Early growth response protein 1
ETS	E26 transformation specific
FACS	Fluorescence-activated cell sorting
FCS	Fetal calf serum
FISH	Fluorescence *in situ* hybridisation
Fms	Colony stimulating factor receptor 1a
FSC	Forward scatter
G-CSF	Granulocyte colony stimulating factor
GESTALT	Genome-editing of synthetic target arrays for lineage tracing
GMP	Granulocyte-macrophage progenitor
GvHD	Graft versus host disease
Gy	Grays
HCD	High-cholesterol diet
HCT	Hematopoietic stem cell transplant
HLA	Human leukocyte antigen
HLA-DR	Human leukocyte antigen D related
hpa	Hours post amputation
hpf	Hours post fertilisation
hpi	Hours post injection
hpt	Hours post treatment
HSB	Hyperactive sleeping beauty
HSC	Hematopoietic stem cell
HSPC	Hematopoietic stem and progenitor cell
ICM	Intermediate cell mass
Id1	DNA-binding inhibitor protein 1
IFN	Interferon
Ig	Immunoglobulin
IL	Interleukin
iNOS	Inducible nitric oxide synthase
IP	Intraperitoneal

IR	Irradiation
Irf	Interferon regulatory factor
Jam1a	Junction adhesion molecule 1a
Klf6a	Krüppel-like factor 6a
LC	Langerhans cell
Lck	Lymphocyte-specific protein tyrosine kinase
Lin	Lineage
LMPP	Lymphoid-primed multipotent progenitor
L-plastin	Leukocyte-specific actin-binding protein
LPS	Lipopolysaccharide
LSK	Lin- Sca1+ cKit+
LT-HSC	Long term hematopoietic stem cell
Lyz	Lysozyme
M1	Classically activated pro-inflammatory macrophage
M2	Alternatively activated anti-inflammatory macrophage
MAPK	Mitogen-activated protein kinase
MEP	Megakaryocyte-erythrocyte progenitor
MG	Microglia
MHC	Major histocompatibility complex
MLP	Myeloproliferative leukemia protein
Mpeg	Macrophage-expressed gene
mpf	Months post fertilisation
MPP	Multipotent progenitor
Mpx	Myeloperoxidase
MTZ	Metronidazole
MyD88	Myeloid differentiation primary response gene 88
MYH10	Non-muscle myosin heavy chain IIB
NF-κB	Nuclear factor κ-light-chain-enhancer of activated B cells
NLR	NOD-like receptor
NLS	Nuclear localisation signal
NOD	Nucleotide-binding oligomerization domain
OTC	Oxytetracycline

PAMP	Pathogen-associated molecular pattern
PB	Peripheral blood
PBI	Posterior blood island
PBS	Phosphate-buffered saline
PCR	Polymerase chain reaction
PFA	Paraformaldehyde
PGE2	Prostaglandin E2
PLM	Posterior lateral-plate mesoderm
poly I:C	Polyinosinic:polycytidylic acid
PRR	Pattern recognition receptor
PS	Penicillin streptomycin
qRT-PCR	Quantitative real-time polymerase chain reaction
R848	Resiquimod
RBI	Rostral blood island
RO	Retro-orbital
ROS	Reactive oxygen species
Sca1	Stem cell antigen 1
SCF	Stem cell factor
SCID	Severe combined immune deficiency
SD	Standard deviation
Sdf1a	Stromal-derived factor 1a
SLAM	Signalling lymphocytic activation molecule
SMX	Sulfamethoxazole
SP	Side population
SSC	Side scatter
ssRNA	Single-stranded RNA
ST-HSC	Short term hematopoietic stem cell
Tal1	T cell acute lymphocytic leukemia 1
TALEN	Transcription activator-like effector nuclease
TCR	T cell receptor
TEP	Transepithelial protrusion
Tg	Transgenic

TGFβ	Transforming growth factor β
TIR	Toll-interleukin-1 receptor
TLR	Toll-like receptor
TNF	Tumor necrosis factor
TRIF	TIR-domain-containing adapter-inducing IFN-β
TRITC	Tetramethylrhodamine
tSNE	T-distributed stochastic neighbour embedding
Ubi	Ubiquitous
VDA	Ventral wall of the dorsal aorta
WBM	Whole bone marrow
WKM	Whole kidney marrow
wpf	Weeks post fertilisation
wpt	Weeks post treatment
WT	Wild type
ZFN	Zinc finger nuclease

Table of Contents

List of Figures

All videos that feature in figures can be accessed via the following link qrgo.page.link/U8g9z

List of Tables

List of Appendices

Chapter 1

Introduction

Chapter 1 | Introduction

1.1 Hematopoietic stem cells

Hematopoietic stem cells (HSCs) were first described by Till & McCulloch in 1961. They are defined by their ability to carry out stable multilineage reconstitution of the hematopoietic system following sequential transplantation in ablated hematopoietic stem cell transplant (HCT) recipients. HSCs are rare, multipotent and self-renewing cells that maintain blood production throughout the life of vertebrate organisms (Till & McCulloch, 1961; Metcalf & Moore, 1971). They are responsible for the production of all mature and differentiated hematopoietic cells (Ng & Alexander, 2017). HSCs maintain steady-state hematopoiesis to ensure sufficient erythrocytes and leukocytes are in circulation throughout an organism's lifespan. They also come into action during emergency haematopoiesis to replenish the immune system with leukocytes (Boettcher & Manz, 2017).

Broadly, there are two main groups of HSCs that have been described in mammals: long-term HSCs (LT-HSCs) and short-term HSCs (ST-HSCs) (Morrison & Weissman, 1994). LT-HSCs go through asymmetric division to self-renew and maintain a population of LT-HSCs for the life span of the animal and produce ST-HSCs, or lineage-specific progenitors. LT-HSCs are capable of reconstituting the immune system in the long term. ST-HSCs and multipotent progenitors (MPPs), on the other hand, are only capable of reconstituting the immune system in the short term as their potential for self-renewal is limited and they are eventually depleted (Morrison & Weissman, 1994; Challen *et al*., 2009). In this way, the maintenance of LT-HSCs into adulthood is crucial to the maintenance of a healthy immune system.

1.1.1 Hierarchy model of hematopoiesis

Hematopoiesis has classically been defined as a hierarchical process with LT-HSCs at the top of the hierarchy, being the most primitive cells and giving rise to all other blood cell types by stepwise progression through intermediate progenitors (Fig 1.1). In this hierarchical model, LT-HSCs first give rise to ST-HSCs, which then differentiate to MPPs, which in turn give rise to oligopotent progenitors known as lymphoid-primed multipotent progenitors (LMPPs) and common myeloid progenitors (CMPs). These oligopotent progenitors have very high

proliferative potential, while also having very limited self-renewal potential (Manz & Boettcher, 2014). MPPs have been shown to have no detectable self-renewal capacity (Yang *et al*., 2005). In an adult human weighing approximately 70 Kg, it has been estimated that ~10^{11}-10^{12} mature blood cells are generated daily under steady-state conditions (Gordon *et al*., 2002), of which approximately 0.5-1 X 10^{11} are granulocytes (Dancey *et al*., 1976). Thus, intermediate progenitors with limited or no self-renewal potential must be continually replenished by HSCs. LMPPs were hypothesised to give rise to pro-lymphocytes or common lymphoid progenitors (CLPs), which can produce T- and B-cells that have limited self-renewal capacity. CMPs, on the other hand, would first go through another progenitor fate decision to generate either bipotent granulocyte-macrophage progenitors (GMPs) or megakaryocyte-erythrocyte progenitors (MEPs) (Akashi *et al*., 2000; Cheng, Zheng & Cheng, 2019) before further proliferation to generate terminally differentiated granulocytes, macrophages, erythrocytes, and megakaryocytes (Fig 1.1). Most of these terminally differentiated cells have a limited life span and must therefore be continually replenished. During infection or injury, the turnover of innate immune cells significantly increases and can lead to demand-driven emergency hematopoiesis.

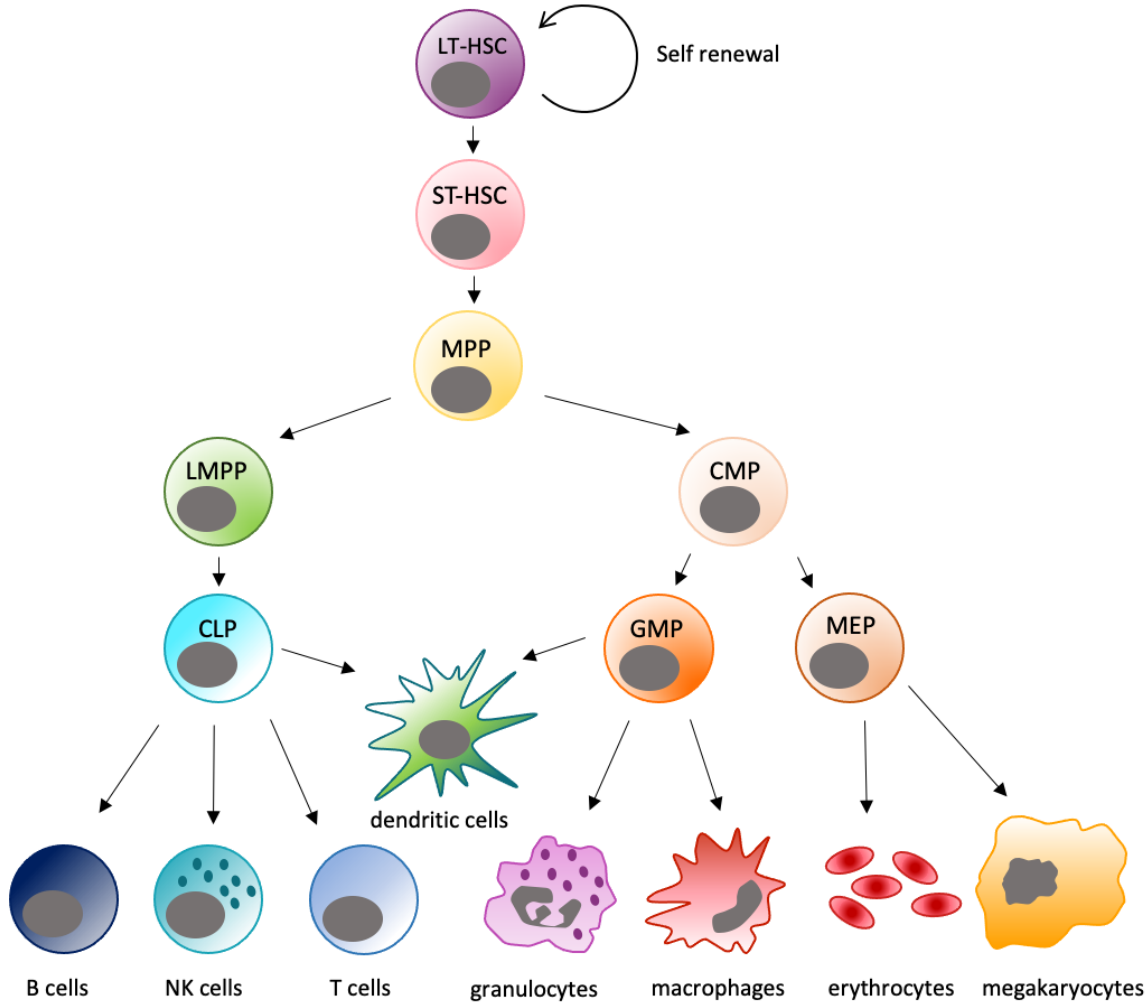

Fig. 1.1 Classical hierarchy model of hematopoiesis

Schematic representation of the hierarchy model of hematopoiesis. LT-HSCs are at the top of the hierarchy and possess self-renewal potential. According to this model there is a step wise progression through ST-HSCs, multipotent progenitors (MPPs) followed by either lymphoid multipotent progenitors (LMPP) or common myeloid progenitors (CMPs) toward terminally differentiated hematopoietic cells.

1.1.2 Continuum model of hematopoiesis

The hierarchical model of hematopoiesis was based predominantly on bulk identification and analysis of cells according to cell surface marker expression and transplantation studies. However, this has not been able to fully recapitulate the intricacies of hematopoiesis or the heterogeneity and plasticity of the hematopoietic stem and progenitor cell (HSPC) population. For example, there have been a number of studies that were able to experimentally convert lymphoid lineage cells to macrophages (Kondo *et al*., 2000; Iwasaki-arai *et al*., 2003; Xie *et al*., 2004). In recent years, as single cell sequencing methodologies and computational analysis have been increasingly applied to the study of hematopoiesis, a continuum model of hematopoiesis has been proposed. In this model, it is suggested that

HSCs gradually acquire bias towards a particular lineage, rather than passing through discrete hierarchical progenitor cells (Velten *et al*., 2017; Macaulay *et al*., 2016; Karamitros *et al.,* 2018). Cheng, Zheng & Cheng describe mouse studies that provide evidence for the heterogeneity of HSCs with myeloid or lymphoid bias (Chen, Zheng & Cheng, 2019). Lineage-biased HSCs have also been identified in zebrafish. Tang *et al*. performed single-cell RNA sequencing on fluorescence-activated cell sorting (FACS) sorted *Runx*:GFP+ HSPCs from adult zebrafish. T-distributed stochastic neighbour embedding (tSNE) analysis showed heterogeneity within the hematopoietic compartment and led to the identification of erythroid-primed HSCs, in addition to classically defined HSCs (Tang *et al*., 2017). A number of mouse and human studies have found that HSC bias and differentiation occurs via gradual, continuous changes in gene expression and cell potential, rather than binary cell fate decisions or by progressing through discrete hierarchical progenitors (Quesenberry *et al*., 2014; Velten *et al*., 2017; Zheng *et al*., 2018; Karamitros *et al.,* 2018). Macaulay *et al*. were able to use single-cell RNA sequencing and computational reconstruction of thrombocyte development in zebrafish to identify and place individual cells within a population along a pseudotime continuum as they differentiated from stem cell to mature thrombocyte (Macaulay *et al*., 2016). Nevertheless, the verdict is still out between the hierarchical and continuum models of hematopoiesis. There have been conflicting results in studies of human HSCs using single-cell RNA sequencing. Recent work on human HSCs has focused on extending single-cell RNA sequencing analysis from classically defined HSCs by using the transmembrane protein mucosialin (hereafter cluster of differentiation (CD) 34) positive CD34+ cells to investigating whole bone marrow lineage negative cells, irrespective of CD34 expression. Using this method, evidence for hierarchical branchpoints of fate decision was found, which led to the identification of the basophil branch point (Pellin *et al*., 2019). Furthermore, sialomucin (CD164) was identified as a new marker for the earliest branches of human HSC specification.

To understand native hematopoiesis, it is important to study the behaviour of HSCs and progenitors under physiological conditions. Most studies that have supported the hypothesis that HSCs are the drivers of hematopoiesis come from transplantation studies, which require pre-treatment to disrupt the niche, which places donor HSCs under hematopoietic stress (Cheng, Zheng & Cheng, 2019). Ablative pre-treatments used in most transplantation studies

have been shown to impact the behaviour of HSCs, as well as alter niche factors that are important in controlling hematopoiesis. Therefore, transplant studies cannot be used to elucidate the behaviours and dynamics of HSCs and progenitors during steady state hematopoiesis (Crane *et al.*, 2017; McBrien, 2017; niche factors described in more detail in section 1.5). However, elegant lineage-tracing studies have been carried out to study native, steady state hematopoiesis. These are discussed in more detail in section 1.4.3.

1.2 Purification of HSCs

1.2.1 Identification of human HSCs

The definitive method to identify HSCs is through *in vivo* HCT reconstitution assays using cells that have been selected based on a combination of cell surface markers. Isolation of HSCs has largely been carried out by the use of antibodies and FACS. The markers used to define HSCs have changed over the last two decades as new methods, such as single-cell RNA sequencing, have made it possible to investigate HSCs in more detail. Historically, human HCSs have largely been defined by their expression of CD34, which is not present on the surface of differentiated cells (Verfaillie *et al*., 1990). Undifferentiated cells also do not express so-called lineage (Lin) markers that are expressed on the surface of mature and terminally differentiated blood cells. Furthermore, the CD34+ Lin- population can be further purified to achieve greater reconstitution potential by excluding cells that express ADP-ribosyl cyclase (CD38) and the major histocompatibility class II antigen Human Leukocyte Antigen D Related (HLA-DR) (Terstappen *et al*., 1991; Brandt *et al*., 1988; Hénon *et al*.,1998). In addition, the CD34+ CD38- population is heterogeneous for the expression of thymocyte antigen 1 (thy1, hereafter CD90), CD45A and CD49f, and can be selected for greater long-term multilineage reconstitution potential based on these cell surface markers (Shimazaki *et al*., 2004; Baum *et al*., 1992). Via limiting dilution assays, it was found that Lin- CD34+ CD38- CD90+ CD45A- CD49f+ cells had the highest frequency of HSCs in humans (Notta *et al.,* 2011). More recently, studies using single-cell RNA sequencing have brought the utility of CD34 as a selection marker for human HSCs into question and have identified a new marker, sialomucin (CD164), which showed a greater distinction in expression levels between early and late progenitors when compared to either CD34 or CD38. It has been suggested that the application of CD164 as a selection marker may increase HSC purity and, hence, HCT outcomes (Pellin *et al*., 2019).

1.2.2 Identification of mouse HSCs

Mouse studies have been central to developing an understanding of HSC biology and phenotype. However, the phenotype of mouse HSCs does not fully recapitulate the cell surface markers found on human HSCs. In fact, mouse HSCs are identified in part by the absence of CD34 expression (Wilson *et al*., 2007). In addition, mouse HSCs are typically isolated from the Lin-, stem cell antigen 1 (Sca1) positive and stem cell factor receptor (cKit) positive population in the bone marrow (BM). This is commonly referred to as Lin- Sca+ Kit+, or collectively abbreviated as LSK (Spangrude *et al*., 1988). This population of LSK cells has been the benchmark HSC population against which HSC potential is measured when new markers are identified. For example, murine CD34- LSK cells can be further refined for increased reconstitution potential by selecting for signalling lymphocytic activation molecule (SLAM) receptors 1 and 2, also known as CD150 and CD48 respectively (Kiel *et al*., 2005). Mouse HSCs were found to express high levels of CD150 but not CD48. Hence, the enriched HSC population can be defined as CD34- LSK CD150+ CD48-. Although this population makes up less than 0.01% of BM cells, 47% of single cells isolated from this population led to long-term reconstitution (Kiel *et al*., 2005). However, despite the wealth of knowledge surrounding cellular and molecular mechanisms that regulate HSC biology, there remain difficulties in interpreting mouse studies of hematopoiesis. This can in part be attributed to inconsistencies in selection parameters for HSC purification, differences in gating strategies for FACS and modifications to the assays used (Batsivari *et al*., 2020).

1.3 Zebrafish hematopoiesis

In the last two decades, zebrafish (*Danio rerio*) have become an attractive model to study hematopoiesis and HSC biology owing to their many unique advantages over higher vertebrate organisms. Due to the relative ease with which transgenic animals can be produced, a large number of transgenic lines have been generated to express fluorescent proteins, driven by cell-type specific promoters (Table 1.1 & 1.2). Similarly, since the advancement of gene-editing technologies such as zinc finger nucleases (ZFN), transcription activator-like effector nucleases (TALENs) and the clustered regularly interspaced short palindromic repeats (CRISPR) /Cas9 system, many reverse genetic studies have been carried out to interrogate the functions of specific genes. In addition, large-scale forward genetic studies, using DNA mutagenic agents such as ethyl-nitroso-urea (ENU) to induce mutagenesis, have led to the

identification of many essential genes required for hematopoiesis (Weinstein *et al*., 1996; Ransom *et al*., 1996). Other advantages of zebrafish include their high fecundity, whereby a given pair is able to produce approximately 200-300 progeny each week (Meeker & Trede, 2008), their *ex vivo* fertilisation and the transparency of the early embryos. These characteristics allow the development of the vertebrate organism to be studied from the single-cell stage. In addition, a number of genetic screens have led to the identification of optically transparent adult mutant zebrafish lines known as *Casper* and *TraNac*, which cannot produce melanophores or iridophore pigment cells, the cells responsible for the black and silver stripes respectively (Lister *et al*., 1999; D'Agati *et al*., 2017). This has further enabled the visualisation and imaging of the fluorescent protein-expressing cells in adult transgenic fish. In addition to the availability of transparent mutant lines, there are also mutant lines that are incapable of initiating definitive hematopoiesis and can survive a bloodless phase, which in mouse models has resulted in embryonic lethality (Soza-ried *et al*., 2010; Sood *et al*., 2010). As a result, zebrafish have become a very valuable model organism to study immunology, HSC and HCT biology. The use of zebrafish has led to a greater understanding of HSC specification, the anatomical locations they arise from, the niches they occupy at different developmental stages and the dynamics of HSC engraftment following HCT.

1.3.1 Primitive hematopoiesis

Vertebrates are known to undergo distinct waves of hematopoietic activity linked to early development and adult stages. In zebrafish, there are two waves of hematopoiesis: the primitive and the definitive waves. Blood formation from the primitive wave gives rise to erythrocytes as well as myeloid cells, such as neutrophils and macrophages of the innate immune system. The erythrocytes ensure adequate oxygenation of tissues in the rapidly developing embryo. The macrophages and neutrophils protect against pathogens which may infect the embryo due to the *ex vivo* development of zebrafish embryos. Furthermore, macrophages carry out phagocytosis of apoptotic cells that arise during development. Macrophages may also be involved in the regulation of the morphology of the vascular system (Lobov *et al*., 2005; Fantin *et al*., 2010). In zebrafish, the primitive wave of hematopoiesis is initiated at two distinct sites, one of which is in the intermediate cell mass (ICM) blood islands. These are intra-embryonic and found along the bilateral stripes of the posterior lateral-plate mesoderm (PLM), between the notochord and yolk sac and in between the

somites. The other site is known as the rostral blood islands (RBI) and originates from the anterior lateral-plate mesoderm (ALPM). The RBI generates primitive macrophages, embryonic microglia and neutrophils (Herbomel *et al*., 1999; Bennett *et al*., 2001; Lieschke *et al*., 2002). In birds and mammals, the equivalent of the cells formed in the ICM are formed in the yolk sac. In contrast to the zebrafish, the mammalian and bird yolk sacs are extra embryonic and have a vascular bed where the blood islands are formed. In amniotes, primitive erythropoiesis is initiated in the yolk sac, which constitutes the only site of primitive erythropoiesis (Yamane, 2018).

1.3.2 Specification of primitive hematopoietic cells in zebrafish

The embryonic primitive wave of hematopoiesis is thought to start with the transient production of bipotential hemangioblast cells during early gastrulation. These cells are capable of producing either hematopoietic progenitors or vascular endothelial progenitors in the ICM and are characterised by early expression of PAS-domain-containing bHLH transcription factor *cloche* (also known as *npas41*), a master regulator of T cell acute lymphocytic leukemia 1 (*tal1*, formerly *Scl*) and E26 transformation specific (ETS) related protein (*etsrp*, also known as *etv2*), which are involved in the earliest stages of hematopoietic and endothelial specification respectively (Reischauer *et al*., 2016; Liao *et al*., 1997). *Cloche* mutants have been used to study the ontogeny of endothelial and hematopoietic cells as they lack primitive blood cells and endocardial heart cells due to the absence of *gata1* and *gata2* transcription factors (Stainier *et al*., 1995). However, there are some fate mapping studies which appear to both confirm the presence of bipotential hemangioblasts and also indicate that separate hematopoietic and vascular endothelial progenitors can arise directly from the ventral mesoderm, rather than forming a transient common hemangioblast progenitor (Vogeli *et al*., 2006). Hence, the existence of a common bipotential hemangioblast continues to be the subject of debate and research.

The earliest markers for primitive hematopoiesis in the ICM are present between 6 and 10.5 hours post fertilisation (hpf; 2-somite stage) of the zebrafish embryo and are punctuated by the expression of *tal1*, *gata2b* and *lmo2* and ETS family transcription factors such as *fli1a*, *fli1b* and *etsrp* by differentiating hemangioblasts in the ICM (Butko *et al*., 2015; Gering *et al*., 1998; Patterson *et al*., 2007). In both zebrafish and mammals, *tal1*, *gata2* and *lmo2* are all important

upstream regulators of *gata1*, an erythrocyte transcription factor, and *pu.1*, a myeloid transcription factor. The balance between erythrocyte and myeloid output is controlled by antagonism between Pu.1 and Gata1 transcription factors, which regulate myeloid versus erythroid output of bipotent erythromyeloid progenitors (EMPs) (Rhodes *et al*., 2005). Subsequently, by approximately 12 hpf (5-somite stage), cell fate is irreversibly determined as ICM cells start to express either *gata1a*, *pu.1* or *kdrl*, leading to formation of erythroid or myeloid precursors or angioblast cells respectively (Bertrand *et al*., 2007; Galloway *et al*., 2005; Liao *et al*., 1997). At approximately 19 hpf (20-somite stage), cells in the ICM start to co-express the neutrophil and erythrocyte markers *myeloperoxidase* (*mpx*) and *gata1*, possibly representing early myeloerythroid cells (Warga *et al*., 2009; Bertrand *et al*., 2007; Glenn *et al*., 2014). Zebrafish erythrocytes remain nucleated and primitive erythrocytes enter circulation at approximately 24 hpf, coinciding with the commencement of the heartbeat (Long *et al*., 1997). These are the only erythrocytes in circulation until approximately 4 days post fertilisation (dpf) and can be distinguished from definitive erythrocytes by their expression of the embryonic hemoglobin genes *hbae1.1, hbae3, hbae5, hbbe1.1, hbbe1.2, hbbe1.3, hbbe2* and *hbbe3* (Tiedke *et al*., 2011; Nefedochkina *et al*., 2016; Brownlie *et al*., 2003; Ganis *et al*., 2012).

In parallel, cells in the RBI express *estrp*, *tal1* and *pu.1* by 10 hpf (Herbomel *et al*., 1999; Bennett *et al*., 2001; Lieschke *et al*., 2002). Later, by approximately 16-18 hpf (17-18-somite stage), these cells express the pan leukocyte marker *leukocyte-specific actin-binding protein* (*l-plastin,* also known as *lcp1*) (Herbomel, Thisse & Thisse, 2001). Around the same time, RBI-derived cells also start to express myeloid-specific genes such as *interferon regulatory factor 8* (*irf8*) and *CCAAT enhancer binding protein 1* (*cebp1*), with the expression of *irf8* leading to macrophage progenitor cell fate while *cebp1* expression determines neutrophil progenitor cell fate (Li *et al*., 2011; Jin *et al*., 2016). By 24 hpf, neutrophil progenitors start differentiating by expression of *mpx* and *lysozyme* (*lyz)* and, by 36 hpf, they are fully mature as can be seen by Sudan Black staining (Bennett *et al*., 2001; Liu *et al*., 2002; Jin *et al*., 2012). Meanwhile, by the 25-somite stage, primitive macrophages start to express *colony stimulating factor receptor 1a* (*csfr1a,* also known as *fms*), *macrophage expressed gene 1* (*mpeg1*), *mfap4*, *ptpn6* and the chemokine receptor *cscr3.2* (Walton *et al*., 2015; Zakrzewska *et al*., 2010; Herbomel, Thisse & Thisse, 2001). At 2.5 dpf, RBI-derived microglia start to colonize the zebrafish brain (Xu *et al*.,

2016), where they are eventually replaced by cells from the definitive wave of hematopoiesis at approximately 15 dpf (Ferrero *et al*., 2018).

1.3.3 Transient wave of definitive hematopoiesis

Prior to the onset of HSC specification from the hemogenic endothelium of the ventral wall of the dorsal aorta (VDA), there is a transient wave of definitive hematopoiesis which forms EMPs at ~24-48 hpf. These progenitors arise from the posterior blood island (PBI). EMPs are characterised by the expression of *gata1* and *lmo2* and can be isolated by FACS as early as 24 hpf (Bertrand *et al*., 2007). By 72 hpf, *gata1*+ and *lmo2*+ cells are no longer detectable in the developing zebrafish embryo. Specification of EMPs is dependent on *cmyb* and *runx1* but does not require *notch*, as shown by *mindbomb* mutants of Notch signalling (Bertrand *et al*., 2010; Burns *et al*., 2005). This differentiates EMPs from HSCs (Burns *et al*., 2005). Fate mapping studies suggest that EMPs arise from *lmo2*+ cells from PLM derivatives. These progenitors give rise to erythrocytes and myeloid cells, as evidenced by the initial detection of *gata1* and *pu.1* followed by *mpx* transcripts respectively. They are capable of producing a range of myeloid cells including granulocytic neutrophils, monocytes and macrophages (Bertrand *et al*., 2007). However, EMPs lack lymphoid potential and hence are not multipotent HSPCs. Furthermore, mouse models have shown that EMPs can only give rise to erythroid and myeloid cells transiently following engraftment of transplanted cells and, unlike HSCs, they cannot reconstitute a myeloablated recipient long term (McGrath *et al*., 2015). Zebrafish transplantation studies demonstrated that EMP cells home to the PBI in transplanted recipients and do not home to definitive sites of hematopoiesis such as the caudal hematopoietic tissue (CHT), the whole kidney marrow (WKM) or the thymus (Bertrand *et al*., 2007).

1.3.4 Definitive hematopoiesis

The second wave of definitive hematopoiesis is initiated at around 26-30 hpf in the hemogenic endothelium of the VDA and gives rise to HSCs that maintain hematopoiesis throughout the life span of the zebrafish. The VDA is sometimes referred to as the aorta gonad mesonephros (AGM), as this is the mammalian equivalent to the VDA where HSCs are formed during embryogenesis. HSCs are capable of giving rise to cells in each lineage including erythrocytes, myeloid cells and lymphoid cells, and are maintained via symmetric and asymmetric divisions

leading to self-renewal in the niche. Once HSCs have budded from the VDA, they enter the circulation and home to the CHT, located at the posterior end of the developing zebrafish embryo, where the cells embed at 2 dpf. The CHT is considered to be the zebrafish equivalent to the mammalian foetal liver, being the embryonic niche to support the expansion of definitive HSCs that have seeded there (Murayama *et al*., 2006). In the CHT, HSCs give rise to embryonic neutrophilic granulocytes, monocytes, macrophages and erythrocytes. Around 3 dpf, HSCs colonize the developing thymus and at 4 dpf, HSCs also migrate to the pronephric tissue that will mature into the adult WKM, constituting the hematopoietic niche in adult zebrafish (Kissa *et al*., 2008). The WKM is the zebrafish equivalent of the mammalian BM and is the site of adult hematopoiesis where cells of each blood cell lineage are produced.

1.3.5 Specification of zebrafish definitive hematopoietic cells

Zebrafish HSC specification is induced by *notch1a/b* receptor-mediated signalling which regulates the expression of definitive hematopoietic transcription factor *runx1*, also known as *acute myeloid leukaemia protein 1* (Burns *et al*., 2005; Kim *et al*., 2014). *runx1* is a highly conserved member of the runt-domain containing family of transcription factors and is required for the induction of the endothelial-to-hematopoietic transition (EHT), which enables cells of the hemogenic endothelium to be specified as hematopoietic cells (Sood *et al*., 2010; Kissa & Herbomel, 2010). However, as in mice, *runx1* is no longer required following EHT (Chen *et al*., 2009). The proteins Runx1 and core binding factor beta (Cbfβ) together form a heterodimer that is required for HSC budding from the VDA, thus enabling cells to enter circulation. However, Cbfβ heterodimerization with Runx1 does not appear to be required in either the primitive wave of hematopoiesis or during the transient wave of EMP production, as these processes were Cbfβ independent. Nevertheless, knockdown of the *runx1* gene does significantly impact primitive hematopoiesis (Bresciani *et al*., 2014; Burns *et al*., 2002; Kalev-Zylinska *et al*., 2002; Kissa & Herbomel, 2010). *tal1* is also required for the specification of definitive HSCs. Due to a whole genome duplication event that occurred in teleost, there are two isoforms of this gene, *tal1α* and *tal1β*. Of these, *tal1β* is expressed in endothelial cells in the VDA that undergo EHT and is required for HSC specification. On the other hand, *tal1α* was found to be expressed at a later stage and to be involved with HSC budding from the VDA (Zhen *et al*., 2013). In addition, Jing *et al*. found that adenosine signalling was involved in regulation of HSPC emergence in the zebrafish embryo. Through stimulation of the A2b

receptor and cAMP-PKA dependent pathway, adenosine signalling induced expression of *cxcl8* and *tal1β*, which were found to increase the number of *runx*1+ and *cmyb*+ cells in the VDA (Jing *et al*., 2015). In the same year, Butko *et al*. described *gata2b* as a key regulator of EHT upstream of *runx1* expression in the hemogenic endothelium of the VDA (Butko *et al*., 2015). *runx1* and *cmyb* are co-expressed at 36 hpf but are regulated in a hierarchical manner as *runx1* is responsible for the downstream induction of *cmyb*, which is also required for HSC budding from the VDA. In 2016, using whole mount in situ hybridisation and bisulfite sequencing, Gore *et al*. were able to show that the *de novo* DNA methyl transferase *dnmt3bb.1* is required for the epigenetic maintenance of *cmyb* following HSC specification and budding from the hemogenic endothelium. This causes methylation of intron 1 of the *cmyb* gene. The expression of *dnmt3bb.1* is induced by *runx1* and ensures continued *cmyb* expression following downregulation of *runx1* (Gore *et al*., 2016). It was shown that in *dnmt3bb.1* mutant fish, *cmyb* expression decreases by 72 hpf and, consequently, there are decreased *rag1* and *l-plastin* expressing cells and reduced HSPCs in the zebrafish WKM.

1.4 Identifying definitive HSCs in zebrafish

Both human and mouse HSCs are purified through a combination of highly selective monoclonal antibodies against cell surface markers described earlier in sections 1.2.1 and 1.2.2. In part due to the relatively recent uptake of zebrafish as a model organism to study HSCs, there are limited anti-zebrafish antibodies commercially available. Furthermore, previous attempts to develop highly specific monoclonal antibodies against teleost leukocytes showed only limited success. This could possibly be the result of the highly divergent glycosylation patterns in teleost being identified as foreign by the rodent immune system (Traver *et al*., 2003). Nevertheless, due to the genetic tractability of zebrafish, a rapidly increasing array of transgenic lines are being developed. Several transgenic lines have been described that express fluorescent proteins in HSPCs (Table. 1.1).

1.4.1 Transgenic lines with fluorescent protein-expressing HSPCs

Traver *et al*. first described a way to identify major blood cell lineages from the zebrafish WKM by flow cytometry analysis. The authors described the use of forward and side scatter (FSC and SSC), which indicate cell size and granularity respectively, to identify erythrocytes (FSC^{low}), lymphocytes (FSC^{inter}, SSC^{low}), precursors (FSC^{high}, SSC^{inter}) and myeloid cells (FSC^{high},

SSC^{high}). They found that cells with long-term multilineage hematopoietic reconstitution ability resided among the lymphoid compartment (FSC^{inter}, SSC^{low}) in the WKM (Traver *et al*., 2003). Later, Lin *et al.* generated a transgenic line where GFP expression is driven by the thrombocyte-specific integrin alpha 2b (itga2b, hereafter CD41). The *Tg(CD41:GFP)* transgenic zebrafish drive expression of GFP in mature thrombocytes (Lin *et al*., 2005). While the CD41:GFP^{high} cell population marked mature thrombocytes, the CD41:GFP^{low} population was found to contain HSCs capable of long-term multilineage reconstitution following primary and secondary transplantation in sublethal gamma-irradiated recipients (Lin *et al*,. 2005; Ma *et al*., 2011). Importantly, CD41:GFP is expressed in definitive HSCs from the larval stage and throughout adulthood. This same transgenic line was utilised in transplantation assays in the aforementioned study by Traver *et al*. Interestingly, the authors described the presence of CD41:GFP^{low} cells within the precursor compartment and CD41:GFP^{high} cells within the lymphoid compartment of the FSC/SSC scatter plot. However, this conflicted with the conclusion that HSCs are found within the lymphoid compartment. In 2007, North *et al*. generated the *Tg(cmyb:*e*GFP)* transgenic zebrafish to study the effect of prostaglandin E2 (PGE2) on HSC expansion in the embryo (North *et al*., 2007). However, GFP expression in *Tg(cmyb:eGFP)* transgenic zebrafish is not maintained post larval stages and therefore cannot be utilised to purify HSCs from the adult WKM (Bertrand *et al*., 2010). In 2009, Lam *et al*. published a study about the two isoforms of *runx1*, driven by either the P1 or P2 promoters in the zebrafish embryo. It was found that GFP was expressed by EMPs in the PBI of *Tg(runx1P1:EGFP)* embryos between 18 and 24 hpf. However, expression was no longer detected by either investigating the presence of GFP or by *in situ* hybridisation by 48 hpf. On the other hand, expression of GFP driven by the P2 promoter was first observed at the 6-somite stage in the notochord, followed by expression in hematopoietic cells arising from the VDA at 22 hpf. Continued expression of GFP was detected in a small number of definitive HSCs in the WKM of 1-month old *Tg(runx1P2:EGFP)* zebrafish (Lam *et al*., 2009). However, GFP expression in this transgenic was not specific to hematopoietic cells as neuronal cells in the brain and spinal cord were also GFP positive.

More recently, Tamplin *et al*. set out to generate a transgenic line that expressed fluorescent protein (mCherry or GFP) more selectively in definitive HSPCs. The expression of fluorescent protein in the transgenic is driven by a highly conserved cis-regulatory enhancer element

identified 23.5 kb downstream of the ATG translation initiation codon of exon one, within the first intron of the mouse *Runx1* locus (termed +23; Nottingham *et al*., 2007). This regulatory element was found to be important for the binding of key regulators of mouse hematopoiesis: *Gata2*, *Runx1*, *Ets*, *Tal1* and *Lmo2*, and hence was found to be driving *Runx1* expression and HSC emergence in the mouse. Tamplin *et al*. generated two transgenic lines: the *Tg(Runx1+23:GFP)* line which drives the expression of cytosolic EGFP (hereafter *Tg(Runx:GFP)*), and the *Tg(Runx1+23:NLSmCherry)* line where a nuclear localisation signal is attached to the mCherry fluorophore (hereafter *Tg(Runx:mCherry*). These lines were utilised to observe the emergence of HSPCs from the VDA and seeding of the perivascular niche in the CHT. The authors impressively demonstrated the interaction and remodelling of endothelial and stromal cells around the HSPCs upon their arrival in the CHT (Tamplin *et al*., 2015). They confirmed that the fluorophores were expressed in definitive HSPCs at all sites of definitive hematopoiesis in both transgenic zebrafish lines through the use of long-term transplantation. Limiting dilution transplant experiments indicated a stem cell frequency of ~1 in 35 among *Runx*:mCherry+ cells (Tamplin *et al*., 2015). Furthermore, the expression of mCherry in the *Tg(Runx:mCherry)* line overlapped significantly with the *cmyb*:GFP+ cells and *CD41*:GFP+ cells in all major hematopoietic tissues of the zebrafish embryo. In addition, Tamplin *et al*. demonstrated that *Runx*+ cells are still present in the adult zebrafish, making it possible to isolate them by FACS.

Transgenic Line	Expression pattern	Reference
Tg(CD41:GFP)	GFP expressed in thrombocytes (high) and HSPCs (low) in embryo and adult	Lin *et al*., 2005
Tg(cmyb:eGFP)	GFP expression lost in adult stages	North *et al*., 2007
Tg(Rux1P2:EGFP)	Unclear whether GFP expression persists in adulthood. GFP expression in HSPCs and neuronal cells	Lam *et al*., 2009
Tg(Runx1+23:NLSmCherry) *Tg(Runx1+23:GFP)*	Fluorescent protein expression in HSPCs in adult and embryo. *Tg(Runx1:NLSmCherry)* line exhibits broader mCherry expression	Tamplin *et al*., 2015
Tg(scl-α:d2EFGP) *Tg(scl-β:d2EGFP*	GFP expressed in HSPCs in the intermediate cell mass in embryos	Zhen *et al.,* 2013
Tg(gata2a:eGFP)	GFP expressed in eosinophils (high) and in *Runx1*:mCherry+ HSPCs (low) in adult	Traver *et al.,* 2003 Kobayashi *et al.,* 2019

Table 1.1 List of transgenic lines that have been used to study zebrafish HSPCs.

This table indicates the promoters used to drive fluorescent protein expression and the resultant expression pattern at different stages of development.

1.4.2 Alternative parameters used to isolate zebrafish HSPCs

In addition to attempts to generate transgenic zebrafish lines that express fluorescent proteins in HSPCs specifically, other methods have also been utilised to identify this rare population of cells. The ability of HSCs to efflux the DNA binding fluorescent Hoechst 33342 (Hoechst) dye is highly conserved among vertebrate species and has been used to enrich for HSCs in mammalian systems and teleost fish (Goodell *et al*., 1996; Kobayashi *et al*., 2008). Cells that expel Hoechst dye are known as side population (SP) cells. Kobayashi *et al*. first identified the presence of SP cells with hematopoietic activity in teleost kidney with an elegant transplantation model using ginbuna carp (Kobayashi *et al*., 2006). In their experiments, the authors used triploid (S3n) clones as donors and tetraploid (S4n) fish with 1 set of goldfish chromosomes as recipients. As such, irradiation or other myeloablative preconditioning was not required for successful transplantation. Subsequently, the group also demonstrated the presence of SP cells in zebrafish WKM (Kobayashi *et al*., 2008). Furthermore, Kobayashi *et al*. showed that zebrafish SP cells with hematopoietic activity relied on the expression of ATP-binding cassette (ABC) transporters to expel the fluorescent dye. These transporters have also been associated with Hoechst dye efflux in mammalian

systems (Zhou *et al*., 2001; Scharenberg *et al*., 2002; Kim *et al*., 2002). While the zebrafish possess 4 paralogous copies of the mammalian gene, it was found that only one of these, *zABCg2a*, was expressed and directly linked to the SP phenotype in zebrafish (Kobayashi *et al*., 2008). Additionally, Tsinkalovsky *et al*. showed that *zABCg2*a-expressing zebrafish SP cells also expressed key HSC-associated genes such as *tal1*, *lmo2*, and *cmyb* (Tsinkalovsky *et al*., 2007). Subsequently, a comparative microarray gene expression analysis between zebrafish, mouse and human HSCs identified 40 highly conserved regulators of HSCs that were upregulated in each species. Of these, *gata2*, *early growth response protein 1* (*erg1*) and DNA-binding inhibitor protein 1 (*id1*) were found, by *in situ* hybridisation, to be co-expressed with *zABCg2a* transporter protein in zebrafish (Kobayashi *et al*., 2010). Finally, in agreement with the presence of HSCs among the SP population, Ma *et al*. found that ~22.5 % of SP cells were also CD41:GFP^{low} (Ma *et al*., 2011).

1.4.3 Lineage tracing and in vivo visualisation of HSC emergence and native hematopoiesis

A number of studies have been carried out to directly visualise the birth and behaviour of HSCs from the VDA, as well as their subsequent seeding of the CHT and other hematopoietic tissues. Owing to the difficulty of generating specific antibodies against zebrafish hematopoietic cells (Traver *et al*., 2003) and the difficulty of identifying HSCs by single cell-specific promoters (Lin *et al*., 2005; North *et al*., 2007; Lam *et al*., 2009), cell- and lineage-tracing approaches have been engineered to gain a better understanding of HSC ontogeny. One such method involves photoactivatable caged fluorochromes which are not fluorescent when caged but fluoresce when UV is applied to break covalent bonds of the caged fluorochrome in a cell-specific manner. This method was first applied for cell tracing in zebrafish embryos by Murayama *et al*. who were able to identify definitive HSPCs that emerged from the area between the dorsal aorta and axial vein, and subsequently migrated to the CHT before colonizing the thymus and WKM (Murayama *et al*., 2006). In 2007, Jin *et al*. utilised photoinducible caged fluorescein to map the fate of fli:GFP+ endothelial cells in the VDA and were able to show that some of these cells later colonize the thymus and express *rag2* (a lymphocyte-specific marker). By doing so, they were among the first to show the existence of the hemogenic endothelium in zebrafish (Jin *et al*., 2007). At the same time, Bertrand *et al*. showed, using photoactivated uncaging of rhodamine, that CD41:GFP+ cells from the VDA,

but not the PBI, can colonize the thymus and express *rag2*, indicating that HSCs come from the VDA (Bertrand *et al*., 2007).

Valuable insights have been gained about HSC ontogeny using laser-activated caged fluorochromes. However, the application of this technology is limited to the first few days of zebrafish development as the caged fluorochrome dyes, which are injected at the 1-8 cell stage, are diluted through cell division in the developing embryo. As a result, alternative technologies using the Cre/Loxp system have been developed for lineage tracing in more mature zebrafish. Bertrand *et al*. crossed *Tg(cmyb:GFP)* transgenic fish with *Tg(kdrl:mCherry)* transgenic fish that expresses mCherry in endothelial cells. With the resultant *Tg(cmyb:GFP; kdrl:mCherry)* transgenic fish, they were able to confirm that HSCs arise directly from the hemogenic endothelium of the VDA via the fate change of *kdrl*:mCherry+ endothelial cells as they transition to become *cmyb*:GFP+ hematopoietic stem cells. Furthermore, they showed that emerging HSCs from the VDA do not enter the aortic lumen but instead migrate to the caudal vein (Bertrand *et al*., 2010). These results were in agreement with observations from Kissa *et al*. who found that nascent CD41:GFP+ HSCs entered circulation via the axial vein as opposed to the dorsal aorta (Kissa *et al*., 2008). Furthermore, Bertrand *et al*. carried out lineage tracing using *Tg(kdrl:Cre; β-actin:Loxp-STOP-Loxp-dsRed*^{express}) to demonstrate that cells deriving from kdlr+ cells in the VDA lead to robust, long-term multilineage population of the adult WKM and thymus, and that *de novo* production of HSCs permanently ceases in larval zebrafish. In this transgenic, *kdrl*+ vascular endothelial cells are driven to express *cre* recombinase, which permanently excises the *loxp* cassette. As a result, dsRed is expressed in *kdrl*+ cells. As the expression of dsRed is under the β-actin promoter, it continues to be expressed even following cellular division in every lineage that derived from cells which expressed *kdrl*. They showed that by 6 months of age, 96% of myeloid cells in the WKM expressed the dsRed marker. Hence, the team was able to demonstrate that all HSPCs derive from the vascular endothelium in the VDA (Bertrand *et al*., 2010). Using a similar strategy, Kobayashi *et al*. generated *Tg(jam1a:Cre*^{ert2}*; β-actin:Loxp-STOP-Loxp-dsRed)* transgenic zebrafish to trace the lineage of *junctional adhesion molecules 1a* (*jam1a*) positive cells. These cells were found to regulate HSC fate by mediating downstream Notch signalling, which is required for HSC specification (Kobayashi *et al*., 2014). Similarly, Butko *et al*. utilised *Tg(gata2b:gal4; UAS:Cre; β-actin:Loxp-STOP-Loxp-dsRed)* transgenic zebrafish to show that

embryonic Notch-dependent gata2b+ cells contribute to adult hematopoiesis and initiate *runx1* expression. In this system, newly emerging HSPCs that express *gata2b* drive the expression of *gal4*, which in turn drives the expression of the UAS promoter responsible for the downstream expression of *cre*. The Cre enzyme then excises the loxp cassette, resulting in the expression of dsRed in all subsequent cells derived from the gata2b+ parent cells (Butko *et al*., 2015).

With the advent of single-cell sequencing technologies, these too have been applied to zebrafish to gain a deeper understanding of the ontogeny of the immune system. Using a system named *ScarTrace*, Alemany *et al*. carried out single-cell sequencing to identify the clonal origin and cell type of adult WKM cells and traced all hematopoietic cells back to a small number of embryonic MPPs (Alemany *et al*., 2018). Genome-editing technologies have also been used to carry out lineage tracing. McKenna *et al*. carried out proof of principle experiments of their genome-editing of synthetic target arrays for lineage tracing (GESTALT) system on zebrafish to show that the majority of cells from each organ could be traced back to a small number of embryonic progenitors. The technology relies on the transgenic insertion of an array of CRISPR/cas9 target sites, called a barcode, that is successively edited and can be used to elucidate cell lineages by sequencing (McKenna *et al*., 2016). Similarly, the Cre/Loxp system has been utilised to generate the *zebrabow* fish in which *cre* drives recombination to generate unique combinations of fluorescent proteins to be expressed, leading to a 'zebrabow' of colours. This has been applied to carry out lineage analysis in embryos and adult zebrafish (Gupta & Poss, 2012; Pan *et al*., 2013; Henninger *et al.*, 2017). In particular, Henninger *et al.* used this system to investigate hematopoiesis and found that during the peak of HSC production from the aortic endothelium, there were approximately 30 HSC clones which would generate the entire hematopoietic system. Furthermore, the group were able show that clonal diversity is reduced upon hematopoietic stress such as the effects of sublethal irradiation and transplantation.

Furthermore, mouse models have also been utilised to investigate steady state hematopoiesis. In a doxycycline inducible mouse model, hyperactive sleeping beauty (HSB) transposon was transiently activated during development to generate stable genetic tags in cells and their downstream hematopoietic progeny. Sun *et al.* were able to demonstrate that the majority of

hematopoietic output in steady state in adults comes from MPPs rather than HSCs, as transplantations studies previously suggested (Sun *et al.,* 2014). Specifically, the group showed that for at least 1 year, granulocyte production was driven by progenitors with limited long-term engraftment potential. Similar results were subsequently found in stable genetic tagging and barcoding mouse models, which indicated that adult hematopoiesis is driven predominantly by MPPs and ST-HSCs, rather than LT-HSCs (Busch *et al.,* 2015; Pei *et al.,* 2017). However, Pei *et al.* also showed that when HSCs were labelled with the polylox barcoding system at the fetal liver stage, their progeny contributed to multiple lineages in adult mice. Interestingly, the Camargo group were able to demonstrate, through subsequent use of the doxycycline inducible HSB transposon system, that LT-HSCs gave rise to a significant proportion of megakaryocyte restricted progenitors during steady state hematopoiesis. Their work suggests that this may be a major role of un-perturbed LT-HSCs (Rodriguez-Fraticelli *et al.,* 2018).

1.4.4 Identification of zebrafish hematopoietic lineages

Due to the limited availability and success in generating zebrafish-specific antibodies to visualise and isolate specific immune cells, a large array of transgenic lines have been produced in zebrafish to study the immune system and hematopoiesis under homeostasis and inflammatory conditions. An overview of transgenic lines available with fluorescent proteins expressed under cell type-specific promoters is summarised in Table 1.2. However, this is not an exhaustive list of all transgenic lines generated to visualise immune cells in zebrafish. As discussed already, several transgenic lines have been created to visualise the emergence and subsequent behaviour of HSPCs, which have been summarised in section 1.4.1 (Table 1.1).

Cell type	Transgenic Line	Reference
Thrombocytes HSPCs	*Tg(CD41:GFP)*	Lin *et al*., 2005
HSPCs	*Tg(Runx1:NLSmCherry)* *Tg(Runx1:GFP)*	Tamplin *et al*., 2015
T cells	*Tg(lck:GFP)*	Langenau *et al*., 2004
CD4+ T cells and macrophages	*Tg(CD4-1:mcherry)*	Dee *et al*.,2016
Lymphoid cells	*Tg(rag2:GFP)*	Langenau *et al*., 2003
B cells	*Tg(IgM:GFP)*	Page *et al*., 2013
B cells	*Tg(CD79: GFP)*	Liu *et al*., 2017
Pro-inflammatory tnfa+ cells	*Tg(tnfα:GFP)*	Marjoram *et al*., 2015 Nguyen-Chi *et al*.,2015
Neutrophils	*Tg(mpx:GFP)*	Renshaw *et al*., 2006
Myeloid cells	*Tg(lysC:dsRed)* *Tg(lyz:GFP)*	Hall *et al*., 2007
Macrophages	*Tg(mpeg:mCherry)*	Ellet *et al*., 2011
Macrophages	*Tg(fms:mCherry)*	Dee *et al*., 2016 Gray *et al*., 2011
Macrophages	*Tg(mfap4:YFP)*	Walton *et al*., 2015
Eosinophils	*Tg(gata2a:GFP)*	Traver *et al*., 2003
All cells	*Tg(ubi:GFP)*	Mosimann *et al*., 2011
All cells	*Tg(β-actin:GFP)*	Burket *et al*., 2008

Table 1.2 List of transgenic lines used to study zebrafish hematopoietic cells.

This table indicates promoters used to drive fluorescent protein expression and which cell types express fluorescent protein driven by each promoter.

1.5 Steady-state and emergency hematopoiesis

During steady-state hematopoiesis, HSCs are responsible for ensuring sufficient numbers of erythrocytes, myeloid and lymphoid cells are in circulation at any given time to oxygenate the blood and carry out immune surveillance. Many complex interactions between cell-intrinsic and cell-extrinsic factors controlling steady-state and emergency hematopoiesis have been elucidated in mammalian systems. The evolution of adaptive immunity coincided with the emergence of jawed vertebrates, a group to which teleost fishes such as the zebrafish and also mammals belong. As a result, both the adaptive and innate branches of the immune system

are highly conserved between mammals and zebrafish (Herbomel, Thisse & Thisse, 1999). Zebrafish possess the same main blood cell populations as humans including erythrocytes, macrophages, neutrophils, eosinophils, T cells, B cells and mast cells (Meeker & Trede, 2008; Moss *et al*., 2009; Renshaw & Trede, 2012; Nguyen-Chi *et al*., 2015; Pereiro *et al*., 2015; Dee *et al*., 2016). Many of the molecular mechanisms found to regulate zebrafish hematopoiesis have also been shown to be conserved among higher vertebrates. Therefore, results from zebrafish are largely also translatable to mammalian systems.

1.5.1 The HSC niche

HSCs require a highly specialised microenvironment to sustain hematopoiesis and maintain their self-renewal potential. This microenvironment is known as the HSC niche and plays a key role in enabling HSCs to divide without initiating the differentiation of daughter cells. In mammalian organisms, the HSC niche resides in the bone marrow. However, during stress conditions, extramedullary local sites, such as the spleen and liver, have been identified as sites of hematopoiesis. In both mammals and zebrafish, HSCs are drawn to their niche through interactions between the HSC chemoattractant Sdf1 (or Cxcl12), expressed by stromal niche cells, and the HSC membrane-bound Cxcr4, the cognate receptor for Sdf1 (Glass *et al*., 2011; Tamplin *et al*., 2015). Tamplin *et al*. suggest that once the HSCs arrive in the correct anatomical location, an additional signal in circulation (possibly a lipid) is required for cell extravasion from the vascular lumen to enter the niche. Zebrafish have two *sdf1* genes, *sdf1a* and *sdf1b*, owing to a genome duplication event. Of these, *sdf1a* is required for HSC homing and is upregulated in a dose-dependent manner following irradiation. In adult mammals, this niche resides in the bone marrow, while in zebrafish and other teleost fish the HSC niche is found in the renal tissue of the kidney, known as the whole kidney marrow (WKM). *sdf1a* is highly expressed by renal tubules in the WKM which makes up most of the marrow and likely makes up part of the HSC niche (Glass *et al*., 2011). Interestingly, *sdf1a* is not only expressed in the renal tubules of the WKM but is also expressed in the gills and skin. The biological relevance of *sdf1* in these extramedullary locations, and whether or not HSCs home to them, has not been explored further.

Sophisticated methods have been developed for the study of the HSC niche in mouse models. However, these require highly invasive imaging techniques to visualise stem cell interactions

with the niche in the calvarium BM of live mice (Lo Celso *et al*., 2009). Due to the optical translucency of the zebrafish embryo, it has been possible to visualise cell-cell interactions between HSCs and niche cells and gain a deeper understanding of the structure of the embryonic niche in the CHT via minimally invasive imaging. Using correlative light and electron microscopy, Tamplin *et al*. were able to demonstrate that in the CHT, the niche consists of a group of 5-6 endothelial cells in addition to a single stromal cell that is in direct contact with the HSC. These cells arrange themselves around the HSC upon arrival in the perivascular niche of the CHT, in a process they termed cuddling (Tamplin *et al*., 2015). At least one stromal cell is in direct contact with one HSC and orients cell division. Conceptually, there are three possible outcomes of HSC cell division: an asymmetric division whereby one daughter cell maintains stem cell identity and the other begins to differentiate; a symmetric division whereby both daughter cells maintain the same stem cell identity of the mother cell, known as self-renewal; or finally, a symmetric division where neither of the two daughter cells maintain the stem cell identity of the mother cell and both differentiate. While little is currently known about the adult zebrafish WKM niche, it is likely that niche cells are involved in maintaining HSCs by inducing self-renewal.

1.5.2 Factors required for HSC maintenance

Mouse models have been used to help identify key growth factors involved in HSC maintenance. Stem cell factor (SCF) has been shown to bind to the KIT receptor, which is readily expressed by HSCs and is utilised in HSC identification in mouse models to select for LSK populations (Spangrude *et al*., 1988; Morrison & Weissman, 1994; Osawa *et al*., 1996; Adolfsson *et al*., 2001; Shin *et al*., 2014). Similarly, *ckit* is expressed by zebrafish HSCs as well. This receptor-ligand interaction is an important regulator of HSC maintenance (Thorén *et al*., 2008). Scf can be released into circulation and may affect HSCs indirectly. However, it has also been found to be expressed on cell surface membranes of niche-resident cells, indicating that HSC maintenance may be regulated via direct cell-cell contact. Thrombopoietin is involved in thrombocyte and platelet production and binds myeloproliferative leukemia protein (MPL) on the surface of HSCs, and has also been shown to be important in HSC maintenance (De Bruin *et al*., 2013). As mentioned earlier, Cxcl12 is an important HSC homing factor. Once in the niche, continued presence of Cxcl12 is responsible for HSC retention and proliferation. The zebrafish vascular niche is also involved in HSPC expansion under steady-state conditions.

Endothelial cell-derived Krüppel-like factor 6a (Klf6a) is required for both HSPC lodgement and expansion in the larval CHT following HSC emergence from the VDA. Klf6b acts via Ccl25b-Ccr7 chemokine signalling to promote HSPC maintenance. Furthermore, *ex vivo* cell culture studies suggest that this finding is also transferable to mammalian systems (Xue *et al*., 2017).

1.5.3 HSC cell cycle kinetics

Several studies have been carried out to determine the cell cycle dynamics of HSCs in mouse studies with conflicting results. One method to determine the cell cycle kinetics involves the incorporation of a thymidine analogue, 5-bromo-2-deoxyuridine (BrdU), into the DNA of replicating cells for a specified duration. Once BrdU is removed and no longer supplied, it is diluted by half with every cell division event. The level of BrdU present in cells is measured by immunohistochemistry following a set period of time known as a chase. However, doubts have been cast on the validity of using BrdU to identify HSCs. It has been postulated that HSCs may be maintained in quiescence to help reduce random mutations and hence reduce the potential to develop cancer. Furthermore, it has been suggested that in the event of asymmetric division, the daughter cell that maintains stem cell identity may asymmetrically inherit the older chromosomes from the mother cell, while the newly copied chromosomes are inherited by the differentiating cell. However, upon investigating this, Kiel *et al*. found that older chromosomes are not maintained in the daughter stem cell, and that chromosome segregation during cell division is random. Therefore, BrdU would not necessarily be retained by the HSCs (Kiel *et al*., 2007). Furthermore, they were able to show that, on average, less than 6 % of mouse CD150+ CD48- CD41- LSK HSCs retained BrdU. On the other hand, Wilson *et al*. applied a combination of BrdU labelling and histone 2B (H2B)-GFP labelling to identify a highly dormant population of HSCs which divide just 5x over the course of the mouse lifetime under homeostatic conditions. They found, by serial transplantation, that the majority of the stem cell potential resided within this dormant HSC population (Wilson *et al*., 2008). This finding is in agreement with earlier studies that have suggested that the greatest stem cell potential is maintained in quiescent cell populations of the mouse BM (Passegue *et al*., 2005). In addition, Foudi *et al*. showed that transient expression of H2B-GFP was a more specific way to label and track cell dynamics of HSCs in mice. They found that approximately 20 % of CD150+ CD48- LSK HSCs have very slow cell cycle dynamics, as measured by H2B-GFP levels.

Furthermore, they showed that those HSCs with greater H2B-GFP retention had superior long-term reconstitution potential following transplantation (Foudi *et al*., 2009).

In contrast, Takizawa *et al*. demonstrated that mouse HSCs capable of lifelong hematopoietic reconstitution reside in both fast-dividing and quiescent populations. However, the group did find that cells with greater proliferative history return to quiescence more readily (Takizawa *et al*., 2011). Interestingly, this suggests that cell cycling is dynamic throughout the HSC lifetime and, hence, cells may be capable of switching between fast cycling and quiescent states.

Limited work has been done to determine cell cycling dynamics by BrdU in adult zebrafish. In the Dallman lab at Imperial College London, work was done to label CD41:GFP ^{low} HSPCs with BrdU in both adult and larval zebrafish to carry out a chase. However, attempts to expose the fish to BrdU, either via direct injection or immersion in system-water containing BrdU, were unsuccessful and no overlap was observed between CD41:GFP ^{low} and BrdU-retaining cells (McBrien, 2017). However, it is possible that CD41:GFP ^{low} HSPCs were not labelled due to slow cell cycle dynamics. In contrast, van Rooijen *et al.* (2009) successfully caried out a BrdU incorporation assay in 7 dpf larvae following 6h immersion, revealing specific hyperproliferation in hematopoietic tissues.

1.5.4 The effect of inflammatory signalling on adult hematopoiesis

Whether an HSC enters the cell cycle and what the outcome of the division event will be, depends on the interaction between cell-intrinsic and extrinsic factors. Mouse models have been of great importance in elucidating factors involved in HSC maintenance and proliferation. For example, *Scl* (*Tal1*) is highly expressed in LT-HSCs and is responsible for maintaining HSC quiescence and inhibiting cell proliferation and differentiation (Lacombe *et al*., 2010). It has been found in both mouse and zebrafish models that *transforming growth factor beta* (*Tgfβ*) negatively regulates HSPC self-renewal and proliferation by preventing HSCs from entering the cell cycle and keeping them quiescent instead (Tamplin *et al*., 2015; Yamazaki *et al*., 2011; Wang *et al*., 2018). However, in mouse models, cycling cells were not able to re-enter quiescence and *Tgfβ* reduced the self-renewal and long-term reconstitution potential of HSCs, as demonstrated by transplantation assays (Wang *et al*., 2018). Careful

regulation of *Tgfβ* activation is required to ensure HSC maintenance within the niche (Yamazaki *et al*., 2011).

Inflammation occurs as a result of infection or injury. Mature immune cells sense the site of infection or injury by the cytokines and chemokines released at the site by resident immune cells. Resident immune cells detect infection and injury by pattern recognition receptors (PRRs) and initiate signalling cascades which ultimately result in the release of proinflammatory cytokines and chemokines. Upon arrival from the niche or circulation, mature immune cells will combat infection, resolve damage and, ultimately, inflammation. Once the cause of inflammation has been eliminated and the inflammatory response is resolved, homeostatic hematopoiesis resumes.

Injury and infection alter hematopoiesis and initiate a process known as emergency granulopoiesis, leading to a significant increase in myeloid cell output to fight infection and replenish granulocyte cells that have been exhausted over the course of infection (Takizawa, Boettcher & Manz, 2012). Depending on the type of infection, a bias pressure towards either lymphoid or myeloid cell differentiation may be placed on progenitors to repopulate a specific cell type. It is hypothesized that inflammatory cytokines and lineage-specific transcription factors are responsible for directing HSCs to differentiate in a lineage-biased way (Pinho *et al*., 2018). There are 3 proposed mechanisms by which HSCs may respond to inflammation. First, they may recognise pathogen-associated molecular patterns (PAMPS) and damage-associated molecular patterns (DAMPS) directly though PRRs such as toll-like receptors (TLRs) and nucleotide-binding oligomerization domain (NOD)-like receptors (NLRs), resulting in the activation of NFκβ and mitogen-activated protein kinase (MAPK) pathways (Burberry *et al*., 2014; Boettcher & Manz, 2017). Second, HSCs may be alerted to inflammation through recognition of inflammatory cytokines that reach the niche and alter expression profiles of other niche-resident cells such as endothelial cells or supportive stromal cells. Finally, it is possible that circulating HSCs sense inflammation directly by binding free inflammatory cytokines in the blood and then "reporting back" to niche-resident HSCs.

There is growing evidence in mouse and human studies to support the hypothesis that HSCs can detect and respond to PAMPS and DAMPS directly. Nagai *et al*. discovered the expression

of *Tlr2* and *Tlr4* on HSPCs and MPPs (Nagai *et al*., 2006). *Tlr2* senses peptidoglycan and lipoteichoic acid from gram-negative bacteria (Takeuchi *et al*., 1999), and *Tlr4* recognises bacterial lipopolysaccharide (LPS) from gram-negative bacteria (Hoshino *et al*., 1999). Takizawa *et al*. were able to show that an injection of the bacterial immunostimulant LPS increased the cell cycling dynamics of HSCs and, thereby, increased both self-renewal and proliferation capacity of HSCs (Takizawa *et al*., 2017). In addition, knockout mouse models showed that *Tlr2*, *Tlr4* and *Tlr9* agonists were capable of inducing differentiation of wild type (WT) HSCs to macrophages when transplanted into *Tlr*, *Tlr4* and *Tlr9* -/- knockout animals, suggesting direct stimulation of HSCs (Megías *et al*., 2012). Furthermore, human HSCs have also been shown to constitutively express *TLR7*, *TLR8* and *TLR4*. Unlike TLR2 and TLR4, which are found primarily on the plasma membrane, TLR7 and TLR8 are found within intracellular endosomal membranes, hence suggesting that HSCs can be infected and alter hematopoietic output as a response to the intracellular pathogens detected. Indeed, stimulation of TLR7, TLR8 and TLR2 by agonists induced HSC bias toward myeloid lineage differentiation (Sioud *et al*., 2006; De Luca *et al*., 2009).

Indirect signalling is mediated by proinflammatory cytokines such as interferons (IFNs) which have been shown to regulate hematopoiesis not only during inflammation, but also in steady-state conditions, during which they can be involved in regulating HSC maintenance (Baldridge *et al*., 2010). During steady-state conditions, the type 2 IFN γ has been shown to reduce HSC proliferation and differentiation both *in vitro* and *in vivo*. This effect is elicited by an inhibition of notch signalling and suggests increased HSC maintenance (Snoeck *et al*., 1994; Qin *et al*., 2019). However, studies in IFN γ signalling knockout mice have shown that HSCs derived from knockout animals have greater reconstitution potential relative to WT-derived HSCs. This suggests that baseline IFN γ is sufficient to diminish HSC potential (de Bruin *et al*., 2013). Furthermore, this effect appears to be exacerbated by chronic *mycobacterium avium* infection, following which HSCs exhibited significantly reduced reconstitution potential (Baldridge *et al*., 2010). De Bruin *et al*. found that IFN γ signalling did not impact cell cycle entry, differentiation or apoptosis, but rather reduced the number of self-renewal divisions that HSCs underwent. During infection, cytokine-meditated activation of HSCs has been shown to lead to impaired self-renewal capacity in favour of differentiation, particularly to the myeloid lineage (King & Goodell, 2011). HSCs can also directly respond to IFN α which promotes

proliferation. However, chronic stimulation can lead to HSC exhaustion (Essers *et al*., 2009). Similarly, extra-cellular nucleotides, which are also a signal of inflammation and cellular stress, appear to promote proliferation, migration and engraftment of HSCs (Rossi *et al*., 2007).

HSC exposure to IL6 cytokine leads to an expansion of myeloid progenitors and mature myeloid cells (Schurch *et al*., 2014; Chou *et al*., 2012). Similarly, IFNγ production by cytotoxic T cells during infection also leads to increased myeloid cell production (Schurch *et al*.,2014). In addition, Schroder *et al*. have described macrophage activation by IFNγ in an *Ehrlichia muris* infection model (Schroder *et al*., 2004). Later, McCabe *et al*. described the macrophage-dependent reduction in HSC number and function following activation by IFNγ in steady sate and during infection (McCabe *et al*., 2015). Other than cytokines released during infection to recruit hematopoietic cells, reactive oxygen species (ROS) also play a key role in managing an infection. However, ROS are not only released at the site of infection but have also been found to increase in the HSC niche in a neutrophil-dependent manner during bacterial infection. The expression levels of NADPH oxidase in neutrophils determine the resultant ROS levels in the niche, which in turn drive myeloid cell expansion (Kwak *et al*., 2017). Furthermore, increases in ROS levels as a response to sterile inflammation also led to myeloid cell expansion (Zhu *et al*., 2017; Kwak *et al*., 2017).

Granulocyte colony stimulating factor (G-CSF) is a key regulator of hematopoiesis. It has the ability to rapidly call dormant LT-HSCs into proliferation to repopulate the myeloid compartment during emergency granulopoiesis (Wilson *et al*., 2008). During an infection, neutrophils are recruited to the mouse BM and are involved in the release of G-CSF (Manz & Boettcher, 2014). In addition to initiating granulopoiesis, this leads to the suppression of the HSC chemoattractant CXCL12 in the niche, upregulation of CXCR4 on HSCs and, hence, HSC mobilisation into circulation (Schajnovits *et al*., 2011; Petit *et al*., 2002). This is in agreement with results that have demonstrated an increase in G-CSF upon bacterial and fungal infections, leading to both granulopoiesis and HSPC mobilisation into circulation (Lieschke *et al*., 1994; Schuettpelz *et al*., 2014). In addition to their role in G-CSF production in the BM, neutrophils have also been shown to coordinate the rhythmic egress of HSCs from the mouse BM (Casanova-Acebes *et al*., 2013). Together, these results indicate that HSCs do not only

sense cytokines and PAMPs within the niche, but also sample the immune environment at the site of infection. In this way, HSCs may directly respond to emergency hematopoiesis at the site of infection. The ability of HSCs to directly sense and respond to PAMPs and cytokine signalling places them among the primary responders to infection (Nagai *et al*., 2006).

While the explicit expression of TLRs on zebrafish HSPCs has not been investigated, it has been shown that embryonic knockdown of *tlr4* and *myd88* resulted in reduced HSC emergence in larvae as measured by quantification of *runx1*- and *cmyb*-expressing cells by *in situ* hybridisation. In addition, it has recently been shown in a zebrafish larvae model that *Shigella flexneri* infection induced HSPC emergency granulopoiesis to increase neutrophil output. By application of morpholinos, it was demonstrated that Gcsf production is macrophage-independent (Willis *et al*., 2018). Mouse studies have revealed that epithelial cells are a predominant source of G-CSF in response to *Escherichia coli* infection (Ingersoll *et al*., 2008). Interestingly, Willis *et al*. found that larvae that were previously infected with shigella were subsequently protected against lethal doses of shigella. This suggests that the innate immune cells present in larval zebrafish prior to the development of adaptive immunity, which occurs by approximately 3 week post fertilisation (wpf) (Page *et al*., 2013), may have immune memory. Further research would be required to gain a deeper understanding into the mechanisms regulating possible innate immune memory. It has previously been shown that stimulation of zebrafish larvae with LPS also leads to Gcsf-dependent emergency granulopoiesis (Liongue *et al*., 2009; Stachura *et al*., 2013). Taken together, these studies provide evidence that zebrafish hematopoietic cells respond to TLR stimulation by adjusting their hematopoietic output. Following infection and the resultant granulopoiesis, HSPC expansion is required to ensure the HSPC pool is maintained. The zebrafish ortholog for cytokine inducible nitric oxide synthase (iNOS) is known as *nos2a*. *nos2a* acts downstream of the transcription factor *C/ebpβ* to control both HSPC expansion in the larval CHT and granulopoiesis in a Nos2a-dependent manner, as evidenced by an increase in *runx1P2*:GFP+ cells in the CHT and an increase in lyz:dsRed+ neutrophils respectively (Hall *et al*., 2012).

Given that there have been variable results on the outcome of immune stimulation on HSCs, it is important to try and determine whether cell-intrinsic or extrinsic factors result in these conflicting outcomes. McBrien carried out transplantation studies in zebrafish to try and

uncouple the impact of cell-intrinsic and extrinsic immune factors on HSCs. In this work, HCT was carried out either with HSCs derived from donors that experienced systemic inflammatory environment from 8 consecutive intraperitoneal injections of polyinosinic:polycytidylic acid (poly I:C) 48 hours apart, or sham treated donors that did not receive the *Tlr3* and *Tlr22* agonist poly I:C. Conversely, HCT was also carried out using untreated donors into poly I:C treated recipients. The results indicated that HSPCs derived from donors with or without poly I:C treatment resulted in similar recipient survival outcome and similar cell numbers of each blood cell lineage, including *CD41*:GFP+ HSPCs. Similarly, no significant difference was seen in the survival or reconstituting cell numbers in recipient fish that did or did not experience systemic inflammation prior to HCT (McBrien, 2017). Although no significant differences were identified in these HCT experiments, it is worth noting that zebrafish populations are highly heterogeneous and may have highly variable responses to treatment. Consequently, high n numbers are required in order to provide sufficient statistical power to identify potential differences between treatment groups. This is costly both in terms of time and animal numbers. One alternative, which has helped to reduce the number of animals required and increased statistical power, has been competitive transplantation assays between treated and untreated groups using equivalent cell populations that express different fluorescent proteins (Li *et al.,* 2015). In theory, competitive HCT assays could also be done with the *Tg(Runx:mCherry)* and *Tg(Runx:GFP)* transgenic lines, which label HSPCs (Tamplin *et al*., 2015). However, the fluorescent populations in these transgenic lines are not equivalent and the *Runx:mCherry* transgene is expressed more broadly (Tamplin *et al.,* 2015). Thus, the fluorescent cell populations in these transgenic lines must be investigated further to identify equivalent HSPC populations.

1.6 Extramedullary hematopoiesis in lungs and gills

1.6.1 Mammalian extramedullary hematopoiesis in the lungs

Classically, the bone marrow (BM) and WKM have been defined as the hematopoietic organs of mammals and teleost fish respectively. However, there have been several clinical cases of patients with myeloid metaplasia presenting with extramedullary hematopoiesis (EMH), where blood formation occurs outside of the medullary spaces of the BM, in the lungs. This indicates that in a diseased state, the human lungs can contribute to blood formation (Koch *et al.,* 2003; Rumi *et al.,* 2006; Asakura & Colby, 1994; Boula *et al.,* 2005). Furthermore, early

studies investigating platelet production found that post-pulmonary blood vessels of cats had greater counts of platelets compared to pulmonary arteries, suggesting that the lung could be an important site of platelet production (Howell & Donahue, 1937). More recently, it was found in mouse studies that megakaryocytes, large platelet-producing cells, circulate in large numbers in the lung and release platelets, accounting for approximately 50 % of total platelet production (Lefrançais *et al.,* 2017). Furthermore, the authors identified immature megakaryocytes, MPPs and LSK HSCs, indistinguishable from BM LSK cells, in the extravascular spaces of the lungs. HSCs identified from the lung were capable of rescuing HSC deficiency in *c-mpl-/-* BM. Transplanted cells seeded the BM, spleen and recipient lungs. These results indicate that in mice, the lungs are both a primary site of platelet production and possess hematopoietic potential (Lefrançais *et al.,* 2017). These novel observations raise new and interesting questions such as the ontogeny of lung HSCs, whether lung hematopoiesis occurs in healthy humans, the function of lung HSCs in steady state conditions beyond platelet production, and when progenitors arrive in the mouse lung. Furthermore, these results provide exciting opportunities to further investigate the properties of HSC niches by probing at the similarities and differences between the lung and BM microenvironment.

1.6.2 Structure and function of the gills

The gills are the respiratory organs specialised for gas exchange for a large variety of aquatic species including vertebrates such as fish and amphibians, as well as invertebrates such as molluscs (Griffith, 2017). However, as the present study focused on zebrafish, this next section will describe the teleost gill specifically. The teleost gill consists of a left and a right set of arches. Each set further consists of 4 arches and a pseudobranch (Evans *et al.*, 2005). Each individual arch consists of a bony arch structure to which 2 sets of filaments are attached on one side and tooth-like 'rakers' are attached on the other. The filaments are divided into the primary lamellae, which protrude perpendicular to the arch, and several rows of secondary lamellae which protrude from both sides of the primary lamellae and are parallel to the arch. Gas exchange occurs only in the secondary lamellae (Rombough, 2007). The organisation of the filaments, much like alveoli in lungs, significantly increases the surface area to volume ratio of the gills, thereby increasing the efficiency of gas exchange at the surface. The lumen of the secondary lamellae is covered by a single-cell layer of squamous epithelial cells (Olson,

2002). This short diffusion path also ensures efficient gas exchange at the surface of the gill. The rate of diffusion is further maximised by the countercurrent flow of blood within the gills relative to the flow of water from the mouth of the fish to the secondary lamellae of the gills (Evans *et al.*, 2005). While gas exchange is an important function of the gills, they also carry out other key roles including osmoregulation, pH regulation, ionoregulation and excretion of nitrogenous waste (Evans *et al.,* 2005). This is an important distinction between the function of the mammalian respiratory system and the varied functions of teleost gills. Indeed, a number of functions carried out by the teleost gill more closely resemble the functions of the mammalian kidney.

1.6.3 Gill hematopoiesis

As described above (section 1.5.1), the hematopoietic organ in adult zebrafish is the WKM. The HSC chemoattractant cytokine *sdf1a* is not only highly expressed in the WKM but also in the skin and gills, suggesting that HSCs may be recruited to these organs as well (Glass *et al.,* 2011). In mammals, the expression of SDF1 at extramedullary sites has been associated with a range of hematopoietic migration events such as the recruitment of HSCs to injury sites (Abbott *et al.,* 2004), migration of megakaryocytes following myeloablative irradiation (Dominici *et al.,* 2009) and retention of myeloid lineage cells in tissues (Grunewald *et al.,*2006). However, the expression of SDF1 has also been associated with the recruitment of HSCs to the liver during EMH. Indeed, the expression levels of *Sdf1* in the liver were inversely proportional to BM *Sdf1* levels (Mendt & Cardier, 2015). Taken together with recent findings describing the mouse lung as a primary site for hematopoiesis (Lefrançais *et al.,* 2017), it may be interesting to investigate whether there is evolutionary conservation between the hematopoietic function of the lungs and the teleost gill. Furthermore, in bivalves such as pacific oysters (*Crassostrea gigas*), which evolved over 500 million years ago (Campbel & Reece, 2002), the major site of hematopoiesis is found in the gills (Jemaa *et al*., 2014; Li *et al.,* 2017). Indeed, hemocyte precursors and stem cell-like cells in the gill filaments were found to increase hematopoietic output upon primary and secondary immune stimulation with *Vibrio splendidus* (Zhang *et al.,* 2014; Li *et al.,* 2017). In addition, a Runx transcription factor termed *Cg*Runx was identified in *Crassostrea gigas*. This transcription factor had a conserved runt domain which possessed 63-75 % sequence similarity with human and zebrafish Runx proteins. Furthermore, *Cg*Runx was highly expressed specifically in the nuclei of hemocytes

in gill filaments (Song *et al.,* 2019). These results give evidence of the existence of gill hematopoiesis in pacific oysters, and it may be possible for hematopoietic activity to be conserved in zebrafish gills. This possibility is worth investigating further. Indeed, gaining a deeper understanding of other hematopoietic niches will help uncover the important shared factors involved in HSC maintenance across niches in different tissues and anatomical locations.

1.7 Hematopoietic stem cell transplantation

There are several inherited and acquired hematological diseases and malignancies (Table 1.3) that are treated by HCT (Gyurkocza, Rezvani & Strob, 2010), a technique that has been in the clinic since 1958. Furthermore, HCT can be used to reconstitute the hematopoietic system of cancer patients following radiation or chemotherapy. In short, the haematopoietic system is first ablated in the recipient using radiation or chemotherapy to eliminate the immune system and to create space in the marrow. Subsequently, cells from a human leukocyte antigen (HLA)-matched donor are transplanted. This enables the donor-derived cells to repopulate the HSC niche in the BM and reconstitute the recipient immune system with healthy cells. Despite the relatively common application of this procedure, the associated morbidity and mortality remain high. Therefore, given the clinical utility of HCT to treat hematological disease and aid in recovery following cancer treatment, the importance of gaining a better understanding of the factors affecting the HCT outcome is evident.

Using zebrafish to study the challenges posed by HCT offers significant advantages. For example, using optically transparent mutant *Casper* or *TraNac* fish as recipients means that transplanted fluorescent protein-expressing cells and their progeny can be visualised and tracked over time *in vivo* (White *et al*., 2008). Being able to track the localisation and behaviour of transplanted cells means that defects caused by mutant genes that lead to disease can be assessed, and therapeutic strategies tested.

Type of disease	Application of HSC transplant
Hematological malignancy	Leukaemia
	Myeloma
	Lymphoma
Non-malignant acquired blood disorder	Aplastic anaemia
Genetic /inherited blood disorders	Thalassemia
	Sickle cell anaemia
	Severe combined immune deficiency (SCID)
	Diamond Blackfan anaemia

Table 1.3 List of diseases that can be treated by hematopoietic cell transplantation in the clinic.
This table indicates groups of diseases based on malignancy and inheritability of disease.

1.7.1 Zebrafish models of hematopoietic stem cell transplantation

The gold standard for the functional identification of hematopoietic stem cells and the quantification of their purity within a population is the use of limit dilution assays. These involve transplantation of a serially-diluted population of cells (meaning that the HSC content is reduced for each subsequent transplant recipient) into preconditioned animals which have received a sublethal dose of irradiation. Theoretically, a single HSC should be able to engraft in the host niche, self-renew and reconstitute a lethally irradiated animal long term. Transplanted cells are assessed for their *stemness* by measuring the long-term survival of the recipient and whether or not multilineage reconstitution has occurred. In addition, the most rigorous test for HSCs involves the subsequent re-transplantation of HSCs isolated from the engrafted recipient into another myeloablated recipient. This enables the long-term assessment of the self-renewal and multilineage potential of the transplanted cells.

In zebrafish, HCT studies were first carried out by transplanting adult kidney marrow cells into embryos at 48 hpf. At this timepoint, the embryos have not yet developed lymphocyte populations. Cells from the adult kidney marrow expressing GFP under the *β-actin* promoter were used. *β-actin* is expressed by most cell types, including leukocytes. This meant that all donor-derived leukocytes expressed GFP, thus enabling the quantification of the

hematopoietic contribution from the donors. Furthermore, Traver *et al*. demonstrated that major blood cell lineages, namely erythrocytes, lymphocytes, myelomonocytes and precursors could be identified based on the FSC and SSC properties of the cells (Traver *et al*., 2003). Erythrocytes do not express *β-actin*:GFP. Therefore, double-transgenic *Tg(β-actin:GFP; gata1:dsRed)* donors were generated to assess the donor contribution to the erythrocyte population. Erythrocytes from these transgenic fish express dsRed under the *gata1* promoter, which is specific to red blood cells. By transplanting *gata1*-/- bloodless mutant embryos, which do not survive past 2 wpf under un-manipulated conditions, the group demonstrated long-term survival and multilineage contribution from WKM-derived donor cells (Traver *et al*., 2003).

Due to the presence of adaptative immunity, transplantation of adult kidney marrow cells into adult recipients requires a sub-lethal dose of irradiation to ablate the hematopoietic compartment, including HSPCs and immune cells. This process is known as myeloablation preconditioning. In addition to reducing competing host HSCs and eliminating immune cells, myeloablative radiation is also believed to 'make space' in the niche for donor cells to engraft. It is hypothesized that there are a limited number of fixed niche spaces (Bhattacharya *et al.,* 2006; Czechowicz *et al.,* 2007). It was shown by Tamplin *et al*. that upon the arrival of HSCs, niche cells remodel around the incoming HSCs in the zebrafish HCT (Tamplin *et al*., 2015). This suggests that niche spaces may not be fixed and may instead be limited only by the abundance of niche cells, such as stromal cells in the marrow. Interestingly, Shimoto *et al.* (2017) found that there are many more niche spaces and niche cells in the mouse bone marrow than those occupied by endogenous HSCs, suggesting that niche spaces are not as limited as previously thought. In their study, Shimoto *et al.* carried out transplantation experiments with very large numbers of purified HSCs into unconditioned mice and found that donor HSCs engrafted without replacing endogenous HSCs (Shimoto *et al.,* 2017). This novel observation led to further questions regarding the function of unoccupied niche spaces at steady state, and the factors involved in limiting the number of HSCs occupying niches in the marrow. It is currently unknown whether the same is true in zebrafish. However, observations made by Tamplin *et al.* indicate the possibility that further niche cells may be available to cuddle around HSCs in zebrafish too. On the other hand, Fraint *et al.* (2020) found that *runx1*$^{W84X/W84X}$ homozygous mutants, 80% of which are incapable of initiating definitive hematopoiesis

(discussed further in section 1.7.3), exhibited significantly improved engraftment compared to heterozygous mutants capable of generating definitive HSCs. The group postulated that this was the case as more HSC niches were available in the homozygous compared to heterozygous mutants. It would be interesting to investigate the availability of HSC niches further, for example by assessing the abundance of supportive stromal cells in the zebrafish CHT and adult WKM.

Transplantation of WKM cells into adult zebrafish is carried out by intracardiac injection to deliver the cells into circulation (Traver *et al*., 2004). Engrafted WKM donor cells home to the WKM of the recipient and rescue >70% of lethally irradiated recipients. In recipients of a WT background, donor cell contribution has classically been assessed by flow cytometry. However, in *Casper* or *TraNac* transparent mutant recipient fish, both of which have mutations in the pigment-encoding genes *mitfa* and *roy*, it has become possible to visualise engrafted cells *in vivo* (Li *et al*., 2015; White *et al*., 2008). A major benefit of using transparent mutant fish as recipients is the ability to monitor transplanted cells in the same organism longitudinally over time and to observe the progression of donor cell engraftment and reconstitution of the immune system (McBrien, 2017). Furthermore, the ability to study the progression of engraftment longitudinally within the same animal provides more informative results and reduces the number of animals subjected to transplantation when compared to a strategy of harvesting animals at each timepoint of interest. However, a detailed characterisation of the events determining the success of engraftment has not been carried out yet. Addressing this is one of the objectives of this thesis.

The characterisation of HSCs in adult zebrafish has, in part, relied on HCT assays. In humans and mammalian HCT studies, immune-matching is carried out to increase the likelihood of successful engraftment. Immune-matching involves matching donor and recipient major histocompatibility complex (MHC) haplotypes. This can lead to a greater rate of donor cell engraftment and increased recipient survival. Immune-matching decreases immunologic rejection of donor cells and reduces the likelihood of graft versus host disease (GvHD) developing. However, it is important to note that early zebrafish HCT experiments did not carry out immune-matching between donor and recipient fish. Indeed, by approximately 4 weeks post irradiation, once the recipient hematopoietic compartment recovers, donor WKM

cells are rejected by the recipient. When immune-matching is carried out, both donor cell engraftment efficiency and recipient survival increase (de Jong *et al*., 2011). However, as opposed to mammals, teleost fish MHC genes are not encoded at individual loci. Instead, teleost possess multiple MHCI and MHCII loci located on different chromosomes (Sültmann *et al*., 1994), making MHC genotypes considerably more difficult to predict. As a result, it is difficult to routinely carry out immune-matching in zebrafish as this would require inbreeding which, in zebrafish, results in inbreeding depression. Therefore, isogenic and congenic zebrafish populations are rare and difficult to maintain. One solution to overcome this is the application of techniques to generate gynogenetic diploid fish. Walker, Walsh & Moens described the application of early pressure to generate gynogenetic diploid zebrafish using UV-light inactivated sperm to fertilise egg cells. Using this procedure, gynogenetic diploid zebrafish were successfully generated and raised (Walker, Walsh & Moens, 2009). Gynogenetic diploid zebrafish have been successfully utilized to carry out transplantation of cancerous cells into unirradiated, immunologically identical recipients (Smith *et al*., 2010; Mizgireuv & Revskoy, 2006). While this represents an effective way of achieving immune-matching, generating such fish requires specialist equipment, is labour intensive and, once successfully generated, such fish are difficult to maintain.

1.7.2 Irradiation preconditioning

An alternative to immune-matching is the use of irradiation preconditioning prior to HCT. A sub- lethal dose of irradiation is capable of eliminating large populations of rapidly dividing cells, such as those of the haematopoietic system (Traver *et al*., 2004). Zebrafish lymphoid, myeloid and precursor populations are particularly radiosensitive and exhibit the most significant reduction in cell numbers 24h and 5 days post 30 grays (Gy) of irradiation (McBrien, 2017). This type of preconditioning is required for 2 main reasons. Firstly, it stops the recipient immune cells attacking the donor cells and causing rejection of the transplanted cells. Secondly, killing hematopoietic cells in their niche was hypothesized to create space in the niche for transplanted donor cells to move into and engraft (Hess *et al*., 2013). In humans, myeloablation also increases homing and engraftment of transplanted HSCs, mediated by increased CXCL12 levels in the irradiated host (Ponomaryov *et al*., 2000). However, there are also complications that accompany total body irradiation treatment. Irradiation does not discriminate between haematopoietic cells and any other rapidly dividing cell type and will

therefore result in lethal DNA damage in any rapidly dividing cell including skin cells and gut epithelial cells (Prise *et al*., 2005). In addition to the targeted effects of radiation, off-target effects can be caused by both the ROS produced by damaged cells and by the subsequent systemic inflammation that ensues. McBrien used qPCR to demonstrate a systemic increase in transcript levels of the inflammatory cytokines *il1β*, *tumor necrosis factor α (tnfα)*, *il6* and *ifnγ1.1* in zebrafish 24 hours post 30 Gy irradiation (administered in two 15 Gy doses 24 hours apart). In addition, increased transcript levels of the HSC chemo attractant *cxcl12a* were also identified in the zebrafish (McBrien, 2017).

In mice, the LT-HSCs, the most quiescent population of HSCs, are affected in a limited way by irradiation treatment which targets rapidly dividing cells. However, following irradiation, dormant HSCs are called into action to re-enter cell cycling by inflammatory cytokines such as IFNα and G-CSF (Wilson *et al*., 2008; Essers *et al*., 2009). Similar results are obtained following 5-fluorouracil (5-FU) treatment, which has been found to activate quiescent HSCs and lead to their expansion (Zhao *et al*., 2014; Itkin *et al*., 2012). Following cessation of 5-FU treatment, HSCs re-enter quiescence. This is modulated by niche cells upregulating *Cxcl4* and *Tgfβ* expression, thereby limiting "the duration of the regenerative response" (Hérault *et al*., 2017). Given the impact of inflammatory cytokines on adult hematopoiesis (see 1.5.4), the systemic inflammation following irradiation poses a clear challenge to research which aims to investigate the effect of inflammation on HSC biology following HCT.

1.7.3 Mutants of definitive hematopoiesis

Bloodless mutant fish, which have been identified following ENU mutagenesis screens, present an alternative to gynogenetic diploid zebrafish lines, immune-matching and irradiation. Soza-ried *et al*. published the characterisation of a mutant line, *cmyb*^{t25127}, which contains a single base pair missense mutation (Ile181Asn) within the highly-conserved DNA-binding domain of *cmyb*. Fish that are homozygous for this mutation (hereafter referred to as *cmyb* mutants, with WT and heterozygous clutch mates referred to collectively as non-mutant siblings) cannot initiate their definitive wave of haematopoiesis and, therefore, exhibit a complete absence of blood cells once the blood cells of the primitive hematopoietic wave are exhausted by approximately 20 dpf. In contrast to heterozygous null mutant mice, which are embryonic lethal, *cmyb* mutant zebrafish can survive a period of bloodlessness. However,

owing to the absence of an immune system and erythrocytes in the mutant line, these fish do not survive past ~14 wpf (Soza-Ried *et al*., 2010). In addition, these fish exhibit growth defects and remain stunted compared to age-matched WT fish. *cmyb* mutants also do not reach sexual maturity and, as a result, cannot be inbred. However, survival can be rescued by HCT at 6-9 wpf. As these mutants have no immune cells, they do not require myeloablative irradiation preconditioning for allogenic HCT. This is beneficial as the widespread cell death induced by irradiation results in inflammation, as discussed above. This inflammation is likely to alter the recipient niche and may also affect the transplanted donor cells. Many questions still remain regarding the effect that inflammation has on HSPC engraftment and their early post-transplant behaviour. Therefore, it is important to establish models to study HCT in the absence of inflammation.

cmyb mutant zebrafish have already been used for both allogenic and xenogeneic transplant studies. Hess *et al*. have demonstrated that allogenic transplantation of *cmyb* mutant fish results in stable multilineage long-term engraftment of donor HSCs. Using limit-dilution assays, they estimated that the adult zebrafish WKM contains one HSC in every ~38140 WKM cells, which is broadly in line with the findings of previous studies which calculated 1 in every ~65500 cells to have HSC potential when immune-matching was carried out between donors and recipients (Hess *et al*., 2013; de Jong *et al*., 2011). Furthermore, Hess *et al*. carried out serial transplantation of WKM cells from successfully reconstituted *cmyb* mutant fish into new *cmyb* mutants. They were thus able to show that the transplanted HSCs not only successfully engraft within the mutant niche, but also that the niche within the *cmyb* mutant WKM is capable of supporting and maintaining HSCs in the long term. In addition, the group did not identify symptoms of GvHD, such as flared scales (also known as dropsy), abdominal oedema or the presence of ascites, in transplant recipients (de Jong *et al*., 2011) despite significant MHCI and MHCII allelic polymorphism identified between donor and recipient (Hess *et al*., 2013). Subsequently, the group successfully carried out xenogeneic transplantation of goldfish WKM cells into *cmyb* mutant fish without myeloablative preconditioning. Stable multilineage reconstitution of definitive hematopoiesis was observed in the *cmyb* mutant fish, despite 128 million years of independent evolution between goldfish and zebrafish (Xu *et al*., 2014). Once again, serial transplantation was carried out which demonstrated the ability of the WKM of *cmyb* mutant fish to support and maintain goldfish HSCs within their niche (Hess

et al., 2016). However, the reconstitution of hematopoiesis in the WKM appeared lymphoid-biased and led to fewer myelomonocytic cells compared to WKM of WT goldfish, possibly indicating differences in niche signals received by transplanted HSCs. Furthermore, although xenogeneic transplantation of goldfish WKM was successful, in competitive transplantation assays WT zebrafish WKM cells outcompeted goldfish WKM cells (Hess *et al*., 2016). Nevertheless, the studies were able to demonstrate that *cmyb* mutant fish do not require myeloablative preconditioning prior to HCT, and that stable multilineage reconstitution is achieved in the recipient fish in the absence of GvHD symptoms.

The *runx1*$^{W84X/W84X}$ zebrafish mutant of definitive hematopoiesis was also identified from ENU mutagenesis screening (Jin *et al*., 2009). The mutation leads to truncation of the Runx1 protein whereby the Cbfβ binding domain, DNA binding domain and nuclear localisation signal (NLS) are lost, rendering the protein non-functional. Homozygosity for the *runx1*$^{W84X/W84X}$ mutation, similar to the *cmyb* mutants, renders the fish unable to initiate definitive hematopoiesis, leading to bloodless zebrafish once circulating blood cells from the primitive wave are depleted by approximately 8-12 dpf (Sood *et al*., 2010). Strikingly, however, it was found that ~20% of homozygous mutant fish survive an initial bloodless phase and reinitiate blood formation between 15-21 dpf. Unlike *Runx1* knockout mice, which are embryonic lethal, these fish can mature into fertile adults and display multilineage hematopoiesis, albeit with reduced WKM cellularity among myeloid and precursor populations. When incrossed, offspring displayed a similar ratio of survival and recovery from the bloodless phase, whereby ~80% survived only until 21 dpf and ~20% survived into adulthood, suggesting that definitive hematopoiesis can be initiated in the absence of functional *runx1* in zebrafish by alternative salvage pathways (Sood *et al*., 2010). These zebrafish make it possible to study later stages of adult hematopoiesis in the absence of *runx1*. However, their utility in transplantation studies is limited to transplants in embryos because the bloodless fish which do not recover were found to die during larval/ juvenile stages, and those which survive initiate endogenous blood formation. Recently, Fraint *et al. (*2020) demonstrated the utility of *runx1*$^{W84X/W84}$ mutants for transplantation studies in the absence of myeloablative pre-conditioning in 2 dpf embryos. Using this system, the group showed that transplantation into homozygous mutants led to significantly improved engraftment compared to heterozygous mutants capable of generating their own definitive HSCs. This

indicated that recipients with empty HSC niches exhibited a greater extent of donor HSC engraftment. However, at 2 dpf, the homozygous mutant fish that will remain bloodless cannot be distinguished from the 20% which will recover, because at this stage all of the fish still possess primitive hematopoietic cells. In addition, the 20% of *runx1*$^{W84X/W84X}$ mutants that exhibit the rescue phenotype would present with chimerism. This limits the utility of this model to study the behaviour of donor cells in the absence of host cells. Indeed, Fraint *et al.* defined engraftment at ≥5% donor-derived myeloid chimerism and found that 2 months after transplantation, 59% of surviving fish were engrafted (Fraint *et al.,* 2020).

Finally, a recent development in zebrafish HCT studies has been the generation of *forkhead box N1 (foxn1)/Casper* mutant zebrafish (Lv *et al.,* 2020). These mutant fish are both transparent, enabling *in vivo* visualisation of transplanted cells, and have a T cell deficiency. As these fish are capable of generating definitive HSCs, donor cell must outcompete the endogenous HSCs that occupy the WKM niche. However, due to their T cell immunodeficiency, these adult zebrafish do not require irradiation preconditioning prior to allogenic and xenogeneic transplantation of normal or malignant cells. Using this model, the authors demonstrated that nonconditioned *foxn1*/*Casper* mutants exhibited a similar extent of engraftment as irradiated *Casper* fish in erythroid, myeloid and precursor lineages. However, engraftment of lymphoid cells was limited, possibly due to the thymus defect caused by the *foxn1* mutation. Furthermore, the authors compared the engraftment capabilities of *CD41*:GFP ^{low} HSPCs, isolated from adult and embryo donors, in adult *foxn1*/*Casper* recipients. These experiments showed that transplanted embryonic *CD41*:GFP ^{low} HSPCs led to both more successful long-term engraftment and greater expansion of progeny at 90 dpt, consistent with previous findings in mice (Arora *et al.,* 2014; Bowie *et al.,* 2007). This new mutant line presents a valuable tool for the study of normal and malignant hematopoiesis through transplantation and subsequent *in vivo* imaging of transplanted cells.

1.8 Remaining questions and aims of this thesis

HSCs are vitally important cells that maintain hematopoiesis throughout vertebrate life. Each single HSC has the ability to be serially transplanted and continue to sustain hematopoiesis even past the life span of the donor organism. Their ability to do so has meant that HSCs have significant clinical applications in the treatment of hematological diseases, autoimmune

disorders and to reinstate healthy hematopoiesis following cancer treatment. Although HCT has been studied for many years, there remain a number of unanswered questions that are important to our understanding of HCT and to develop ways of improving recipient outcomes. Zebrafish provide a new and unique opportunity to study transplanted donor cells in the live recipient by minimally invasive imaging techniques and without the need for surgery, owing to the optical transparency of juvenile transparent mutant fish. This has opened up the field to study previously difficult to observe cell behaviours, such as the initial homing location of transplanted cells, the reaction of niche cells to the arrival of donor cells, as well elucidating potential differences between the zebrafish embryonic CHT and the adult WKM niche, and the effect of immune stimulation on HCT outcome. In addition, there may be potential to utilise early post-transplant imaging data to predict long-term HCT outcomes.

While significant progress has been made in understanding the ontogeny of HSCs in embryonic zebrafish and the factors governing their emergence, maintenance and proliferation, little is currently known about the niche and the factors required for self-renewal and maintenance of HSCs in the adult zebrafish WKM. Furthermore, the HSCs and their niche in the adult WKM are yet to be fully characterised. This can in part be attributed to difficulties in reliably isolating and visualising a pure population of HSCs from the WKM. Hence, one of the aims of this thesis is to further characterise the cells expressing fluorescent proteins in the recent *Tg(Runx:mCherry)* and *Tg(Runx:GFP)* transgenic lines (Tamplin *et al*., 2015) and assess whether they could be used for subsequent competitive repopulation assays. Furthermore, this thesis aims to gain a deeper insight into the responses that fluorescent protein-expressing *Runx*+ cells can elicit in response to immune stresses such as viral mimetics and antibiotic treatment.

Another key aim of this thesis is to assess the effectiveness of the HCT model using bloodless *cmyb* mutant fish and assay *Tg(Runx:mCherry)* fluorescent HSPCs. In addition to the application of these bloodless mutant fish for HCT assays, the immunological and regenerative capabilities of these fish will also be investigated in order to better understand the recipient environment.

Finally, this thesis aims to refine the HCT procedure by carrying out longitudinal live *in vivo* imaging of recipients to assess whether there are early post-transplant predictors of engraftment and long-term survival. By doing so, this thesis aims to significantly reduce the use of survival as a readout for HCT success or failure by instead humanely killing animals which are not predicted to have engrafted and, therefore, are unlikely to survive long term. This could reduce the severity of the HCT procedure in zebrafish from severe to mild and make a contribution to the replacement, reduction, and refinement of animal use for experimental purposes (Guidance on the Operation of the Animals (Scientific Procedures) Act 1986).

In summary, the aims of this thesis are to:

- Further characterise fluorescent cell populations in *Tg(Runx:mCherry)* and *Tg(Runx:GFP)* transgenic lines.
- Assess the response of *Runx*+ cells to antibiotics and immune stimuli.
- Investigate whether *cmyb* mutant zebrafish are capable of regeneration or mounting an immune response.
- Determine early predictors of long-term survival and reconstitution in *cmyb* mutant zebrafish following HCT.

Chapter 2

Materials and Methods

Chapter 2 | Materials and Methods

2.1 Zebrafish maintenance

Wild Type, mutant and transgenic zebrafish strains used in this study (summarised in Table 2.1) were bred and maintained according to standard practices and all procedures conformed to the UK Home Office requirements (ASPA 1986) under the project licence P5D71E9B0 and personal licence I48C3E7BB. Zebrafish life stages were classified as seen in Table 2.2. The transgenic *Tg(IgM:GFP)* line was kindly provided by Dr Adam Hurlstone (University of Manchester) and the *Tg(Runx:mCherry)* and *Tg(Runx:GFP)* lines were provided to the Dallman lab by Dr Owen Tamplin (University of Illinois at Chicago).

In all experiments with adult zebrafish, 3-18 months post fertilisation (mpf) fish were used unless otherwise stated. Both male and female zebrafish were used in equal numbers where possible and breeding stocks allowed. In experiments using *cmyb* mutants, 5-8 wpf fish were used. Due to age and growth retardation, gender could not be determined for these fish. Following all experimental procedures and treatment regimens, fish were maintained in static tanks at 28.5 °C with their water replaced daily. *cmyb* mutant fish received 200 mL fresh E2 medium daily and tanks were cleaned weekly. Fish were monitored twice daily for breathing, feeding and swimming behaviour to check for any signs of ill health.

Name of Line	Advantage	Reference
Wild Type (WT)	No genetic modifications	
Mutants	**Advantage**	**Reference**
tra$^{-/-}$*nacre*$^{-/-}$	Lack pigment producing iridophores and melanocytes due to mutations in *mpv17* and *mitfa* genes making them optically translucent.	(Kraus *et al*., 2013; Wenz *et al*., 2020; White *et al*., 2008)
cmyb $^{-/-}$	Immune deficient fish. Do not require irradiation to ablate HSPCs prior to transplant	(Soza-Ried *et al*., 2010; Hess *et al*., 2013)
Transgenics	**Cells expressing the transgene**	**Reference**
Tg(Runx:mCherry)	Hematopoietic stem and precursor cells	(Tamplin *et al*., 2015)
Tg(Runx:GFP)	Hematopoietic stem and precursor cells	(Tamplin *et al*., 2015)
Tg(lyz:GFP)	Myeloid cells. Predominantly neutrophils	(Hall *et al*., 2007; Wittamer *et al*., 2011)
Tg(lyzC:dsRed)	Myeloid cells. Predominantly neutrophils	(Hall *et al*., 2007; Wittamer *et al*., 2011)
Tg(mpx:GFP)	Predominantly neutrophils	(Renshaw *et al*., 2006)
Tg(mpeg1.1:Caspase1biosensor) *Referred to as Tg(mpeg1.1:SECFP-YPet) in this thesis*	Predominantly macrophages	(Andrews, 2016; Ramel, personal communication)
Tg(ubi:GFP)	Ubiquitous GFP expression	Mosimann *et al*., 2011
Tg(CD41:GFP)	Hematopoietic stem and precursors cells (GFP low) and Thrombocytes (GFP high)	Lin *et al*., 2005
Tg(lck:GFP)	T and NK lymphocytes	(Langenau & Zon, 2005)
Tg(IgM:GFP)	IgM expressing B lymphocytes	(Page *et al*., 2013)

Table 2.1 Overview of zebrafish lines used in this study.

Developmental stage	Age
Embryo	0 - 5 days post fertilisation
Larvae	6 - 30 days post fertilisation
Juvenile	1 - 2 months post fertilisation
Adult	2 + months post fertilisation

Table 2.2 Classification of zebrafish life stages at different ages.

Embryos obtained from individual crosses or tank crosses were initially reared at a density of 50 embryos per petri dish in 50 mL system water containing 0.3 ppm methylene blue (M9140; Sigma-Aldrich), which was changed daily. Embryos were cleaned daily to remove unfertilised eggs and chorions of hatched fish. At 6 dpf, 50 larvae were transferred into 3-litre tanks with standard E2 embryo growth medium (15 mM sodium chloride [S7653; Sigma-Aldrich], 0.5 mM potassium chloride [P9333; Sigma-Aldrich], 1 mM magnesium sulfate [M7506; Sigma-Aldrich], 150 µM potassium phosphate monobasic [P5655; Sigma-Aldrich], 50 µM sodium phosphate dibasic [S7907; Sigma], 1 mM calcium chloride [C5670; Sigma-Aldrich], 0.7 mM sodium bicarbonate [S6297; Sigma-Aldrich] and 10 U/mL penicillin/ streptomycin [15070-063; Life Technologies]). 200 mL of E2 medium was added daily until 14 dpf, at which stage WT and transgenic larvae were transferred onto the aquarium system supplied with a combination of dechlorinated tap water and reverse osmosis water at a ratio of 1:5. *cmyb* mutant fish were maintained in static tanks on the bench, receiving 200 mL E2 daily and tanks cleaned weekly. Fish were reared and maintained at 28.5℃ on a 14 hours light and 10 hours dark cycle and fed twice a day using a combination of brine shrimp *Artemia* and dry food. Larvae were fed standard zebrafish larval food (ZM; ZM system). At 6-8 dpf larvae received ZM000, 9-14 dpf ZM100 and juveniles from 15 dpf to 2 mpf received ZM200 twice daily. Adults were fed dry food (Hikari Tropical Micro Pellets; Hikari). Due to their small size, *cmyb* mutant fish were not fed adult dry food but were instead maintained on ZM200.

2.2 Genotyping

2.2.1 Obtaining genomic DNA from tail fin amputation

To collect tissue for genotyping and/or investigate tail fin regeneration, animals were anaesthetised with 170 mg/L tricaine (MS222; E10521; Sigma-Aldrich) and a caudal fin amputation was performed with a sterile scalpel. Adult fish were recovered in system water,

while *cmyb* mutants and juvenile fish were recovered in E2 medium and kept off flow until genotyping was complete. *cmyb* mutants used for tail fin regeneration studies were kept in static tanks with E2 medium.

Genomic DNA was prepared from tail fin tissue using "TaqMan sample to SNP" kit (Applied Biosystems) as per manufacturer's instructions with minor adjustments: tissue was added to 10 µL lysis solution, boiled at 95˚C for 10 minutes followed by cooling to 4 ˚C. Next, 10 µL stabilising solution was added and mixed by pipetting up and down.

2.2.2 Identification of cmyb ^{t25127} mutant fish

cmyb breeding stocks are heterozygous mutants. Therefore, each generation must be genotyped for heterozygous fish. Homozygous mutants were not genotyped until after an experiment. Polymerase chain reactions (PCRs) to identify heterozygous and homozygous fish were set up using 1 µL of genomic DNA (obtained as described above), 10 µL 2X Taq PCR master mix (Qiagen), 1 µL of each primer (10 mM; Fwd (5'-TTTGGAAGAACTTGAGGGT-3') and Rev (5'-AGTGGAAATGGCACCTGAA-3')) and 7 µL PCR grade water. The samples were run in a thermal cycler (Applied Biosystems) on the following program: 94 °C for 4 minutes, 40 repeats of (94 °C for 30 s, 54°C for 30 s, 72°C for 1 minutes), finally 72°C for 5 minutes. Next, the products were purified using the QIAquick PCR clean-up kit (Qiagen) according to manufacturer's instructions. Samples were eluted in nuclease-free water. Then, 5 µL of each sample were loaded with 1 µL purple gel loading dye (B7025S; New England BioLabs) and run on a 1.5% agarose TBE gel to confirm the presence of product. This did not distinguish mutants from non-mutants.

The *cmyb*^{t25127} mutation can be detected on a 2.5% agarose TBE gel, following a 2-hour incubation in a 37 ˚C water bath of 25 µL PCR product, 3 µL 10X buffer and 0.5 µL Hpy188iii restriction enzyme (New England BioLabs). The resulting samples were loaded onto a 2.5% agarose gel with ethidium bromide (1:1000) using 6 µL orange loading dye (New England BioLabs). The samples were run at 65 V for 35 minutes. Enzyme digestion of the PCR products resulted in 2 bands for homozygotes (184 & 260 bp), 4 bands for heterozygotes (114, 146, 184 & 260 bp) and finally 3 bands for WT fish (114, 146 & 184 bp, Table 2.3).

Genotype	Band length			
	114	146	184	260
WT	✔	✔	✔	
Heterozygote	✔	✔	✔	✔
Homozygote			✔	✔

Table 2.3 Bands when genotyping *cmyb* mutants by PCR and restriction digest.

2.2.3 Identification of transgenic Runx fish by genotyping

Fish were reared and maintained as described above. During the juvenile stage, genomic DNA was obtained from tail fin tissue as described above. To identify the transgene, initially PCRs were carried out using 1 µL genomic DNA with 10 µL 2X Taq PCR Master mix (Qiagen), 1 µL of each primer (10 mM; Fwd (5'-ACTGATAACGTGGGCAGCTT-3')) and Rev (5'-GCTCTGCACTGCACTAAGGA-3') and 7 µL of PCR grade water. The samples were run in a thermal cycler (Applied Biosystems) program: 94 ˚C for 5 minutes, 35 repeats of (94 ˚C for 30 s, 60 ˚C for 1 minutes, 72 ˚C for 30 s), finally 72 ˚C for 7 minutes. The resulting amplicons were mixed with 4 µL purple loading dye (New England Biolabs) and run on 1% agarose gel with ethidium bromide (1:1000) at 65 V for 35 minutes. The primer sequences are specific for the mouse genome-derived P1 enhancer sequence of *Runx1*. Therefore, only DNA derived from *Tg(Runx:GFP)* and *Tg(Runx:mCherry)* fish (Tamplin *et al*., 2015) contains the target sequence. This method could only determine the presence or absence of the enhancer sequence; it could not distinguish between hetero- or homozygosity.

2.2.4 Identification of transgenic Runx fish by screening

As increasingly powerful microscopes became available in the lab, live *in vivo* fluorescence microscopy was used to identify the transgene. Embryos at 4 dpf were anaesthetised using 200 mg/L tricaine (MS222; E10521; Sigma-Aldrich) and placed on the lid of a 48-well plate in individual droplets of water. Using the Leica M205 FCA stereomicroscope and Leica EL6000 external light source for fluorescence excitation, fluorescent protein-expressing hematopoietic cells were screened for in the CHT of embryonic fish. The filters used were the Leica ET mCherry (Article Number: 10450195; Excitation nm: ET560/40x; Emission nm: ET630/75m), as well as the ET GFP (Article Number: 10447408; Excitation nm: ET470/40x; Emission nm: ET525/50m).

This is a refined method to identify transgenic fish as no procedure has to be carried out for identification after 5 dpf. This method allows for identification of heterozygous and homozygous fish, as homozygous fish express more fluorescent protein and their cells are brighter.

2.3 Tissue harvest

2.3.1 Schedule 1 euthanasia of zebrafish

Fish were culled using anaesthetic overdose by placing into system water containing 400 mg/L tricaine (MS222; E10521; Sigma Aldrich). Following loss of operculum movement, secondary confirmation was carried out by destruction of the brain.

2.3.2 Whole kidney marrow

The whole kidney marrow (WKM) was dissected as described by Gerlach *et al*. (2011). In short, following decapitation, the thorax was opened ventrally and the intraperitoneal organs were removed. Using fine forceps, the kidney was gently rolled away from the dorsal wall, starting from the head kidney, and collected. The dorsal aorta, which runs directly adjacent to the kidney, cannot be separated from the kidney and was included in kidney samples, making it WKM.

2.3.3 Gut tissue harvest

To dissect the gut tissue, the thorax was opened ventrally following decapitation, giving access to internal organs, which were then removed. The gut was separated from other internal organs and stretched out to isolate distal and proximal portions where necessary.

2.3.4 Gill tissue harvest

To collect gill tissue, fish were euthanized as described above, followed by removal of the operculum from one or both sides to expose the gill tissue. Next, the required number of gill arches were detached and resected from the gill cavity using fine forceps. Coagulated blood adherent to the gills and other non-gill tissue was removed.

2.3.5 Peripheral blood harvest

Following euthanasia by anaesthetic overdose (described above), the skin around the heart was removed and the heart was punctured using a 10 µL pipette tip filled with 0.9X phosphate-buffered saline (PBS) at room temperature. As the heart was punctured, the PBS was dispensed into the heart cavity. Subsequently, peripheral blood was gently aspirated from the heart while massaging the body of the fish. Harvested blood was dispensed into 1 mL of 0.9X PBS. Coagulated blood was filtered and removed using a 40 µM cell strainer (Falcon). Where required, the concentration of blood cells was determined using a haemocytometer (x 10^4 cells/ mL).

2.4 Flow cytometry analysis for hematopoietic cell populations

Flow cytometry was carried out on single cell suspensions in 0.9X PBS and 2% foetal calf serum (FCS), using 4 or 5 laser BD LSR Fortessa analyser (BD Biosciences) in the Department of Life Sciences Flow Cytometry Facility (Imperial College London). A minimum of 20,000 cells were acquired from any given tissue. Data was analysed using FlowJo™ software (Becton, Dickinson & Company). Where indicated, cell viability was assessed by resuspension of cells in 0.9X PBS with 1 µg/mL 4',6-diamino-2-phenylindole dihydrochloride (DAPI; D9542; Sigma Aldrich) 3 minutes before flow cytometry analysis. Gating for hematopoietic cells was based on the WKM-gating strategy from Traver *et al*. (2003). This gating was also used to identify hematopoietic cells in other tissues.

Fluorescence activated cell sorting (FACS) was carried out on a FACS Aria (BD Biosciences) cell sorter by Dr Jane Srivastava or Dr Jessica Rowley in the Department of Life Sciences Flow Cytometry Facility (Imperial College London).

2.4.1 Whole kidney marrow tissue preparation

WKM was dissected as described above. Singe cell suspensions were created by massaging the kidney tissue through 40 µM cell strainer into 0.9X PBS supplemented with 2-5% FSC, using the rubber tip of a 1 mL syringe plunger.

2.4.2 Gill tissue preparation

Whole gill tissue was dissected as described above and placed into 1X PBS on ice. Next, PBS was aspirated, and 2-4 gill arches were placed into 100 µL PBS with 2 mg/mL collagenase P (Roche) and incubated at 37 ˚C for 10 minutes. After 5 and 10 minutes, the tissue was pipetted up and down to aid dissociation of gill tissue. Cells were centrifuged at 1000 rcf for 4 minutes at 4 ˚C and the resultant supernatant removed. The samples was resuspended in 100 µL PBS and, with the remaining tissue, gently massaged through a 40 µM cell strainer into 250 µL 0.9X PBS supplemented with 2-5% FCS using the rubber tip of a 1 mL syringe plunger.

2.4.3 Peripheral blood

Whole blood was collected as described above. The samples were strained to remove coagulated blood. The single cell suspensions were subjected to flow cytometry analysis or FACS directly.

2.5 Whole mount immunostaining of zebrafish tissues

2.5.1 Fixation of gill

Following euthanasia and dissection of tissues as described above, whole gill arches were submerged and fixed in 4% paraformaldehyde (PFA; 18814; Polysciences Inc) overnight at 4 ˚C.

2.5.2 Staining for RFP, GFP and Draq5

Following fixation in PFA overnight, tissues are washed twice in PBS and stored in PBS for no longer than 1 month at 4 ˚C before being stained. All of the following steps were carried out in 1.5 mL or 2 mL microcentrifuge tubes. Tissues were washed twice for 1 minute in deionised water (dH_2O), transferred to ice-cold acetone (Sigma Aldrich) for 10 minutes at -20 ˚C, rinsed with dH_2O twice, washed twice for 20 minutes in PBST (PBS, 0.05% Triton X-100, 0.05% Tween-20 (P1379; Sigma Aldrich)), then incubated in blocking buffer (PBST, 1% DMSO (D2650; Sigma Aldrich) with 5% donkey serum (D9663; Sigma Aldrich) and 5% goat serum for 30 minutes. Next, samples were incubated in blocking buffer with polyclonal chicken anti-GFP (1:1000, Abcam; ab13970) and/ or polyclonal rabbit anti-RFP (1:1000, MBL; PM005) overnight at 4 ˚C, washed 4 times in PBST for 20 minutes and incubated in blocking buffer

containing polyclonal donkey anti-chicken-AF488 (1:250, Jackson Immuno-Research; 703-545-155) and/or polyclonal goat anti-rabbit-AF555 (1:300, ThermoFisher Scientific; A-32737) for 4 hours at RT and washed 4 times in PBST for 20 minutes (Table 2.4). Finally, tissues were stored in PBST until they were imaged. When nuclear staining was carried out, DRAQ5 (1:1000, ThermoFisher Scientific) was used as per manufacturer's instructions, then rinsed in PBST on the same day as imaging was carried out.

Antibody	*Species*	*Dilution*	*Transgenic Targets*	*Source*
Primary antibodies				
Anti-RFP	Rabbit	1:1000	*Runx:mCherry*	MBL (PM005)
Anti-GFP	Chicken	1:1000	*lck:GFP, lyz:GFP, CD41:GFP IgM:GFP, Runx:GFP*	Abcam (ab13970)
Secondary antibodies				
Anti-rabbit AF555	Goat	1:300		ThermoFisher Scientific (A-32737)
Anti-Chicken AF488	Donkey	1:250		Jackson ImmunoResearch (703-545-155)

Table 2.4 List of antibodies use for whole mount immunostaining of zebrafish tissues

2.6 Imaging

All confocal and widefield imaging was carried out in the Facility for Imaging by Light Microscopy (Faculty of Medicine, Imperial College London).

2.6.1 Stereomicroscopy

Routine handling, screening and imaging of zebrafish larvae and adults was carried out on a Leica M205 FCA stereomicroscope fitted with a Leica DFC7000 T camera and Leica EL6000 external light source for fluorescence excitation controlled by the Leica LAS X software. The filters used were the ET GFP (Article Number: 10447408; Excitation nm: ET470/40x; Emission nm: ET525/50m) and ET mCherry (Article Number: 10450195; Excitation nm: ET560/40x; Emission nm: ET630/75m).

2.6.2 Widefield microscopy

Directly before imaging, individual fish were anaesthetised with 170 mg/L tricaine (MS222; E10521; Sigma-Aldrich) and gently placed on a 35 mm glass-bottomed dish (Ibidi, µ-Dish 35 mm, high Glass Bottom; 81158) with a small anaesthetic droplet around them to ensure they did not dry out. All fish were fully recovered no later than 11 minutes after placing into anaesthetic solution.

Live *in vivo* imaging of recipient fish was carried out on a widefield Zeiss Axiovert 200M inverted microscope fitted with a Hamamatsu Flash 4 camera, pE4000 coolLED system light source and the following Zeiss filter cubes: GFP (excitation 470/40, emission 525/50) and mCherry (excitation 562/40, emission 624/40). The microscope was controlled by Velocity software, which was later replaced by ZEN blue pro software. Data was collected using 10X (EC Plan-Neofluar 10X 0.30 Ph1) and 20X (LD Plan-Neofluar 20X 0.40 KORR) objectives.

2.6.3 Confocal microscopy

Fixed and stained gill tissues were placed on a 35 mm glass-bottomed dish (Ibidi, µ-Dish 35 mm, high Glass Bottom; 81158) and covered in a small droplet of PBST to prevent them from drying out. Image acquisition of immunoassayed gill tissue to visualise tissue structure and labelled cells was carried out on a Leica SP5 inverted confocal microscope controlled by Leica Application Suite software. Images were acquired on 5X (PL FLUOTAR 5X 0.12), 10X and 20X (HC PL APO 20X 0.70 CS) objectives as indicated.

2.6.4 Image analysis

All image processing and quantification was carried out using FIJI software (Schindelin *et al.*,2012; Rueden *et al.*, 2017) or Icy software (de Chaumont *et al.*, 2012).

To analyse the abundance of cells in recipients post-transplant or for characterisation studies, FIJI software was used. Cell tracking was carried out using TrackMate FIJI plugin (Tinevez *et al.,* 2017). The brightness and contrast of each channel were adjusted for each image to ensure both bright and dim cells were included in the analysis. To determine the post-transplant score of cells in circulation, videos were used as this made it possible to view highly motile cells that could not be detected in individual images.

Detection and quantitative analysis of *lyz*:GFP+ cell in the gills following R848 treatment was performed with Icy software. First, maximum projections were generated from z-stacks of gills, then regions of interest were defined manually to select the first 20 secondary lamellae of each arch (including equivalent region of primary lamellae). Cells within this region were detected and quantitatively analysed using the spot detector plugin (Olivo-Marin, 2002). Secondary gill lamellae that were significantly damaged or obstructed were excluded from analysis.

2.7 Antibiotic treatment

2.7.1 Short-term penicillin and streptomycin treatment of adult fish

Six *Tg(Runx:mCherry; lyz:GFP)* females per group were randomly selected and distributed to treatment and non-treatment tanks. The fish were placed in 3 L capacity system tanks filled with 2 L of system water per group. From each tank, 200 mL system water was removed per day followed by addition of 200 mL fresh system water +/- penicillin (10 U/mL) streptomycin (10 µg/mL) (PS) (15070-063; Life Technologies), to mimic a 10% exchange for a period of 14 days.

2.7.2 Long-term penicillin and streptomycin treatment of juvenile fish

Penicillin (10 U/mL) streptomycin (10 µg/mL) (PS) (15070-063; Life Technologies) was administered on a daily basis to larval zebrafish from 6 dpf for 7 weeks. Ten larval fish per group were kept in 1L tanks and administered 200 mL E2 +/- PS per day until tanks filled. Tanks were replaced once a week. E2 medium was prepared with 15 mM sodium chloride (S7653; Sigma-Aldrich), 0.5 mM potassium chloride (P9333 Sigma-Aldrich), 150 µM potassium phosphate monobasic (P5655; Sigma-Aldrich), 1 mM magnesium sulfate (M7506, Sigma-Aldrich), 50 µM sodium phosphate dibasic (S7907; Sigma-Aldrich), 1 mM calcium chloride (C5670; Sigma-Aldrich), 0.7 mM sodium bicarbonate (S6297; Sigma- Aldrich) and 10 U/mL penicillin streptomycin (15070-063; Life Technologies).

2.7.3 Oxytetracycline treatment of adult fish

Six adult *Tg(Runx:mCherry; lyz:GFP)* fish were randomly selected and placed in 1 L capacity tanks filled with system water +/- 50 mg oxytetracycline (OTC; Sigma-Aldrich). OTC was

dissolved on day of use. The water in each tank and OTC were replaced daily. Treatment continued for 10 days.

2.8 Immunostimulant challenges

2.8.1 Poly:IC treatment

Fish treated with poly I:C were anaesthetised with 170 mg/L tricaine (MS222; E10521; Sigma Aldrich) and received a single intra-peritoneal (IP) injection with a gauge 30 Hamilton syringe of 2 µL containing 10 µg poly I:C (P1530; Sigma Aldrich).

2.8.2 Immersion of cmyb mutant fish in R848

Between 1 and 8 *cmyb* mutant fish aged 5-7 wpf were placed into a single well of a 24-well plate with 1 mL of E2 medium. Subsequently, the medium was aspirated and replaced with 500 µL E2 containing 0.5 mg/mL R848 (tlr-r848-r; InvivoGen). The fish were challenged by immersion for 10 minutes. Next, the R848 medium was aspirated and replaced with fresh E2, and the fish were transferred into a small tank with 200 mL E2 medium for 1-8 hours according to the experimental timepoint.

2.8.3 Gill application of R848 on transgenic fish

R848 was dissolved in endotoxin-free water at a concentration of 0.5 mg/mL. Adult zebrafish were anaesthetised in 168 mg/mL tricaine (MS222; E10521; Sigma Aldrich) and placed laterally on a Petri dish. The operculum and gills were dried with tissue prior to application of 5 µL of 0.5 mg/mL R848 (tlr-r848-r; InvivoGen). Following treatment, fish were recovered from anaesthesia in aquarium system water.

2.9 Hematopoietic cell transplantation

2.9.1 Donor cell sorting

Donor WKM or gills were harvested and prepared for FACS as described above (see section 2.3 & 2.4). The resulting cells were resuspended in 0.9X PBS and 5% FCS, creating a single cell suspension. Cells were sorted at 2000 events/ s on BD FACSAria III by Dr Jane Srivastava or Dr Jessica Rowley in the Department of Life Sciences Flow Cytometry Facility (Imperial College London) to obtain the population of interest. Sorted cells were gated to exclude debris (using

FSC/SSC, both of which use 488 nm laser and 480/10 filter). Cells were then split based on their fluorescent reporter and fluorescence intensity for either GFP (488 nm laser, 490/20 filter) or mCherry (561 nm laser, 480/10 filter). The cells were sorted into 200 µL of 5% FCS 0.9 X PBS at 4 ˚C.

2.9.2 Donor cell preparation

The concentration of sorted cells was determined using a haemocytometer (x10^4 cells/ mL) following centrifugation at 1000 rpm for 4 minutes and resuspension of cells in 150 µL 0.9X PBS 2% FCS.

Carrier cells were obtained from WT or TraNac fish following anaesthetic overdose using 400 mg/L tricaine (MS222; E10521; Sigma Aldrich). Following cessation of operculum movement, the skin around the heart was removed with fine forceps and the exposed heart was punctured using a 10 µL pipette tip containing 1X PBS. As the heart was punctured, the PBS was simultaneously dispensed. Next, the blood was slowly aspirated from the heart cavity while massaging the fish. The aspirated blood was dispensed into 1 mL of room temperature 1X PBS and immediately pipetted up and down to stop the blood from coagulating. The concentration of peripheral blood cells was determined using a haemocytometer (x10^4 cells /mL).

Next, 2000 sorted donor cells were mixed with 10^5 peripheral blood cells, centrifuged at 1000 rpm for 10 minutes at 4 ˚C and resuspended in 1 µL.

2.9.3 Retroorbital injection of cmyb mutant fish with donor cells

All transplants were carried out by retro-orbital (RO) injection as originally described by Pugach *et al*. (2009), with modification as described by McBrien (2017). In short, transparent *cmyb* mutant recipients (*cmyb*$^{-/-}$, *tra*$^{-/-}$ *nacre*$^{-/-}$) were anaesthetised with 168 mg/mL tricaine (MS222; E10521; Sigma Aldrich) and placed laterally on an anaesthetic-soaked sponge. Glass pulled needles were cut to size and used to carry out injections. Needles were mounted on a micromanipulator and connected to an IM 300 micro-injector (Narishige, Japan). Needles were inserted at a 45˚ angle between the eye and the socket and situated near the heart. Fish were injected with a 1 µL suspension of 2000 *Runx*+ cells and 10^5 peripheral blood carrier cells

unless otherwise stated. Post-transplant, fish were recovered from anaesthesia in fresh E2 medium in individual small tanks.

2.9.4 Post- transplant care

Following transplant recovery, individual recipient *cmyb* mutant fish were maintained in separate static tanks with E2. Each recipient fish was housed socially with 3 WT companion fish of the same size (2 to 3 weeks younger). WT fish could be distinguished from recipient fish by eye due to the presence of pigment-producing melanophores in WT fish. Due to growth retardation of recipient fish, the companion fish were kept size matched to recipients for the duration of the experiments. 200 mL E2 medium was added to tanks daily and tanks were cleaned on a weekly basis to remove food debris and waste. All fish were monitored for adverse signs of health twice daily and those exhibiting adverse effects such as lack of motility, gasping for air, oedema or difficulty to stay balanced, were humanely culled with anaesthetic overdose (400 mg/L tricaine; MS222; E10521; Sigma Aldrich). Survival data of these fish was recorded and included in the survival analysis. Recipients were subjected to imaging to develop a post-transplant tracking system at 3, 6, 8, 10, 15, 22 and 29 days post-transplant (dpt). Widefield microscopy was carried out as described above (see section 2.6).

2.10 Measuring gene transcript levels by qRT-PCR

2.10.1 mRNA extraction from whole tissue

Zebrafish tissues were homogenized in 200 µl of TRIzol (15596026; ThermoFisher Scientific) using a pellet pestle cordless motor (Sigma Aldrich). Total RNA was extracted using the PureLink™ RNA Micro Kit (12183016; ThermoFisher Scientific) with DNAse treatment according to the manufacturer's protocol. Quality and concentration of RNA were measured using a Nanodrop 1000 or NanoDrop One spectrophotometer (ThermoFisher Scientific).

2.10.2 mRNA extraction from sorted cells

50,000 cells (250 µL) of interest were FACS sorted directly into 750 µL TRIzol™ LS reagent (10296028; ThermoFisher Scientific) and maintained at 4 ˚C. To homogenize cells, samples were pipetted up and down directly after collection. Samples were transferred to 2 mL phase lock gel heavy tubes for subsequent RNA isolation steps. Phenol chloroform total RNA

isolation was carried out according to manufacturer's instructions. Next, RNA samples were cleaned using RNA Clean & Concentrator™ -5 kit and treated with DNase (R1014; Zymo Research). Quality and concentration of RNA were measured using a Nanodrop 1000 or NanoDrop One spectrophotometer (ThermoFisher Scientific).

2.10.3 cDNA synthesis

For transcripts analysis, 125ng RNA were used per sample to synthesise complementary DNA (cDNA) using the High-Capacity cDNA Reverse Transcriptase Kit (Applied Biosystems) with random primers. Before further use, cDNA was diluted 1:5 with water.

2.10.4 Relative gene transcript analysis

Taqman primer and probe-based quantitative polymerase chain reaction (qPCR) reactions were prepared using 1 µL cDNA and 9 µL Taqman Fast Universal 2X Mastermix (Applied Biosystems) and water. qPCR reactions using oligonucleotide primers (0.5 µL each of forward and reverse primers) were prepared using 5 µL SyBr Green Mastermix 2X (Applied Biosystems), 1 µL cDNA and water. Reactions were run in duplicate or triplicate on a 7500 Fast Real Time PCR System Machine (Applied Biosystems) and the cycle threshold (Ct) was set at 0.2.

Transcript levels were analysed relative to 18S levels by calculating the ΔCt between the gene of interest and 18S for each sample. Relative transcript levels were calculated by 2^-ΔCt. Samples with undetected transcripts were reported as having a relative transcript level of 0. When fold change was calculated, 18S Ct values were used to normalise Ct values of genes of interest. Fold change was determined relative to the median of control samples using the 2-ΔΔCt method (Livak & Schmittgen, 2001).

2.10.5 List of primers and probes

Gene	Assay type	TaqMan assay ID / SYBR primer sequences
18S	TaqMan	4319413E
il1β	TaqMan	Dr03114368_m1
ifnγ1-2	TaqMan	Dr0381923_m1
ifnϕ1	TaqMan	Dr03100938_m1
tnfα	TaqMan	Dr03126850_m1
cxcl18b	TaqMan	Dr03436643_m1
runx1	TaqMan	Dr03074179_m1
cmyb	TaqMan	Dr03432766_m1
lyz	TaqMan	Dr03099436_m1
mpeg1.1	TaqMan	Dr03439207_g1
rag1	TaqMan	Dr03131481_m1
GFP	TaqMan	Mr03989638
16S	SYBR	F: 5'-TCCTACGGGAGGCAGCAGT-3' R: 5'-GGACTACCAGGGTATCTAATCCTGTT-3'
lck	SYBR	F:5'-ACGCCGAAGAAGATCTC-3' R: 5'-GCTTGGGGCAGTTACA-3'
IgM	SYBR	F: 5'- GAAGCCTCCAATTCTGTTGG-3' R: 5'-CCGGGCTAAACACATGAAG-3'
pax5	SYBR	F: 5'-CTGATTACAAACGCCAAAAC-3' R: 5'-CTAAATTATGCGCAGAAACG-3'
c-kit	SYBR	F: 5'-CCAGCCGGACACATGGAAAT-3' R: 5'-CTGCGGTTTGCTGATGACA-3'
mCherry	SYBR	F: 5'-CCCCGTAATGCAGAAGAAG-3' R: 5'-TTGGTCACCTTCAGCTTGG-3'

Table 2.5 List of qRT-PCR primers and probes

2.11 Statistical analysis

Data analysis was carried out using Microsoft Excel followed by statistical analysis and graphical representation on GraphPad Prism 5-9.0 software (CA, USA). When comparing 2 groups, Student's t-tests were carried out with Welch's correction if the standard deviation was significantly different. If a population did not have normal distribution, the non-parametric Mann-Whitney test was used. One-way analysis of variance (ANOVA) with Tukey's multiple comparison test was used to compare 3 or more groups. If data was non-parametric, the Kruskal-Wallis test with Dunn's multiple comparison test was used. The Log rank test was used to compare survival. P values greater than 0.05 were deemed non-significant, denoted as ns. Statistical significance denoted as *P<0.05, **P<0.01, ***P<0.001, ****P<0.0001. Error bars indicate standard deviation (SD).

Chapter 3

Runx1+23 Transgenic Characterisation

Chapter 3 | *Runx1+23* Transgenic Characterisation

This chapter presents the work carried out to further characterise *Runx* transgenic zebrafish, as published by Tamplin *et al*. (2015). The aim was to better understand the population of cells expressing fluorescent proteins in these transgenic fish throughout developmental and adult stages. This chapter sets out to characterise the localisation of transgenic *Runx*+ cells in adult zebrafish tissues, as well as their HSC potential. A better understanding of the cells that express fluorescent proteins in these transgenics will have important implications for the use of these transgenic fish for HCT studies. Identifying the population with the greatest stem cell potential for transplantation will have an impact on the survival of transplant recipients.

3.1 Introduction

3.1.1 Runx1 expression throughout zebrafish development

Runx1 is a highly conserved gene that regulates definitive hematopoiesis in all vertebrates. It has a conserved gene structure and function (Speck & Gilliland, 2002; Levanon & Groner, 2004), forming a heterodimer with Cbfβ to regulate HSC budding from the ventral wall of the dorsal aorta (VDA) (Bresciani *et al*., 2014). Vertebrate *runx1* has two isoforms, generated by differential usage of the P1 or P2 promoters. Lam *et al*. generated two transgenic zebrafish lines, *Tg(runx1P1:EGFP)* and *Tg(runx1P2:EGFP)*, to characterise the expression of each *runx1* isoform, and found that each is expressed in discrete hematopoietic sites (Lam *et al*., 2009). The *runx1P1* isoform was found to be maternally expressed in the unfertilized oocyte and transcripts remained present until approximately 4 hpf, as detected by quantitative real-time PCR (qRT-PCR). In contrast, the *runx1P2* isoform transcript was predominantly detected from 14 hpf onwards. GFP fluorescence was first detected in *Tg(runx1P1:EGFP)* transgenic fish at 18 hpf in the posterior lateral-plate mesoderm (PLM), but this was mostly gone by 24 hpf once the posterior blood island (PBI) had formed. The P1 promoter drove expression of *runx1* in the early stages of definitive erythromyeloid progenitor (EMP) formation before being down regulated (Lam *et al*., 2009). Interestingly, morpholino knockdown indicated that *runx1P1* was not necessary for either primitive or definitive hematopoiesis. Expression of GFP was also driven by the *runx1P1* promoter in the olfactory placode and neuronal and somitic tissues.

The *runx1P2* promoter on the other hand was not detected in the PBI region, and instead was found to drive expression of GFP in definitive HSPCs in the VDA by 22 hpf, followed by their migration to the thymus by 4 dpf and pronephros, which eventually becomes the WKM, by 5 dpf. Expression of the P2 isoform was first detected at the 6-somite stage in the notochord, followed by the establishment of distinct neuronal expression by the 12-somite stage (Lam *et al*., 2009). Together, this indicated specific expression driven by the P2 promoter of *runx1* in definitive hematopoietic sites but not primitive sites, as well as neuronal expression as GFP fluorescence was abundant in the brain and spinal cord. *runx1P2* promoter continued to drive GFP expression in HSPCs in the WKM in 1-month old zebrafish. Subsequently, *Tg(runx1P2:EGFP)* transgenic zebrafish were crossed with *Tg(kdrl:NLSmCherry)* zebrafish and double positive progeny were utilised to visualise the emergence of HSCs from the VDA (Lam *et al*., 2010).

Most recently, another zebrafish *runx1* reporter line was generated which has led to the discovery that HSC-forming hemogenic endothelium derived from the arterial endothelium. Using the *TgBAC(runx1P2:citrine)* transgenic line, it was found that *runx1* expression was dependent upon earlier arterial programming by the *notch* ligand *dll4*. This led the authors to hypothesize that the arterial endothelium was a precursor to the hemogenic endothelium (Bonkhofer *et al*., 2019). Citrine expression in this transgenic was found to recapitulate endogenous hematopoietic expression of *runx1P2*. However, in contrast to the findings by Lam *et al*., where EGFP was detected by 22 hpf in *Tg(runx1P2:EGFP)* transgenic zebrafish, citrine expression was first detected in *TgBAC(runx1P2:citrine)* transgenic fish at 23-24 hpf. Citrine was also detected in spinal cord neurons but not in *runx1*+ Rohon-Beard neurons (Bonkhofer *et al*., 2019).

Interestingly, as discussed in the introduction (section 1.7.3), the *runx1*^{W84X} mutant line exhibited impaired HSC formation in most of the homozygous mutants, whereby no definitive HSCs were present at 5 dpf. However, approximately 20% were capable of surviving a bloodless phase and could form a reduced number of definitive HSCs in the CHT, which eventually migrated to the kidney despite the absence of functional *runx1*. Although a reduced number of HSCs formed, *runx1*^{W84X} mutants exhibited also reduced numbers of myeloid and

precursor cells in the adult WKM (Sood *et al*., 2010). All in all, Sood *et al.* demonstrated that zebrafish HSCs can form even in the absence of functional *runx1*.

3.1.2 Runx1 expression in thrombocytes

In addition to its significance in the formation of definitive HSCs, *runx1* is also involved in the regulation of zebrafish thrombocyte development. Thrombocytes are the zebrafish equivalent of platelet-producing megakaryocytes. Sood *et al.* found that *runx1*^{W84X} mutants had defective thrombocyte differentiation. Furthermore, it has been found that patients with heterozygous *RUNX1* mutations in humans also developed familial platelet disorders with thrombocytopenia (Michaud *et al*., 2002). Additionally, it has been reported in humans and mice that *RUNX1*-mediated silencing of a *non-muscle myosin heavy chain IIB (MYH10)* is important for correct megakaryocyte maturation. In the absence of functional RUNX1 proteins, MYH10 was found to build up in platelets, leading to thrombocytopenia (Antyony-Debré *et al*., 2012).

Building upon the work carried out by Bonkhofer *et al.*, Koth *et al.* utilised the *TgBAC(runx1P2:citrine)* transgenic line generated in earlier work in combination with the *runx1*^{W84X} mutant line to investigate scar deposition following heart cryoinjury. The group demonstrated the way in which *runx1* was specifically upregulated in cardiomyocytes following heart injury and led to decreased myocardial proliferation and survival. In the *runx1*^{W84X} mutant zebrafish, on the other hand, both proliferation of myocardial cells and their survival was greater, while fibrosis was reduced. Furthermore, they showed that *runx1*+ endocardial cells and *runx1*+ thrombocytes accumulated in WT zebrafish (Koth *et al*., 2020).

Several groups have been able to provide evidence suggesting there is overlap between *runx1*+ cells and *CD41*:GFP+ cells. In their work, Tamplin *et al.* crossed *Tg(Runx:mCherry)* zebrafish to *Tg(CD41:GFP)* fish and used confocal microscopy in the CHT region of 72 hpf embryos to show a 60 ± 12% overlap between *CD41*:GFP+ HSPCs and *Runx*:mCherry+ HSPCs, and 44 ± 8% overlap vice versa (Tamplin *et al*., 2015). Utilising single-cell RNA sequencing technologies, Tang *et al*. also showed significant overlap between the transcriptional programs of *CD41*:GFP+ and *Runx*:GFP+ cells from the WKM (Tang *et al*., 2017). As discussed in Chapter 1, the *CD41*:GFP^{low} population has been used to isolate HSPCs, whereas the *CD41*:GFP^{high} cells

are mature thrombocytes (Lin *et al*,. 2005; Ma *et al*., 2011). Interestingly, Tang *et al.* found that *CD41*:GFP^{low} and *Runx*:GFP+ cells did not cluster together in a defined group in a principal component analysis but instead were found to be a highly heterogenous population of cells. *CD41*:GFP+ and *Runx*:GFP+ cells followed two main trajectories: either that of classically defined HSPCs or erythroid-primed HSCs. Finally, they also found that classically defined HSPCs, erythroid-primed HSPCs and thrombocytes had closely related transcriptional programs. Most recently, Koth *et al*. (2020) also showed that *runx1*:citrine+ cells also expressed the thrombocyte marker *CD41* (also known as *itga2b*).

3.1.3 Runx1 is required for B cell formation and maturation

runx1, in partnership with c*bfβ*, is required for regulation of B cell lymphocyte development and maturation. In *runx1*^{W84X} mutant zebrafish, Chi *et al.* have shown that functional *runx1* is required for successful V(D)J rearrangements in B cells. Interestingly, it was found that T cell development remains unaffected in *runx1*^{W84X} mutants, and that the reduction in B cells was linked to increased apoptosis rather than decreased proliferation. In adult zebrafish, the abundance of *IgM*:GFP+ cells (Page *et al*., 2013) decreased from 30% of total WKM live cells in WT fish to approximately 4 % in the mutant, indicating that *runx1* plays an important role in B cell maturation and differentiation in adult zebrafish (Chi *et al*., 2018). The requirement of *runx1* for B cell maturation is not specific to zebrafish and is conserved in mice and humans, too. Indeed, *RUNX1* mutations in patients can lead to acute lymphoblastic leukaemia and mouse studies have shown that *Runx1* is required for promoting the survival and development of B cell progenitors (Niebuhr *et al*., 2013).

3.1.4 Runx1 transgenic lines used to identify hematopoietic stem and precursor cells in adult zebrafish

As discussed in the main introduction, a number of transgenic lines have been generated to aid in the study of HSCs and HSPCs in zebrafish (Section 1.4.1). Most of these, particularly the *Tg(cmyb:eGFP)* and *Tg(runx1p2:EGFP)* transgenic lines, have focused on the study of HSPCs in the zebrafish embryo (North *et al*., 2007; Lam *et al*., 2009). However, this thesis aims to focus on investigating HSPCs in adult zebrafish in order to utilise these in HCT studies. The transgenic lines *Tg(Runx:mCherry)* and *Tg(Runx:GFP)* have been shown to drive expression of fluorescent proteins in both embryonic and adult-derived HSPCs (Tamplin *et al*., 2015). In

these transgenic lines, expression of fluorescent protein is driven by an evolutionarily highly conserved cis-regulatory element shared between human, mouse, dog, chicken, frogs, zebrafish and opossum, located approximately 23.5 kb downstream of the translation initiation site of exon one within the first intron of the mouse *Runx1* locus (Nottingham *et al*., 2007). The expression of fluorescent protein in these transgenics was found to be present in cells at all sites of definitive hematopoiesis and was confirmed by HCT (Tamplin *et al*., 2015). Independently, Ng *et al*. also identified a highly conserved non-coding *Runx1* intronic enhancer element located +24 kb downstream of the P1 promoter region. This was shown to be the same as the +23.5 enhancer element identified by Nottingham *et al*. (2007). Differences in the naming of the enhancer elements came about due to different definitions of the +1 site. The +24 enhancer element was found to have hematopoietic-specific activity in both mice and zebrafish and was specifically active in the hemogenic endothelium (Ng *et al*., 2010).

The two transgenic strains *Tg(Runx:mCherry)* and *Tg(Runx:GFP*) differ predominantly in the addition of a nuclear localisation signal in the *Tg(Runx:mCherry)* strain. Therefore, the localisation of GFP would be expected in the cytosol while the mCherry fluorescent protein would be trafficked to and sequestered within the nucleus. However, it was found that the two cell populations were not equivalent, whereby the mCherry fluorophore was expressed in a larger population of cells relative to *Runx*:GFP (Tamplin *et al*., 2015). Although there may be positional differences in the insertion site of the transgene, the difference in population size can likely be attributed to the nuclear localisation signal in the *Tg(Runx:mCherry)* transgenic line, leading to retention of mCherry possibly even after HSPCs start to differentiate. If this is the case, precursor cells and multipotent progenitors would be expected to have retained mCherry fluorescence. Indeed, work carried out in collaboration with Dr. McBrien identified that the *Runx*:mCherry+ cell population was significantly more radiosensitive than the *Runx*:GFP+ cell population. Sub-lethal irradiation led to a significant reduction in the number of *Runx*:mCherry+ cells in the WKM of adult fish 5 days post irradiation. *Runx*:GFP+ cells, on the other hand, did not reduce in cell numbers following irradiation (McBrien, 2017).

The overlap between *Runx*:mCherry and *Runx*:GFP-expressing cells was investigated by Tamplin *et al.* using fluorescence microscopy of the CHT at 72 hpf, which revealed that 13±6 % of *Runx*:mCherry+ cells overlapped with *Runx*:GFP+ cells, and 92±11 % of *Runx*:GFP+ cells

overlapped with *Runx*:mCherry+ cells. This clearly demonstrated that the *Runx*:mCherry population was considerably larger than the *Runx*:GFP population. The difference in the number of cells that express the fluorescent protein likely is reflected in biological differences between these two populations. The aim of this chapter is to further characterize these transgenic lines and determine whether equivalent populations of HSPCs can be isolated for potential future use in competitive transplantation assays in adult zebrafish.

3.2 Aims

This chapter aims to further characterise the *Tg(Runx:mCherry)* and *Tg(Runx:GFP)* transgenic lines generated by Tamplin *et al.* (2015). Fluorescent protein-expressing cells will be investigated during larval and adult stages with a view to utilise adult transgenic fish as HSC donors in subsequent HCT experiments.

More specifically, the aims of this chapter are to:

1. Determine the localisation and abundance of fluorescent protein-expressing *Runx*+ cells.
2. Investigate the similarities and differences between *Runx*:mCherry+ and *Runx*:GFP+ populations in different tissues.
3. Elucidate whether other non-HSC cell types may be expressing the *Runx*:mCherry construct, using a combination of flow cytometry, imaging and gene transcript data.

3.3 Results

3.3.1 The localisation and abundance of fluorescent protein-expressing Runx+ cells

The publication by Tamplin *et al*. (2015) provided a detailed account of the localisation of *Runx*+ HSPCs during the embryonic developmental stages of zebrafish and examined all major hematopoietic tissues of the embryo, including the VDA, CHT, thymus and WKM. In particular, the study characterised the emergence of *Runx*+ cells from the hemogenic endothelium in the CHT. The current project therefore focused on post embryonic stages of zebrafish development and investigated where *Runx*+ cells could be found in larval and juvenile fish, before also studying adult transgenic fish.

3.3.1.1 Runx:mCherry+ cells appear in circulation and embed in the gill tissue

During larval stages of zebrafish development, a significant population of circulating *Runx*:mCherry+ cells were identified (Fig. 3.1A-B). These cells were found throughout the circulatory system, including in distal sites such as the gills (Fig. 3.1C, D). It was possible to track cells in circulation in the CHT, demonstrating the presence of embedded cells in the CHT niche in addition to cells in the vasculature. Unfortunately, due to the long exposure time (200 µS) and the dynamic movement of cells through the gill vasculature, it was not possible to accurately track circulating cells in gill tissue (nevertheless, videos are accessible via QR codes and URLs in each figure). While it has previously been reported that a small pool of HSPCs is continuously released into circulation during steady-state hematopoiesis in mammalian systems (Massberg *et al*., 2007), the functional purpose of these circulating *Runx*:mCherry+ cells in the larval zebrafish remains unclear. They may go on to seed the WKM, the definitive site of adult hematopoiesis, or later the thymus to form lymphoid cells.

The presence of circulating *Runx*+ cells continued into the larval and juvenile stages of the zebrafish development (Fig. 3.2), and even into adulthood (Fig. 3.3). Furthermore, in addition to the published presence of embedded *Runx*+ cells in the CHT and later the WKM and thymus (Tamplin *et al*., 2015), I found that juvenile fish at 21 dpf contain a small number of embedded *Runx*+ cells in their gills (Fig. 3.2). Therefore, changes in localisation of *Runx*+ cells throughout the development of the zebrafish were investigated.

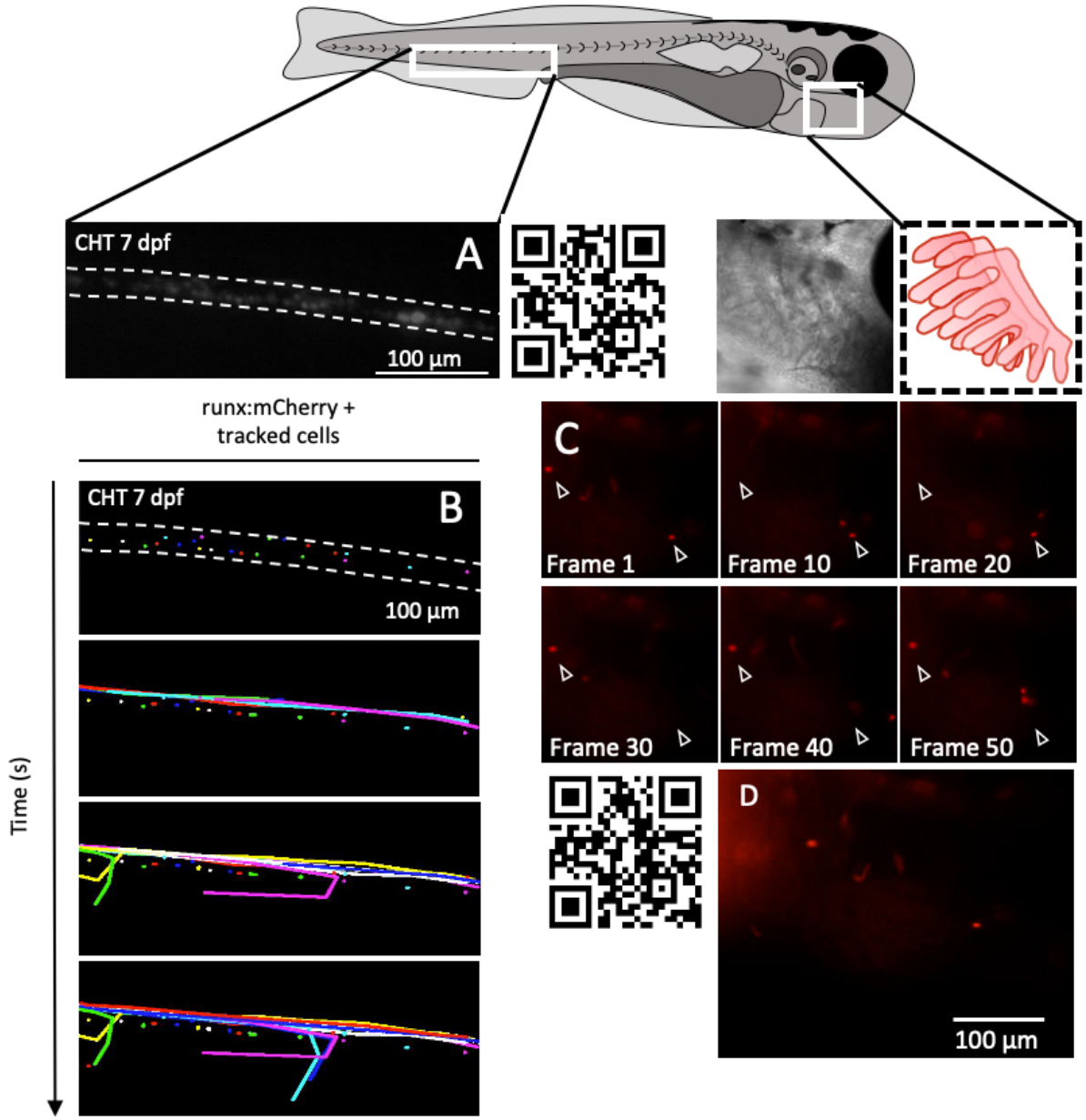

Fig. 3.1 Presence of circulating *Runx*:mCherry+ cells in 7 dpf zebrafish larvae.

(A) Widefield live intravital microscopy of 7 dpf *TraNac Tg(Runx:mCherry)* CHT. Fluorescent cells in grey. Cartoon of zebrafish indicates areas imaged. Video is taken at a single z slice. The video can be viewed by using the adjacent QR code or at this link qrgo.page.link/m45Mv. **(B)** Manual cell tracking data of *Runx*:mCherry+ cells in the CHT area and in circulation in the blood of 7 dpf *TranNac Tg(Runx:mCherry)* fish. Stationary cells indicate HSPCs lodged in the CHT; lines indicate the movement of cells in circulation. Cell tracking was carried out using Fiji manual tracking plugin (Tinevez *et al.*, 2017). **(A-B)** Dotted line indicates location of CHT. **(C-D)** Live intravital microscopy of 7 dpf *TranNac Tg(Runx:mCherry)* fish gills. **(C)** Unfilled arrow heads show *Runx*:mCherry+ cells in circulation through the gill (fluorescent cells in red). N= 5. Representative video can be viewed using adjacent QR code or at this link qrgo.page.link/Ny1tT.

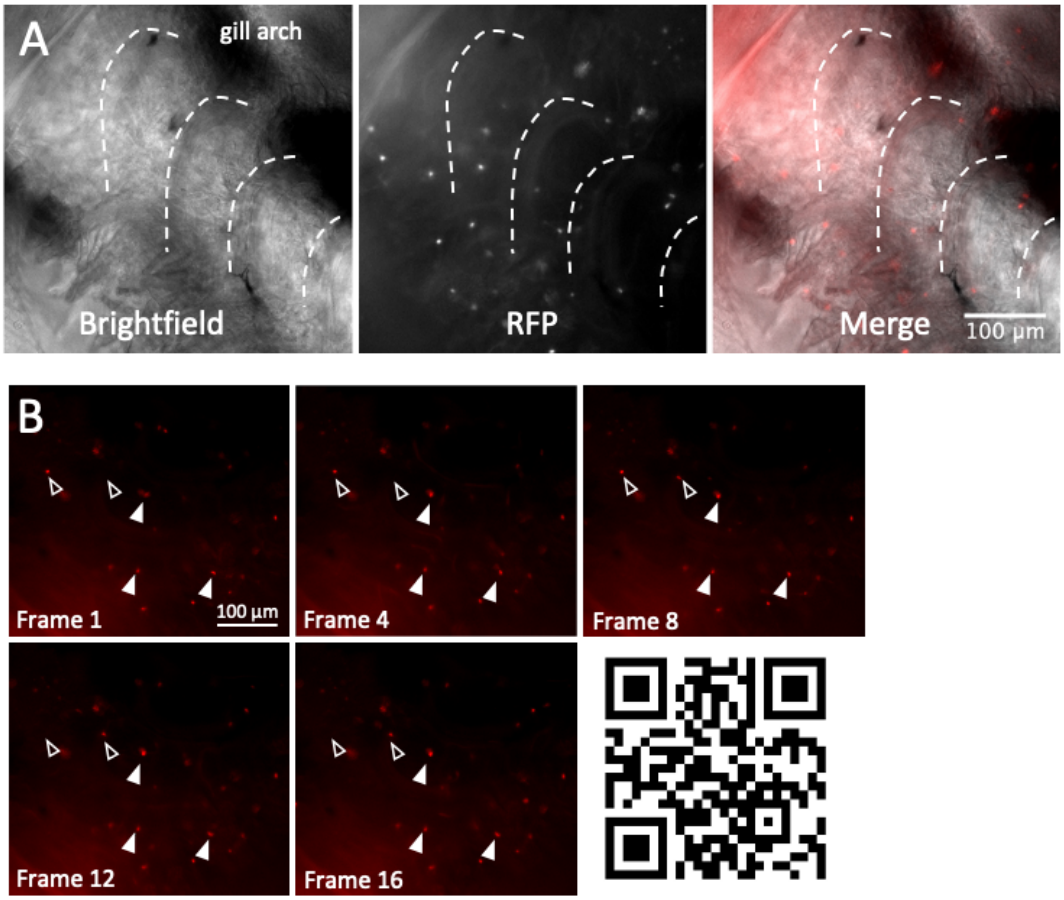

Fig. 3.2 Presence of *Runx*:mCherry+ static cells in the zebrafish gills from 21dpf.

(A) Widefield live intravital microscopy of 21 dpf *TraNac Tg(Runx:mCherry)* gills. Brightfield and fluorescent images of gills are taken at a single z slice. Brightfield image are included to indicate focal plane. **(B)** mCherry fluorescence observed in the gills of 21 dpf of *TraNac Tg(Runx:mCherry)* fish. Filled arrowheads indicate stationary cells in the gill. Unfilled arrowheads indicate the location of cells that move in circulation. Video can be viewed by using adjacent QR code or at this link qrgo.page.link/bmc7r.

It was found that between 7-14 dpf, the only *Runx*+ cells that were present in the gills were those in circulation in the blood. However, from approximately 21 dpf onward, embedded *Runx*+ cells started to appear in the gill tissue (Fig. 3.2 & 3.3). The number of these resident cells appeared to increase between 21-35 dpf and then stabilised as fish matured and reached adulthood (Fig. 3.3). Ultimately, a quantitative flow cytometry time course would be required to confirm this.

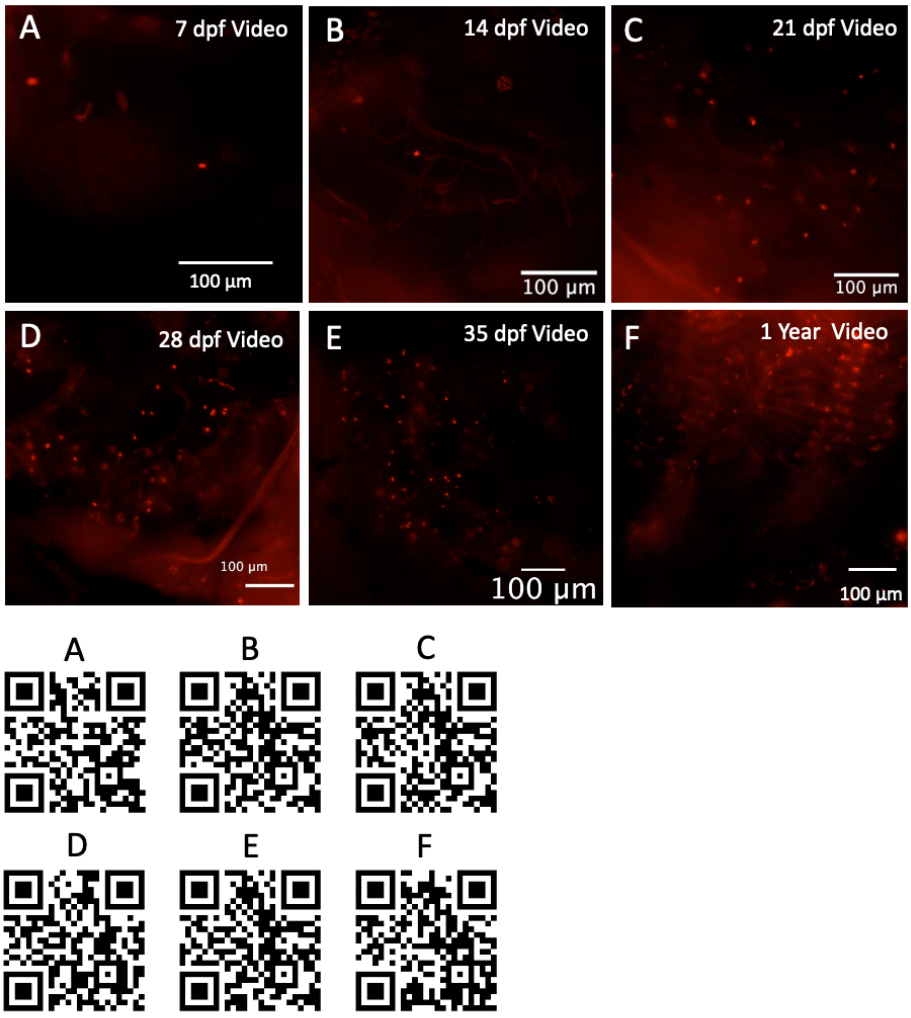

Fig. 3.3 Developmental time course of *Runx*:mCherry+ cells in gill tissue.

Widefield live intravital fluorescence microscopy of *TraNac Tg(Runx:mCherry)* gills. Videos taken at a single z slice. Videos of *Runx*:mCherry + cells in circulation in zebrafish gills at 7 dpf **(A,** qrgo.page.link/mrgtk**)**, 14 dpf **(B,** qrgo.page.link/vzz4k**)**, 21 dpf **(C,** qrgo.page.link/R3tKk**)**, 28 dpf **(D,** qrgo.page.link/qFjax**)**, 35 dpf **(E,** qrgo.page.link/5SJ3F) and 1 year post fertilisation **(F,** qrgo.page.link/Vj4R9**)**. N=5, representative videos shown. Image stabilisation was carried out using Fiji software. Scale bars represent 100 µM. Cell tracking was not possible due to required long exposure time of 200 µs and dynamic movement of cells in circulation. Videos can be viewed using corresponding QR codes and URLs.

3.3.2 Characterising blood cell populations in whole kidney marrow, gill and blood

Following the identification of *Runx*:mCherry+ cells in the gills and peripheral blood, in addition to their previously known presence in the WKM of adult zebrafish, the abundance of *Runx*:mCherry+ cells in these adult tissues was investigated. Understanding the abundance of *Runx*:mCherry+ cells and other major blood cell populations could shed light on whether the *Runx*:mCherry+ cells in each niche may have distinct organ-specific functions. As described by Traver *et al.* (2003), hematopoietic cell populations in the WKM can be readily identified by flow cytometry by distinguishing forward and side scatter properties (Fig. 3.4E). These

provide information on the size and granularity of the cells, respectively. For this approach, single cell suspensions were prepared from each tissue from individual adult transgenic zebrafish and analysed by flow cytometry. Live single cells were identified by selecting for singlet cells, excluding auto-fluorescent cells and FSC ^{low} debris (Fig. 4 A-D). The flow cytometry gating for major blood cell lineages was confirmed by determining which compartments contained established reporter cells, such as *lyz*:GFP+ and *Runx*:mCherry+. Indeed, *lyz*:GFP+ cells localised to the myelomonocyte compartment and *Runx*:mCherry ^{high} cells to the lymphocyte compartment (Fig. 4 E-G) as previously described (Hall *et al.,* 2007; Tamplin *et al.,* 2015).

It was observed that the gating of major blood cell populations, as defined by Traver *et al.* (2003), could accurately be applied to the WKM and the peripheral blood (PB) (Fig. 3.4E-G & 3.5A). However, the gill appeared to possess another dominant population, which partially overlapped with the precursor and myelomonocyte gates (Fig. 3.5D). Using transgenic markers for myelomonocytes, such as *Tg(lyz:GFP)*, which has previously been reported to identify 57.4±3.5 % of all cells within the myelomonocyte compartment (Hall *et al*., 2007), it became clear that there was a discrepancy in the number of events within the myelomonocyte compartment and the number of *lyz*:GFP+ cells present in the gills (Fig. 3.5G & I). Previous work by Dr. Wane in the Dallman lab (Wane, 2021) also found that *fli*:GFP+ cells, which express fluorescent protein in endothelial cells (Lawson & Weinstein, 2002), fall in both the precursor and myelomonocyte compartments in the gill, indicating that cells of a non-hematopoietic lineage also contribute to these gates. Therefore, although myeloid cells would be expected in the myelomonocyte compartment of the gill and, likewise, precursor cells would be expected in the precursor compartment, it cannot be assumed that the number of events present in these gates are a true reflection of the number of myelomonocyte and precursor cells in the gill.

The most abundant hematopoietic cell type in the three tissues investigated (WKM, blood and gill) were the erythrocytes which contributed on average 26.3 % and 44.3 % to live cells in the WKM and gill respectively. Unsurprisingly, they account for the greatest proportion of cells within the PB, where 79.2±10 % of all live single cell events were found within the erythrocyte compartment (Fig. 3.5 & 3.6). Lymphocytes make up approximately 22-26 % of live cells in

both the WKM and the gills. However, there are very few present in the blood (1.7 %). The abundance of myelomonocytes was the greatest in the WKM with an average of 21.0 %, compared to 9.8 % in the gill and 0.6 % in the blood. However, given the contribution of non-hematopoietic lineages to this compartment in the gill, the number of myelomonocytes in the gill is likely to be an overestimation. Indeed, *lyz*:GFP+ cells only contribute 0.5 % on average to live cells in the gill, compared to 9.8 % of live singe cells within the myelomonocyte gate. Meanwhile in the WKM *lyz*:GFP+ cells make up on average 17.2 % of live cells, this is much more similar to the contribution of live single cells to the myelomonocyte compartment (21 %) in the same tissue. As it may be expected, WKM contains the largest proportion (7.7 %) of hematopoietic precursor cells relative to the blood and gills, which contain 0.9 % and 5.5 % respectively. Once again, within the gills, this number is unlikely to reflect the true number of precursor cells present in the tissue. However, a similar trend is observed in the population size of *Runx*:mCherry+ cells which make up 3.9, 0.3 and 1.1 % of live single cells in the WKM, blood and gill respectively (Fig. 3.5 & 3.6).

For the purpose of identifying blood cell populations in the WKM and blood, the gates described by Traver *et al.* (2003) to identify major blood cell populations were used. However, to investigate blood cell populations in the gill, I in part relied on the use of fluorescent protein-expressing cells, such as *lyz*:GFP+ and *Runx*:mCherry+ cells, to more accurately reflect the abundance of myeloid and precursor cells respectively. In addition, the lymphocyte and erythrocyte compartments, based of FSC/SSC, were also used to determine the abundance of these blood cell populations in the gills.

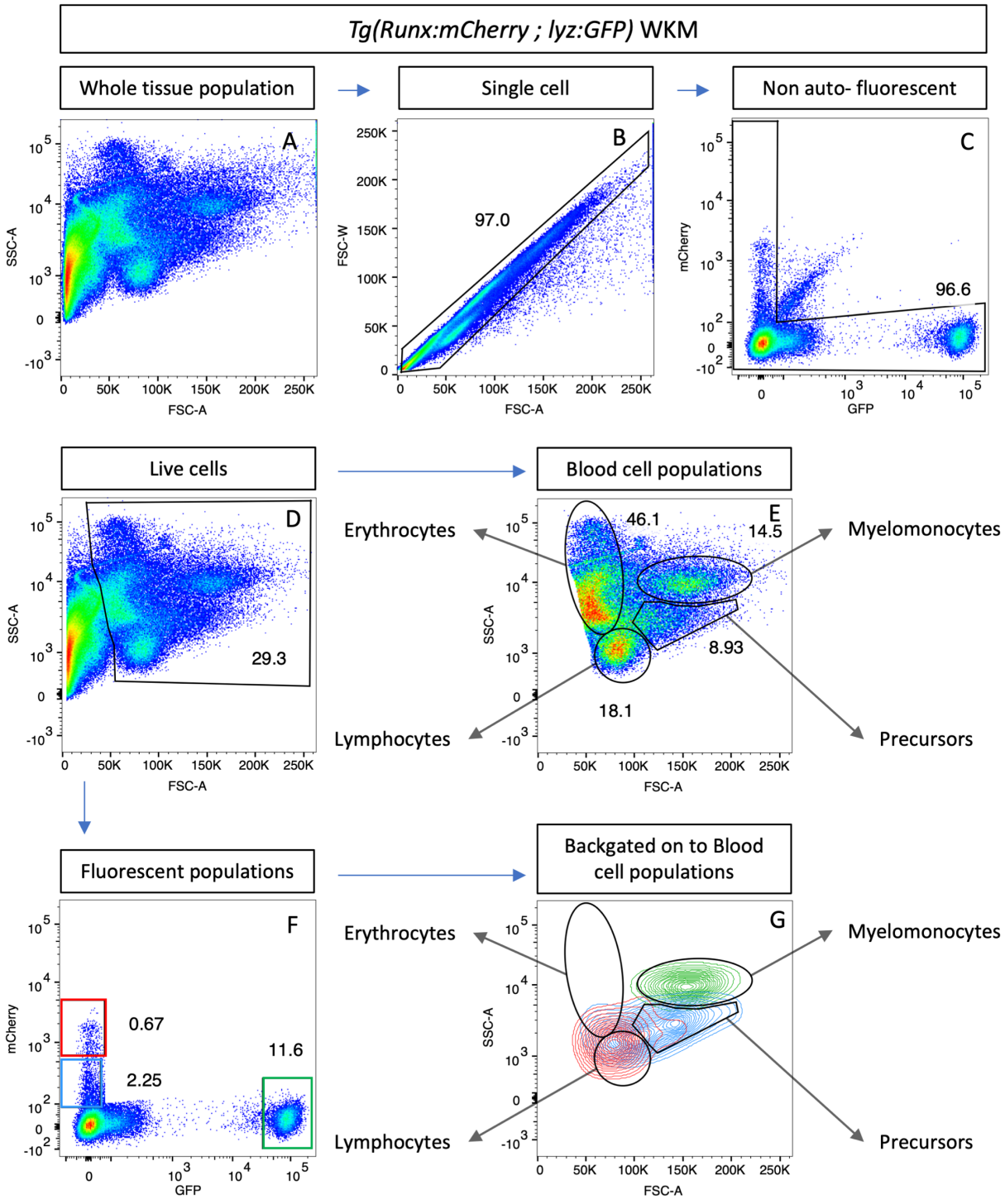

Fig. 3.4 Flow cytometry gating strategy to identify live single cells and fluorescent cell populations.

A single cell suspension of WKM tissue from *Tg(Runx:mCherry; lyz:GFP)* fish was analysed to identify live single cells using flow cytometry. (**A**) Ungated FSC-A/SSC-A profile of a representative WKM. (**B**) Singlet cells were selected on FSC-W/FSC-A. (**C**) Auto-fluorescent events were excluded based on mCherry/GFP. (**D**) FSC ^{low} debris was excluded on SSC-A/FSC-A. (**E**) Black outlines indicate gates of major blood cell populations. (**F**) mCherry/ GFP plot with gating of fluorescent populations. Red box outline represents gating for mCherry ^{high} cells, blue box outlines the gate for mCherry ^{low} cells and the green box outline shows gating for GFP+ cells. Values adjacent to gates reflect the percentage of events within each gate compared to total events in the whole plot. (**G**) Back-gating of fluorescent cells to identify the FSC/SSC gates they are found within.

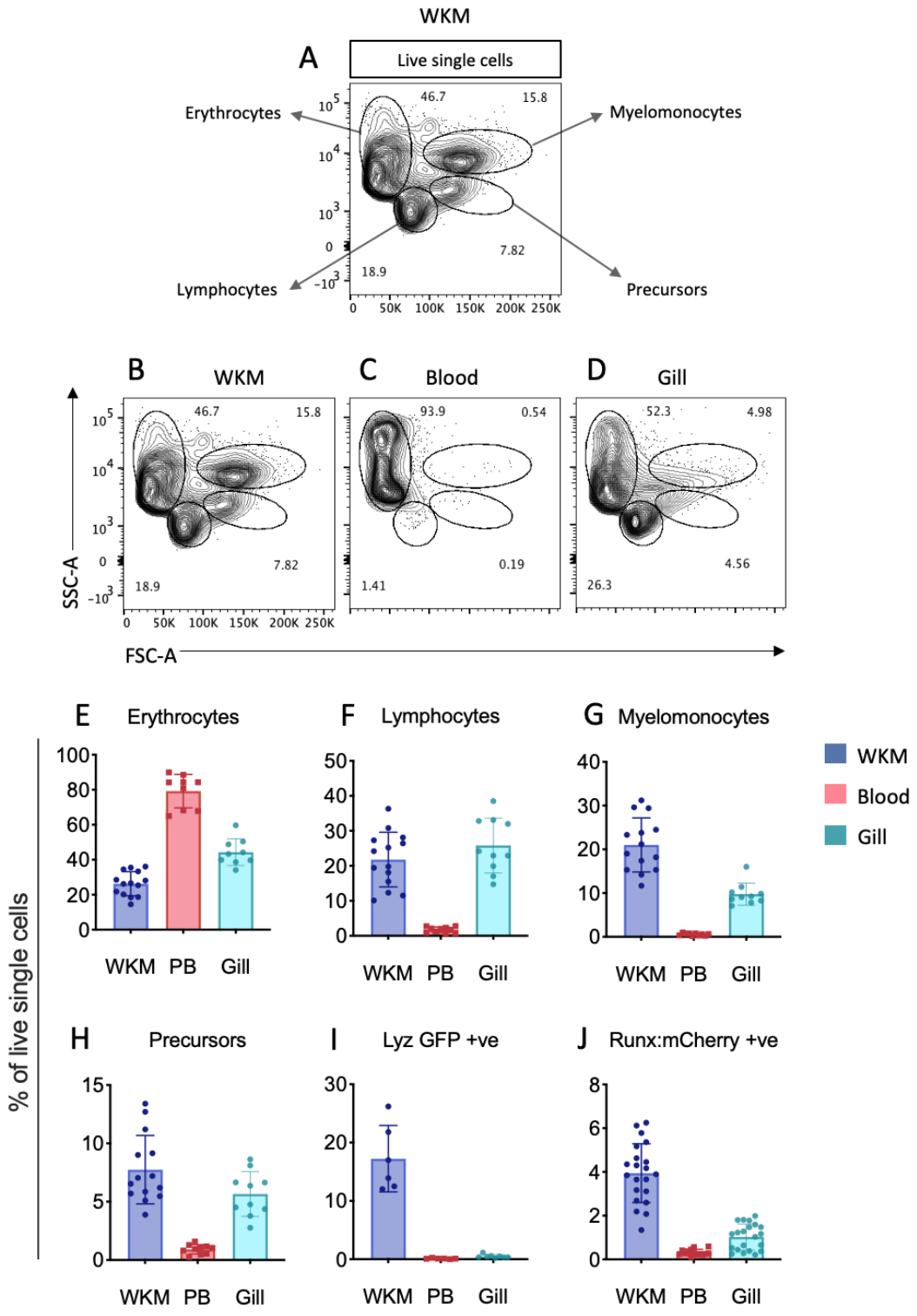

Fig. 3.5 Characteristic FSC/SSC plots of blood, gill and WKM, as well as their composition.

Adult WT, *Tg(Runx:mCherry)* and *Tg(Runx:mCherry; lyz:GFP)* fish were dissected and WKM, PB and gill tissues were harvested in order to determine the composition of cell populations. **(A)** Gating of major blood cell populations on WKM based on FSC/SSC as described by Traver *et al*. (2003). **(B, C & D)** Representative FSC/SSC plots of WKM, PB and gill single cell suspensions from individual fish with typical blood cell gating applied. **(E-J)** Individual dots represent 1 fish. N= 6-21. Mean and standard deviation (SD) shown. Percentage contribution of erythrocytes **(E)**, lymphocytes **(F)**, myelomonocytes **(G)** and precursors **(H)** to live single cells in WKM, PB and gills. **(I)** Proportion of *lyz*:GFP+ cells as a percentage of live singe cells in each of the WKM, PB and gill tissues. **(J)** Proportion of *Runx*:mCherry+ cells as a percentage of live single cells in each of the WKM, PB and gill tissues.

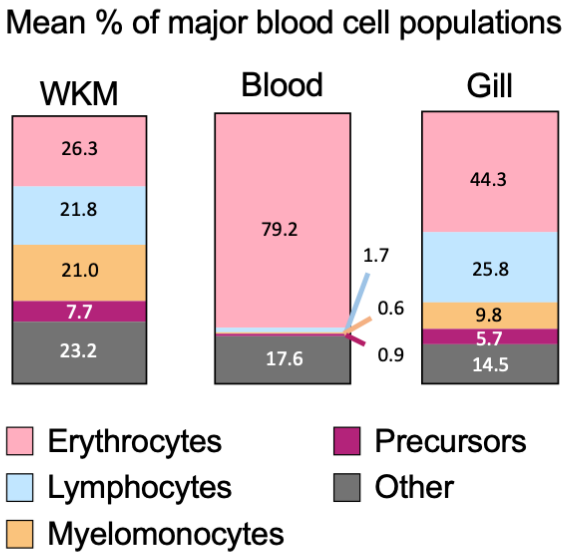

Fig. 3.6 Cell composition of WKM, blood and gill tissues.

Flow cytometry FSC/SSC was used to determine the mean average proportion of erythrocytes, lymphocytes, myelomonocytes and precursors as a percentage of live single cells in WKM, blood and gill tissues of adult WT zebrafish. N= 9.

3.3.3 Identification of Runx+ cells by flow cytometry

The next objective was the quantification of both *Runx*:mCherry+ and *Runx*:GFP+ (collectively referred to as *Runx*+) cells in adult zebrafish by flow cytometry to further dissect the populations. Tamplin *et al.* (2015) showed that *Runx*+ cells possessed the same size and granularity as cells found in the lymphocyte compartment (which has been shown to contain HSCs (Traver *et al.,* 2003)). This study corroborated these findings and showed that *Runx*+ cells from the WKM localised to the lymphocyte gate (Fig. 3.4F & G, 3.7A-C). Based on fluorescence intensity, different populations of *Runx*:mCherry+ cells could be identified in the WKM of adult zebrafish, there being a clear distinction between mCherry ^{high} and ^{low} fluorescence intensity. The mCherry ^{low} population was more abundant and comprised approximately 3.0 % of all the live single cell events in the kidney and 77.6 % of the entire mCherry+ compartment. In contrast, mCherry ^{high} was found to have contributed an average of 0.9 % of the WKM and 22.4 % of all mCherry + cells (Fig. 3.7E & H). Of these, it was found that on average ~72.2±9.8 % of *Runx*:mCherry ^{high} cells were in the lymphocyte compartment, while ~12.0±8 % appeared in the precursor compartment (Fig. 3.7F). The remaining ~16 % were outside of either compartment. *Runx*:mCherry ^{low} cells in the WKM appeared to lie predominantly in the precursor compartment (~46.6±8 %). However, they were next most abundant in the lymphocyte compartment, where ~34.1±7.5 % of them were found (Fig. 3.7D & G). Of the remaining ~19.3 % of *Runx*:mCherry ^{low} cells, 4.7±3 % were found in the erythrocyte compartment and 5.7±4.5 % were found in the myelomonocyte compartment (Fig. 3.7D).

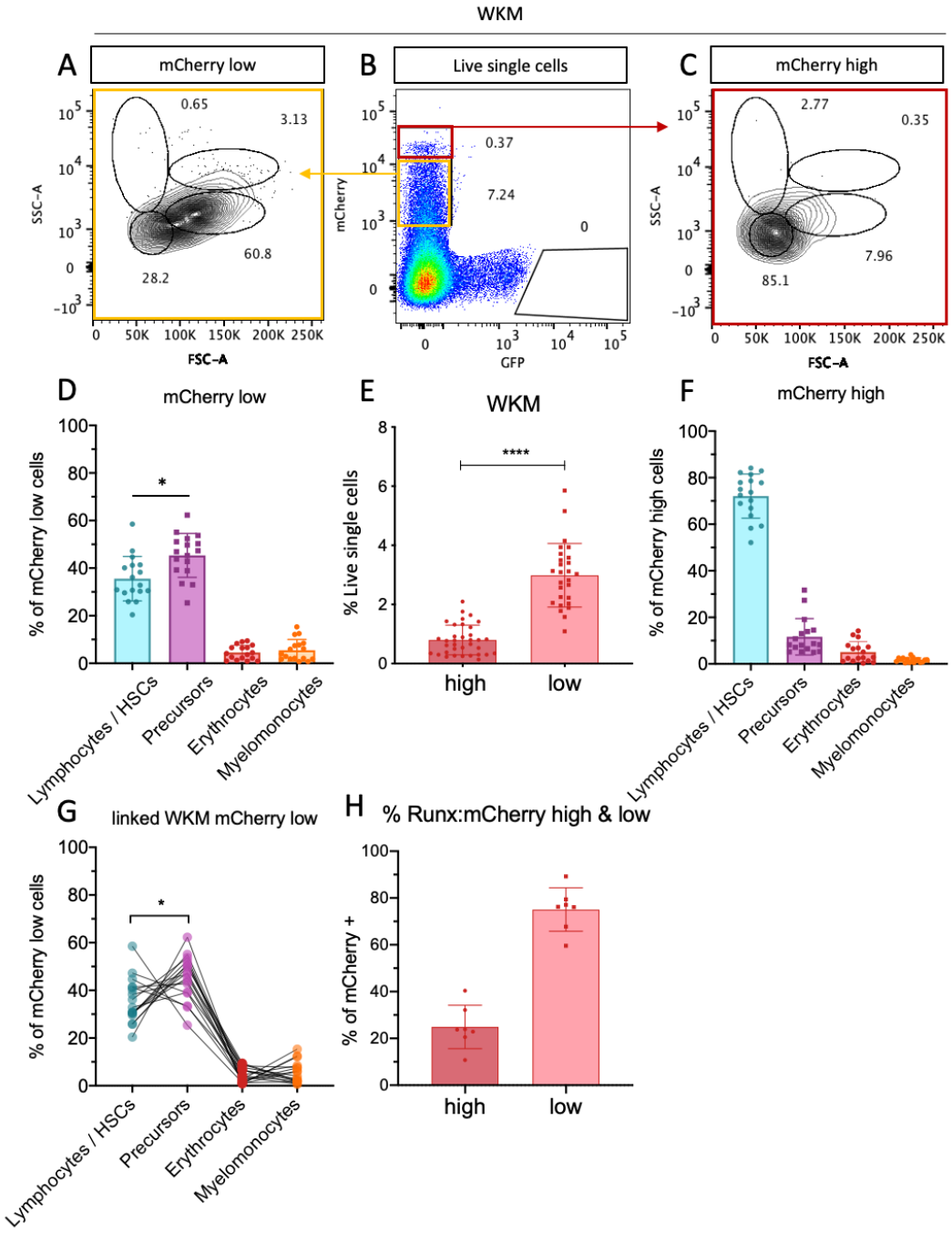

Fig. 3.7 Characterisation of *Runx*:mCherry+ cells in adult zebrafish WKM.

Tg(Runx:mCherry) transgenic WKM was harvested from adult zebrafish to quantify the *Runx*:mCherry ^{high} and *Runx*:mCherry ^{low} cells as a percentage of total live cells and dissect the differences between *Runx*:mCherry ^{high} and ^{low} cells. N=7-27. **(A)** *Runx*:mCherry ^{low} cells plotted on FSC/SSC to determine the gate in which the majority of cells lie. Values on plot reflect the percentage of cells within each gate relative to total events in plot. **(B)** mCherry/GFP plot of *Tg(Runx:mCherry)* WKM. Red box indicates gating for *Runx*:mCherry ^{high} cells and yellow box indicates gating for *Runx*:mCherry ^{low} cells. **(C)** *Runx*:mCherry ^{high} cells plotted on FSC/SSC to determine which gate the majority of cells lie in. 85% of *Runx*:mCherry ^{high} events were found in the lymphocyte gate and 8% in the precursor gate. **(D)** Percentage of all *Runx*:mCherry ^{low} cells which were found in different gates. **(E)** The proportion of *Runx*:mCherry ^{high} and ^{low} cells as a percentage of live single cells in the WKM. **(F)** Percentage of all *Runx*:mCherry ^{high} cells which were found in different gates. **(G)** Percentage of all *Runx*:mCherry ^{low} cells which were found in different gates for individual fish, linked values. **(H)** The proportion of *Runx*:mCherry ^{high} and ^{low} cells as a percentage of all *Runx*:mCherry+ cells in the WKM. Each dot represents 1 fish. Error bars indicate SD. *P < 0.05, **P < 0.005, ***P < 0.0005, ****P < 0.00005. T-Test.

The presence of *Runx*:mCherry+ cells was confirmed by flow cytometry in the adult gill tissue. Strikingly, the predominant population of *Runx*:mCherry+ cells in the gill were *Runx*:mCherry ^{high}. These contributed 1.1 % to all live single cells and 97.5 % to the total mCherry+ population (Fig. 3.8B, E & G). Like those *Runx*:mCherry ^{high} cells found in the WKM, ~ 86.6±11.6 % of *Runx*:mCherry ^{high} cells in the gill appeared in the lymphocyte compartment, while only ~0.9±0.7 % appeared in the precursor compartment (Fig. 3.8C & F). The much smaller and occasionally absent population of *Runx*:mCherry ^{low} cells in the gill contributed ~0.1±0.1 % of live cells. Of these, ~34.9±10.3 % were found in the lymphocyte compartment (Fig. 3.8A, B, D & E). This data suggests that either other, non-HSPC cell types were also expressing *Runx*:mCherry, or that there was a population of HSPCs or other precursors in the gill expressing the *Runx*:mCherry transgene.

The population of *Runx*:mCherry+ cells found in the blood had a significantly lower abundance than either in the gill or WKM and only made up a total of ~0.4±0.4 % of live single cells. Similarly to the gill, the *Runx*:mCherry+ cells found in the circulating blood were also predominantly *Runx*:mCherry ^{high} (87.5 %, Fig. 3.9B, E & F). These cells were found principally in the lymphocyte compartment (~ 77.2±12.7 %), with only ~ 9.3±4 % found in the precursor compartment. Conversely, the *Runx*:mCherry ^{low} cells in the blood were rare (~0.2 % of live single cells) and of these, ~40.5±8.6 % were located in the precursor compartment and ~19 ± 10.3% in the lymphocyte compartment (Fig. 3.9C, F & A, D).

In contrast to the distribution of *Runx*:mCherry+ cells, only one population of *Runx*:GFP+ cells was found in each examined tissue (Fig. 3.10A-C). In the WKM, much like the *Runx*:mCherry ^{high} cells, *Runx*:GFP+ cells were found to scatter predominantly in lymphocyte compartment (81.6±10.4 %), while an average of 5±6.7 % of cells were in the precursor compartment (Fig. 3.10D & G). Meanwhile, the *Runx*:GFP + population in the gill was found to be almost entirely restricted to the lymphocyte compartment (94±3.4 %), with less than 2.5 % of cells found in any other compartment (Fig. 3.10E & H). Finally, in the blood, a small population of circulating *Runx*:GFP+ cells was found, predominantly in the lymphocyte compartment (88.3±1.5 %), with 5.3±1 % among the precursors (Fig. 3.10F & I).

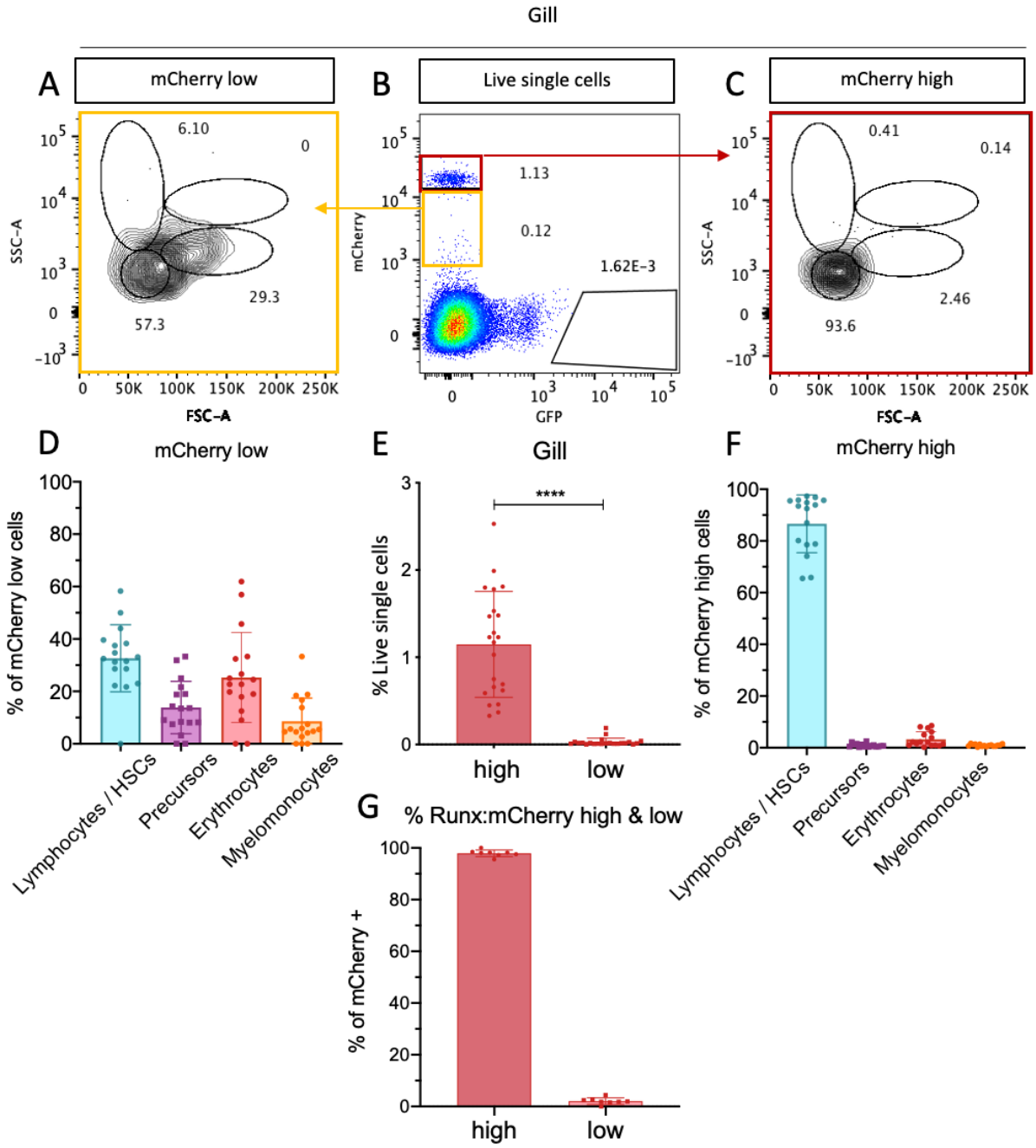

Fig. 3.8 Characterisation of *Runx*:mCherry+ cells in adult zebrafish gill.

Tg(Runx:mCherry) transgenic gills were harvested from adult zebrafish to quantify the *Runx*:mCherry ^{high} and ^{low} cells as a percentage of total live cells and dissect the differences between *Runx*:mCherry ^{high} and ^{low} cells. N=8-17. **(A)** *Runx*:mCherry ^{low} cells plotted on FSC/SSC to determine which gate the majority of cells lie in. Values on plot reflect the percentage of cells within each gate relative to total events in plot. **(B)** mCherry/GFP plot of *Tg(Runx:mCherry)* gills. Red box indicates gating for *Runx*:mCherry ^{high} cells and yellow box indicates gating for *Runx*:mCherry ^{low} cells. **(C)** *Runx*:mCherry ^{high} cells plotted on FSC/SSC to determine which gate the majority of cells lie in. 93% of *Runx*:mCherry ^{high} events were found in the lymphocyte gate. **(D)** Percentage of all *Runx*:mCherry ^{low} cells which were found in different gates. **(E)** The proportion of *Runx*:mCherry ^{high} and ^{low} cells as a percentage of live single cells in the gill. **(F)** Percentage of all *Runx*:mCherry ^{high} cells which were found in different gates. **(G)** The proportion of *Runx*:mCherry ^{high} and ^{low} cells as a percentage of all mCherry+ cells in the gill. Each dot represents 1 fish. Error bars indicate SD. *P < 0.05, **P < 0.005, ***P < 0.0005, ****P < 0.00005. T-Test.

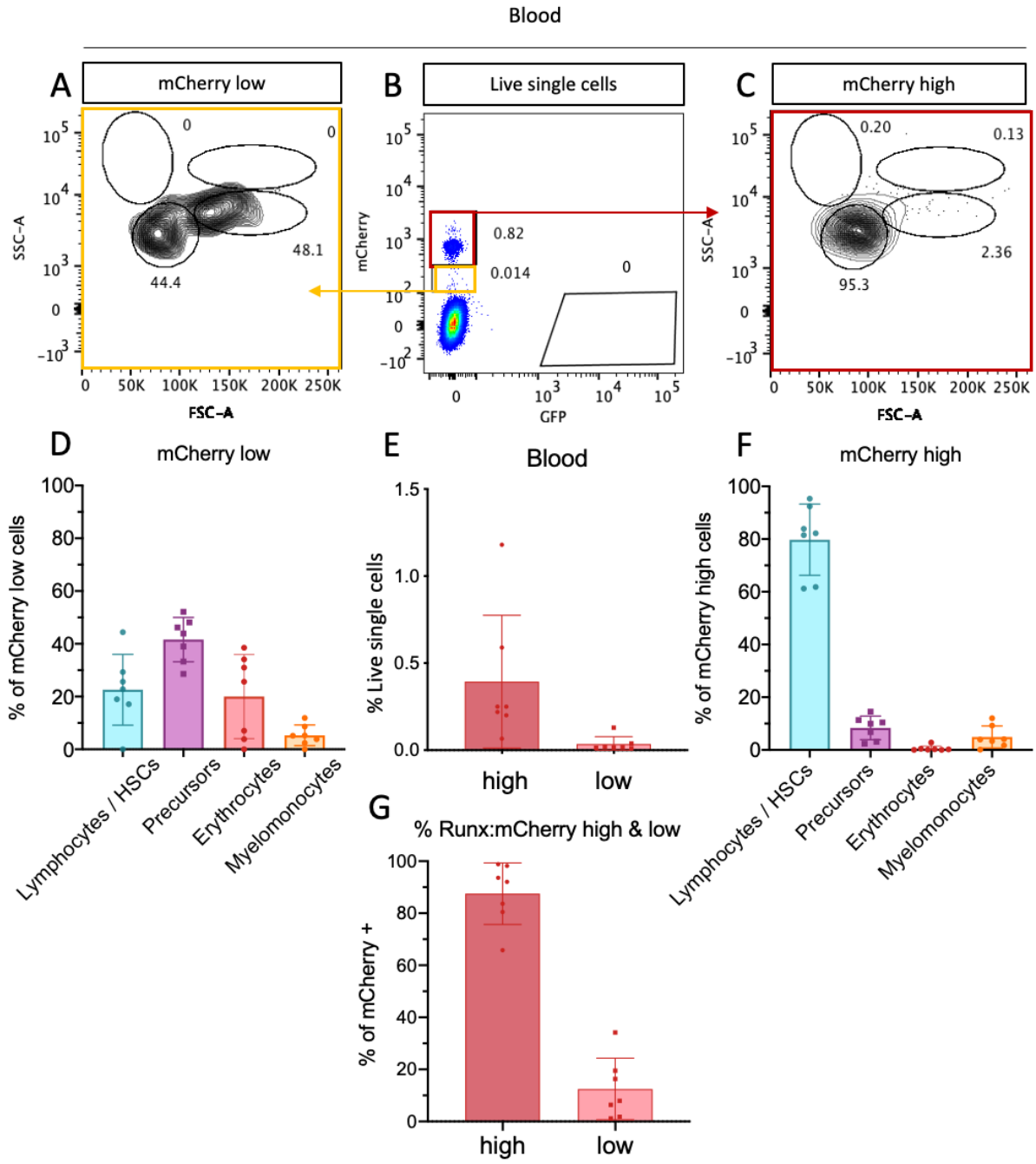

Fig. 3.9 Characterisation of *Runx*:mCherry+ cells in adult zebrafish blood.

Tg(Runx:mCherry) transgenic blood was harvested from adult zebrafish to quantify the *Runx*:mCherry ^{high} and ^{low} cells as a percentage of total live cells and dissect the differences between *Runx*:mCherry ^{high} and ^{low} cells. N=7. **(A)** *Runx*:mCherry ^{low} cells plotted on FSC/SSC to determine which gate the majority of cells lie in. Values on plot reflect the percentage of cells within each gate relative to total events in plot. **(B)** mCherry/GFP plot of *Tg(Runx:mCherry)* blood. Red box indicates gating for *Runx*:mCherry ^{high} cells and yellow box indicates gating for *Runx*:mCherry ^{low} cells. **(C)** *Runx*:mCherry ^{high} cells plotted on FSC/SSC to determine which gate the majority of cells lie in. 95% of *Runx*:mCherry ^{high} events found in lymphocyte gate. **(D)** Percentage of all *Runx*:mCherry ^{low} cells which are found in different gates. **(E)** The proportion of *Runx*:mCherry ^{high} and ^{low} cells as a percentage of live single cells in blood. **(F)** Percentage of all *Runx*:mCherry ^{high} cells which were found in different gates. **(G)** The proportion of *Runx*:mCherry ^{high} and ^{low} cells as a percentage of all mCherry+ cells in blood. Each dot represents 1 fish. Error bars indicate SD. *P < 0.05, **P < 0.005, ***P < 0.0005, ****P < 0.00005. T-Test.

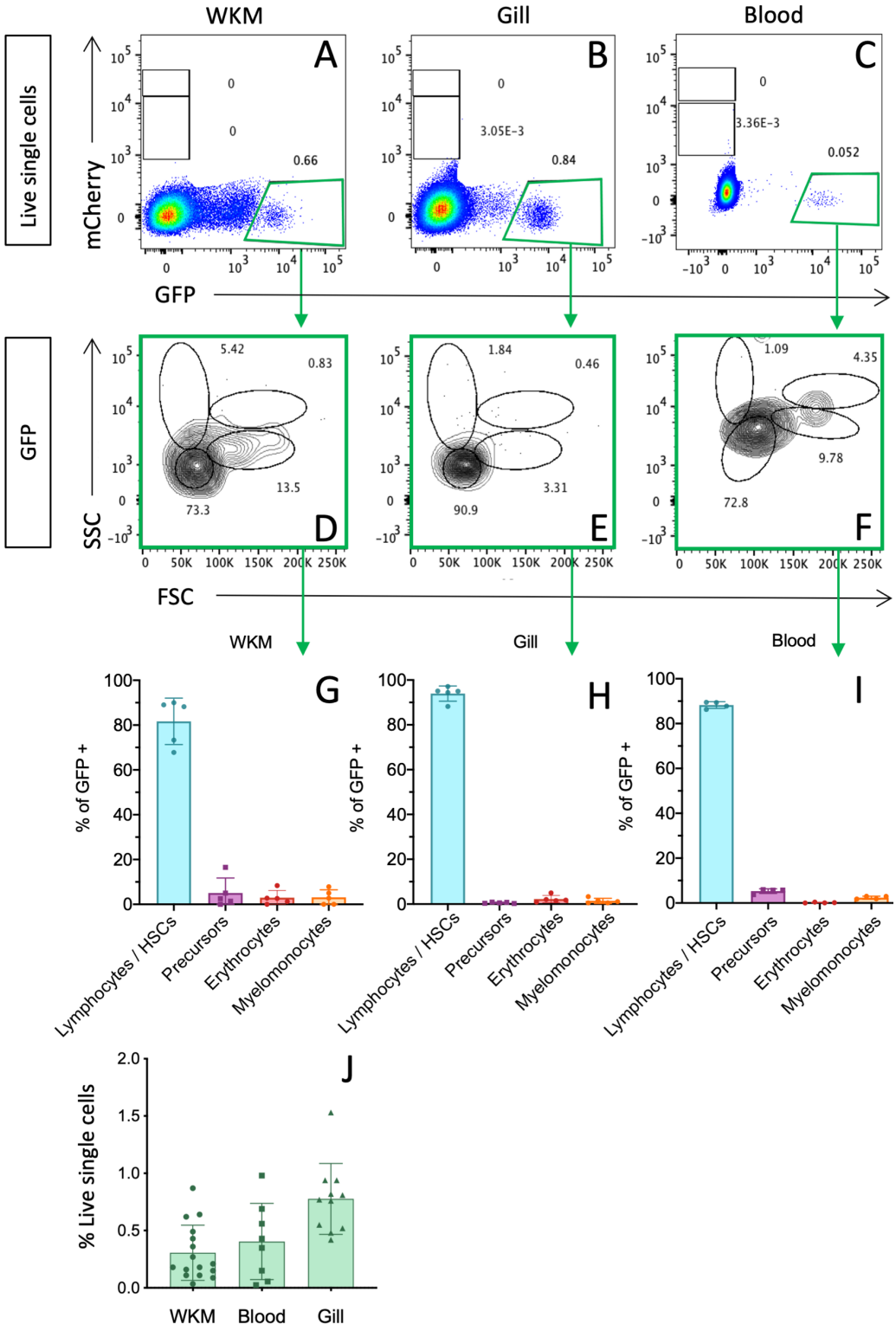

Fig. 3.10 Characterisation of *Runx*:GFP+ cells in adult zebrafish WKM, gill and blood.

Tg(Runx:GFP) transgenic WKM, gill tissue and blood were harvested from adult zebrafish to quantify the *Runx*:GFP+ cells as a percentage of total live cells and determine which FSC/SSC gate the cells were found in. N=5. **(A-C)** mCherry/ GFP flow cytometry plots. Green box indicates gating of *Runx*:GFP+ cells in each tissue. **(D-F)** *Runx*:GFP+ cells plotted on FSC/SSC to determine in which gate the majority of cells lie. Values on plot reflect the percentage of cells within each gate relative to total events in plot. **(G-I)** Percentage of all *Runx*:GFP+ cells in each tissue which were found in different FSC/SSC gates. **(J)** The proportion of *Runx*:GFP+ cells as a percentage of live single cells in each tissue. N= 9-15. Each dot represents 1 fish. Error bars indicate SD.

When *Runx*:mCherry ^{high} and ^{low} populations were compared to the *Runx*:GFP+ population, it was found that the population size of *Runx*:GFP+ cells was similar to that of *Runx*:mCherry ^{high} cells found in each of the tissues. On the other hand, *Runx*:mCherry ^{low} cells were much more abundant in the WKM and less abundant in either the gill or blood (Fig. 3.11). Given the similar population sizes between *Runx*:mCherry^{high} and *Runx*:GFP+ cells, it was hypothesised that these populations may be equivalent. Understanding the overlap between these fluorescent protein-expressing cells may help isolate HSCs to a higher purity, thereby improving the study of HSCs in zebrafish. To determine whether this was the case, adult *Tg(Runx:mCherry)* and *Tg(Runx:GFP)* fish were crossed and analysed by flow cytometry. Some of this work was carried out in collaboration with Chloe Tubman (MRes. Imperial College London).

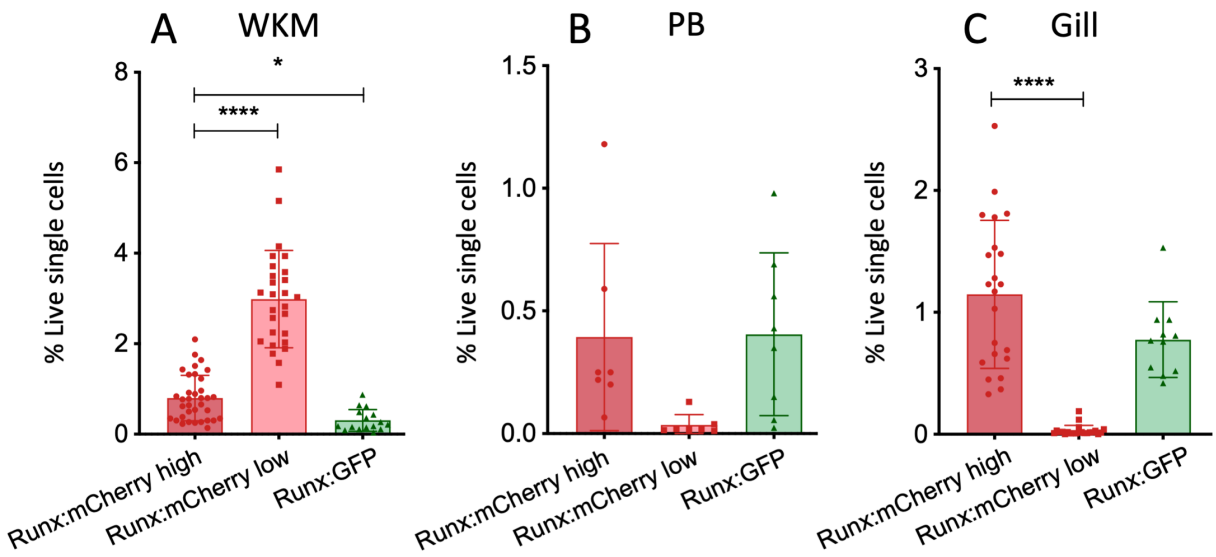

Fig. 3.11 Comparison of *Tg(Runx:mCherry)* and *Tg(Runx:GFP)* cells in WKM, blood and gill tissue.

WKM, blood and gill tissue were harvested from adult transgenic *Tg(Runx:mcherry)* and *Tg(Runx:GFP)* zebrafish and analysed by flow cytometry. **(A)** The proportion of *Runx*:mCherry ^{high} and ^{low} cells compared to *Runx*:GFP+ cells as a percentage of live single cells in the WKM. **(B)** The proportion of *Runx*:mCherry ^{high} and ^{low} cells compared to *Runx*:GFP+ cells as a percentage of live single cells in blood. **(C)** The proportion of *Runx*:mCherry ^{high} and ^{low} cells compared to *Runx*:GFP+ cells as a percentage of live single cells in the gill tissue. N= 7-35. Each dot represents 1 fish, mean and SD are shown. *P < 0.05, **P < 0.005, ***P < 0.0005, ****P < 0.00005. One-way ANOVA.

3.3.4 Similarities and differences between Runx:mCherry+ and Runx:GFP+ populations

In the WKM, it was difficult to discern the overlap of the two cell populations when examining *Runx*:mCherry; *Runx*:GFP samples, owing to the low fluorescence intensity of *Runx*:GFP+ cells and an auto-fluorescent population that was regularly observed in WKM samples (Fig. 3.12A). It was necessary, therefore, to remove some samples where auto-fluorescent cells interfered

with identification of double positive populations. Consequently, the number of double positive cells may be an underestimation in the WKM. In blood and gill tissues, which generally have a much clearer GFP/mCherry profile, overlapping populations were more readily discernible.

In the WKM, 0.5±0.2 % of live single cells were found to be GFP+ mCherry+. This was similar to both the mCherry ^{high} population found in the *Tg(Runx:mCherry)* fish, as well as the GFP+ population found in *Tg(Runx:GFP)* fish (Fig. 3.12G). As seen in both single transgenic fish, the double positive cells were also found predominantly within the lymphocyte compartment (77.6±15.3 %) (Fig. 3.12A & D). Interestingly, most *Runx*:mCherry ^{high} cells were overlapping with *Runx*:GFP+ cells (90.9±11.5 %) and nearly all *Runx*:GFP+ cells (99.7±0.4 %) were overlapping with *runx*:mCherry ^{high} cells (Fig. 3.12B & E). However, *Runx*:mCherry ^{low} cells did not overlap with the *Runx*:GFP+ cells (Fig. 3.12A, C & F). Taken together, this showed that the *Runx*:mCherry ^{high} population was roughly equivalent to the *Runx*:GFP+ population. Differences between fluorescent protein-expressing cell populations in *Tg(Runx:mCherry)* and *Tg(Runx:GFP*) may be linked to positional effects of the insertion sites of the transgenes, or to the presence of GFP in the cytosol while mCherry is trafficked to the nucleus (Tamplin *et al*., 2015). Of *Runx*:mCherry ^{high} and ^{low} cells together, 22.2±12.2 % overlapped with *Runx*:GFP+ cells (Fig. 3.12C & F). These data from adult WKM are concordant with the results of Tamplin *et al*. (2015), which found that 13±6 % of *Runx*:mCherry+ cells overlapped with *Runx*:GFP in the CHT of 3 dpf embryos.

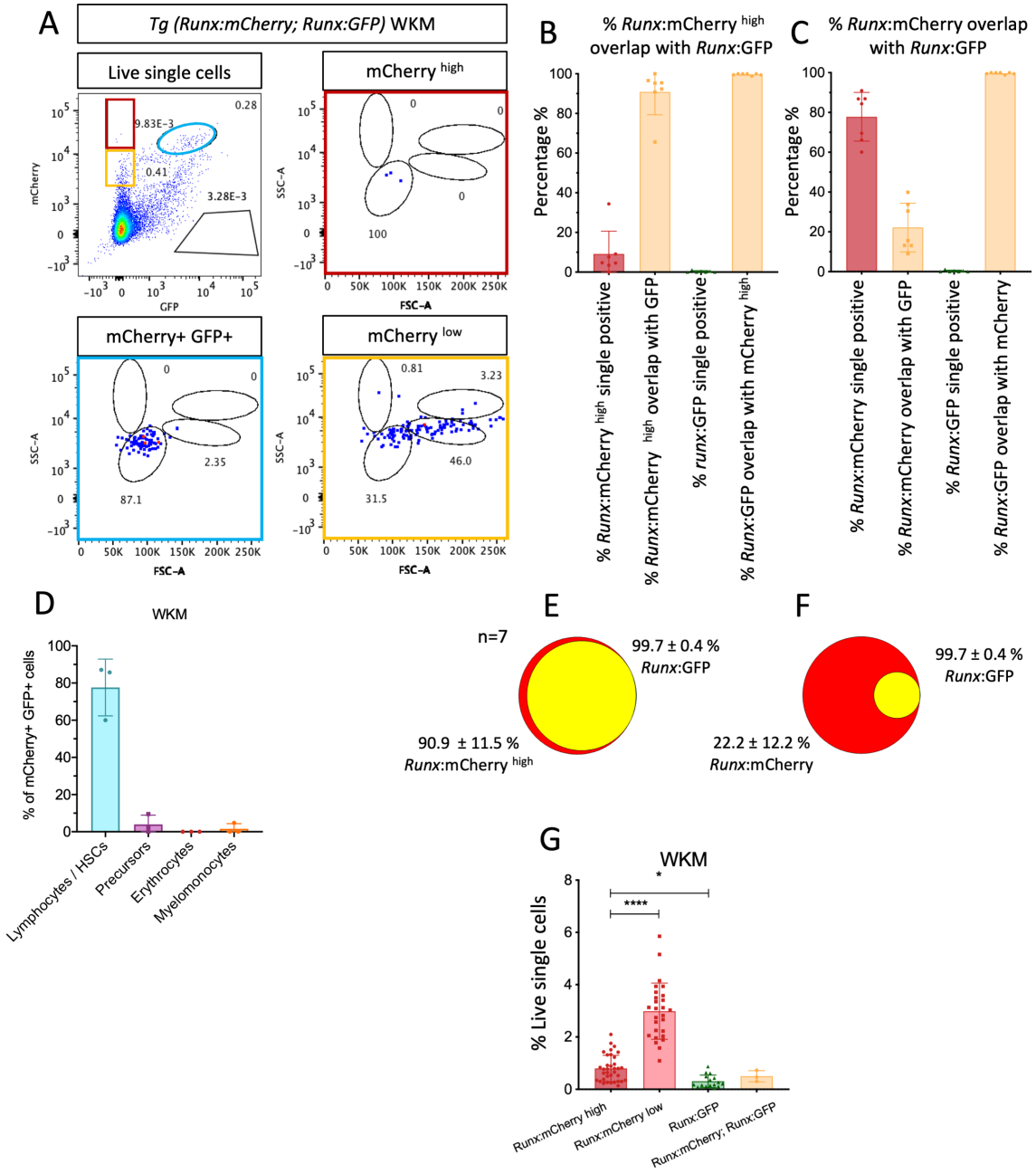

Fig. 3.12 The overlap of *Runx*:mCherry+ and *Runx*:GFP+ cells in the WKM of adult zebrafish.

Singe cell suspensions of transgenic *Tg(Runx:mCherry; Runx:GFP)* WKM from adult zebrafish were analysed by flow cytometry. N=7. Sample processing and data acquisition was carried out in collaboration with Chloe Tubman (MRes. Imperial College London). **(A)** Representative mCherry/GFP plot of *Tg(Runx:mCherry; Runx:GFP)* WKM. Red box indicates gating for *Runx*:mCherry ^{high} cells and yellow box indicates gating for *Runx*:mCherry ^{low} cells. Blue oval for *Runx*:mCherry+ *Runx*:GFP+ cells and black outline for *Runx*:GFP+ cells. Back-gating of each population on FSC/SSC shown. **(B)** The proportion of *Runx*:mCherry ^{high} single positive cells as a percentage of all *Runx*:mCherry ^{high} cells, the overlap of *Runx*:mCherry ^{high} cells with *Runx*:GFP+ cells, proportion of single positive *Runx*:GFP cells compared to all *Runx*:GFP+ cells and the overlap of *Runx*:GFP+ cells with *Runx*:mCherry ^{high} cells. **(C)** The proportion of *Runx*:mCherry (high and low) single positive cells as a percentage of all *Runx*:mCherry+ cells, the overlap of *Runx*:mCherry+ cells with *Runx*:GFP+ cells, proportion of single positive *Runx*:GFP cells relative to all *Runx*:GFP+ cells and the overlap of *Runx*:GFP+ cells with *Runx*:mCherry+ cells. **(D)** Percentage of *Runx*:mCherry+ *Runx*:GFP+ double positive cells found in different FSC/SSC gates. **(E&F)** Venn diagrams representing the overlap between *Runx*:mCherry ^{high} **(E)** or all *Runx*:mCherry+ cells **(F)** and *Runx*:GFP+ cells in WKM. **(G)** Comparison of the proportion of different *Runx*+ populations of all live single cells in the WKM. Each dot represents 1 fish. Mean and SD are shown. *P < 0.05, **P < 0.005, ***P < 0.0005, ****P < 0.00005. One-way ANOVA.

Both in the peripheral blood and gill, the *Runx*:mCherry ^{high} populations overlapped greatly with the *Runx*:GFP+ (97.4±0.7 % in the blood, 98.1±1.8 % in the gill), with only a few *Runx*:mCherry ^{high} events not being *Runx*:GFP+ (Fig. 3.13 & 3.14). The remaining single-colour *Runx*:mCherry ^{high} cells were all found in the lymphocyte compartment. In the blood, the entire *Runx*:GFP+ population overlapped with the *Runx*:mCherry+ population, with only a small *Runx*:mCherry ^{low} population not overlapping both in the gill and in the blood (Fig. 3.13 & 3.14). However, a small number of *Runx*:GFP single positive cells were identified in some gills (Fig. 3.13C & F). In order to further investigate, confocal microscopy was carried out on immunoassayed gills of *Tg(Runx:mCherry; Runx:GFP)* zebrafish. In line with the flow cytometry data, many GFP+ mCherry+ double positive cells were identified, as well as a small number of mCherry single positive cells. The cytosolic GFP and nuclear localised mCherry signal were observed (Fig. 3.15). However, no GFP single positive cells were identified in the gills, highlighting the rarity of these cells. Immunoassayed samples had a small amount of background non-specific immunofluorescence. Cells were distinguished from background autofluorescence by assessing size, morphology and the presence of nuclei, as identified by Draq5 nuclear staining.

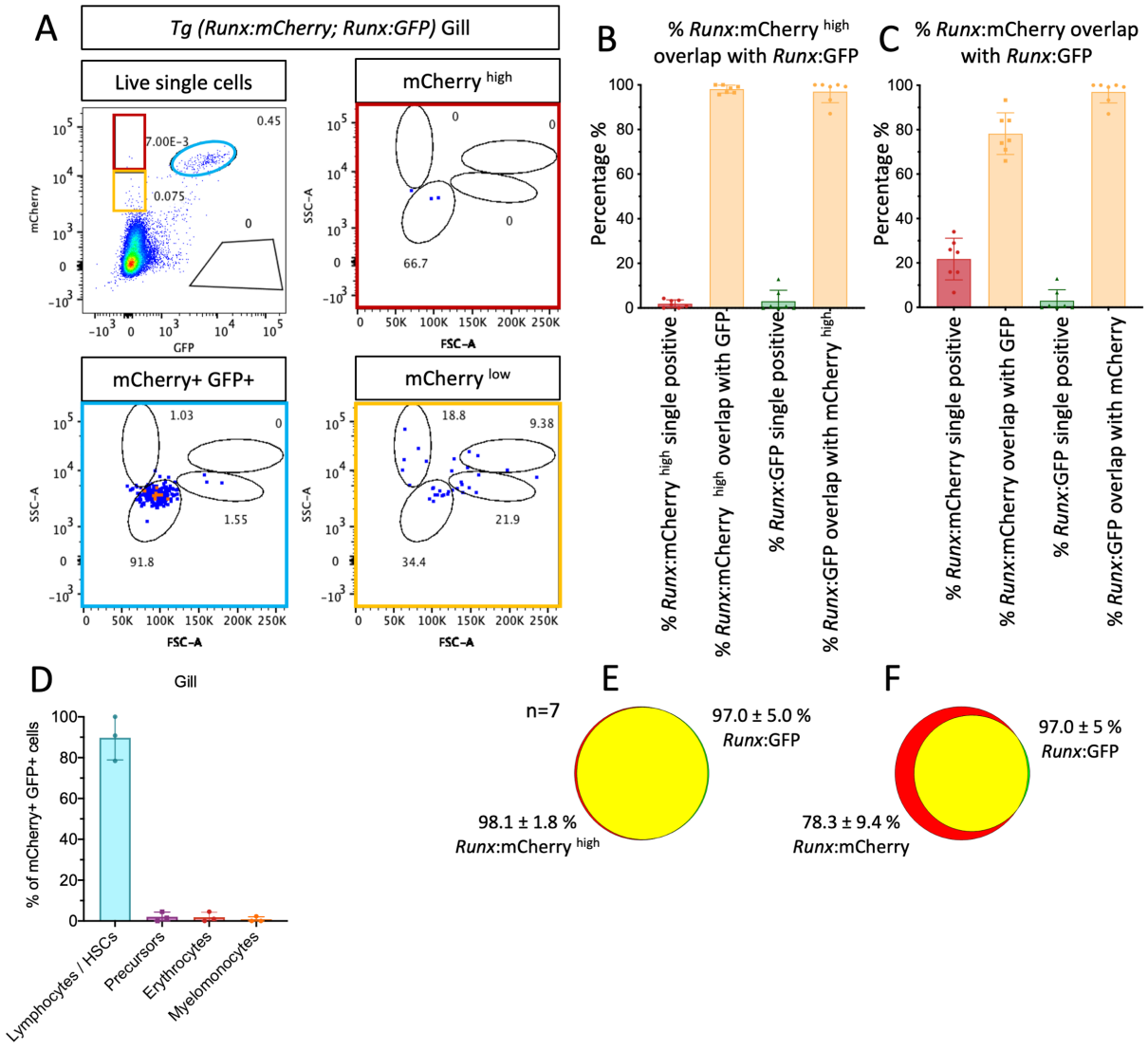

Fig. 3.13 The overlap of *Runx*:mCherry+ and *Runx*:GFP+ cells in the gills of adult zebrafish.

Singe cell suspensions of transgenic *Tg(Runx:mCherry; Runx:GFP)* gills from adult zebrafish were analysed by flow cytometry. N=7. Sample processing and data acquisition was carried out in collaboration with Chloe Tubman (MRes. Imperial College London). **(A)** Representative mCherry/GFP plot of *Tg(Runx:mCherry; Runx:GFP)* gills. Red box indicates gating for *Runx*:mCherry ^{high} cells and yellow box indicates gating for *Runx*:mCherry ^{low} cells. Blue oval for *Runx*:mCherry+ *Runx*:GFP+ cells and black outline for *Runx*:GFP+ cells. Back-gating of each population on FSC/SSC shown. **(B)** The proportion of *Runx*:mCherry ^{high} single positive cells as a percentage of all *Runx*:mCherry ^{high} cells, the overlap of *Runx*:mCherry ^{high} cells with *Runx*:GFP+ cells, proportion of single positive *Runx*:GFP cells compared to all *Runx*:GFP+ cells and the overlap of *Runx*:GFP+ cells with *Runx*:mCherry ^{high} cells. **(C)** The proportion of *Runx*:mCherry (high and low) single positive cells as a percentage of all *Runx*:mCherry+ cells, the overlap of *Runx*:mCherry+ cells with *Runx*:GFP+ cells, proportion of single positive *Runx*:GFP cells relative to all *Runx*:GFP+ cells and the overlap of *Runx*:GFP+ cells with *Runx*:mCherry+ cells. **(D)** Percentage of *Runx*:mCherry+ *Runx*:GFP+ double positive cells found in different FSC/SSC gates. **(E&F)** Venn diagrams representing the overlap between *Runx*:mCherry ^{high} **(E)** or all *Runx*:mCherry+ cells **(F)** and *Runx*:GFP+ cells in gills. Each dot represents 1 fish. Mean and SD are shown. *P < 0.05, **P < 0.005, ***P < 0.0005, ****P < 0.00005. One-way ANOVA.

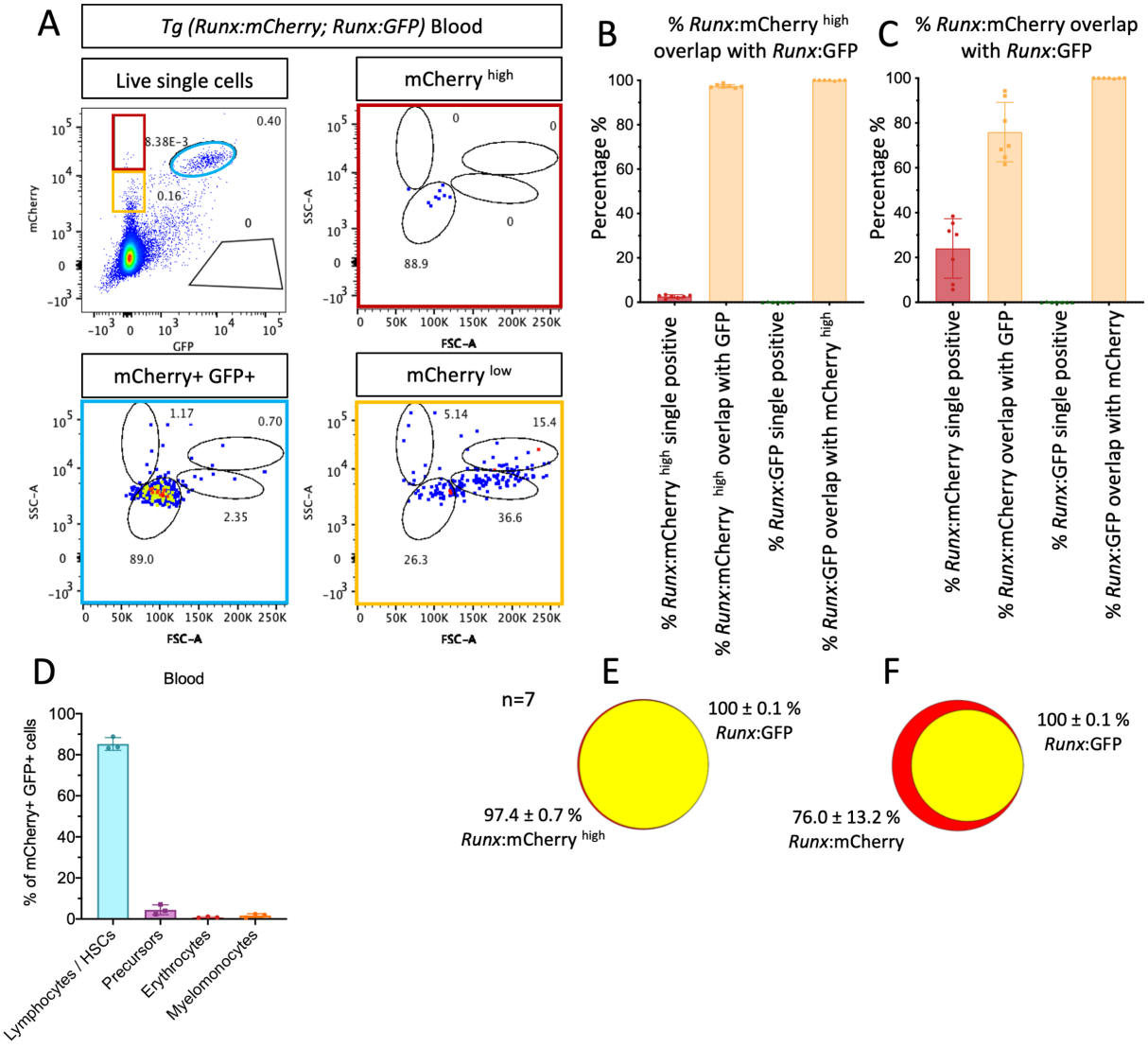

Fig. 3.14 The overlap of *Runx*:mCherry+ and *Runx*:GFP+ cells in the blood of adult zebrafish.

Singe cell suspensions of transgenic *Tg(Runx:mCherry; Runx:GFP)* blood from adult zebrafish were analysed by flow cytometry. N=7. Sample processing and data acquisition was carried out in collaboration with Chloe Tubman (MRes. Imperial College London). **(A)** Representative mCherry/GFP plot of *Tg(Runx:mCherry; Runx:GFP)* blood. Red box indicates gating for *Runx*:mCherry ^{high} cells and yellow box indicates gating for *Runx*:mCherry ^{low} cells. Blue oval for *Runx*:mCherry+ *Runx*:GFP+ cells and black outline for *Runx*:GFP+ cells. Back-gating of each population on FSC/SSC shown. **(B)** The proportion of *Runx*:mCherry ^{high} single positive cells as a percentage of all *Runx*:mCherry ^{high} cells, the overlap of *Runx*:mCherry ^{high} cells with *Runx*:GFP+ cells, proportion of single positive *Runx*:GFP cells compared to all *Runx*:GFP+ cells and the overlap of *Runx*:GFP+ cells with *Runx*:mCherry ^{high} cells. **(C)** The proportion of *Runx*:mCherry (high and low) single positive cells as a percentage of all *Runx*:mCherry+ cells, the overlap of *Runx*:mCherry+ cells with *Runx*:GFP+ cells, proportion of single positive *Runx*:GFP cells relative to all *Runx*:GFP+ cells and the overlap of *Runx*:GFP+ cells with *Runx*:mCherry+ cells. **(D)** Percentage of *Runx*:mCherry+ *Runx*:GFP+ double positive cells found in different FSC/SSC gates. **(E&F)** Venn diagrams representing the overlap between *Runx*:mCherry ^{high} **(E)** or all *Runx*:mCherry+ cells **(F)** and *Runx*:GFP+ cells in blood. Each dot represents 1 fish. Mean and SD are shown. *P < 0.05, **P < 0.005, ***P < 0.0005, ****P < 0.00005. One-way ANOVA.

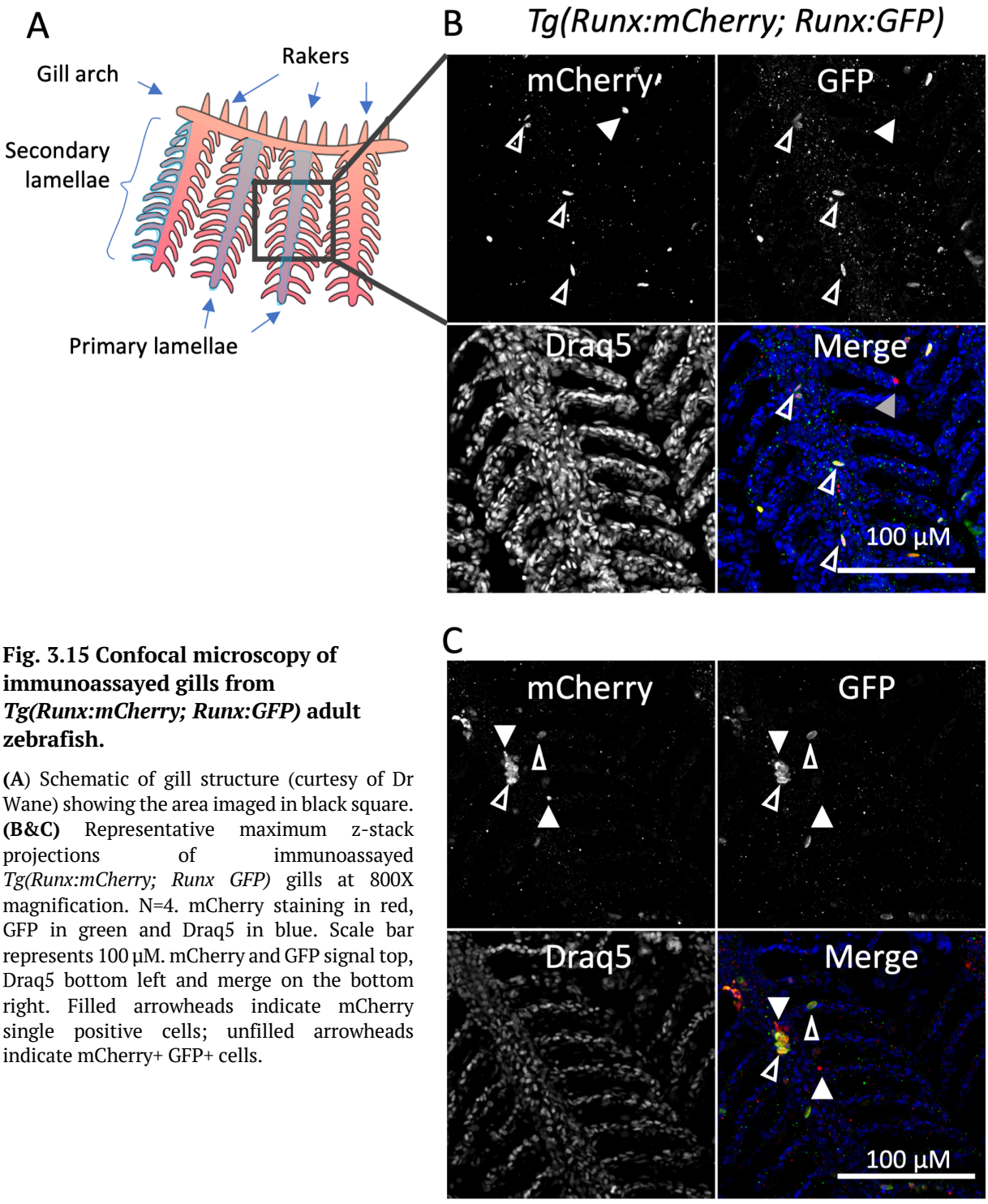

Fig. 3.15 Confocal microscopy of immunoassayed gills from *Tg(Runx:mCherry; Runx:GFP)* adult zebrafish.

(A) Schematic of gill structure (curtesy of Dr Wane) showing the area imaged in black square. **(B&C)** Representative maximum z-stack projections of immunoassayed *Tg(Runx:mCherry; Runx GFP)* gills at 800X magnification. N=4. mCherry staining in red, GFP in green and Draq5 in blue. Scale bar represents 100 µM. mCherry and GFP signal top, Draq5 bottom left and merge on the bottom right. Filled arrowheads indicate mCherry single positive cells; unfilled arrowheads indicate mCherry+ GFP+ cells.

3.3.5 Investigation of the cell types that express the Runx:mCherry construct

There was a relatively high abundance (1.1 %) of *Runx*:mCherry+ cells embedded in and circulating through the gill. 97.5 % of these cells were *Runx*:mCherry ^{high} and were found in the lymphocyte compartment by flow cytometry. As previously suggested, cells other than lymphocytes may be found within the lymphocyte scatter gates and these were investigated for the expression of the *Runx*:mCherry transgene. The promoter element driving fluorophore expression in the *Runx* transgenic construct originated from a mouse P1 enhancer sequence of *Runx1* (Tamplin *et al.,* 2015; Nottingham *et al.,* 2007). In order to elucidate which other cell types may express the fluorophore, it was important to investigate other cell types that express upstream transcription factors that would activate the *Runx1* enhancer and drive the transcription of the fluorophore downstream of the transgenic mouse P1 enhancer element.

3.3.5.1 Investigating the overlap of Runx:mCherry+ and IgM:GFP+ cells in the lymphocyte compartment

It has been established that *Runx1* is active in the development of B cells in both mammals and zebrafish (Chi *et al*., 2018; Niebuhr *et al*., 2013). Additionally, both B cells and the *Runx*+ cells from the zebrafish gill are found in the lymphocyte compartment by flow cytometry. Furthermore, this study has shown that emergence of embedded *Runx*:mCherry+ cells in the gill coincides with the development of adaptive immunity in the zebrafish (Fig. 3.2 & 3.3) (Trede *et al*., 2001; Page *et al.,* 2013). Consequently, it was hypothesised that the *Runx*+ cells that were observed embedded in the gill could be a type of B cell. To further investigate this hypothesis, *Tg(Runx:mCherry)* transgenic zebrafish were crossed to *Tg(IgM:GFP)* zebrafish in which *IgM*+ B cells express GFP. This enabled the detection of any double positive cell population. However, in the tissues under consideration in this study (WKM, blood and gill), no double positive population was found either by flow cytometry, or by immunostaining and confocal microscopy (Fig. 3.16).

In order to accurately discern double positive cells, the lymphocyte compartment was interrogated specifically. This was done to rule out auto-fluorescent cells that could contaminate the live cell compartment without being confined to a major blood cell lineage, and instead being spread evenly throughout the FSC/SSC dot plot. Through this analysis, it was found that there is 0 % overlap between *Runx*+ and *IgM*+ cells in the tissues investigated

(Fig. 3.16A-C). The distinct localisation of each fluorescent protein-expressing cell type in the gill was confirmed through imaging of single and double positive fish of each transgenic line. *IgM*:GFP+ cells were largely found in the arch of individual gills, with a relatively small number of fluorescent protein-expressing cells found in the primary and secondary lamellae. *Runx*:mcherry+ cells, on the other hand, were found evenly spread throughout the primary and secondary lamellae, with very few cells localised in the gill arches (Fig. 3.16D, F, G). However, discerning *Runx*:mCherry+ cells in the gill arch was more difficult due to significant background fluorescence in the arch following immunostaining in some cases.

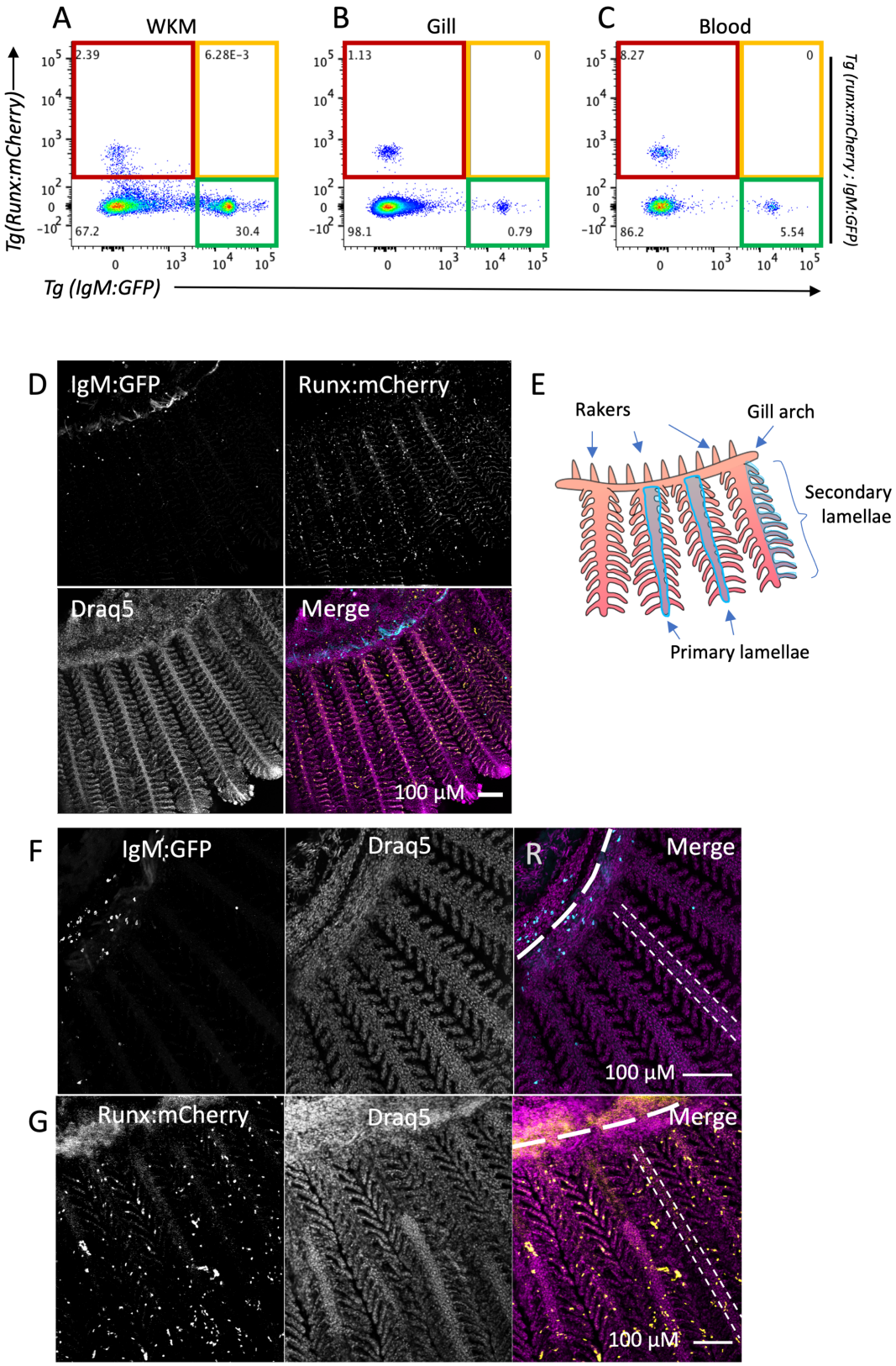

Fig. 3.16 Flow cytometry and confocal microscopy of adult *Tg(Runx:mCherry; IgM:GFP)* tissues.

WKM, gill and blood were collected from adult *Tg(Runx:mcherry; IgM:GFP)* zebrafish and analysed by flow cytometry. (**A-C**) mCherry/GFP plots of lymphocyte population, with gating of fluorescent populations. Red box outline indicates gating for mCherry+ cells, yellow box outline for mCherry+ GFP+ cells and the green box outline shows gating of GFP+ cells. Values within gates reflect the percentage of events within each gate relative to total

events in the lymphocyte compartment in FSC/SSC plot. N=3. (**D**) Representative maximum z-stack projections of immunoassayed *Tg(Runx:mCherry; IgM:GFP)* gills at 170X magnification. **(D,F,G)** mCherry staining in yellow, GFP in cyan and Draq5 in magenta. Scale bar represents 100 µM. mCherry and GFP signal top, Draq5 bottom left and merged on the bottom right. **(E)** Schematic of gill structure. **(F,G)** Representative maximum z-stack projections of immunoassayed *Tg(IgM:GFP)* **(F)** and *Tg(Runx:mcherry)* **(G)** transgenic zebrafish gills at 340X magnification. R represents gill rakers, thick dashed line indicates location of gill arch and thin dashed line outlines a primary lamella.

3.3.5.2 Investigating the overlap of Runx:mCherry+ and lck:GFP+ cells in the lymphocyte compartment

To determine whether *Runx*+ cells coincide with *lymphocyte-specific protein tyrosine kinase* (*lck)*+ cells in the zebrafish, confocal microscopy was utilised. Initially, due to the abundance of *lck*+ cells in the gill, it appeared that there may have been overlap between *Runx*+ and *lck*+ cells. However, high magnification and z resolution revealed that mCherry and GFP fluorescence did not come from the same cells. Furthermore, flow cytometry analysis revealed that there was no overlap between *Runx*:mCherry+ and *lck*:GFP+ cells in the lymphocyte compartment of the gill, blood and WKM of adult zebrafish (Fig. 3.17A-C).

3.3.5.3 Investigating the overlap of Runx:mCherry+ and CD41:GFP+ cells in the lymphocyte compartment

At the embryonic stage, there is significant (44±8 %) overlap of *Runx*:mCherry+ cells with *CD41*:GFP+ cells, and 60±12 % overlap of *CD41*:GFP+ with *Runx*:mCherry+ cells in the CHT (Tamplin *et al*., 2015). The group investigated the overlap between these cells in the CHT at 72 hpf by confocal microscopy. At this stage, the *CD41*:GFP+ cells present in the CHT are *CD41*:GFP ^{low} HSPCs. Circulating mature *CD41*:GFP ^{high} thrombocytes arise in the developing zebrafish from approximately 72 hpf onwards (Lin *et al*., 2005). However, *c-mpl* ^{high} and CD41:GFP+ thrombocyte precursor cells were identified as early as 42 hpf (Bertrand *et al*., 2008). Given the overlap between *CD41*:GFP+ and *Runx*:mCherry+ cells in HSPCs and their closely related transcriptional programming (Tang *et al*., 2017), it was hypothesised that *CD41*:GFP ^{high} thrombocytes may also express *Runx1* and, hence, could express the *Runx*:mCherry transgene. Unfortunately, a cross between *Tg(Runx:mCherry)* and *Tg(CD41:GFP)* fish was not possible in the duration of this project due to time constraints. However, the fluorescent cells in each strain were investigated independently. Examination by immunostaining and confocal microscopy of the gills from each transgenic line individually revealed a similar distribution of the *Runx*:mCherry+ cells in the gill to that

observed in *CD41*:GFP+ gills (Fig. 3.18). Two distinct cell distribution patterns were observed in both lines. Firstly, in most samples fluorescent cells were evenly distributed throughout the gill structure with no obvious bias between the primary and secondary lamellae, or the proximal and distal tip of primary lamellae (Fig. 3.18). The second cell distribution pattern, which was rarer and has only been observed in *Runx*:mCherry+ and *CD41*:GFP+ transgenic fish, was the presence of clusters of fluorescent protein-expressing cells at the base (proximal end) of primary lamellae (Fig. 3.19A & B). This distribution of fluorescent protein-expressing cells was not observed in either *IgM*:GFP+ or *lck*:GFP+ gills. However, an insufficient number of animals have been studied for the distribution of cells specifically to determine the frequency or significance of this phenotype. Immunostaining and confocal microscopy of *Tg(Runx:mCherry)* and *Tg(CD41:GFP)* gills was carried out by Chloe Tubman (MRes. Imperial College London).

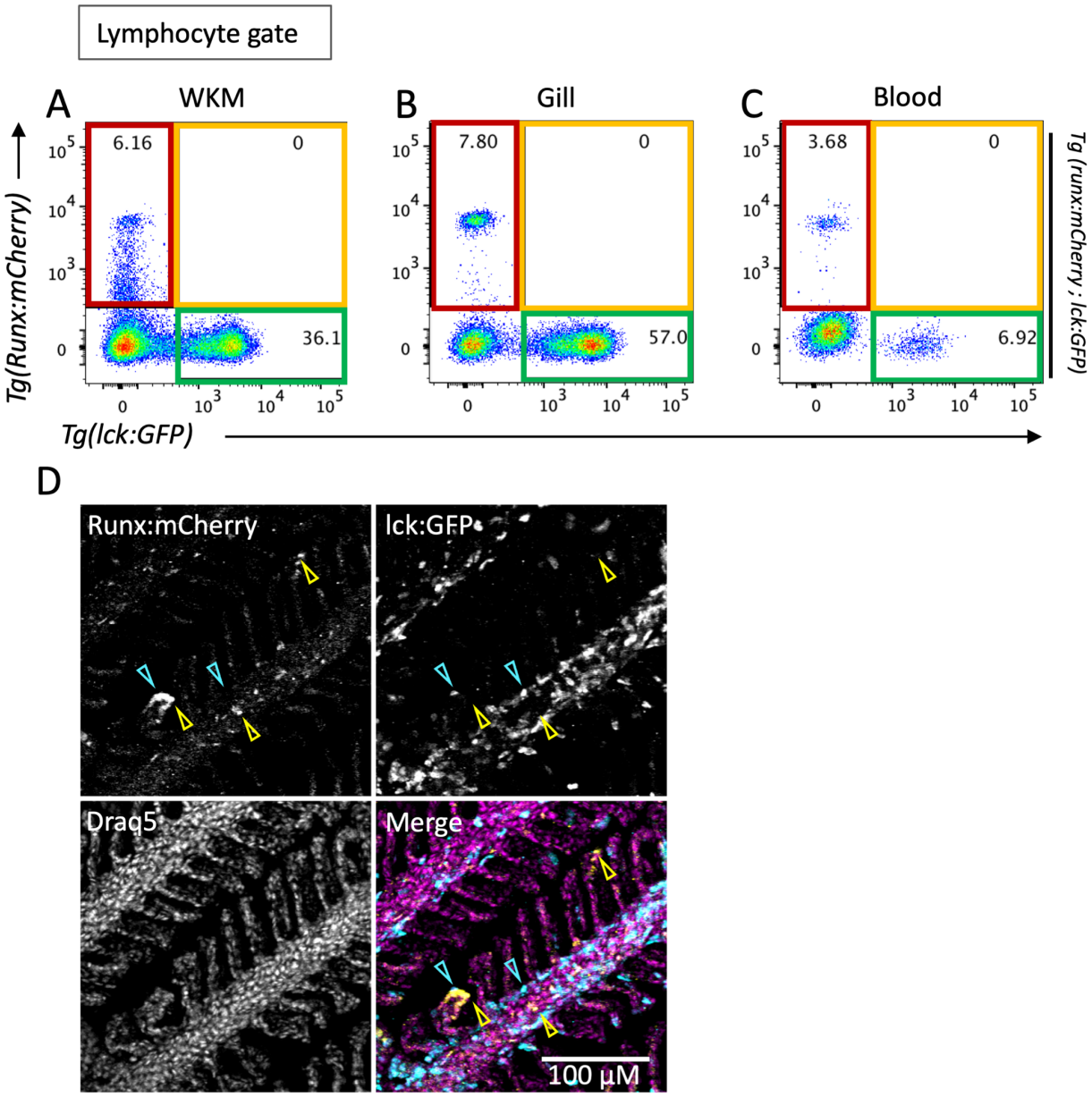

Fig. 3.17 Flow cytometry and confocal microscopy of adult *Tg(Runx:mCherry; lck:GFP)* tissues.

WKM, gill and blood were collected from adult *Tg(Runx:mCherry; lck:GFP)* zebrafish and analysed by flow cytometry. (**A-C**) mCherry/GFP plots of lymphocyte compartment, with gating of fluorescent populations. Red box outline indicates gating for *Runx*:mCherry+ cells, yellow box outline for mCherry+ GFP+ cells and the green box outline shows gating of *lck:GFP*+ cells. Values within gates reflect the percentage of events within each gate relative to total events in the lymphocyte compartment in FSC/SSC plot. N=7. **(D)** Representative maximum z-stack projection of immunoassayed *Tg(Runx:mCherry; lck:GFP)* gills at 400X magnification. mCherry staining in yellow, GFP in cyan and Draq5 in magenta. Scale bar represents 100 µM. mCherry and GFP signal top, Draq5 bottom left and merge on the bottom right. Unfilled cyan and yellow arrow heads indicate *lck*:GFP+ and *Runx*:mCherry+ cells respectively.

Furthermore, flow cytometry analysis, carried out in collaboration with Chloe Tubman (MRes. Imperial College London) has confirmed that both *Runx*:mCherry ^{high} cells and *CD41*:GFP ^{high} thrombocytes were found largely in the lymphocyte compartment of WKM and gill tissues. Of the *CD41*:GFP ^{high} cells in the WKM, 79 % (SD 6.8 %) were found in the lymphocyte compartment. This number was 88 % (SD 1.6 %) in the gill tissue (Fig. 3.19). The population sizes, in terms of percentage of all live single cells, of both *Runx*:mCherry ^{high} and *CD41*:GFP ^{high} cells were similar in the gill and WKM (Fig. 3.20). In the WKM, it was found that *Runx*:mCherry ^{high} cells contribute 0.8 % to live single cells while *CD41*:GFP ^{high} cells contribute on average 0.3 %. However, the discrepancy between these can partially be attributed to differences in the number of fish analysed. Furthermore, the difference was not found to be statistically significant. Indeed, these results were consistent with findings from Ma *et al,* (2011) who showed that 0.81 ± 0.41% of WKM cells were *CD41*:GFP ^{high} cells . In the gill, the *Runx*:mCherry ^{high} population represented 1.1 % of live cells and the *CD41*:GFP ^{high} population represented 0.9 %. Meanwhile, the *Runx*:mCherry ^{low} and *CD41*:GFP ^{low} cells constituted 0.03 % and 0.08 % of live cells in the gill respectively. Although there were some similarities in the distribution and abundance of *Runx*:mCherry ^{high} cells and *CD41*:GFP ^{high} cells in the gill, no conclusions relating to co-expression of the transgenes can be drawn from a comparison between fluorescent protein-expressing cells in different animals. However, it would be interesting to build upon this data in the future by crossing these lines to investigate potential overlap between *CD41*:GFP+ and *Runx*:mCherry+ cells in the WKM and gill tissue.

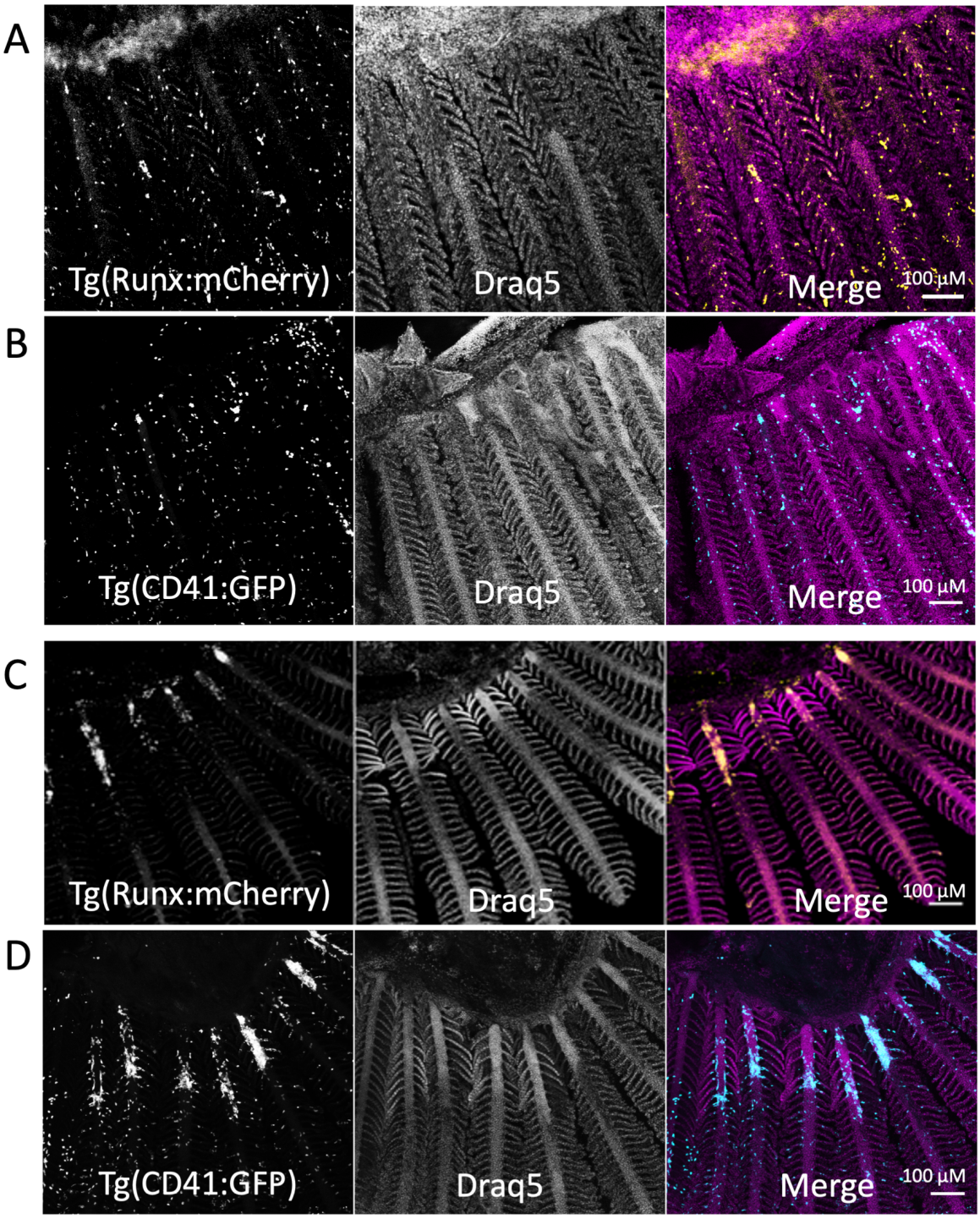

Fig. 3.18 Comparison of *Runx*:mCherry+ and *CD41*:GFP+ cell distributions in the gill.

(A,B) Representative maximum z-stack projection of immunoassayed *Tg(Runx:mCherry)* **(A)** and *Tg(CD41:GFP)* **(B)** gills at 170X magnification. **(C,D)** Maximal z-stack projection of rare phenotype in *Tg(Runx:mCherry)* **(C)** and *Tg(CD41:GFP)* **(D)** gills at 170X magnification. N=4, for each transgenic. Sample processing and data acquisition were carried out by Chloe Tubman (MRes. Imperial College London). mCherry staining in yellow, GFP in cyan and Draq5 in magenta. Scale bar represents 100 µM. mCherry / GFP signal on the left, Draq5 centre and merge right.

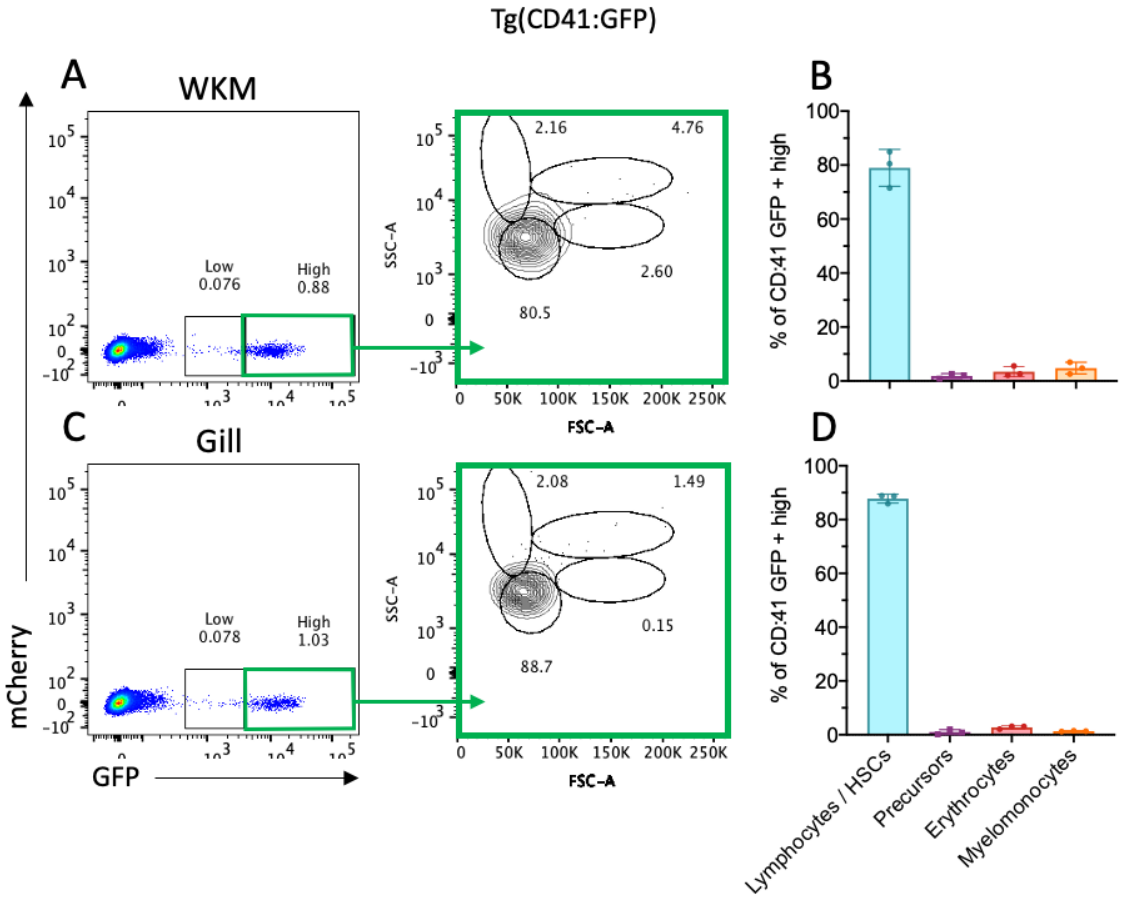

Fig. 3.19 Characterisation of *CD41*:GFP+ cells in adult zebrafish WKM and gill.

Sample processing and data acquisition was done in collaboration with Cloe Tubman (MRes. Imperial College London). *Tg(CD41:GFP)* transgenic WKM and gill tissue were harvested from adult zebrafish to quantify the *CD41*:GFP ^{high} cells as a percentage of total live cells and determine which FSC/SSC compartment the cells were found in. Values on plot reflect the percentage of cells within each gate relative to total events in plot. N=3. **(A, C)** mCherry/ GFP flow cytometry plots. Green box indicates gating of *CD41*:GFP ^{high} cells in each tissue followed by the back gating of *CD41*:GFP ^{high} cells to determine which FSC/SSC compartment they are found in. **(B, D)** Percentage of all *CD41*:GFP ^{high} cells found in different FSC/SSC gates. Mean and SD are shown. Each dot represents 1 fish.

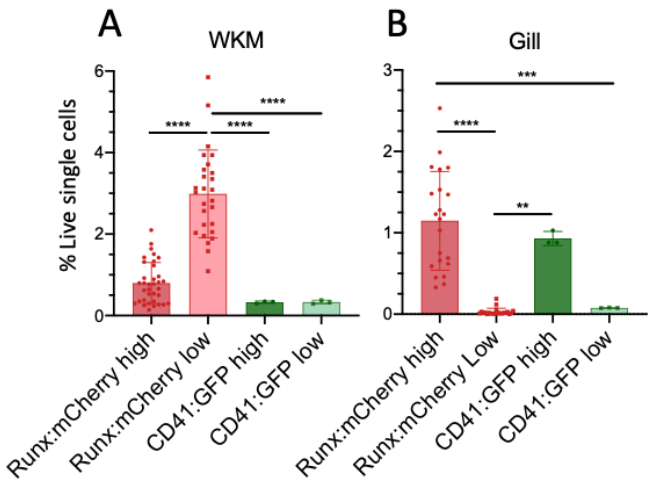

Fig. 3.20 Comparison of the proportion of *Runx*:mCherry+ and *CD41*:GFP+ cells in WKM and gill tissue.

WKM and gill tissue were harvested from adult transgenic *Tg(Runx:mcherry)* and *Tg(CD41:GFP)* zebrafish and analysed by flow cytometry. **(A, B)** The proportion of *Runx*:mCherry ^{high} and ^{low} cells compared to *CD41*:GFP ^{high} and ^{low} cells as a percentage of live single cells in the WKM **(A)** and the gill **(B)** N=3-35. Each dot represents 1 fish. Mean and SD shown. *P < 0.05, **P < 0.005, ***P < 0.0005, ****P < 0.00005. One-way ANOVA.

3.3.6 Characterisation and quantification of immune cells found in the flow cytometry lymphocyte compartment of zebrafish

Owing to the abundance and variety of hematopoietic reporter cells found within the lymphocyte compartment in different transgenics, it was important to quantify the proportion of different cell types that contributed to this compartment as a whole. For this purpose, transgenic lines that are known to express fluorescent proteins in cells found within the lymphocyte compartment were investigated, including *Tg(lck:GFP)*, *Tg(IgM:GFP)*, *Tg(CD41:GFP)* and *Tg(Runx:mCherry)*. The WKM, gills and blood from individual fish were harvested and analysed by flow cytometry. As previously highlighted, there was no overlap between *Runx*+ cells and either *lck*+ or *IgM*+ cells (Fig. 3.16, 3.17). Therefore, the data from these cell populations could be utilised to determine their contribution to the lymphocyte compartment as a whole. However, the same could not be assumed for the *CD41*+ cells, as the overlap between them and *Runx*+ cells has not been determined in adult zebrafish. It must also be noted that the possible overlap between *lck*+ and *IgM*+ cells has not been investigated by microscopy in this study. However, as will be described in detail later in this chapter, transcript analysis carried out on sorted cell populations suggests that there was no co-expression of *lck* or *IgM* in *IgM*:GFP+ or *lck:*GFP+ cells. *lck*:GFP+ sorted cells were not found to express B cell-specific genes and likewise, *IgM*:GFP+ cells were not found to express *lck* (Fig. 3.25 & 3.26).

In the WKM, *lck*:GFP+ cells were found to comprise the largest population within the lymphocyte compartment, contributing 38.3 % (SD 14.4 %) on average, followed by *IgM*:GFP+ cells at 21.5 % (SD 5.6 %). The *Runx*:mCherry+ cells contributed a total of approximately 5.8%, with *Runx*:mCherry ^{low} cells contributing 3.5 % (SD 0.7 %) and *Runx:*mCherry ^{high} cells 2.3 % (SD 0.5 %; Fig. 3.21I & 3.22).

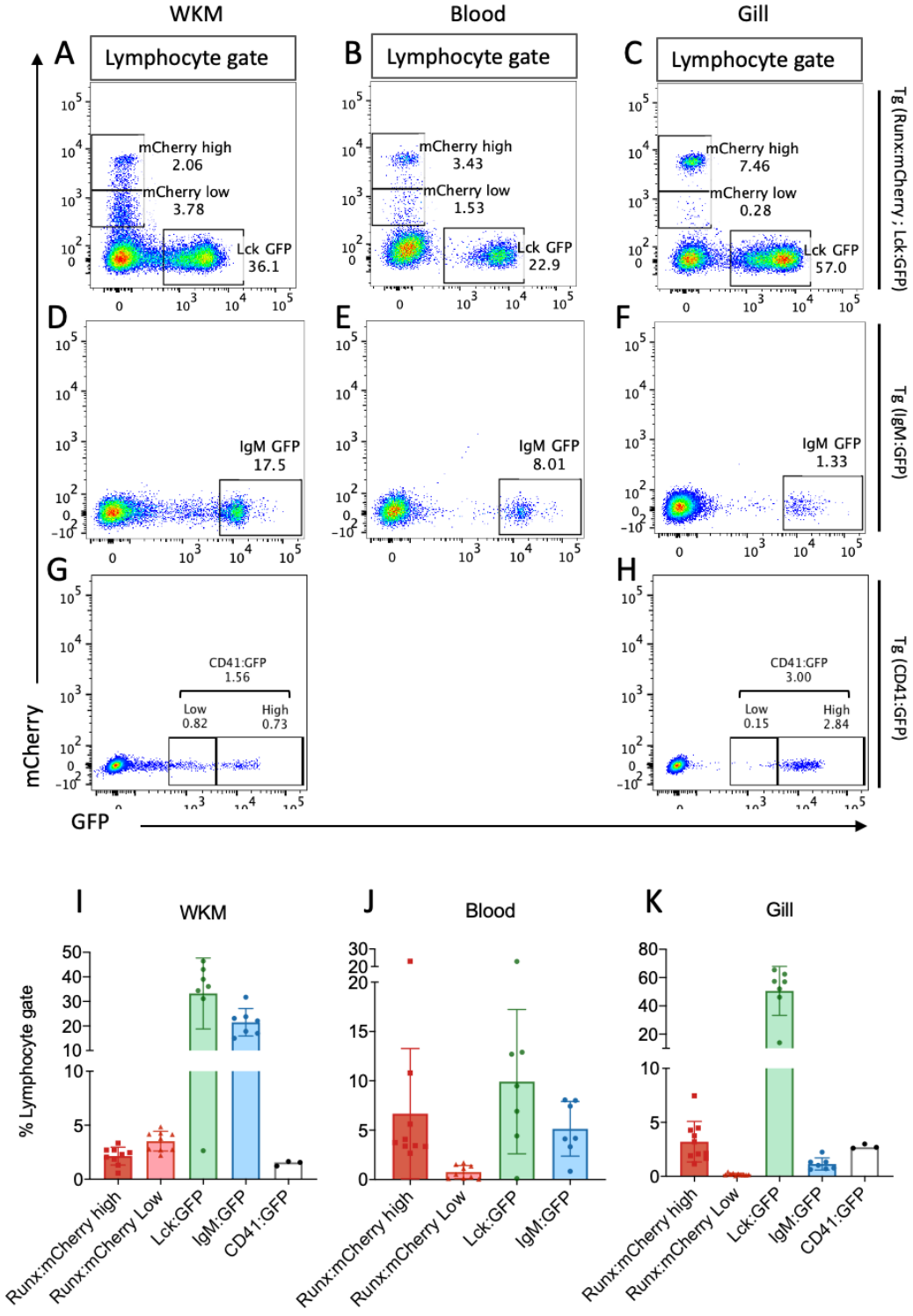

Fig. 3.21 Dissection of the adult zebrafish lymphocyte compartment in WKM, gill and blood.

WKM, gill and blood were harvested from adult *Tg(Runx:mCherry; lck:GFP)*, *Tg(IgM:GFP)* and *Tg(CD41:GFP)* zebrafish and single cell suspensions were analysed by flow cytometry. (A-H) mCherry/GFP plots of the lymphocyte compartment of each transgenic line. Top row: *Tg(Runx:mCherry; lck:GFP)* WKM (**A**) blood (**B**) and gill (**C**). Middle row: *Tg(IgM:GFP)* WKM (**D**) blood (**E**) and gill (**F**). Bottom row: *Tg(CD41:GFP)* WKM (**G**) and gill (**H**). Sample processing and data acquisition of *Tg(CD41:GFP)* fish was carried out in collaboration with Chloe Tubman (MRes. Imperial College London). (**I-K**) Quantification of the proportion each transgenic fluorescent protein-expressing cell type contributed to lymphocyte compartment as a percentage in the WKM (**I**), blood (**J**) and gill (**K**). N= 3-7. Each dot represents 1 fish. Bar graphs show mean and SD.

In the gill, *lck*+ cells remained the dominant population, making up an average of 56 % (SD 17.3 %) of the lymphocyte population. However, the *IgM*+ cells only contributed 1.1 % (SD 0.6 %) in the gill, while the *Runx*:mCherry ^{high} cells contributed 3.2 % (SD 2 %) on average. This was similar to the percentage of *CD41*+ cells at 2.7 % (SD 0.2 %) (Fig. 3.21K & 3.22). Meanwhile, the *lck*+ population was significantly lower in the blood than in either the WKM or gill, contributing only 11.6 % (SD 7.3 %) to the lymphocyte compartment in the blood. *IgM*+ cells contributed 5.8 % (SD 2.8 %) and *Runx*:mCherry ^{high} cells 6.7 % (SD 7.4 %) to the lymphocyte compartment on average. In one fish, an overwhelming 23 % of the lymphocyte compartment in the blood was occupied by *Runx*:mCherry ^{high} cells (Fig. 3.21J & 3.22).

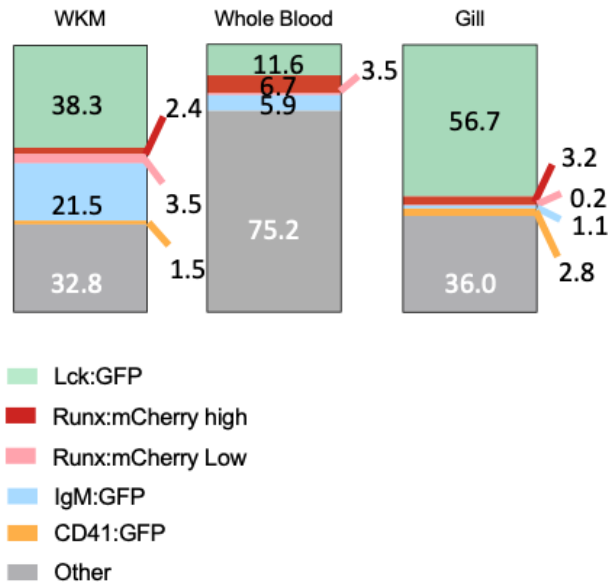

Fig. 3.22 Comparison of the proportions that transgenic fluorescent protein-expressing cells contribute to the lymphocyte compartment in the WKM, blood and gills.

Stacked bar charts indicating the proportion, as a percentage, that *lck*:GFP, *Runx*:mCherry ^{high}, *Runx*:mCherry ^{low}, *IgM*:GFP and *CD41*:GFP cells contributed to the lymphocyte compartment. Values within each band indicate the mean average percentage. N= 3-7.

3.3.7 Transcript analysis in Runx+ cells in WKM and gill

Using flow cytometry, a difference between *Runx*:mCherry ^{high} and ^{low} cells was identified based on their size and granularity (FSC/SSC, Fig. 3.7). Furthermore, *Runx*:mCherry ^{high} cells have been shown to reside, in abundance, in the gill and head kidney of adult zebrafish (Fig. 3.3 & 3.8; Tamplin *et al*., 2015). On the other hand, *Runx*:mCherry ^{low} cells were much more abundant in the WKM and were only found in low numbers in the blood and gills. It is believed that HSPCs reside among the *Runx*:mCherry ^{high} population as these cells have the expected FSC/SSC properties (Traver *et al* 2003). However, the function of *Runx*:mCherry ^{high} cells in the gills remains elusive. *Runx*:mCherry ^{high} and ^{low} cells may have distinct functions that have not been fully elucidated and which may depend on their inter-tissue localisation.

In order to gain a better understanding of the functional differences between *Runx*:mCherry+ populations in different tissues and those that are present with different fluorescence intensities, gene transcript profiles were investigated. Using FACS, large populations of *Runx*:mCherry ^{high} and ^{low} cells were isolated from the WKM and gills of individual fish where possible. When insufficient cell numbers were harvested for transcript analysis from individual fish, 3 or more transgenic fish were pooled in order to obtain at least 100,000 cells per sample. This enabled higher quality of RNA to be isolated and analysed. To sort fluorescent protein-expressing cells, live single cells were selected followed by application of gates for fluorescent populations of interest: *Runx*:mCherry ^{high} and ^{low}, *lyz*:GFP+, *lck*:GFP+ and *IgM*:GFP+. When isolating *Runx*:mCherry ^{high} and ^{low} cells from WKM, gates were applied based on fluorescence intensity, followed by gates selecting for FSC ^{low} and FSC $^{mid\text{-}high}$ for *Runx*:mCherry ^{high} and ^{low} cells respectively (Fig. 3.23). RT-qPCRs were subsequently carried out to assay the transcript levels of key genes across each population.

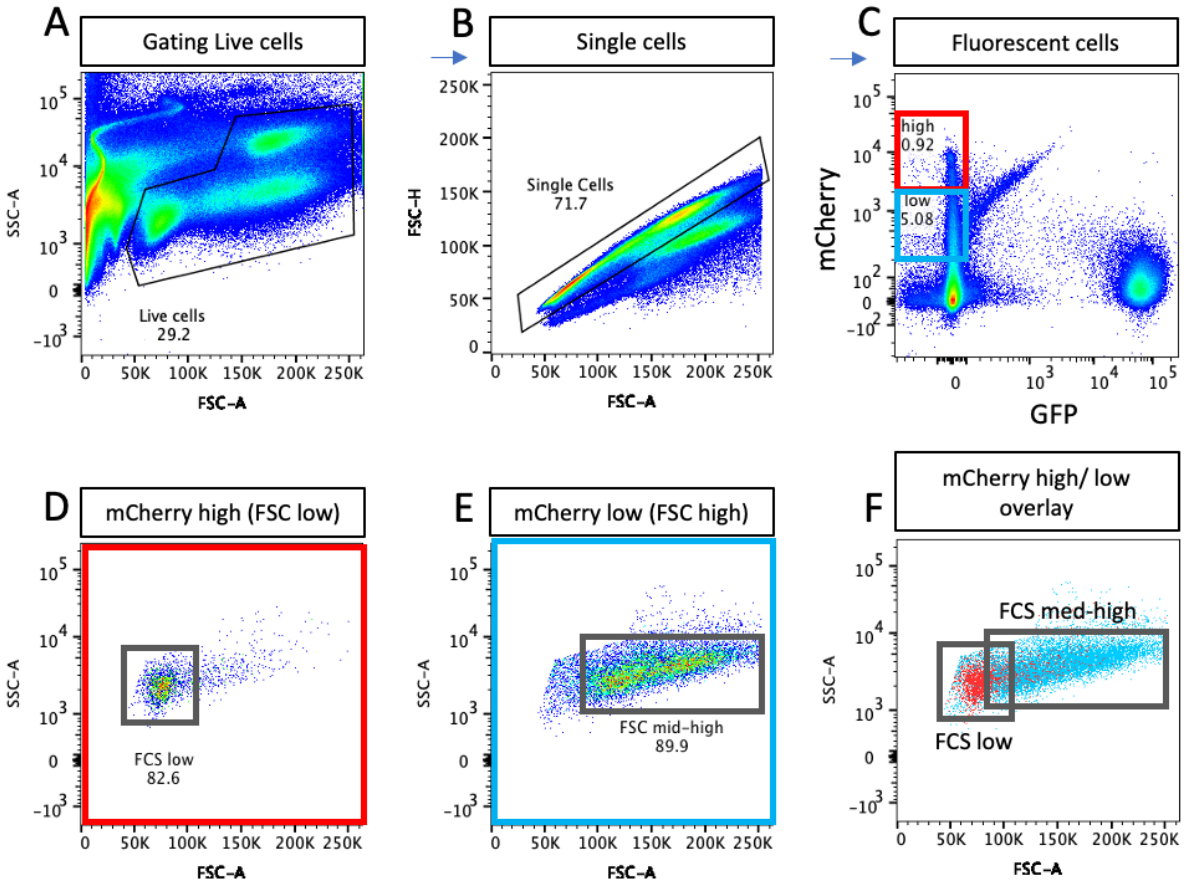

Fig. 3.23 FACS gating strategy to sort *Runx*:mCherry ^{high} and ^{low} populations.

Single cell suspension of WKM tissue pooled from 4 *Tg(Runx:mCherry; lyz:GFP)* fish. (**A**) Representative FSC-A/SSC-A profile. Black lines indicate gating for live cells. (**B**) Gating to exclude doublet cells. (**C**) mCherry/ GFP plot with gating for *Runx:*mCherry ^{high} and ^{low} populations. Red box outline represents gating for *Runx*:mCherry ^{high} cells, blue box outline gates for *Runx:*mCherry ^{low} cells. (**D**) FSC/SSC plot of *Runx*:mCherry ^{high} cells. Grey box outline represents gating for FSC ^{low} cells which were sorted for RNA isolation. (**E**) FSC/SSC plot of *Runx*:mCherry ^{low} cells. Grey box outline represents gating for FSC $^{medium-high}$ cells which were sorted for RNA isolation. Values adjacent to gates reflect the percentage of events within each gate relative to total events in the whole plot. (**F**) Overlap of **D** and **E** to show relationship of *Runx:*mCherry ^{high} and ^{low} cells on FSC/SSC.

Based on the findings of Chi *et al*. (2018), Zhang *et al*. (2010) and Ryo *et al*. (2010), it was hypothesized that *Runx*:mCherry ^{high} cells in the gill may correspond to *immunoglobulin Z* (*IgZ)*-expressing B cells. It has been shown that the expression of *runx1* is required in B cell development in zebrafish and mammals (Chi *et al*., 2018; Niebuhr *et al*., 2013). To investigate this hypothesis, mature B cell marker (*IgM*) and B cell development markers (*pax5* and *rag1*) were assayed on the sorted cell populations. In addition, a combination of HSC markers (*ckit*, *cmyb* and *runx1*) were utilised to determine whether *Runx*:mCherry ^{high} or ^{low} cells may harbour HSPCs in the WKM.

Due to inevitable variation in the number of cells sorted for each population, 18S values were highly variable between samples, meaning that samples with low 18S levels would have fewer transcripts overall. To determine whether the transcript levels of genes of interest were low due to low abundance in the sorted population specifically or due to low overall RNA levels, detection limits of new probes were assessed. In order to elucidate detection limits, two-fold dilution series of a single cell WKM suspension was carried out. With each dilution, cycle threshold (Ct) values were expected to increase by 1. The dilution series was used as the standard curve to determine the line of best fit and hence, the detection limit of each probe. The point at which the change in Ct of each probe was no longer directly proportional to the Ct of 18S ribosomal RNA was used as a cycle cut-off for reliable detection of transcripts of each gene of interest (Fig. 3.24). This enabled more accurate interpretation of gene transcript levels. Samples with relatively low but detectable gene of interest transcript levels relative to 18S were found above the standard curve within the white quadrant. Samples that had such low gene of interest transcript levels that they were undetectable despite reliable 18S values, were found in the yellow quadrant. Samples where 18S Ct values were too high (indicating low RNA levels) for gene transcripts to be detected by the probe, were found within the red quadrant. Finally, samples found within the blue quadrant indicated particularly high gene of interest transcript levels, such that they were detected by the probe despite a high Ct value for 18S. An example of this is seen in *IgM*:GFP+ cells from the WKM: 18S transcripts levels were low but high levels of *rag1* and *pax5* were detected (Fig. 3.24A & E).

Using these standard curves, any gene expression that was found to be above the detection limit for a given probe was appropriately represented in comparative gene expression graphs. mCherry transcript levels were used as a control for the quality of FACS sorting and RNA isolation for *Runx*+ cells that were sorted based on mCherry fluorescence intensity. The data verified that fluorescence intensity was proportional to transcript levels of the fluorophore, as the *Runx*:mCherry ^{high} population in the WKM and gill had the highest mCherry transcript levels relative to 18S, while the *Runx*:mCherry ^{low} population had a much lower mCherry transcript levels relative to 18S (Fig. 3.25A). Similarly, GFP transcript levels reflected the GFP fluorescence intensity that had previously been observed by microscopy (Fig. 3.25B).

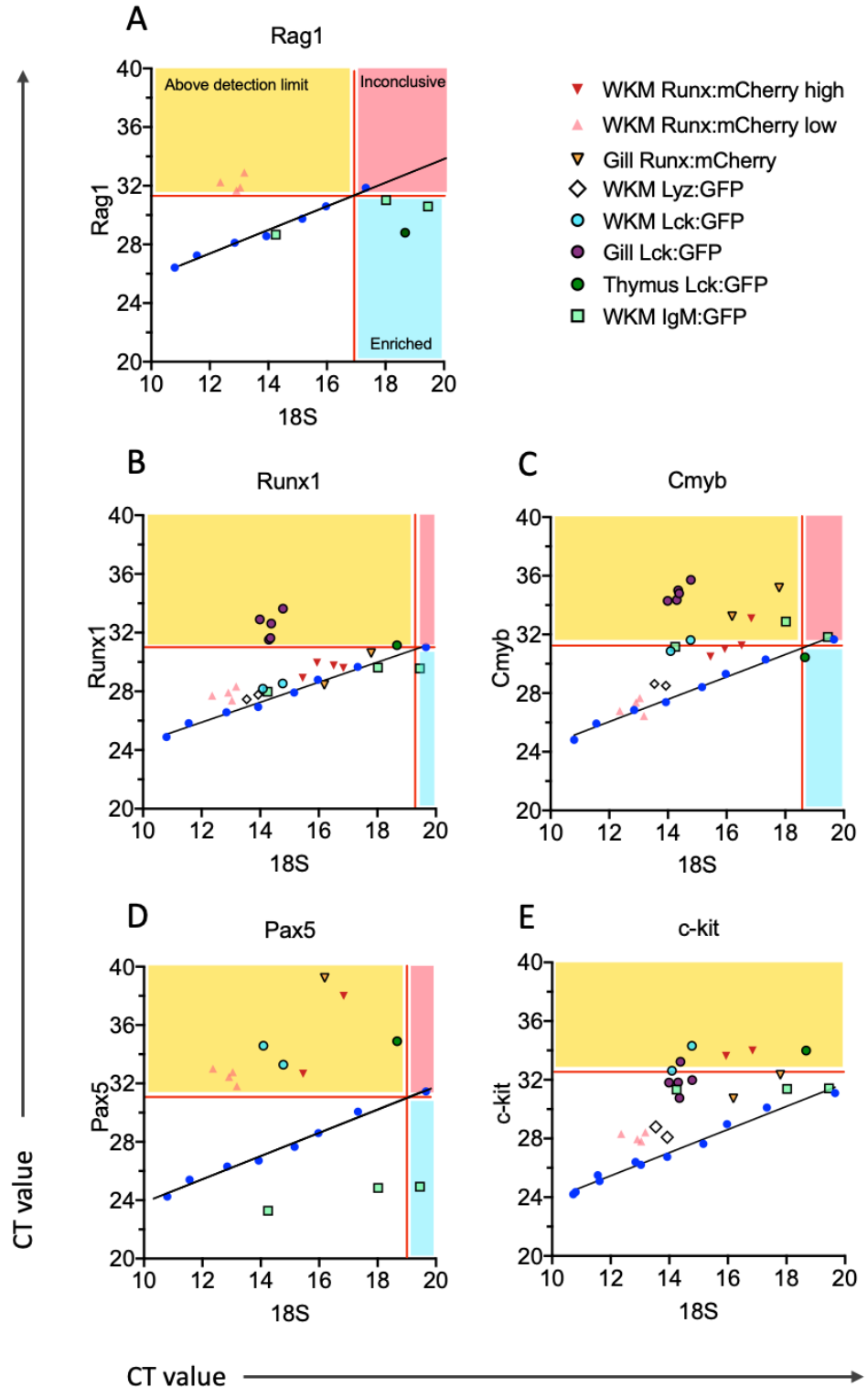

Fig. 3.24 Standard curves and detection limits for *rag1*, *runx1*, *cmyb*, *pax5* and *ckit* qPCR probes.

Standard curves for qPCR probes were created using 1 in 2 serial dilution of untreated adult WT WKM FACS sorted cells comparing Ct value for 18S housekeeping gene (x axis) and gene of interest (y axis). Standard curves shown by blue dots and line of best fit. Detection limits of each probe were determined by assessing SD of triplicate Ct values. Detection limits indicated by horizontal red lines. Yellow areas above detection limit depict low gene transcript level compared to 18S value. Red areas indicate inconclusive gene transcript values due to low 18S expression. Blue areas depict where gene transcript level is high compared to 18S value, indicating enrichment. (**A**) *rag1*, (**B**) *runx1*, (**C**) *cmyb*, (**D**) *pax5* and (**E**) *ckit*. Each dot indicates 1 sample.

rag1 expression was found to have been highest in *IgM*+ cells and in a thymus *lck*+ population. However, detectable (albeit low) levels of *rag1* transcripts were also found in the *Runx*:mCherry ^{low} population isolated from WKM (Fig. 3.25C). These findings are consistent with the hypothesis that these cells are precursor cells which could be lymphoid primed. *rag1* was not detected in any other sampled population. Interestingly, the data showed that *runx1* transcript levels were highest in *IgM*+ cells found in the WKM, corroborating that these cells express *runx1* in order to mature. However, flow cytometry data has shown that *Runx*:mCherry+ cells did not overlap with *IgM*:GFP+ cells, suggesting that the +23 enhancer element in the *Runx*:mCherry transgene is not activated by transcription factors involved in B cell maturation. Nevertheless, it was reassuring to see that *runx1* transcript levels in fluorescent protein-expressing cells followed the same pattern as mCherry transcript levels as this suggests that fluorescence intensity of the transgene is reflective of the endogenous *runx1* expression levels within these cells (Fig. 3.25D). It has previously been reported that transgenic expression of fluorescent proteins under this enhancer element is not reflective of endogenous *runx1* expression in non-hematopoietic cells in zebrafish. Instead, the enhancer was described as a hematopoietic site-specific promoter element (Ng *et al*., 2010).

It was hypothesized that *IgM*+ cells from the gill may be more mature B cells than those *IgM*+ cells found in the WKM, where B cell maturation occurs. However, gene transcript levels of *IgM*+ cells from the gill were not analysed. Due to the low prevalence of *IgM*:GFP+ cells in the gill, it was not considered ethical to harvest a large number of animals in order to isolate a sufficient population of *IgM*+ cells to analyse their gene transcript profiles by qRT-PCR. Single-cell transcriptomics could be a way for these cells to be analysed without requiring a large number of zebrafish to be harvested.

The transcript levels of *lyz* and *lck* were found only to be high in *lyz*;GFP+ and *lck*:GFP+ cells respectively (Fig. 3.25E & F). Concordant with the involvement of *lck* in T cell development, which occurs in the zebrafish thymus (Langenau *et al.,* 2004), the data indicates that relative *lck* transcript levels were highest in cells found in the thymus, and lower in those found in the WKM or gill. However, *lck* transcript levels in the WKM and gill were similar (Fig. 3.25F). The mature B cell marker *IgM* and B cell maturation marker *pax5* were only expressed to detectable levels in *IgM*:GFP + sorted cells (Fig. 3.26A & B).

Finally, unexpected results were obtained for the HSC marker genes *ckit* and *cmyb*. The *Runx*:mCherry ^{low}, FSC $^{med\text{-}high}$ population isolated from the WKM had higher levels of both *cmyb* and *ckit* transcripts than the *Runx*:mcherry ^{high}, FSC ^{low} population from the same tissue. Power calculations indicated that between 4-9 samples were required per group to achieve 85% power for transcript level measurements of *ckit, cmyb* and *runx1*. Thus, additional experimental replicates may be required to assess the significance of these results. Nevertheless, enrichment of *ckit* and *cmyb* marker genes within the *Runx*:mCherry ^{low} population may indicate that these cells also harboured multipotent HSCs. Protein expression analysis and HSC transplant studies could help to further shed light on functional differences between *Runx*:mCherry ^{high} and ^{low} populations. Another unexpected result was that *ckit*, but not *cmyb*, transcript levels were high in *Runx*:mCherry ^{high} cells isolated from gill tissue and *lyz*+ cells isolated from the WKM (Fig. 3.26C & D). Furthermore, *cmyb* transcript levels were highest in the *lck*+ population from the thymus and *IgM*+ cells from the WKM, suggesting that these fluorescent protein-expressing cells may harbour some progenitor cells or that *cmyb* may be involved in the maturation of lymphocytes.

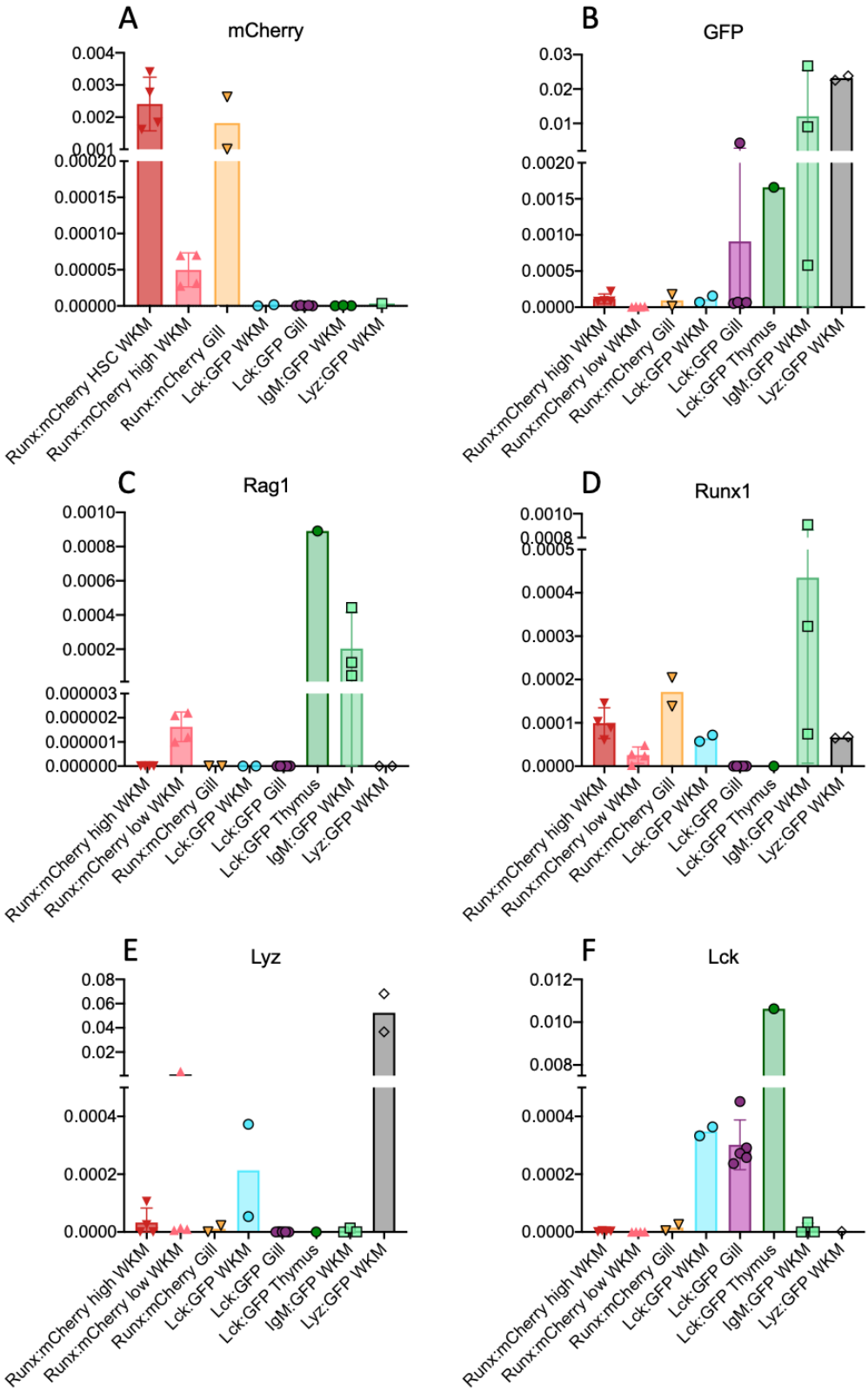

Fig. 3.25 Transcript levels of hematopoietic cell marker genes in FACS-sorted populations.

qRT-PCR analysis of *mCherry* (**A**), *GFP* (**B**), *rag1* (**C**), *runx1* (**D**), *lyz* (**E**) and *lck* (**F**) mRNA transcript levels in sorted *Runx*:mCherry ^{high} and ^{low} WKM cells, *Runx*:mCherry+ gill cells, *lck*:GFP+ WKM, gill and thymus cells, *IgM*:GFP+ and *lyz*:GFP+ cells from the WKM. Gene transcript levels were calculated as ratio relative to 18S using 2^-(ΔCt). Each dot is 1 sample from either 1 fish (*lck*:GFP+ samples) or a pool of up to 6 fish for *Runx*:mCherry+ samples. N=1-6. Data pooled from 4 experiments. Error bars and SD shown only for samples with 3 or more data points.

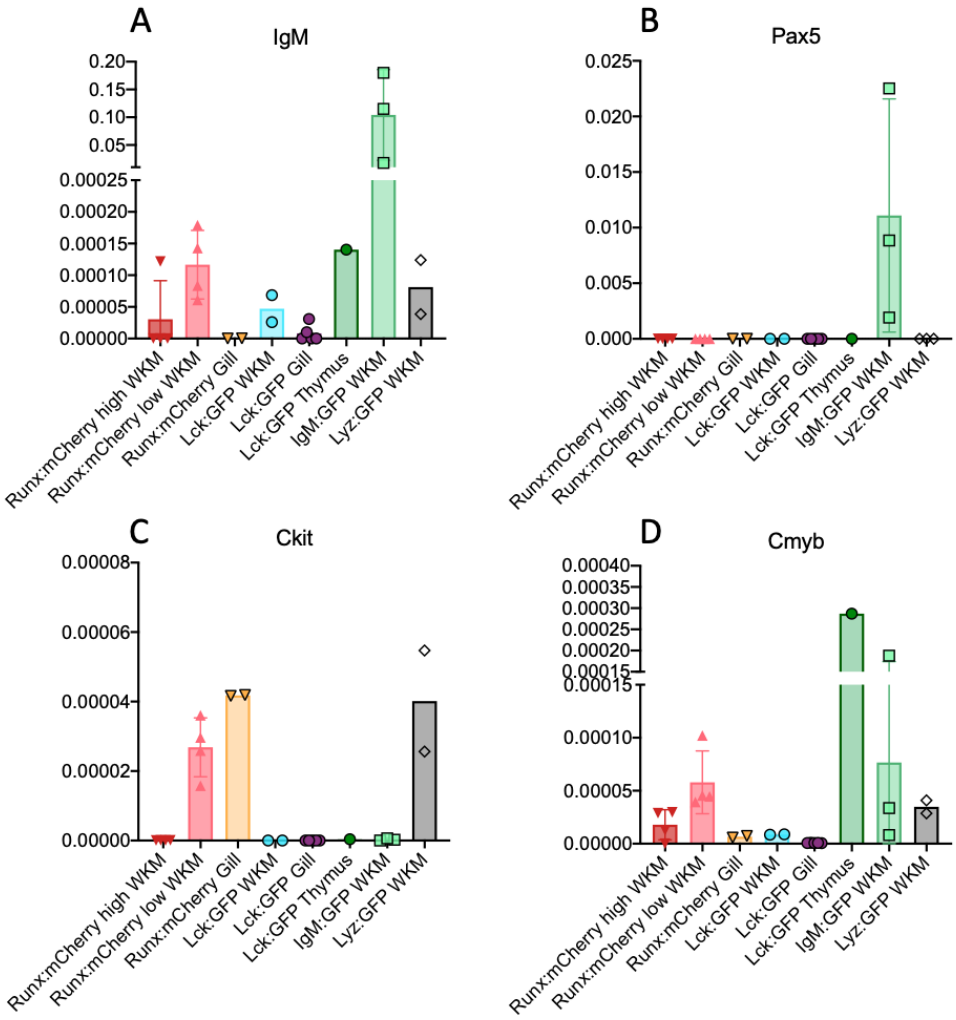

Fig. 3.26 Transcript levels of B cell and HSPC marker genes in FACS-sorted populations.

qRT-PCR analysis of *IgM* (**A**), *pax5* (**B**), *ckit* (**C**) and *cmyb* (**D**) mRNA transcript levels in sorted *Runx*:mCherry ^{high} and ^{low} WKM cells, *Runx*:mCherry+ gill cells, *lck*:GFP+ WKM, gill and thymus cells, *IgM*:GFP+ and *lyz*:GFP+ cells from the WKM. Gene transcript levels were calculated as ratio relative to 18S levels using 2^-(ΔCt). Each dot is 1 sample from either 1 fish (*lck*:GFP+ samples) or a pool of up to 6 fish for *Runx*:mCherry+ samples. N=1-6. Data pooled from 4 experiments . Error bars and SD shown only for samples with 3 or more data points.

3.4 Summary

Runx:mCherry+ cells were found in the peripheral blood and embed into the gill tissue at approximately 21 dpf. In the WKM, distinct *Runx*:mCherry ^{high} and ^{low} populations exist with differential FSC/SSC properties. The majority of *Runx*:mCherry ^{high} cells were found in the lymphocyte compartment, while the *Runx*:mCherry ^{low} cells were found predominantly in the precursor compartment. In the peripheral blood and the gill, the majority of *Runx*+ cells present were *Runx*:mCherry ^{high}.

Investigating the overlap between the *Tg(Runx:mCherry)* transgenic line and the *Tg(Runx:GFP)* line, it was found that the *Runx*:GFP+ cells overlap almost exclusively with *Runx*:mCherry ^{high} cells and not *Runx*:mCherry ^{low} cells in the WKM, gill and blood.

Assessing the overlap of *Runx*:mCherry+ cells with other fluorescent protein-expressing cell types, it was found that the *Runx*:mCherry+ populations within the WKM, blood and gill do not overlap with *lck*:GFP+ lymphocytes or *IgM*:GFP+ B cells. The abundance of *Runx*:mCherry ^{high} and *CD41*:GFP ^{high} cells in the WKM and gill appear similar by flow cytometry and a similar distribution of cells was observed in the gill tissue by microscopy.

Gene transcript analysis of sorted *Runx*:mCherry+ populations revealed that the *Runx*:mCherry construct does not label *runx1*-expressing B cells in the WKM of adult zebrafish. It was also found that *Runx*:mCherry ^{low}, FSC $^{med-high}$ cells had higher levels of *cmyb* and *ckit* transcripts compared to the *Runx*:mCherry ^{high}, FSC ^{low} population.

3.5 Discussion

The aim of this chapter was to further characterise fluorescent protein-expressing cell populations in the *Tg(Runx:mCherry)* and *Tg(Runx:GFP)* transgenic lines generated by Tamplin *et al*. (2015). To achieve this aim, the localisation and abundance of these cells were investigated over time, similarities and differences between *Runx*:mCherry+ and *Runx*:GFP+ populations were scrutinised and gene transcript data was used to try and determine whether other non-HSPCs could also express the *Runx*:mCherry transgene.

3.5.1 Embedded Runx:mCherry+ cells are found in the gill

Runx:mCherry+ cells were observed in circulation from as early as 4 dpf in transgenic zebrafish, in addition to their presence in the CHT where they embed following their arrival form the VDA (Fig. 3.1; Tamplin *et al*., 2015). The abundance of cells in circulation aided in screening of transgenic fish as these cells were more readily identified, particularly in heterozygous fish which exhibited dim mCherry fluorescence. In juvenile zebrafish gills, however, *Runx*:mCherry+ cells were not only observed in circulation. It was found that, by 21 dpf, a small number of *Runx*:mCherry+ cells were lodged in the gill tissue and the abundance of *Runx*:mCherry+ cells increased in the gills over time until adulthood was reached (Fig. 3.2 & 3.3). Interestingly, the timing at which *Runx*:mCherry+ cells started to colonise the gill at 21 dpf appears to coincide with the functional development of adaptive immunity in zebrafish (Lam *et al.,* 2004; Page *et al.,* 2013; Chi *et al.,* 2018; Trede *et al*., 2001; Hu *et al.,* 2010). This is also when *IgM*:GFP+ B cells and *IgZ* transcript levels have been shown to arise in the developing zebrafish (Page *et al*., 2013).

The data collected in this study showed that *Runx*:mCherry ^{high} cells were abundant in the PB and also embedded in the gills of juvenile and adult zebrafish. It is unclear whether these *Runx*:mCherry ^{high} cells are HSPCs that are recruited from the WKM to the gill during development to coincide approximately with the development of adaptive immunity, or whether other hematopoietic cells that may express the transgene are recruited. Indeed, it is also unclear whether *Runx*:mCherry ^{high} cells are recruited to the gill or whether they arise in the gill tissue. It is hypothesized that they are recruited to the tissue from the WKM due to the abundance of *Runx*:mCherry ^{high} cells that are in circulation throughout development.

Ultimately, lineage tracing would be required to determine the ontogeny of gill *Runx*:mCherry+ cells.

Whether gill-derived *Runx*:mCherry+ cells are HSPCs, capable of reconstituting hematopoiesis in mutants of definitive hematopoiesis, has been tested through transplantation assays in Chapter 5 (section 5.3.6). These results indicate that *Runx*:mCherry ^{high} cells isolated from gills are not capable of long-term multilineage reconstitution but may be capable of short term erythroid output (Fig. 5.15C). Although the gills have not previously been described as an extramedullary site of hematopoiesis in zebrafish, it has been discovered in recent years that the mouse lung can host extramedullary hematopoiesis (EMH) in steady state conditions. Indeed, the lung was found to be a primary site of platelet biogenesis in mice (Lefrançais *et al.*, 2017). In addition, the human lung has been shown to host EMH in patients presenting with myeloid metaplasia (Koch *et al.,* 2003; Rumi *et al.,* 2006; Asakura & Colby, 1994; Boula *et al.,* 2005). Thus, the presence of *Runx*:mCherry ^{high} cells, which have previously been characterised as HSPCs (Tamplin *et al.,*2015), in the zebrafish gills raises interesting questions about whether there is evolutionary conservation in the function of gills and lungs as a site for hematopoiesis, platelet production, and as a niche for HSPCs (Lefrançais *et al.*, 2017). The similar abundance and distribution of *CD41:*GFP+ and *Runx*:mCherry+ cells in the gill could indicate that the *Runx*:mCherry+ cells identified in the gill may be involved in thrombocyte biogenesis. Unfortunately, as *Tg(Runx:mCherry; CD41:GFP)* zebrafish were not generated during the course of this project, it was not possible to assess the thrombocyte out-put of transplanted cells using flow cytometry or *in vivo* microscopy. However, it remains a possibility that gill *Runx*:mCherry+ cells contribute to thrombocyte biogenesis. The presence of *Runx*:mCherry+ cells in the gills also raises other interesting questions. For example, if the gills can provide a niche for HSPCs, how does this niche compare to the WKM niche, what factors govern the abundance of HSPCs in the gill and how is their arrival in gill tissue coordinated?

In this chapter, the hematopoietic cell composition of the zebrafish gill was investigated. Much of this work was carried out by flow cytometry analysis. The gating strategy described by Traver *et al*. (2003) for the identification of erythrocytes, lymphocytes, precursors and myelomonocytes in the WKM has also been applied to the gill. However, it is worth noting

that the gill tissue is not identical to the WKM tissue and some non-hematopoietic cells have been found to scatter in similar ways to previously-identified hematopoietic cells (Fig. 3.5D). For example, *Fli*:GFP+ endothelial cells scatter across the precursor and myelomonocyte compartments (Wane, 2021). This is important information when utilising flow cytometry for the characterisation of cells in the gill as the number of events found within these compartments cannot be said to be an accurate representation of the number of precursor or myelomonocytic cells present within the gill tissue. Indeed, very few *lyz*:GFP+ neutrophils, which have been shown to comprise 57.4±3.5 % of all cells within the myelomonocyte compartment (Hall *et al*., 2007), reside in the gill tissue. However, a large proportion of cells in the gill tissue possess the same FSC/SSC properties as myelomonocytes (Fig. 3.5G & I). More accurate data for the abundance of precursors and myelomonocytes can be obtained by investigating fluorescent protein-expressing cells driven by cell type-specific promoters such as *lyz*:GFP or *Runx*:mCherry.

3.5.2 Bright and dim populations of Runx:mCherry+ cells in the WKM, gill and blood

This chapter investigated the characteristics of bright and dim fluorescent *Runx*:mCherry+ cells. It was found that the major population in the WKM is comprised predominantly of *Runx*:mCherry ^{low} cells while the *Runx*:mCherry ^{high} population contributed on average less than 25% to the total *Runx*:mCherry+ population (Fig. 3.7). In contrast, the major *Runx*:mCherry+ population in both the blood and the gills was unexpectedly found to consist of *Runx*:mCherry ^{high} cells (Fig. 3.8 & 3.9). Furthermore, there was a clear distinction between the FSC/SSC properties of *Runx*:mCherry ^{high} versus *Runx*:mCherry ^{low} cells, which were consistent across different tissues, whereby the *Runx*:mCherry ^{high} population was FSC ^{low} and the *Runx*:mCherry ^{low} cells were FSC $^{med-high}$, indicating possible functional differences between the *Runx*:mCherry ^{high} and ^{low} populations.

Based on findings by Traver *et al*., it was hypothesized that the FCS^{low}/ SSC^{low} compartment contained lymphocytes and long-term repopulating HSCs (Traver *et al*., 2003). This would suggest that the *Runx*:mCherry ^{high} population possesses multilineage, long-term hematopoietic repopulation potential. Indeed, this was the assumption made by Tamplin *et al*. (2015), who hypothesized that *Runx*:mCherry ^{low} cells are predominantly progenitors as these scatter in the SSC $^{low-med}$ FSC $^{med-high}$ fraction, which has been described as the precursor

compartment (Traver *et al*., 2003). However, very recent work by Kobayashi *et al*., published after the cessation of the experimental work presented in this thesis, used *Runx*:mCherry+ cells in combination with *gata2a*:GFP to enrich for HSPCs in the zebrafish WKM. Interestingly, the HSPC-enriched population of *Runx*+ *gata2a*+ cells, with increased long-term reconstitution potential, was found within the FSC $^{med\text{-}high}$ precursor compartment by flow cytometry. Furthermore, the group found no long-term reconstitution potential at 16 weeks post transplant among the *Runx*+ *gata2a*- (FSC $^{low\text{-}mid}$) population of cells in HCT studies (Kobayashi *et al*., 2019). This may suggest that those *Runx*:mCherry ^{high} cells which scatter predominantly in the lymphocyte compartment may either have a reduced HSC potential or reduced abundance of HSCs among this population. The work of Kobayashi *et al.* (2019) indicates that the HSC potential within *Runx*+ cells may lie within the FSC$^{med\text{-}high}$ population. Data presented in this chapter has indicated that only a small proportion (12.0±8 %) of *Runx*:mCherry ^{high} cells are found within the precursor (FSC $^{med\text{-}high}$) compartment. On the other hand, the majority (46.6±8 %) *Runx*:mCherry ^{low} cells were found within the precursor compartment. Thus, HSC potential residing among the *Runx*:mCherry ^{low} cells remains a possibility worth investigating. If this is the case, it may suggest that some cells within the *Runx*:mCherry ^{high} population in the WKM, gill and PB correspond to a different cell type within the FSC ^{low} population, such as thrombocytes, erythromyeloid precursors or lymphoid cells which express high levels of *runx1*. Indeed, Kobayashi *et al.* (2019) found that the *Runx*+ *gata2a*- population possesses high levels of thrombocyte, myeloid and erythroid marker genes. One way to investigate this further would be to analyse the WKM, gill and blood of fish which possess both the *Runx*:mCherry and *CD41*:GFP transgenes. In this chapter, no overlap was discovered between *Runx*:mCherry+ cells and fully differentiated lymphoid cells. This was in agreement with work from Kobayashi *et al.* (2019) which indicated that the lymphoid marker genes were only detected in *Runx*- populations.

If a subset of *Runx*:mCherry ^{high} cells do indeed correspond to a different cell type, and the *Runx*:mCherry ^{low} population contain a proportion of HSPCs, this could explain why a significant *Runx*:mCherry ^{low} population was only found in the WKM and not in the gill or blood, as the WKM is the adult zebrafish hematopoietic organ (Traver *et al.,* 2003). Alternatively, it may be the case, as indicated by Tamplin *et al.* (2015), that the *Runx*:mCherry ^{low} population represents precursors and lineage-primed progenitors derived from

Runx:mCherry ^{high} cells, such as those identified by Kobayashi *et al.* (2019) in the *Runx*+ *gata2a*- populations. On the other hand, results from Chapter 5 (section 5.3.6) indicate that gill and WKM *Runx*:mCherry ^{high} cells can arise in recipients of WKM-derived *Runx*:mCherry ^{low} cells, suggesting that *Runx*:mCherry ^{low} cells are not derived from *Runx*:mCherry ^{high} cells.

3.5.3 Runx:mCherry^{high} and Runx:GFP+ cell populations are equivalent

In agreement with the findings by Tamplin *et al*. (2015), a smaller population of cells expressed *Runx*:GFP compared to *Runx*:mCherry. In contrast to the *Runx*:mCherry ^{high} and ^{low} populations, only one population of *Runx*:GFP+ cells was identified in this study. In terms of cell abundance in each tissue, as well as their FSC/SSC scatter properties, these cells appeared to correspond most closely to *Runx*:mCherry ^{high} cells (Fig. 3.10 & 3.11). To investigate this further, *Tg(Runx:mCherry)* were crossed *to Tg(Runx:GFP)* zebrafish. This revealed that the total fluorescent populations were not equivalent in the WKM of adult zebrafish, and only 22±12 % of *Runx*:mCherry+ cells overlapped with *Runx:*GFP+ cells. Similarly, Tamplin *et al*. (2015) reported that only 13±6 % of *Runx*:mCherry+ cells overlapped with *Runx*:GFP+ cells in the CHT in double-transgenic embryos. On the other hand, they found that 92±11 % of *Runx*:GFP+ cells overlapped with *Runx*:mCherry+ cells, which is similar to the results reported here with 99.7±0.4 % of *Runx*:GFP+ cells overlapping with *Runx:*mCherry+ cells in the adult WKM (Fig. 3.12). The extent of overlap between *Runx:*mCherry+ and *Runx:*GFP+ cells at different developmental stages suggests that the relative abundance of these cells in the different hematopoietic niches does not change significantly over time.

The hypothesis that *Runx*:GFP+ cells most likely correspond to *Runx*:mCherry ^{high} cells was confirmed by flow cytometry of WKM, blood and gill tissues, as well as confocal microscopy of gills from double-positive *Tg(Runx:mCherry; Runx:GFP)* zebrafish. Indeed, only a small population of *Runx*:mCherry ^{high} cells did not overlap with *Runx*:GFP+ cells in the WKM (Fig. 3.12). In addition, these cells also exhibited close to 100 % overlap in the blood and gills (Fig. 3.13, 3.14 & 3.15) and double-positive cells were found predominantly within the lymphocyte compartment. This demonstrated that *Runx*:mCherry ^{low} cells do not overlap with *Runx*:GFP+ cells. Therefore, it is likely that the non-overlapping compartment of the *Runx:*mCherry+ cell population identified in the CHT of 3 dpf embryos by Tamplin *et al*. was comprised predominantly of *Runx*:mCherry ^{low} cells.

3.5.4 There is no overlap between Runx:mCherry+ and IgM:GFP+ or lck:GFP+ cells

After finding that *Runx*:mCherry ^{high} cells with similar FSC/SSC properties to lymphocytes were abundant in the zebrafish gills, it was hypothesized that *Runx*:mCherry ^{high} cells could identify different, non-HSPC cells. Lymphocytes were investigated first as the FSC/SSC properties matched and because the timing at which *Runx*:mCherry+ cells started to embed in the gill tissue (21 dpf) coincided with the development of adaptive immunity in zebrafish (Lam *et al*., 2004; Page *et al*., 2013; Chi *et al*., 2018; Trede *et al*., 2001; Hu *et al*., 2009). However, no overlap was identified by both flow cytometry analysis and confocal imaging of gill tissue of *Runx*:mCherry+ cells with *IgM*:GFP+ cells and *lck*:GFP+ cells (Fig. 3.16 & 3.17). While this ruled out the possibility that *Runx*:mCherry ^{high} cells correspond to either *lck*:GFP+ T cells or *IgM*:GFP+ B cells, it did not rule out the possibility that they correspond to a different type of lymphocyte. Although many B cells are found in the teleost gill, it has been shown that the mucosal-specific population of B cells in gills are *IgZ2*-positive cells (Sogabe Ryo *et al*., 2010), while *IgM*-positive B cells are most abundant in the PB and WKM. Although there was no transgenic *IgZ* reporter line available to cross with *Tg(Runx:mCherry)* transgenic zebrafish, it has recently been demonstrated that a proportion of *mpeg1.1*+ cells also report B cells, in addition to macrophage cells. Ferrero *et al.* found that brightly fluorescent cells, driven by the *mpeg1.1* promoter, fall within the lymphocyte compartment based on their FSC/SSC properties. Furthermore, using transcriptomic data, the group identified that *mpeg*+ B cells were predominantly expressing *IgZ* antibodies (Ferrero *et al*., 2020). Hence, existing transgenic zebrafish, expressing fluorescent protein under the control of the *mpeg1.1* promoter, could be utilised to determine whether or not *Runx*:mCherry ^{high} cells correspond to *IgZ*+ B cells.

3.5.5 Similar cell distribution between Runx:mCherry ^{high} cells and CD41:GFP+ cells

Flow cytometry and confocal imaging data presented in this chapter have identified similar cell distribution between *Runx*:mCherry ^{high} cells and *CD41*:GFP+ cells. The abundance and FSC/SSC properties of *CD41*:GFP+ cells were investigated in the WKM and gill. In both tissues, *CD41*:GFP ^{high} thrombocytes (Lin *et al*., 2005) gated to the lymphocyte compartment (Fig. 3.19) and were found to contribute a similar proportion to live single cells as *Runx*:mCherry ^{high} cells (Fig. 3.20). In addition, the distribution of *CD41*:GFP+ cells in the gills followed similar patterns to the distribution of *Runx*:mCherry+ cells, whereby they were either spread evenly

throughout the primary and secondary lamellae, which was more common, or were found in clusters at the proximal end of the primary lamellae (Fig. 3.18). A cross between these transgenic lines would be required to determine whether or not the same population of cells express both fluorescent proteins. When the overlap between these two transgenic fluorescent protein-expressing cells was assessed by Tamplin *et al*. in the CHT of 72 hpf embryos by microscopy, it was found that 60±12 % of *CD41*:GFP+ cells overlapped with *Runx*:mCherry+ cells, and 44±8 % of *Runx*:mCherry+ cells overlapped with *CD41*:GFP+ cells (Tamplin *et al*., 2015). This indicated that the *Runx*:mCherry+ population in the embryo is already significantly larger than the *CD41*:GFP+ population. However, the population of *CD41*:GFP+ cells in the CHT before 72 hpf are *CD41*:GFP ^{low} HSPCs (Lin *et al*., 2005; Bertrand *et al*., 2008). Therefore, one might expect that the percentage of overlap between *CD41*:GFP+ and *Runx*:mCherry+ cells will be significantly reduced when mature *CD41*:GFP ^{high} thrombocytes appear. However, high levels of *CD41* transcripts were found in *Runx*:mCherry+ *gata2a*- cells both by RNA-seq and qPCR analysis (Kobayashi *et al*., 2019). Thus, it would be interesting to investigate whether *Runx*:mCherry ^{high} cells in the gill might correspond to the population of *CD41*:GFP ^{high} cells found in the gill. In support of this hypothesis, Antony-Debré *et al*. (2012) have previously demonstrated the importance of *RUNX1* expression in humans and mice in regulating thrombocyte maturation. Furthermore, it was found by Tang *et al*. (2017) that *CD41*:GFP+ and *Runx1*+ cells have overlapping gene transcription profiles and cluster together in a tSNE analysis. Recent work based on the *Tg(runx1P2:citrine)* reporter line, which utilises the P2 promoter of *runx1* to drive citrine expression, has demonstrated that the brightest *runx1P2*:citrine+ cells found at heart cryo-injury sites also expressed *CD41* mRNA, indicating that those cells were likely thrombocytes (Koth *et al*., 2020). However, a cross between the two transgenic lines would be required in order to assess whether the +23 enhancer is activated by transcription factors involved in thrombocyte differentiation.

3.5.6 Transcript analysis suggests that WKM Runx:mCherry ^{low} cells may also harbour HSC-like cells

Gene transcription data confirmed that there are high levels of *runx1* transcripts in *IgM*:GFP+ cells in the WKM (Fig. 3.25), corroborating that *IgM*:GFP+ cells require *runx1* in order to mature (Chi *et al*., 2018). However, flow cytometry data confirmed that *Runx*:mCherry is not expressed in *IgM*+ cells, as no overlap between *Runx*:mCherry+ and *IgM*:GFP+ cells was

observed. This indicates that the +23 enhancer, which drives fluorescent protein expression in *Tg(Runx*:*mCherry)* zebrafish, is not activated by transcription factors involved in B cell development.

It was found that *runx1* transcript levels correlated closely to *mCherry* transcript levels in the isolated *Runx*:mCherry+ populations, such that *Runx*:mCherry ^{high} cells in the WKM and gill were found to have greater *runx1* transcript levels than *Runx*:mCherry ^{low} cells isolated from the WKM. This suggests that the fluorescence intensity of the transgene is reflective of the endogenous *runx1* expression levels within these cells (Fig. 3.25D). This may further suggest that the *Runx*:mCherry ^{low} population is not merely a product of differentiating HSCs, which cease to express *runx1* while retaining some mCherry fluorescence (McBrien, 2017), but rather that there is reduced *Runx1* activation by upstream transcription factors and, hence, reduced *mCherry* expression in these cells.

In their study, Tamplin *et al*. (2015) predicted that 1 in 35 *Runx*:mCherry+ cells were HSPCs, equating to ~ 2.9 % of *Runx*:mCherry+ cells. They did not describe discriminating between *Runx*:mCherry ^{high} and ^{low} populations when sorting for donor cells to transplant. Given that *runx1* transcript levels were high in cells that are not HSPCs (Fig. 3.25D; Chi *et al*., 2018; Ng *et al*., 2010), the *Runx*:mCherry ^{high} population, which was assumed to be the HSC-containing compartment, could contain other hematopoietic cells such as thrombocyte, erythrocyte and lymphoid precursors which are equivalent in size and granularity to lymphoid cells and HSCs (Kobayashi *et al.,* 2019). In particular, the abundance of *Runx*:mCherry ^{high} cells in the gill may suggest that some *Runx*:mCherry ^{high} cells could be non-HSPCs. If this were the case in the gill, the same may be true for the *Runx*:mCherry ^{high} cells found in the WKM.

In this study, it was found that both *cmyb* and *ckit* transcript levels, which are HSC markers, were consistently greater in the WKM *Runx*:mCherry ^{low} population relative to the WKM *Runx*:mCherry ^{high} population (Fig. 3.26). Although gene transcript levels are not directly indicative of protein expression and cell function, work by Kobayashi *et al*. reported that the *Runx*:mCherry+ *gata2a*:GFP+, HSC-enriched population expressed higher levels of HSC-associated gene transcripts, including *meis1b*, *myb* and *kita,* compared to other populations. However, it is important to note that direct parallels cannot be drawn between the

populations assayed by Kobayashi *et al*. and the *Runx*:mCherry ^{high} and ^{low} populations described in this chapter. In particular, there are cells from both the bright and dim *Runx*:mCherry populations the are found within the FSC ^{med} precursor compartment. Thus, cells from either the *Runx*:mCherry ^{high} or ^{low} populations could contribute to the *Runx*:mCherry+ *gata2a*:GFP+ population identified by Kobayashi *et al*. (2019). However, if either the *Runx*:mCherry ^{high} or ^{low} populations were found to be specifically enriched for HSCs, it would be possible to sort *Runx*:mCherry+ cells for a greater HSC purity for transplantation, thereby improving the survival outcome. Furthermore, effective isolation of HSCs to a high concentration will facilitate studies into the biology of HSCs, as well as the molecular mechanisms regulating them.

In conclusion, the data confirmed that fluorescence intensity of *Runx*:mCherry+ cells correlated to both fluorophore gene transcript levels and, indeed, transcript levels of endogenous *runx1* within fluorescent protein-expressing populations. However, it also confirmed that the transgene driven by the +23 enhancer element does not recapitulate endogenous *runx1* expression in the hematopoietic lineages, and did not label IgM+ B cells from the WKM, which exhibit high *runx1* transcript levels. This suggests that IgM+ B cells utilise a different promoter element of *runx1,* such as the P1 or P2 promoters. This may indicate that the *runx*:mCherry transgene is specific to HSPCs. Nevertheless, it remains uncertain whether *Runx*:mCherry ^{high} or ^{low} cells in the WKM harbour the highest concentration of HSCs. In addition, *Runx*:mCherry ^{low}, FSC $^{med\text{-}high}$ cells exhibited higher transcript levels of *cmyb* and *ckit*, suggesting gene transcript signatures more akin to HSCs. However, this population also exhibited higher levels of *IgM* and *rag1* than other *Runx*:mCherry+ populations, while also exhibiting the lowest *runx1* transcript levels. Furthermore, the identity of *Runx*:mCherry+ cells in the gills remains elusive. Of the genes assayed, this population only showed detectable transcript levels of *ckit* and *runx1*. Further gene transcript and functional analysis will be required to better understand the hematopoietic identity of these populations.

Chapter 4

Response of *Tg(Runx:mCherry)* and *cmyb*^{t25127} Mutant Fish to Antibiotic and Immune Stimulants

Chapter 4 | Response of *Tg(Runx:mCherry)* and *cmyb*^{t25127} Mutant Fish to Antibiotic and Immune Stimulants

This chapter presents the work on the response of *Tg(Runx:mCherry)* transgenic zebrafish to antibiotic treatment and immune stimuli. It builds on the *Tg(Runx:mCherry)* characterisation data of the previous chapter, the antibiotic treatment data presented in the thesis of Charlwood (2017), the effect of poly I:C on HSPCs as presented in the thesis of McBrien (2017) and the response of gill tissue to R848 treatment presented by Progatzky *et al*. (2019) (see below). Using *Tg(Runx:mcherry)* transgenic fish enabled the assessment of the effects to treatments in HSPCs and extramedullary cells expressing the mCherry transgene. Furthermore, the effects of the viral mimetic R848 were investigated in *cmyb* mutant fish.

4.1 Introduction

Antibiotics are readily used to treat pathogenic bacteria in both humans as well as livestock. Generally, antibiotic treatment cannot specifically kill just one strain of pathogenic bacteria. Instead, commensal bacteria that live on the skin, in the gut or the respiratory tract of mammals and the gills of fish are also affected. As a result, antibiotic exposure can lead to an imbalance within the commensal microbial community, which in turn can impact the hematopoietic system and its response to subsequent immune challenges (Josefsdottir *et al*., 2016; Yonar, 2012).

4.1.1 The impact of antibiotics in aquaculture

The heavy use of antibiotics in aquaculture has far reaching impacts, particularly because not only fish that are intended to be treated are affected. Antibiotics have been shown to have long-term effects on the wider ecosystem. This is in part because antibiotic particles can accumulate within the sediment, leading to selection of antibiotic resistance in aquatic bacteria, which can result in horizontal transfer of antibiotic resistance between microbes (Santos & Ramos, 2018). It has been hypothesized that horizontal transfer of antibiotic resistance can occur from microbes in fish to those in livestock and humans (Santos & Ramos, 2018). Furthermore, significant antibiotic contamination has previously been identified in drinking water and crop irrigation sources in agriculture (Bu *et al*., 2013). This has been found

to affect the health of school children in Shanghai by long-term low-dose exposure to a combination of 21 contaminating antibiotics, as identified in their urine (Wang *et al*., 2016). Chronic low-dose antibiotic exposure is likely to lead to selection for antibiotic resistance in humans as well. In order to limit the rate at which antibiotic resistance develops, it is important to understand the impact antibiotics have on the immune system and strive for alternative disease prevention methods in aquaculture and agriculture.

4.1.2 Microbial defence against infection

Mammalian and fish mucosal surfaces, such as the gut and gills, host diverse microbial communities which provide protection against pathogens. This is achieved by both direct and indirect interactions such as competition with invading pathogens, the release of antimicrobial agents (Gómez & Balcázar, 2008) and stimulation of the hematopoietic system leading to the maintenance of immune cell populations (Josefsdottir *et al*., 2016; Kelly & Salinas, 2017). Any disruption to this diverse microbiome and its equilibrium between microbial species can lead to increased susceptibility of the host to opportunistic pathogens (Mohammed & Arias, 2015). Furthermore, pathogenic infections can themselves also lead to an imbalance and reduction in bacterial diversity within the microbial community, known as dysbiosis (Reid *et al*., 2017; Rosado *et al*., 2019).

4.1.3 The effect of Oxytetracycline on fish health and immunity

Oxytetracycline (OTC) is one of the most commonly used antibiotics in aquaculture, both as a preventative and a curative treatment for bacterial pathogens (Bu *et al*., 2013; Li *et al*., 2020; Zhou *et al*., 2018). It is metabolically produced by *Streptomyces rimosus* (Finlay *et al*., 1950) and inhibits bacterial protein synthesis by interfering with the 30S rRNA interaction with ammonia-acyl tRNA (Zhang, Cheng & Xin, 2015). OTC is a broad-spectrum antibiotic as it acts against both gram-negative and gram-positive bacteria. Intensive fish farming practices have resulted in the rapid spread of bacterial disease which can have significant economic impacts (Zhou *et al*., 2018; Wei, 2002). Furthermore, due to the extensive use of OTC, there are concerns regarding widespread antibiotic resistance that is emerging in fish farms.

OTC can be administered either through the addition to pellet feed, commonly around 50-100 mg OTC/ kg body weight (Lundén & Byland, 2000), or by addition to water. The latter is

practical in laboratory research with zebrafish as it ensures equal administration to all fish within a given tank independent of feeding habits or competition, which could lead to some fish consuming a higher dose of the antibiotic. In rainbow trout (*Oncorhynchus mykiss*), OTC treatment was found to reduce lymphoid cell mitogenic response to LPS stimulation in the head kidney (Lundén & Byland, 2000). Upon administration of OTC with immunisation, it led to the suppression of antibody production and reduced lymphocyte numbers in circulation (Lundén *et al*., 1998). More recently, two-week OTC treatment has been shown to cause oxidative stress and immune suppression in rainbow trout, as measured by a reduction in blood leukocytes, plasma immunoglobulin levels and reduced bacterial phagocytosis. These impacts were alleviated by the addition of lycopene to the treatment (Yonar *et al*., 2012). Furthermore, 96-hour acute and 28-day long chronic treatment with OTC both led to histological alterations in the gills of rainbow trout. Chronic exposure led to lamellar fusion and changes in tissue architecture, while hypertrophy of mucous cells and hyperplasia of epithelial cells were observed upon acute treatment (Rodrigues *et al*., 2017). The same group subsequently found similar results with the antibiotic erythromycin (Rodrigues *et al*., 2019), indicating that these effects were not unique to OTC antibiotic.

To assess microbial composition in the gills and skin of farmed seabass, Rosado *et al.* utilised 16S rRNA v4 metataxonomics. The group found that both disease outbreak and treatment with OTC led to considerable changes in the microbiome composition in both the gills and skin, and OTC led to a decrease of core microbial diversity in the gill tissue (Rosado *et al*., 2019).

Relatively few studies have investigated the impact of OTC on zebrafish health and microbiome. Barros-Becker *et al.* (2012) demonstrated widespread inflammation in zebrafish larvae following 48h 750ppm OTC exposure by showing a significant increase in *mpx*+ neutrophils in superficial tissues. Four days of 20 μg/L OTC was found to cause a significant increase in reactive oxygen species (ROS) production and apoptosis, in addition to causing developmental delay as exhibited by delayed hatching, shorter body length, increased yolk sac area and un-inflated swim bladders of zebrafish larvae (Zhang, Cheng & Xin, 2015). Long-term impact of high-dose OTC on zebrafish gut health has also been investigated by treating zebrafish for 6 weeks with 80 mg/kg/day in pellet feed. This treatment led to increased oxygen

consumption and decreased alkaline phosphatase (AKP) and acid phosphatase (ACP) levels in the gut, indicating altered gut health. Furthermore, the treatment led to increased mortality following *Aeromonas hydrophila* exposure, indicating that OTC impacted the immune response. The group also investigated the gut microbial diversity and richness, both of which were decreased in OTC-treated zebrafish (Zhou *et al*., 2018). Recently, the long-term low-dose effects of OTC have also been investigated in zebrafish. In agreement with the results described by Zhou *et al.*, two-month treatment of 10 mg/L OTC was found to decrease gut microbial diversity and richness and led to increased cellular energy consumption (Almeida *et al*., 2019a). Interestingly, behavioural and feeding changes were also observed in the OTC-treated group in this study. In a second study, the group investigated the impact of OTC exposure on zebrafish gut microbial communities, specifically by 16S rRNA gene-based metagenomic analysis using Illumina next-generation sequencing. This revealed that both the gut and water microbiome was altered upon OTC administration, even at the lowest concentration of 10 μg/L OTC. Statistically significant increases in gut proteobacteria and actinobacteria, and decreases in gamma proteobacteria were identified at 10 mg/L OTC (Almeida *et al*., 2019b). In partial agreement with this data, Li *et al.* were also able to detect altered gut microbial diversity as evidenced by an increase in fusobacteria and proteobacteria, as well as a decrease in actinobacteria, in zebrafish guts following 1 month of exposure to either 1 μg/L or 100 μg/L of OTC (Li *et al*., 2020). These low doses of OTC were also found to alter thyroid hormone homeostasis (Li *et al*., 2020; Yu *et al*., 2020). However, due to the wide range of OTC concentrations and exposure durations studied, it is not possible to compare these results directly.

4.1.4 Effect of Antibiotics on steady-state hematopoiesis

Antibiotics are commonly prescribed to patients suffering from bacterial infections. They are also commonly used as a pre-emptive measure for transplant patients and patients undergoing invasive surgery that could expose them to potential infection. Regarding hematopoietic cells, it has been reported that 15 % of patients in the US receiving high-dose β-lactam antibiotics, including penicillin, for over 2 weeks present with neutropenia (Olaison *et al*., 1999). It has also been reported in mouse studies that the administration of a 2-week broad spectrum antibiotic cocktail of vancomycin, neomycin, ampicillin and metronidazole resulted in decreased whole bone marrow (WBM) counts and significantly depleted HSPC and

MPP populations in the WBM and PB, both in terms of percentage and in absolute numbers. Mice presented as anaemic and leukopenic, with significantly elevated platelet counts but no change in peripheral granulocytes. Interestingly, the granulocyte, megakaryocyte and erythroid progenitors were not adversely affected by the treatment. The group were also able to show that this effect was not caused by direct suppression of HSCs by the antibiotic but was rather elicited indirectly through the alteration of the gut microbiome and reduced stimulation of hematopoietic cells. Despite significant reduction in HSPCs, their functional capacity was not diminished, as assessed by HCT (Josefsdottir *et al*., 2016).

Although the mechanism was not understood, an appreciation arose in the 1980s for the link between neutropenia and antibiotics, as patients developed neutropenia following 10+ days of high-dose *β-Lactam* antibiotic treatment. Furthermore, neutropenia was attributed to reduced bone marrow cellularity following antibiotic treatment (Neftel *et al*., 1985). In humans, the diversity and richness of intestinal microbiota has been linked to HCT outcome, whereby reduced diversity was associated with increased mortality (Taur *et al*., 2014). In mouse models, the microbiota has been linked to steady-state hematopoiesis by means of driving myelopoiesis. Germ-free mice exhibit reduced myeloid progenitor differentiation potential in both primitive and definitive hematopoiesis. This is rescued following recolonization of the microbiota from WT mice (Khosravi *et al*., 2014). Furthermore, increased complexity of the gut microbiota is associated with a larger bone marrow myeloid cell population. Similarly, broad-spectrum antibiotic treatment was found to reduce myelopoiesis by reducing microbial diversity in the gut. Additionally, germ-free animals also exhibited delayed pathogen clearance (Balmer *et al*., 2014; Khosravi *et al*., 2014). This may also be related to the underdeveloped gut-associated lymphoid tissues in germ-free mice (Round & Mazmanian, 2009).

4.1.5 Effect of antibiotics on the immune response to bacterial infection

As described above, antibiotic treatment is associated with impaired steady-state hematopoiesis and can lead to leukopenia and neutropenia. Antibiotic treatment has also been associated with impaired immune response to infection and delayed pathogen clearance, which in turn has been associated with increased mortality. For example, both germ-free and antibiotic-treated mice infected with *Listeria monocytogenes* were found to have a greater

pathogenic burden and resultant mortality compared to WT animals (Khosravi *et al*., 2014). Similarly, OTC or sulfamethoxazole antibiotic-treated zebrafish experienced greater mortality compared to untreated fish following *Aeromanas hydrophila* exposure (Zhou *et al*., 2018).

4.1.6 Effect of antibiotics on the immune response to viral stimulation

In a neomycin-treatment mouse model of respiratory tract influenza virus, the microbiota was found to modulate the immune response by providing the appropriate signals to initiate pro-*Il-1β* and pro- *Il-18* mRNA expression and activate inflammasomes. Neomycin-treated mice had lower levels of *Il-1β* and pro *Il-18* mRNA. As a result, the microbiota was found to regulate T & B cell responses to the virus in the respiratory mucosa (Ichinohe *et al*., 2011). Impaired T cell response was characterised by reduced *Ifnγ* levels, in addition to fewer antigen-specific cells. Antibiotic-mediated immune impairment was rescued by administration of toll-like receptor (TRL) 4 agonist LPS, indicating that the commensal microbiome is involved in TRL signalling, which has immune-modulatory function. Similarly, another study showed that antibiotic-treated mice exhibited impaired innate and adaptive antiviral immune responses to influenza virus, delayed viral clearance and increased mortality. The associated mortality was partially rescued in antibiotic-treated mice that received poly I:C prior to influenza infection, once again indicating that commensal bacteria have an important role in steady-state TLR signalling by setting the activation threshold of the innate immune system for effective antiviral immune responses (Abt *et al*., 2012).

4.1.7 Pattern recognition receptors

For vertebrate health and immunity, effective pathogen recognition is essential to ensure appropriate immune responses are initiated to eliminate infection. Pathogens and their pathogen-associated molecular patterns (PAMPS) are recognised by pattern-recognition receptors (PRRs) such as TLRs and nod-like receptors (NLRs), which are expressed on a variety of cells including hematopoietic and non-hematopoietic cells in the vertebrate body. As discussed in the introduction (section 1.5.4), HSCs have been found to possess a number of TLRs, including TLR2, TLR4, TLR7, TLR8 and TLR9, stimulation of which leads to the alteration of the hematopoietic output bias, namely toward the myeloid lineage (Nagai *et al*., 2006; Sioud *et al*., 2006; De Luca *et al*., 2009). Although PRRs are an evolutionarily conserved

method of pathogen recognition, species-specific differences exist in the specificity of certain PRRs and their signalling pathways. Zebrafish possess orthologues for many mammalian PRRs, making them a valuable addition to the repertoire of model organisms to investigate pathogen recognition in vertebrates.

4.1.7.1 Toll-like receptors

TLRs are an ancient mechanisms of immune defence conserved between vertebrates and invertebrates (Janeway & Medzhitov, 2002). They are transmembrane proteins found either on the surface of the plasma membrane or intracellular compartments such as endosome membranes or other intracellular vesicles. Intracellular TLRs, such as TLR3, TLR7, TLR8 and TLR9, are involved in the detection of intracellular nucleic acids, such as those that may enter the cell via endocytosis of viral particles. For example, TLR3 detects double-stranded RNA (dsRNA) (Bernard *et al*., 2012) and TLR7 and TLR8 are involved in the detection of single-stranded RNA (ssRNA). Upon ligand binding, TLRs will form homo- or heterodimers, leading to the recruitment of adaptor proteins through common cytoplasmic Toll-interleukin-1 receptor (TIR) domains, such as differentiation primary response 88 (MyD88) or TIR-domain-containing adapter-inducing IFN-β (TRIF). The recruitment of these adaptor proteins leads to further downstream signalling, activation and nuclear translocation of cytokine transcription factors such as nuclear factor κ-light-chain-enhancer of activated B cells (NF-κβ), IRF3 and IRF7, which are responsible for inducing the expression of inflammatory cytokines and interferons (Kawai & Akira, 2010).

Rodents possess 12 TLRs and 10 TLRs have been identified in humans. Many human TLRs possess zebrafish orthologues and conserved adaptor proteins. However, zebrafish also possess additional TLRs not found in mammals, some of which identify similar PAMPs as mammalian TLRS, such as the zebrafish Tlr22 which recognises dsRNA such as poly I:C, the equivalent of mammalian TLR3 (Li *et al*., 2017).

4.1.8 Zebrafish responses to TLR agonists

In the experimental data of this chapter, two TLR agonists have been applied to investigate the zebrafish responses, in particular changes in the *runx*:mCherry+ cell populations in the

gill and WKM. This section will summarise the current understanding of zebrafish responses to these two agonists; poly I:C and R848.

4.1.9 Zebrafish response to poly I:C model of systemic inflammation

Poly I:C is a synthetic short-strand dsRNA molecule of inosinic and cytidylic polymers and is a viral mimetic capable of inducing a robust anti-viral interferon response. It has commonly been utilised to study responses to viral infections by inducing a sterile inflammation in fish and mouse models. Poly I:C induces type I IFNs, which can be produced by most cell types, including HSCs, and leads to downstream signalling and subsequent activation of the immune system (Essers *et al*., 2009; Pietras *et al*., 2014; Sato *et al*., 2009). In one mouse study, a single 10 µg/g injection of poly I:C to induce IFN signalling resulted in the proliferation of HSCs, whereas chronic stimulation caused HSCs to re-enter quiescence, indicating that HSCs can sense and respond to poly I:C directly (Pietras *et al*., 2014).

In teleost, poly I:C can be recognised by two TLRs: Tlr3 and the teleost-specific Tlr22 (Matsuo *et al*., 2008). While the zebrafish genome encodes both of these TLRs, the ligand specificity of these receptors has not been fully elucidated. Transcript analysis by Dr. Wane detected *Tlr3* transcripts in zebrafish heart, gills, spleen, liver, gut and WKM (Dallman lab, personal communication). McBrien (2017) investigated the effect of a single intraperitoneal injection of poly I:C at 1 µg, 10 µg and 50 µg doses on the zebrafish. Results showed that transcript levels of type I (*ifnφ*) and type II interferons (*ifnγ1.1* & *ifnγ1.2*) were significantly increased at 10 µg and 50 µg doses. In addition, the transcript levels of inflammatory cytokines *il-1β*, *tnfα*, *il6*, *il8* and chemokines *cxcl18b* and *cxcl8* were also elevated at 3 hours post treatment (hpt). Interestingly, transcript levels of HSC chemoattractant *cxcl12a* and HSC marker *runx1* were not altered at 3 hpt in response to poly I:C treatment (McBrien, 2017). Furthermore, McBrien also investigated the effect of chronic poly I:C stimulation in zebrafish by injection of 8 consecutive doses of 10 µg poly I:C at 48-hour intervals. One week post treatment, this led to a decrease in *l-plastin* and *mpeg1.1* transcript levels in the WKM. However, transcript levels of HSC markers *runx1* and *cmyb* were unchanged at this timepoint. Flow cytometry analysis indicated an increased proportion of cells within the lymphocyte compartment. However, *CD41*:GFP+ cells within the lymphocyte compartment had declined in abundance, suggesting that the HSPC content may have been reduced in the WKM (McBrien, 2017).

Lin *et al.* recently identified metaphocytes in the gill mucosa and demonstrated that these cells were responsible for mediating the poly I:C-induced local immune response following treatment by immersion. In this experimental set up, poly I:C was able to induce a robust increase in *ifnγ1.1*, *ifnφ1* and *ifnφ2* levels (Lin *et al*., 2020).

4.1.10 HSPC response to R484 stimulation

R848, also known as resiquimod, is a small ssRNA viral mimetic. In humans and mice, it has been characterised as a TLR7 and TLR8 agonist that acts in a MyD88-dependent manner and induces type I IFN and proinflammatory cytokine production (Hemmi *et al*., 2002). Treatment of human *CD34+* HSPCs *in vitro* with R848 has been shown to induce differentiation along the myeloid cell lineage to increase the population of macrophage and monocytic dendritic precursor cells. Furthermore, stimulation of these cells resulted in an increase in *Il-1β*, *IL6*, *IL8*, *TNFα* and *GCS-F* transcript levels. Together, these indicated that stimulation of TLR7/8 can directly influence HSPC behaviour *in vitro* (Sioud *et al*., 2006).

4.1.11 Teleost response to R484 stimulation

The stimulation of rainbow trout (*Oncorhychus mykiss*) leukocytes with R848 *in vitro* resulted in an increase in transcript levels of the proinflammatory cytokines *il-1β*, *il8* and *tnfα*, as well as increased type I interferon *ifnα* (Purcell *et al*., 2006; Palti *et al*., 2010). This response was maintained even following inhibition of endosomal acidification using chloroquine (Palti *et al*., 2010). Interestingly, stimulation of Japanese flounder (*Paralichthys olivaceus*) peripheral blood leukocytes *in vitro* with R848 inhibited viral replication, upregulated immune genes, reduced apoptosis and increased proliferation of blood leukocytes in a Myd88-dependent manner. However, inhibition of endosomal acidification by means of chloroquine significantly diminished the R848-induced antiviral effect and immune response (Zhou & Sun, 2015). These conflicting results could be the product of species- or cell-specific differences or differences in the experimental conditions. A study in salmon also showed that R848 stimulation by intraperitoneal (IP) injection increased type I IFN in the gills and kidney. Furthermore, type I IFN-expressing cells in the gills were found predominantly within the primary lamellae of the gills, as shown by fluorescence *in situ* hybridisation (FISH) (Svingerud *et al*., 2012).

Finally, topical application of R848 to the gills of zebrafish has also been shown to induce a robust inflammatory response by local upregulation of type I and type II interferons (*ifn*α and *ifn*γ, respectively), in addition to *il6*, *il-1*β and *tnf*α proinflammatory cytokines (Progatzky *et al*., 2019). Furthermore, a significant increase in the number of *lyz*:GFP+ neutrophils in the gills was observed at 3 hpt compared to sham treated gills which returned to control levels by 8 hpt. Similarly, a significant increase in the number of *lck*:GFP+ lymphocytes was observed at 3 hpt. However, unlike the *lyz*:GFP+ cells, *lck*:GFP+ lymphocytes were further elevated at 8 hours post R848 treatment. This may indicate that proliferation in leukocytes has occurred, as seen in the leukocytes of Japanese flounders following R848 stimulation *in vitro* (Zhou & Sun, 2015). Although the ability of R848 to stimulate Tlr7/8 in teleost has not been investigated specifically, given the evolutionary conservation of TLRs between teleost and mammals (Li *et al*., 2017), these results suggest that R848 is likely to stimulate these TLRs in zebrafish. This would indicate that there are conserved R848 response pathways between teleost and mammals. Furthermore, orthologues of TLR7 and TLR8 have been identified in zebrafish, with two orthologues present for TLR8 (*tlr8a* and *trl8b*) (Li *et al*., 2017). In addition, Svingerud *et al.* found that salmon cell lines with little or no expression of Tlr7/8 were not able to induce an IFN response when treated with R848 (Svingerud *et al*., 2012).

4.2 Aims

The previous chapter investigated the heterogeneity found among cells expressing the *Runx*:mCherry transgene. To gain a deeper understanding of the functional differences between *Runx*:mCherry+ cells found in the WKM and the gill, this chapter sets out to investigate the effects of antibiotic and/or immune stimuli on *Runx*:mCherry-expressing cells. Furthermore, this chapter aims to investigate whether bloodless *cmyb*^{t25127} mutant fish are capable of responding to a viral-type immune stimulus.

More specifically, the aims of this chapter are to:

1. Assess the response of *Runx*:mCherry+ cells and innate immune cells to antibiotic treatments.
2. Investigate whether the zebrafish response to the viral mimetic poly I:C is altered by antibiotic pre-treatment.
3. Determine whether *Runx*:mCherry+ cells in the gill respond to topical application of R848 viral mimetic and Tlr7 agonist.
4. Assess the ability of bloodless *cmyb*^{t25127}mutant fish to respond to R848 treatment by immersion.

4.3 Results

4.3.1 The response of Runx:mCherry+ cells and innate immune cells to antibiotic treatments

4.3.1.1 Zebrafish response to low-dose penicillin-streptomycin treatment does not significantly alter hematopoietic output

With an appreciation for the *Runx*:mCherry+ population in the WKM, which contains HSPCs involved in steady-state hematopoiesis, the next aim was to determine how these *Runx*:mCherry+ cells of juvenile and adult zebrafish might be affected by antibiotic treatment. Josefsdottir *et al.* (2016) have shown that broad-spectrum antibiotics, including beta-lactam antibiotics, were capable of altering the hematopoietic output of mice through reduction of gut microbial diversity, resulting in reduced bone marrow cellularity and absolute HSC numbers. Furthermore, data from Charlwood (2017) has demonstrated that a dose of 10 U/mL penicillin and 10 µg/mL of streptomycin (PS) broad-spectrum antibiotics was sufficient to induce a reduction in gut microbial diversity. This dose of PS is commonly used in zebrafish-rearing media and has been found to impair gut peristalsis when administered in combination with a high-cholesterol diet (HCD) (Progatzky *et al*., 2014). It is important to understand the impact this dose of PS can have on the hematopoietic output of the zebrafish raised in it. To this end, the hematopoietic output of juvenile transgenic zebrafish reared in E2+ PS media for 7 weeks was assessed by flow cytometry. Embryos were reared in system water and with methylene blue until 5 dpf and subsequently raised in E2 medium ± PS until 8 wpf. It was found that, in the WKM of 8-wpf fish raised with continuous exposure to PS, the number of *Runx*:mCherry+ HSPCs, *lyz*:GFP+ and *mpx*:GFP+ neutrophils were not significantly altered relative to their PS-free siblings. In addition, no change was detected in the proportion of major blood cell populations in the WKM (Appendix 1). However, a small increase in *lck*:GFP+ lymphocytes was detected (Fig. 4.1).

Due to the well-established link between the use of antibiotics for growth promotion of livestock, including fish (Butaye *et al*., 2003; He *et al*., 2010; Carvalho *et al*., 2016), the length and mass of zebrafish reared ± PS were compared. The results showed no difference in length or mass of fish between the two groups overall (Appendix 2). In addition, BMI was calculated for each fish (BMI= kg/ cm^2). However, there was no difference in the BMI of treated and

untreated fish (Fig. 4.1D). This indicates that rearing fish in low-dose PS for a period of 7 weeks does not increase their growth rate.

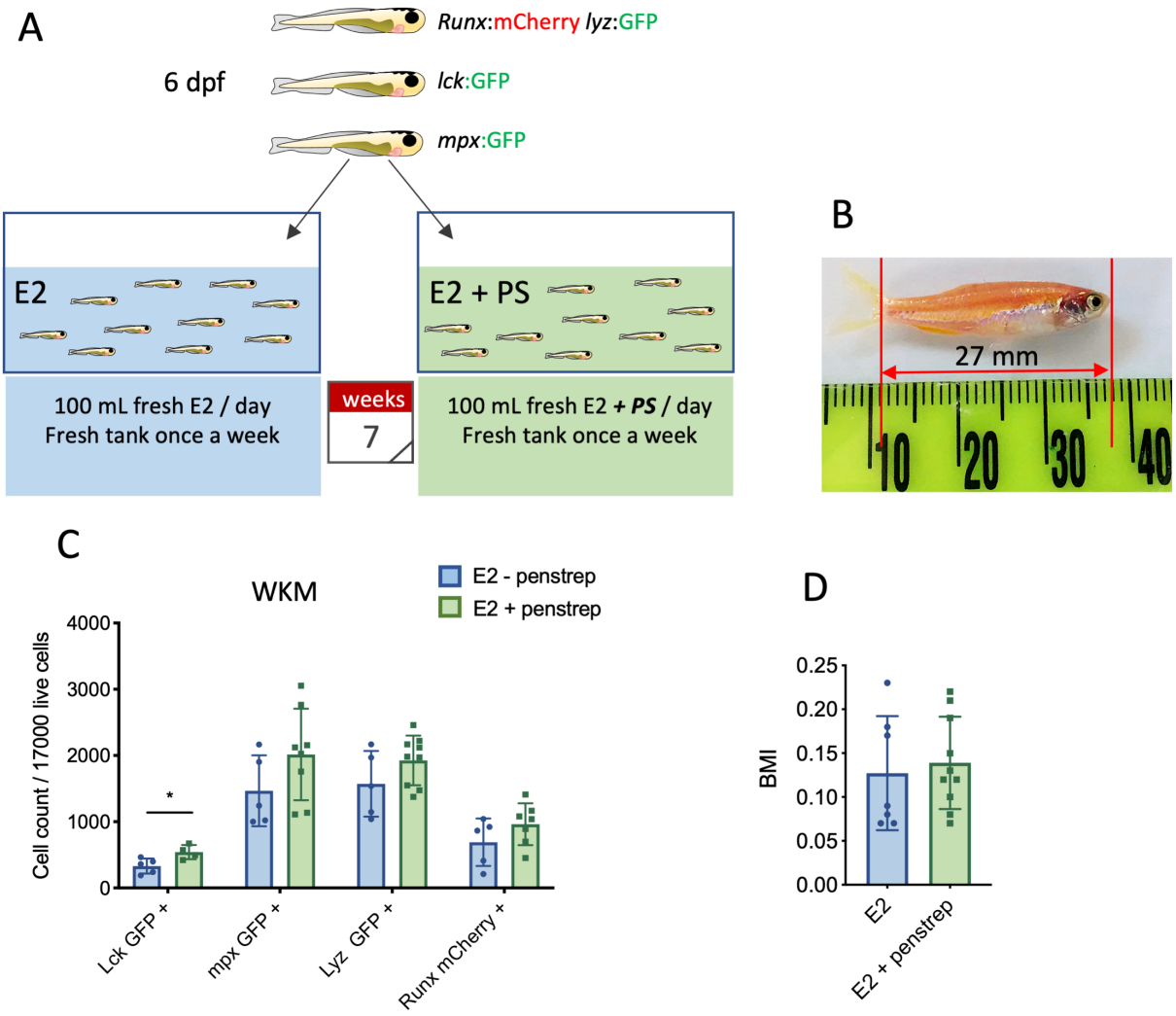

Fig. 4.1 Seven weeks of low-dose PS treatment does not significantly alter hematopoietic output of juvenile fish.

Six dpf, transgenic *Tg(Runx:mCherry; lyz:GFP), Tg(lck:GFP)* and *Tg(mpx:GFP)* fish were placed into E2 medium ± PS (10 U/mL penicillin and 10 µg/mL of streptomycin) and reared in benchtop tanks for 7 weeks. Treatment was administered through the addition of 200 mL E2± PS each day, in addition to a weekly change of tanks. (**A**) Schematic representation of experimental set up. (**B**) Fish size measurement, red lines indicate section of fish measured from head to tail, not including tail fin. (**C**) Single cell suspensions of WKM were subjected to flow cytometry and cell counts/ 17000 live cells were analysed for each transgenic cell type. Each dot indicates 1 fish. N= 5-9. Data pooled from 3 independent experimental repeats. Student's t-test *P < 0.05. (**D**) BMI of zebrafish reared on E2± PS (kg/ cm2). N= 7-10. Mean and SD shown. Where P value is not shown, differences were not statistically significant.

Due to data suggesting that there may be a trend towards increasing cell numbers in the myeloid and lymphoid lineages in zebrafish reared with PS, the effect of short-term PS treatment of adult zebrafish was investigated. As before, a dose of 10 U/mL of penicillin and 10 µg/mL of streptomycin was used. Adult fish received the PS via addition to system water for 2 weeks. This time point was chosen as previous research in human studies and mouse models have shown that 2 weeks of broad-spectrum antibiotics were sufficient to reduce HSC numbers and cause abnormal hematopoiesis, particularly regarding lymphoid cells (Josefsdottir *et al.,* 2016). It was reported that erythro-myelopoiesis remained unaffected in response to broad-spectrum antibiotic treatment. For this experiment, adult *Tg(Runx:mCherry; lyz:GFP*) fish were investigated so that neutrophil output could be assessed concomitantly with HSPC numbers. The data indicates that there was no difference in either *lyz*:GFP+ cells, *Runx*:mCherry+ populations or other major blood cell populations in the WKM of adult fish exposed to low-dose PS for 2 weeks (Fig. 4.2; Appendix 3). For further analysis, a more potent type and dose of antibiotic was investigated subsequently (section 4.3.1.2).

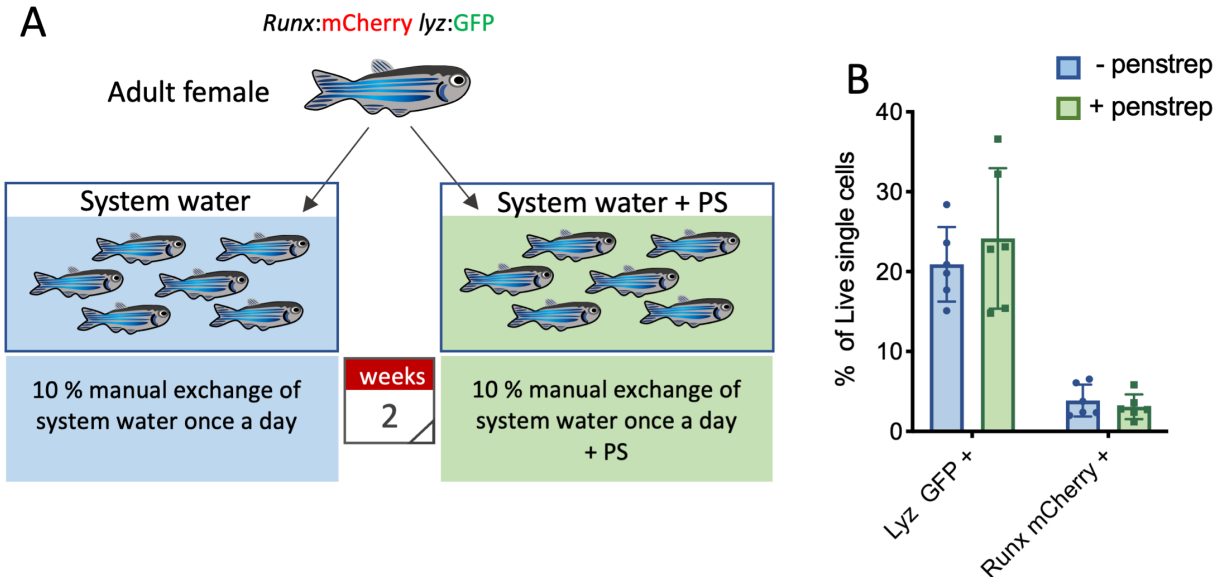

Fig. 4.2 Two weeks of low-dose penicillin streptomycin does not significantly alter hematopoietic output of adult *Tg(Runx:mCherry; lyz:GFP)* zebrafish.

Adult transgenic *Tg(Runx:mCherry; lyz:GFP)* fish were treated in system water ± PS (10 U/mL penicillin and 10 µg/mL of streptomycin) for 2 weeks. Treatment was administered through the addition of system water ± PS each day with 10 % exchange. (**A**) Schematic representation of experimental set up. (**B**) Single cell suspensions of WKM were subjected to flow cytometry. *Runx*:mcherry+ and *lyz*:GFP + cells were analysed as a percentage of live cells. Each dot indicates 1 fish. N= 6. Data pooled from 2 independent experimental repeats. Mean and SD are shown. Where P value is not shown, differences were not statistically significant.

4.3.1.2 Ten-day 50 mg/L OTC exposure reduces gill bacterial load and reduces HSPC cellularity in the WKM of adult zebrafish

Low-dose PS appeared to have minimal impact on WKM cellularity of juvenile fish treated for 7 weeks or adults treated for 2 weeks with 10 U/mL penicillin and 10 µg/mL of streptomycin. Next, OTC, a commonly used antibiotic in aquaculture, was investigated. High doses of OTC have been shown to reduce zebrafish gut bacterial diversity and result in impaired gut health due to increased activity of digestive enzymes and reduced AKP and ACP activity (Zhou *et al*., 2018). To determine whether microbial diversity in the gut reduced WKM HSPC proportions, adult *Tg(Runx:mCherry; lyz:GFP)* zebrafish were treated with 50 mg/L OTC in system water for 10 days. This dose of OTC has been shown not to increase mortality in adult zebrafish (Oliveira *et al*., 2013) but was capable of inducing macroscopic histological changes in the gills of adult rainbow trout (Rodrigues *et al*., 2017). The data indicates that this dose of OTC does not alter the proportion of *lyz*:GFP+ cells in the WKM or gills of adult fish, suggesting that neutrophil output remains unchanged (Fig. 4.3B). In addition, the proportions of each major blood cell lineage in the WKM also remained unchanged (Appendix 4).

Data interrogating the relationship between the OTC treatment and *Runx*:mCherry+ cells in the WKM and gill has shown that there was no change in the number of *Runx*:mCherry+ cells in the gill of treated adult fish. In the WKM, on the other hand, a possible trend towards decreased proportion of *Runx*:mCherry+ cells was found across three independent experiments. The data was pooled and confirmed this trend. However, the change in *Runx*:mCherry+ cells in the WKM is not statistically significant (P=0.067 using the student's t-test; Fig. 4.3C). Furthermore, *Runx*:mCherry ^{high} and ^{low} populations in the WKM were dissected to illuminate whether or not the possible reduction in population size in response to OTC treatment could be attributed to changes in one or both populations. The data revealed no statistically significant difference in either the *Runx*:mCherry ^{high} or *runx*:mCherry ^{low} populations upon OTC treatment (Fig. 4.3 D, E). To assess the biological importance of the trend in reduced WKM *Runx*:mCherry+ cells, the abundance of *Runx*:mCherry+ cells must be correlated with 16S values, which are indicative of bacterial load. If there is a positive correlation between cell abundance and increased 16S, this would indicate that bacterial load can alter the WKM *Runx*:mCherry+ population.

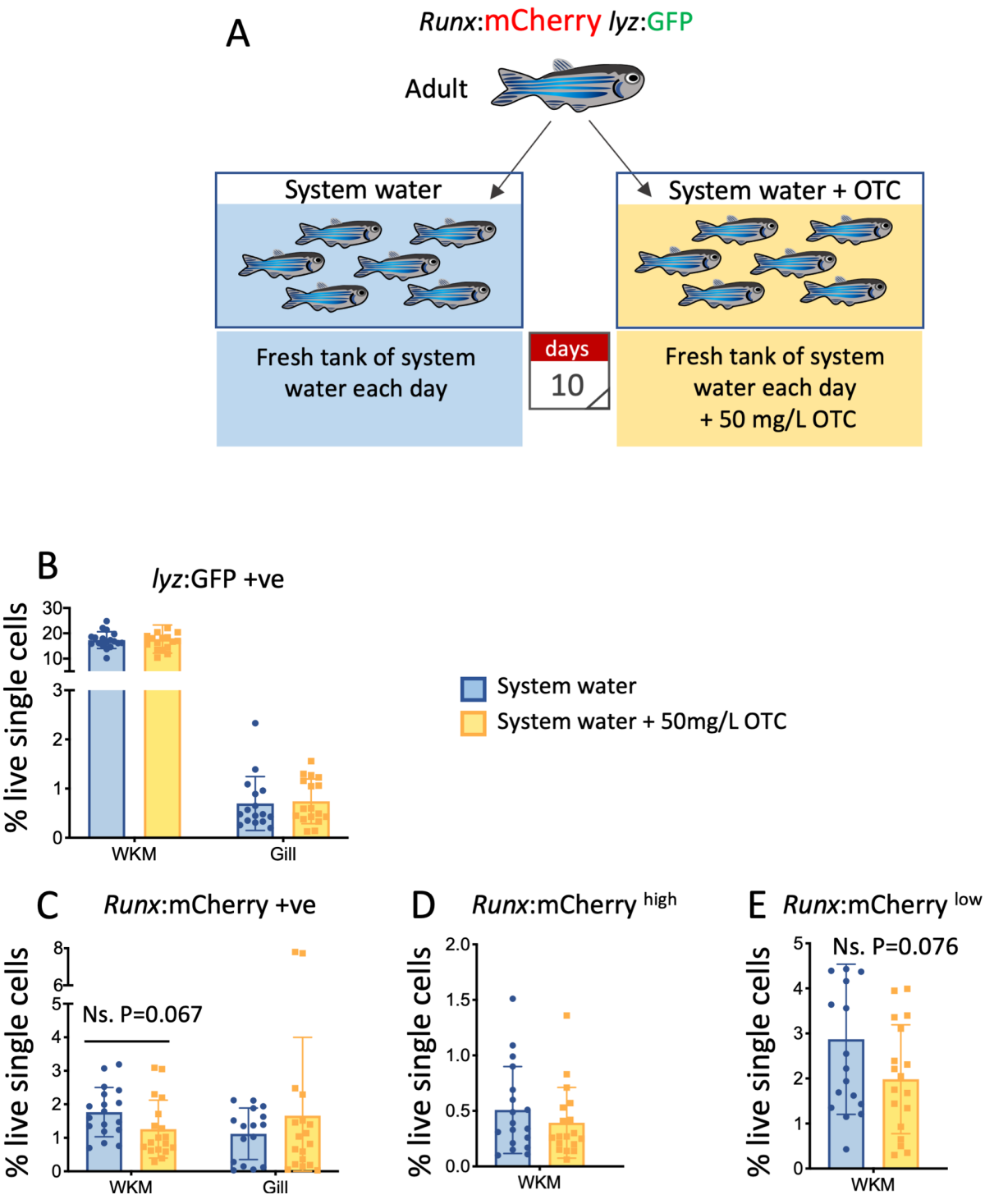

Fig. 4.3 Ten days of OTC treatment of adult *Tg(Runx:mCherry; lyz:GFP)* zebrafish does not alter neutrophil output but may reduce *Runx*:mCherry+ cells in the WKM.

Adult transgenic *Tg(Runx:mCherry; lyz:GFP)* fish were treated in system water ± 50 mg/L OTC for 10 days. Treatment was administered via the replacement of all water ± OTC each day to ensure OTC remained bioactive. (**A**) Schematic representation of the experimental set up. (**B-E**) Single-cell suspensions of WKM and gill tissue were subjected to flow cytometry. Mean and SD are shown. *lyz*:GFP+ (**B**) and *Runx*:mCherry+ cells (**C**) were analysed as a percentage of live cells. (**D, E**) Proportion of *Runx*:mCherry+ cells in WKM were distinguished as *Runx*:mCherry ^{high} (**D**) and *Runx*:mCherry ^{low} (**E**). Each dot indicates 1 fish. N= 16-18. Data pooled from 3 independent experimental repeats. Where P value is not shown, differences were not statistically significant.

The bacterial load of OTC-treated and control fish was compared in the gills, which were directly exposed to the OTC in the water, and also the gut which was exposed to OTC through ingestion. It was found that fish within the control group exhibited highly variable 16S rRNA levels relative to 18S. However, there was a significant reduction in 16S levels in the gills of the OTC-treated group (Fig. 4.4A). In the gut, on the other hand, there was an increase in 16S levels compared to the untreated control (Fig. 4.4B). These findings are consistent with Charlwood (2017), which showed that administration of PS caused reduced bacterial diversity in the gut of embryos while increasing total bacterial load, as measured by 16S levels.

Given the change in bacterial load between the OTC-treated and control groups, as well as the trend indicating a reduction in the percentage of *Runx*:mCherry+ cells in the WKM, it was hypothesized that animals that experienced the greatest change in bacterial load, as measured by 16S rRNA levels, may have the lowest percentage of *Runx*:mCherry+ cells in the WKM. Indeed, a statistically significant positive correlation was identified between the percentage of *Runx*:mCherry+ cells in the WKM and 16S levels in the gills (Fig. 4.4C). However, a positive correlation was not identified between the 16S levels in the gut and *Runx*:mCherry+ cells in the WKM, or 16S levels and *Runx*:mCherry+ cells in the gills. Nevertheless, the correlation between reduced gill bacterial load and reduced percentage of *Runx*:mCherry+ cells in the WKM suggested that HSPCs in the WKM were specifically reduced in response to OTC treatment. Due to the distinct niches occupied, differential gene expression patterns and differential response to OTC treatment between *Runx*:mCherry+ cells in the gills and WKM (Fig. 3.25 & 26), *Runx*:mCherry+ cells in the gills may represent a different cell type to those found in WKM.

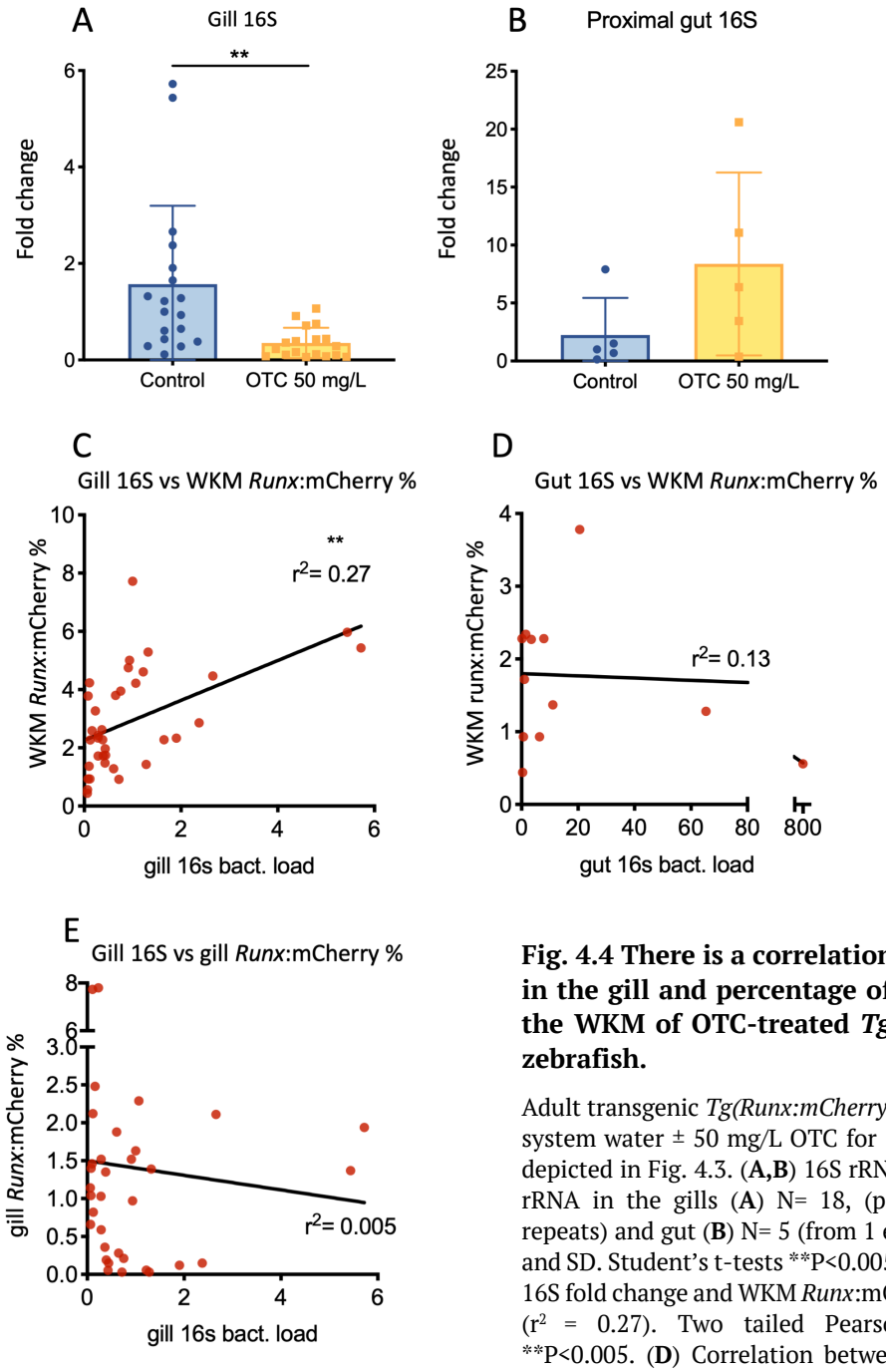

Fig. 4.4 There is a correlation between 16S rRNA load in the gill and percentage of *Runx*:mCherry+ cells in the WKM of OTC-treated *Tg(Runx:mCherry; lyz:GFP)* zebrafish.

Adult transgenic *Tg(Runx:mCherry; lyz:GFP)* fish were treated in system water ± 50 mg/L OTC for 10 days. Experimental set up depicted in Fig. 4.3. (**A,B**) 16S rRNA fold change relative to 18S rRNA in the gills (**A**) N= 18, (pooled from 3 experimental repeats) and gut (**B**) N= 5 (from 1 experiment). Bars show mean and SD. Student's t-tests **P<0.005. (**C**) Correlation between gill 16S fold change and WKM *Runx*:mCherry percentage of live cells (r^2 = 0.27). Two tailed Pearson's correlation coefficient **P<0.005. (**D**) Correlation between gut 16S fold change and WKM *Runx*:mCherry percentage (r^2 = 0.13). (**E**) Correlation between gill 16S fold change and gill *Runx*:mCherry percentage (r^2 = 0.005). Where P value is not shown, differences were not statistically significant.

4.3.2 OTC pre-treatment does not alter the zebrafish response to systemic poly I:C treatment

Having found a correlation between OTC treatment and reduced *Runx*:mCherry+ cells in the WKM, suggesting reduced HSPC numbers in the zebrafish, the ability of OTC-treated zebrafish to respond to immune stimuli such as poly I:C was investigated. Poly I:C was chosen as an immune stimulant as the zebrafish response to IP injection of 5 µL (10 µg) poly I:C has been thoroughly characterised by McBrien (2017), including the effects of two week long stimulation on the HSPC compartment, which indicated reduced *CD41*:GFP+ HSPC numbers in the WKM 1 week post treatment (wpt). To determine how OTC treatment may alter the response to systemic poly I:C treatment, the fish were allocated into one of two groups, water control or OTC treatment. For 10 days, fish were maintained in static tanks in either system water or system water with 50 mg/L OTC, both of which were replaced daily. After 10 days, the groups were split up further for poly I:C and saline control groups. Fish received a 5 µL IP injection of either saline or poly I:C and were harvested for analysis 3 hours post injection (hpi). During the 3 hpi, fish remained exposed to fresh OTC or system water (Fig. 4.5A).

Transcript levels were determined using the ΔΔCt method, normalised to 18S transcript levels. The results reinforced data previously reported by McBrien (2017), which measured the responses to 10 µg poly I:C after 3 hours. There was a significant increase in *cxcl18b* (formerly *cxcl-c1c*) both in fish that remained in water as well as those in OTC. Fish that remained in water exhibited a 70-fold increase in *cxcl18b* expression in the WKM and a ~26-fold increase in the gill, while those that were OTC-treated only showed a small and non-significant increase relative to water-treated fish (82-fold increase in the WKM, 31-fold increase in the gill) (Fig. 4.5 B, C). Interleukin 1 beta (*il1β)* transcripts were also significantly increased following poly I:C treatment (11-fold increase in WKM and 5-fold increase in the gill), and this pattern was not significantly altered by OTC exposure (13-fold increase in the WKM, 3-fold increase in the gill). Zebrafish type 1 interferon *ifnϕ1* transcripts were elevated 24-fold in the WKM of control fish and 26-fold in the presence of OTC, while in the gill this increase was 34-fold and 28-fold respectively. Finally, the type 2 interferon *ifnγ1-2* exhibited an average of 24-fold increase in response to poly I:C treatment in the WKM of control fish and 38-fold increase in OTC-treated fish. In the gill, a 14-fold increase in *ifnγ1-2* transcript levels was detected in the control fish and an 11-fold increase in OTC-treated fish (Fig. 4.5 B, C). Taken together, it appears that the zebrafish response to systemic administration of 10 µg poly I:C

did not become either attenuated or exacerbated by exposure to 50 mg/L OTC over the preceding ten days.

Investigating the abundance of *lyz*:GFP+ and *Runx*:mCherry+ cells in the gills revealed no change in the response to either poly I:C on its own or poly I:C in combination with OTC. In the WKM, no change was observed in the abundance of *lyz*:GFP+ cells across the groups. A small but statistically non-significant reduction in *Runx*:mcherry ^{high} cells was detected in the WKM of OTC-treated groups. No such reduction was evident in the *Runx*:mcherry ^{low} population (Fig. 4.5D-E). However, as shown by McBrien (2017) and Josefsdottir *et al.* (2016), the number of cells does not need to change in order for functional changes to occur in the biology of HSCs and HSPCs. To fully assess whether stem cell potency was affected, transplantation assays would be required.

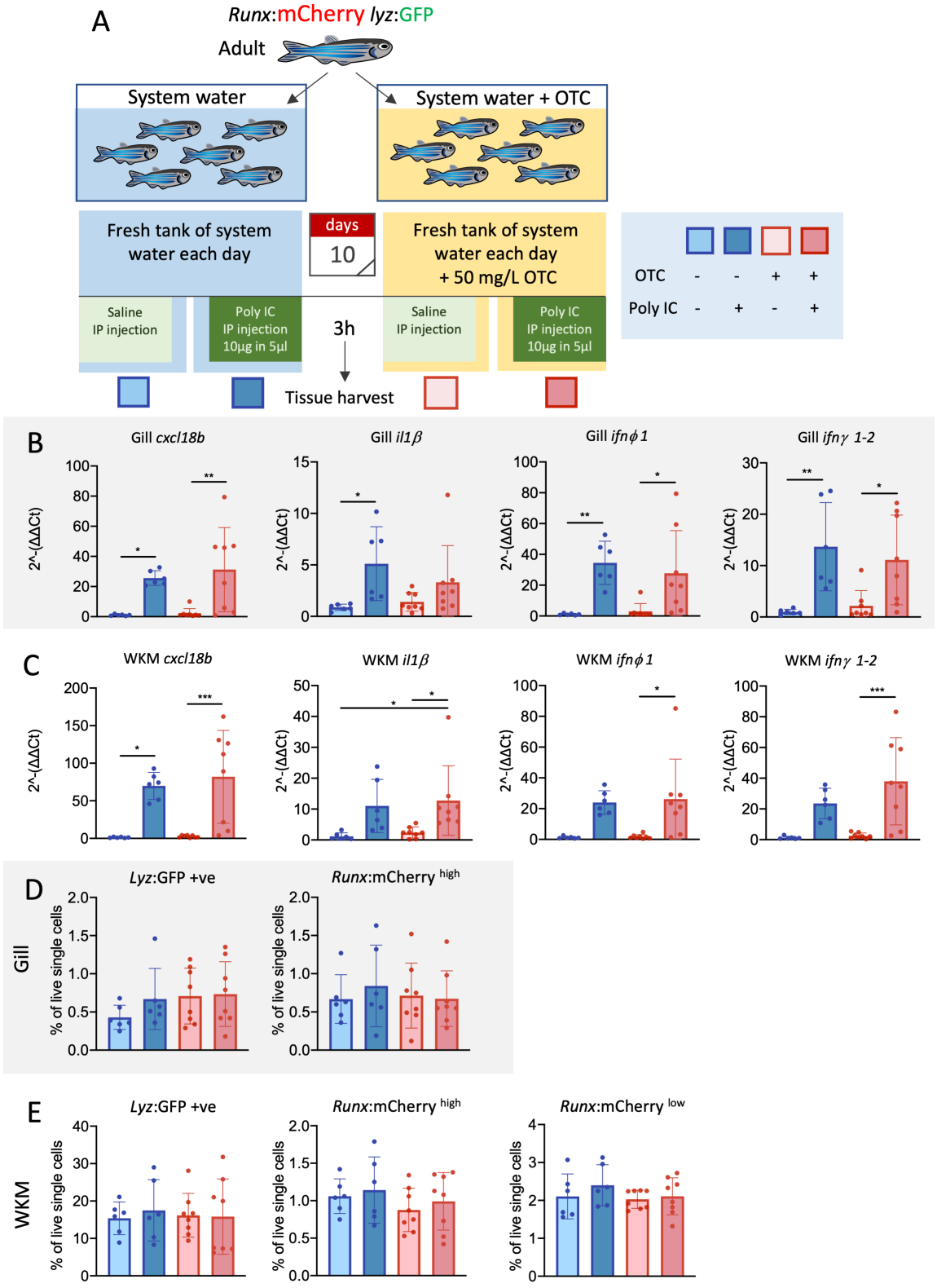

Fig. 4.5 OTC treatment does not alter the immune response to systemic poly I:C treatment of *Tg(Runx:mCherry; lyz:GFP)* zebrafish.

Adult transgenic *Tg(Runx:mCherry; lyz:GFP)* zebrafish were treated in system water ± 50 mg/L OTC for 10 days, as depicted in **(A).** Subsequently, both OTC and control groups were randomly split into two groups for intraperitoneal (IP) injection of poly I:C or saline control. WKM, gill, and gut were harvested at 3 hours post IP injection. (**A**) Experimental set up. (**B,C**) qRT-PCR analysis of the gills (**B**) and WKM (**C**) from water + saline (light blue), water + poly I:C treated (dark blue), OTC + saline (light red) and OTC + poly I:C treated (dark red) zebrafish.

Panel of inflammatory cytokines associated with response to poly I:C includes *cxcl18b*, *il1β, ifnϕ1* and *ifnγ1-2*. Mean and SD are depicted. Individual dots show relative expression values obtained for individual fish. Values for each gene were normalised to 18S and expressed as fold change relative to the median sample in the water + saline treated control group. (**D,E**) Flow cytometry quantification of the percentage of GFP+ and mCherry+ cells in *Tg(Runx:mCherry; lyz:GFP)* zebrafish gills (**D**) and WKM (**E**) 3 hours post poly I:C treatment. Each dot represents the percentage of GFP or mCherry+ cells obtained for one individual fish. The mean and SD are shown. N=6-8. Three experimental replicates were performed, and the data pooled (each experiment following the same trend). *P < 0.05, **P < 0.005, ***P < 0.0005, ****P < 0.00005. One-way ANOVA and Tukey's multiple comparisons test. Where P value is not shown, differences were not statistically significant.

4.3.3 TLR7 and TLR8 agonist R848 may induce a small increase in the abundance of Runx:mCherry+ cells in the zebrafish gill

To further characterise the *Runx*:mCherry+ population in the gill, their response to the TLR7 and TLR8-agonist R848 was investigated. R848 is a single stranded RNA viral mimetic, which has been used in the Dallman lab to study the zebrafish gill response to viral type respiratory challenge. R848 is applied to the gill directly and has been shown to induce a robust cytokine response in the gill tissue, with an early upregulation of *tnfα* and *il1β* mRNA transcripts followed by a later upregulation of *ifnϕ1* and *ifnγ1-2* transcript levels (Porgatzky *et al*., 2019; Dallman lab personal communication). This model of inflammatory gill challenge was chosen as it has been shown to induce a quantitative increase in innate and adaptive immune cells in the adult zebrafish gill. This has been shown by the transient increase in *lyz*:GFP+ neutrophils at 3 hours post challenge, and increases in *lck*:GFP+ lymphocytes at both 3 and 8 hours post challenge, as observed by microscopy (Progatzky *et al*., 2019).

Runx1:mCherry+ cells were found to be abundant in the gills (Fig. 3.3, 3.8) and exhibited high *runx1* and transgene-driven *mCherry* transcript levels (Fig. 3.25). Although, it was not possible in the duration of this project to elucidate what cells comprise this population, results in Chapter 3 showed that *Runx*:mCherry+ cells do not overlap with either *IgM*:GFP+ or *lck*:GFP+ cells in the gill (Fig. 3.16, 3.17). It remains to be uncovered what types of cells express the transgene. By applying inflammatory stimulation to the gill and observing how the cells respond, a deeper insight into the function of this population may be gained.

Tg(Runx:mCherry; lyz:GFP) transgenic zebrafish were treated with R848 by application of 2.5 µg of R848 directly onto the gills. Endotoxin-free water was applied to the gills of fish in the control group. The gills of R848-treated fish were harvested either 3 or 8 hpt so that both any early and late response would be detected (Fig. 4.6A). The gills from the treated side of each

fish were split into 3 groups such that flow cytometry, qPCR and microscopy analysis could be carried out using tissue from the same fish. This experiment was carried out by Dr. Wane (Dallman lab, Imperial College London) in collaboration with A. Scemama (MRes, Imperial College London). The qPCR data confirmed that a robust induction of inflammatory cytokines had taken place at 3 and 8 hpt, following previously established kinetics (Dallman lab, personal communication; Progatzky *et al*. 2019). The expression levels of *ifnγ1-2*, *ifnϕ1* and *cxcl18b* transcript levels were determined as a relative increase compared to 18S transcript levels using the ΔCt method. The data showed that both *ifnγ1-2* and *ifnϕ1* transcript levels increased relative to 18S at 3 and 8 hpt. *cxcl18b* was also increased at 3 and 8 hpt relative to the sham control. However, at 8 hpt, transcript levels had decreased compared to the 3-hour timepoint (Fig. 4.6B). Parallel to qPCR data acquired from the gills, flow cytometry data was also analysed and indicated a trend of transiently increased *lyz*:GFP+ cells in the gills 3 hpt. However, the increase in *lyz*:GFP+ cells was not statistically significant when measured by flow cytometry (Fig. 4.6C; Madina Wane, personal communication). No change was found in the abundance of *Runx*:mCherry+ cells at either 3 or 8 hpt.

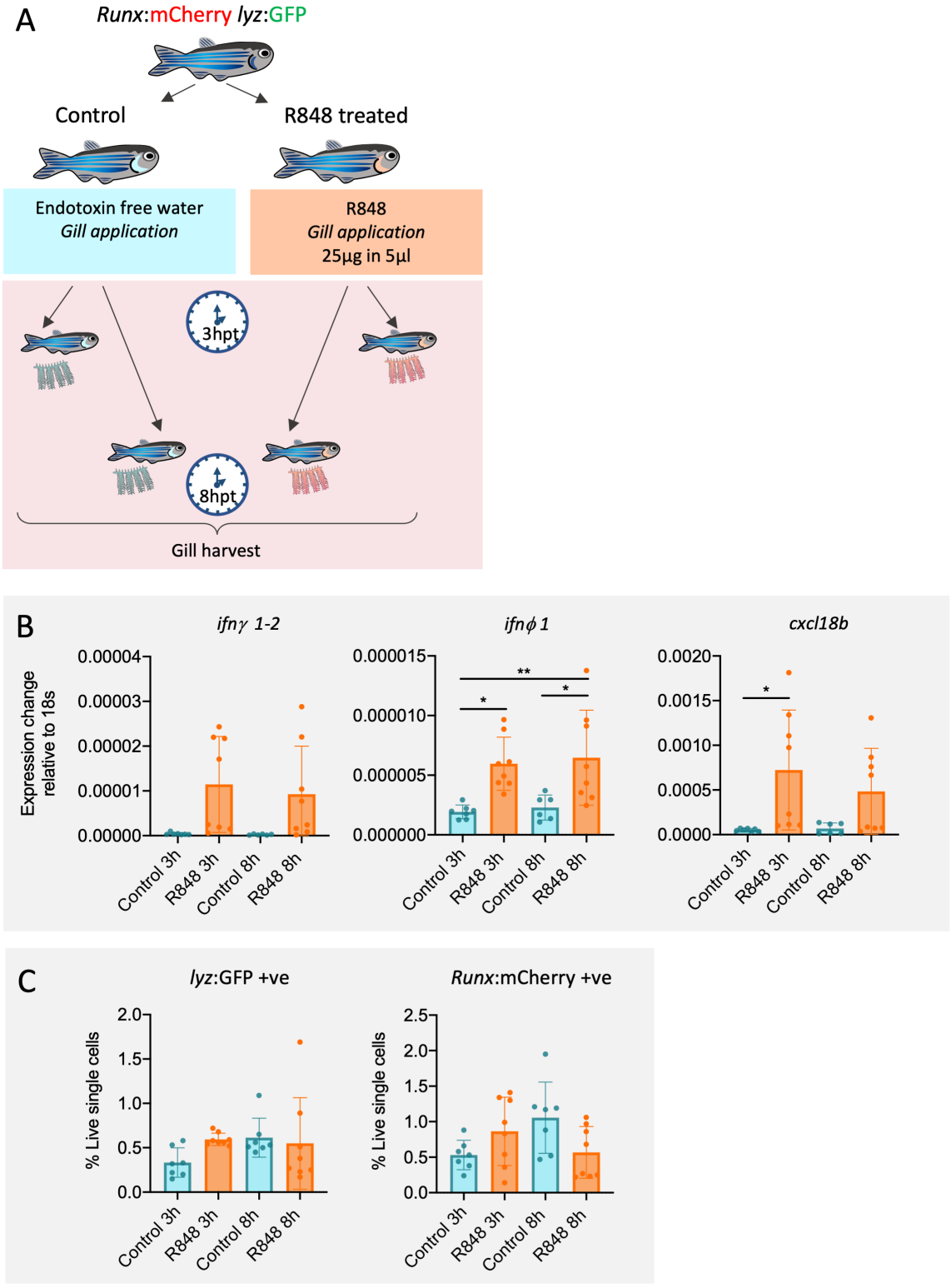

Fig. 4.6 The response of adult *Tg(Runx:mCherry; lyz:GFP)* gills to R848 gill application.

The gills of adult *tg(Runx:mCherry; lyz:GFP)* transgenic zebrafish were treated directly with 2.5 µg R848 delivered in 5 µL endotoxin-free water. Sham treated fish received 5 µL endotoxin-free water only. Gills of fish were first dried with tissue before applying solutions. Gills were harvested 3 or 8 hpt for both control and R848-treated fish. Data pooled from 2 experimental replicates. N=8. Procedure carried out by Dr. Wane (Dallman lab, Imperial College London) in collaboration with A. Scemama (MRes. Imperial College London). (**A**) Schematic of experimental set up. (**B**) qRT-PCR analysis of the gills at 3 and 8 hpt of control and R848-treated gills. The mRNA expression levels of *ifnγ1-2*, *ifnϕ1* and *cxcl18b* are expressed as a ratio relative to 18S transcrip levels using formula 2^-(ΔCt). Each

dot represents the expression levels from one individual fish. Mean and SD are shown. *P < 0.05, **P < 0.005. One-way ANOVA and Tukey's multiple comparisons test. Where P value is not shown, differences were not statistically significant. (**C**) Flow cytometry quantification of the percentage of GFP+ and mCherry+ cells as a proportion of live single cells in *Tg(Runx:mCherry; lyz:GFP)* zebrafish gills at 3 and 8 hpt. Each dot represents the transcript levels from one individual fish. Mean and SD are shown.

Next, the number of *lyz*:GFP+ and *Runx*:mCherry+ cells were quantified in the primary and secondary lamellae by microscopy in order to give an indication of how cell distribution may change. A transient increase in neutrophils was found at 3 hpt, as expected from previous data (Progatzky *et al*., 2019; Fig. 4.7A, B). The increase in neutrophils appeared roughly equal throughout the primary and secondary lamellae of the gills. Although not statistically significant, there appeared to be an indication of a small increase in *Runx*:mCherry+ cells at 3 and 8 hpt in response to R848 (Fig. 4.7A, C). At 3 hpt, there was an average increase from 10 to 16 cells in the area quantified in the primary lamella of the gills, while the number of *Runx*:mCherry+ cells remained constant in the secondary lamellae. There were fewer *Runx*:mCherry+ cells in the 8 hour control samples compared to the 3 hour controls. Nevertheless, at 8 hours, the number of *Runx*:mCherry+ cells appeared to increase in both the primary and secondary lamellae in R848-treated gills relative to the 8-hour control samples. In the primary lamellae of the control group, the average cell count was 4. In R848-treated fish, this count was higher with an average of 11 cells. In the secondary lamellae, the average counts were 4 cells in the control group and 6 in R848-treated fish (Fig. 4.7C). However, these results were not statistically significant. Given the heterogeneity in the abundance *Runx*:mCherry+ cells in untreated zebrafish gills and the resultant high standard deviation (Fig. 3.8E, 4.6C, 4.7C), it was calculated that approximately a further 15 samples would be required per experimental group to achieve a power of 85 %, which was not feasible in this project. In addition, there can be experimental limitation in cell quantification. For example, gills that are partially obstructed or damaged during dissection or staining can limit the number of lamellae that can be used to carry out cell quantification following microscopy. Thus, a greater number of experimental repeats would ensure a greater number of lamellae can be quantified. An increase in the abundance of *Runx*:mCherry+ cells upon R848 treatment would suggest that these cells may be capable of responding to viral-like stimuli.

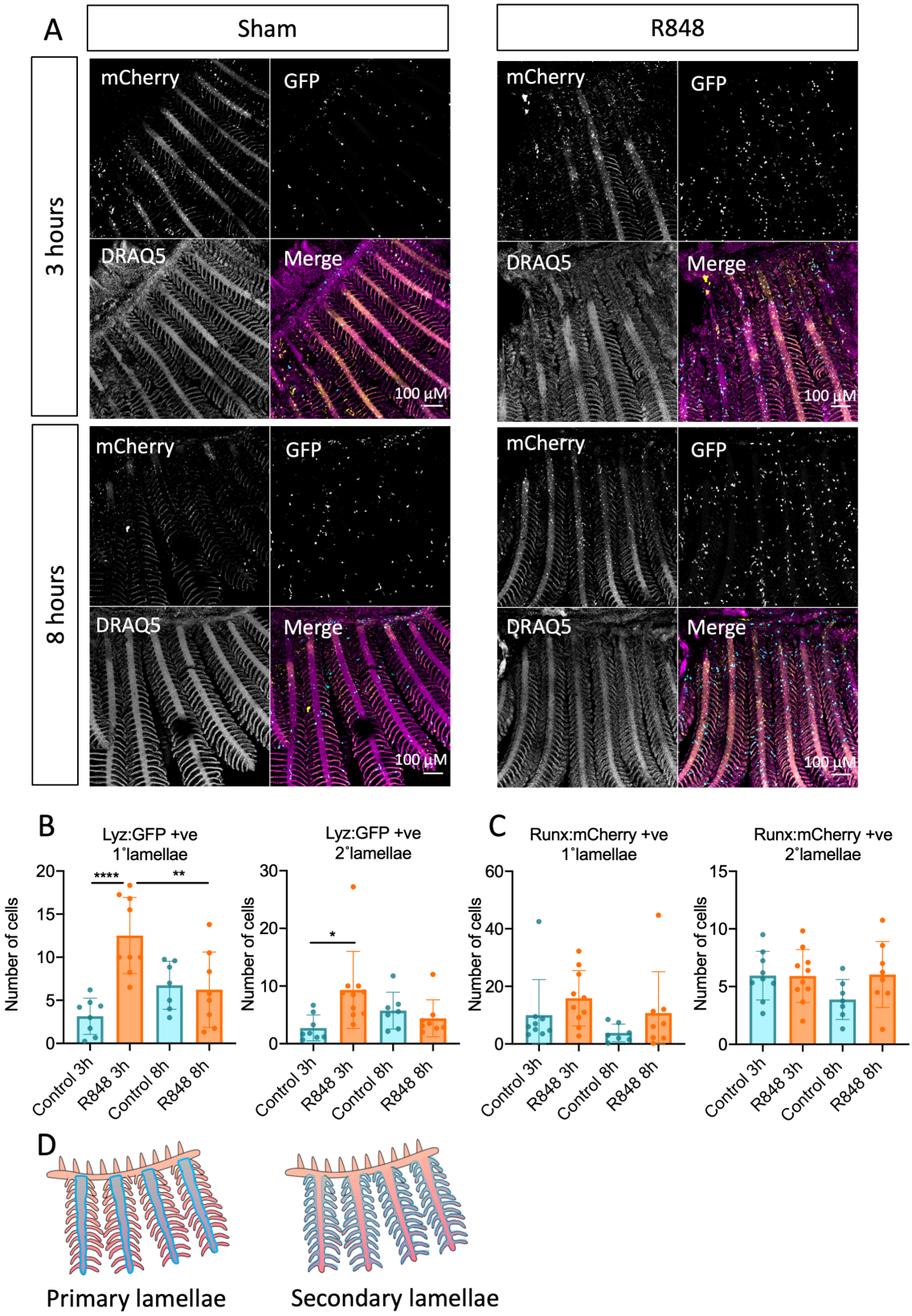

Fig. 4.7 The response of *lyz*:GFP+ and *Runx*:mCherry+ cells in the gills of adult *Tg(Runx:mCherry; lyz:GFP)* transgenic zebrafish in response to R848 gill application.

The gills of adult *tg(Runx:mCherry; lyz:GFP)* transgenic zebrafish were treated directly with 2.5 µg R848 delivered in 5 µL endotoxin free water as described in Fig. 4.6. Gills were harvested 3 or 8 hpt for both sham and R848-treated fish. Data pooled from 2 experimental replicates. N=8. Experiment carried out by Dr. Wane (Dallman Lab, Imperial

College London) in collaboration with A. Scemama (MRes. Imperial College London). Analysis was carried out in collaboration with A. Scemama. (**A**) Representative maximum z-stack projections of immunoassayed control and R848-treated gills harvested 3 and 8 hpt. Images acquired at 170X magnification. mCherry staining of *Runx*:mcherry+ cells in yellow, GFP staining of *lyz*:GFP+ neutrophils in cyan and Draq5 nuclear staining in magenta. Scale bar represents 100 µM. mCherry and GFP signal top, Draq5 bottom left and merged at the bottom right. (**B, C**) Average number of *lyz*:GFP+ (**B**) and *Runx*:mcherry+ (**C**) cells in the primary lamellae and in the 20 secondary lamellae most proximal to the arch, of each filament, at 3 and 8 hpt. Each dot indicates average counts per individual gill. Mean and SD shown. *P < 0.05, **P < 0.005, ***P < 0.0005, ****P < 0.00005. One-way ANOVA and Tukey's multiple comparisons test. Where P value is not shown, differences were not statistically significant. (**D**) Schematic of gill structure. Blue overlay indicates primary and secondary lamellae where cells have been counted for data in (**C**).

4.3.4 Cmyb^{t25127} *mutant fish can partially increase expression of some inflammatory cytokines in response to R848 treatment*

Previous research has shown that zebrafish gills are capable of mounting an immune response to topically applied R848 (Progatzky *et al* 2019). In addition, the data in section 4.3.3 of this chapter further corroborated this research and showed a strong antiviral response via increased *ifnγ1-2*, *ifnϕ1* and *cxcl18b* transcript levels in adult *Tg(Runx:mCherry; lyz:GFP)* zebrafish. Tlr7 and Tlr8 are intracellular receptors found on the luminal side of endosomal and lysosomal membranes. The *cmyb*^{t25127} mutant zebrafish (hereafter referred to as *cmyb* mutants) do not undergo definitive wave of hematopoiesis. However, non-hematopoietic cells also express these receptors. Hence, it is likely that *cmyb* mutant fish express these TLRs on their endosomal membranes to some extent. However, this has not been confirmed and could be assessed by gene transcript analysis in the future. To better understand the antiviral immune response that *cmyb* mutants can elicit, their response to R848 was investigated at 4-6 wpf. Parts of this work were carried out in collaboration with Alice Scemama (MRes. Imperial college London).

As the response of adult zebrafish to topical gill application of R848 has been characterised, the subsequent aim was to investigate the response of *cmyb* mutant gills to R848. Due to the growth retardation exhibited by *cmyb* mutants, it was not possible to apply R848 topically to the gills. Furthermore, it was necessary to pool all 8 gill arches of 7-8 fish in order to obtain sufficient gill mRNA to assay gene transcription levels by qRT-PCR. Therefore, to ensure consistent treatment across fish, the decision was made to pool fish into groups (depending on the timepoint they would be harvested at) and treat pooled fish together by immersion in 500 µL 0.5 mg/ mL R848. This dose was chosen as it is analogous to the concentration of R848 applied to the gills of adult fish in section 4.3.3 of this chapter. To test whether immersion of

juvenile zebrafish could induce a robust antiviral response, 5 wpf WT and *cmyb* heterozygous fish (collectively referred to as non-mutant siblings) which are comparable in size to ~6-week-old *cmyb* mutant fish, were treated by immersion. Treated fish were then transferred into recovery tanks with E2 medium and harvested either 1 or 8 hpt (Fig. 4.8A). The gills of 7-8 fish were pooled for RNA isolation and gene transcript analysis. The decapitated bodies of *cmyb* mutant fish were harvested and analysed individually, and the tail fin was harvested for DNA extraction and genotyping to confirm the genotype of treated fish.

The data revealed that the gills of 5 wpf pooled non-mutant sibling fish can increase antiviral gene transcript levels in response to immersion in R848. Gene transcript levels were measured relative to 18S levels. It was found that *ifnγ1-2* exhibited a significant increase at 8 hpt compared to both control and 1 hpt samples (Fig. 4.8B). Conversely, *ifnϕ1*, *il1β* and *tnfα* transcript levels were increased at 1 hpt, returning to control levels by 8 hpt. However, these fluctuations were not found to be statistically significant (Fig. 4.8C-E). Additionally, although not statistically significant, there appeared to be a trend of increased *cxcl18b* transcript levels at 1 hpt, followed by a further increase at 8 hpt (Fig. 4.8F).

Upon establishing that immersion in R848 can induce an immune response in the gills of juvenile non-mutant sibling fish, the response of *cmyb* mutant fish was assessed next using the same workflow as depicted in Fig. 4.8A. Although the presence of tlr7 or tlr8 receptors in *cmyb* mutant fish has not been confirmed in this study, it was hypothesized that *cmyb* mutant fish would also possess these TLRs as non-hematopoietic cells also express these receptors in healthy fish. Due to limitations in the number of *cmyb* mutant fish that survive to 6 wpf and the necessity to pool 7-8 fish, only a small number of samples were obtained. However, it was evident that the *cmyb* mutant fish, in contrast to their heterozygous and WT counterparts, were not able to induce an *ifnγ1-2* response to R848 either at 1 or 8 hpt (Fig. 4.9A). However, small increases in *ifnϕ1*, *tnfα* and *cxcl18b* transcripts were detected at 1 and 8 hpt (Fig. 4.9B, D & E). However, a greater number of samples would be required to determine the significance of this increase. The pattern of change in gene transcript levels of *il1β* in *cmyb* mutants remained consistent with the pattern found in the non-mutant siblings. There appeared to be an increase at 1 hpt, with expression returning to untreated levels by 8 hpt (Fig. 4.9C).

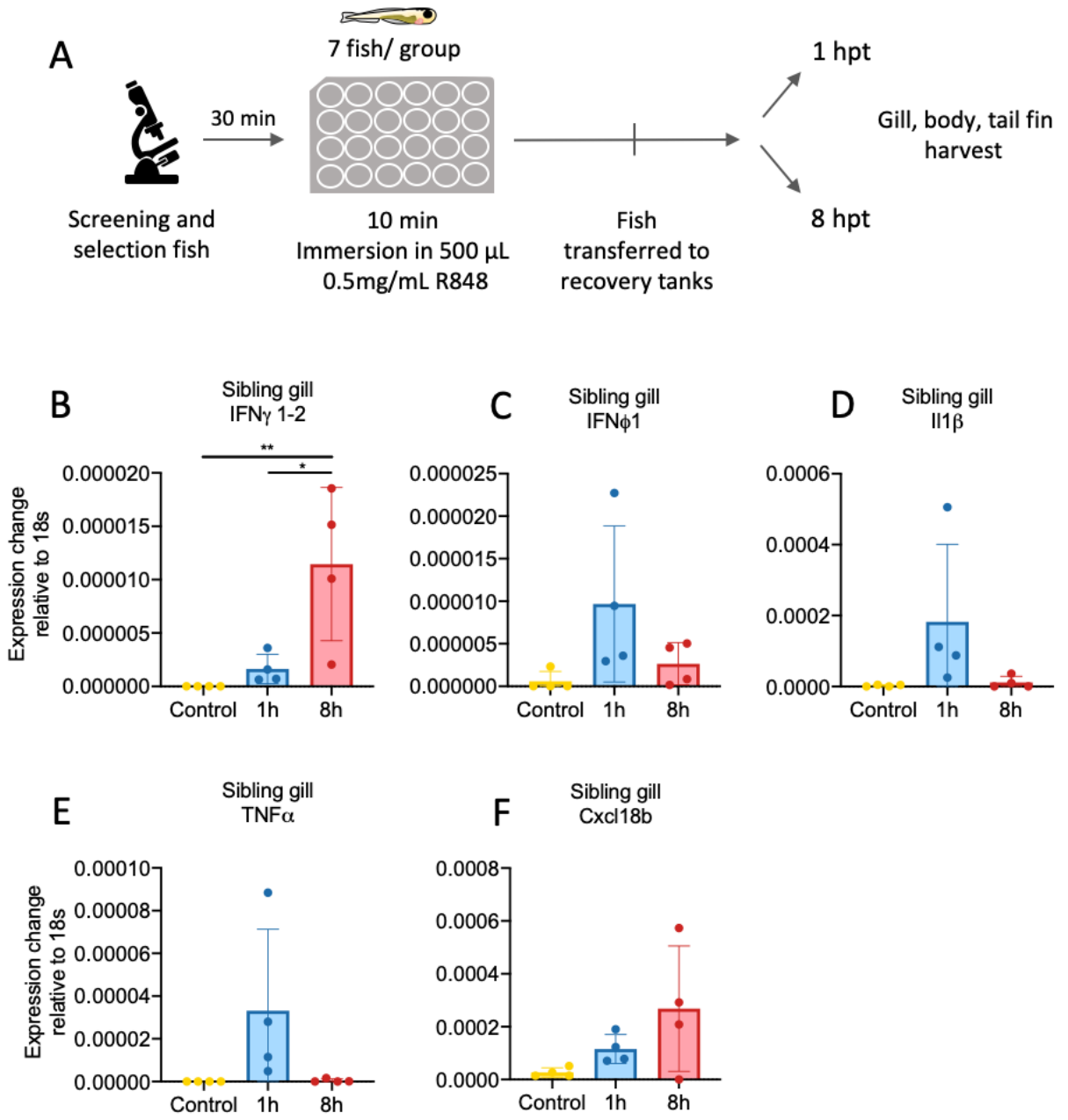

Fig. 4.8 The response of juvenile non-mutant sibling gills to R848 immersion.

A pool of 7-8, 5 wpf non-mutant sibling fish were immersed for 10 minutes in 500 µL of 0.5 mg/mL R848 (or 500 µL of E2 for control fish) in the wells of a 24-well plate. The fish were then transferred to E2 medium. The gills, body and tail fin were harvested at either 1 or 8 hpt for R848-treated fish. Control fish were harvested at 8 hpt. Data pooled from 4 independent experiments carried out in collaboration with A. Scemama (MRes. Imperial College London). N=4. (**A**) Schematic of experimental set up. (**B-F**) qRT-PCR analysis of the gills at 1 and 8 hours post R848 treatment and control. The transcript levels of *ifnγ1-2* (**B**), *ifnϕ1* (**C**), *il1β* (**D**), *tnfα* (**E**) and *cxcl18b* (**F**) are expressed as a ratio relative to 18S levels using formula 2^-(ΔCt). Each dot represents transcript levels from a pool of 7-8 fish. Mean and SD are shown. One-way ANOVA and Tukey's multiple comparisons test *P < 0.05, **P < 0.005. Where P value is not shown, differences were not statistically significant.

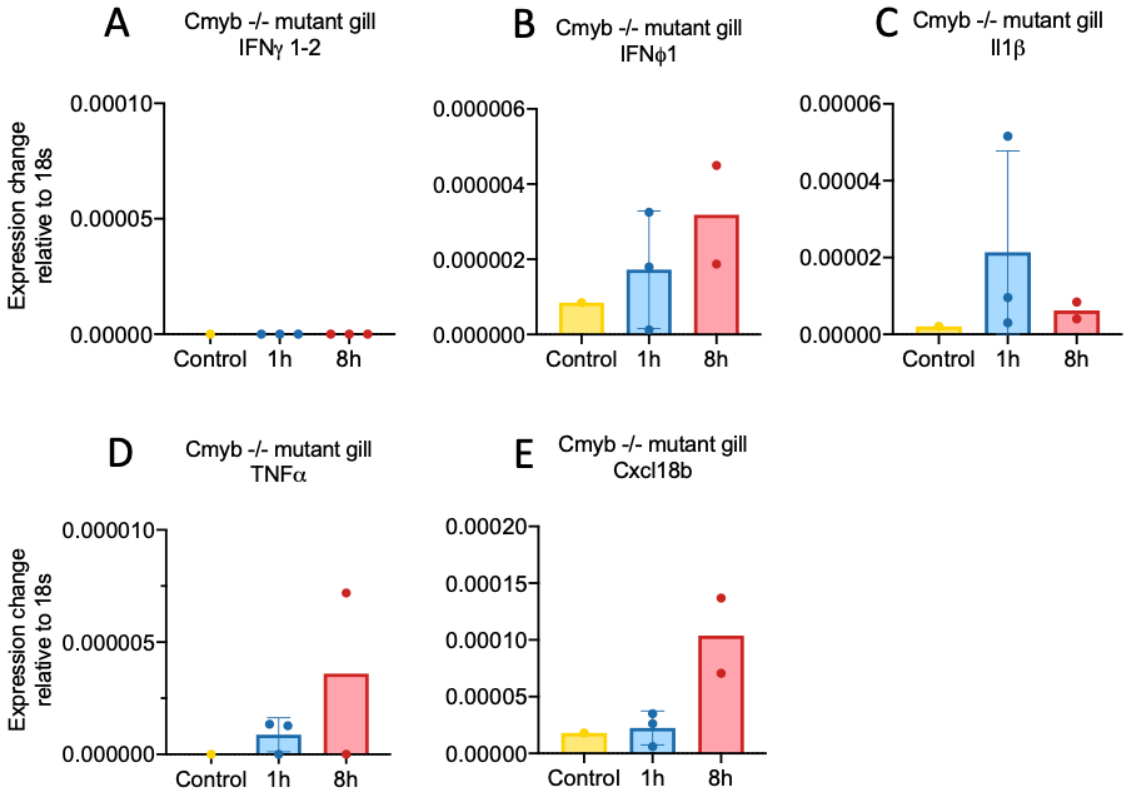

Fig. 4.9 The response of *cmyb* mutant gills to R848 immersion.

Pools of 7 or 8, 6 wpf *cmyb* mutant fish were immersed for 10 minutes in 500 µL of 0.5 mg/mL R848 (or 500 µL of E2 for control fish) in the wells of a 24-well plate. The fish were then transferred to E2 medium. The gills were harvested at either 1 or 8 hpt for R848-treated fish. Control fish were harvested at 8 hpt. Data pooled from 5 independent experiments carried out in collaboration with A. Scemama (MRes. Imperial College London). N=1-3. (**A-E**) qRT-PCR analysis of the gills at 1 and 8 hours post R848 treatment and control fish. The transcript levels of *ifnγ1-2* (**A**), *ifnϕ1* (**B**), *il1β* (**C**), *tnfα* (**D**) and *cxcl18b* (**E**) are expressed as a ratio relative to 18S levels using formula 2^-(ΔCt). Each dot is transcript levels from a pool of 7-8 fish. Mean and SD are shown only for 1h where N≥3.

Following the observation that the gills of *cmyb* mutant fish were capable of responding by increasing transcript levels of some of the genes involved in the antiviral response to R848 treatment, the magnitude of the response was compared directly between pools of *cmyb* mutant and non-mutant sibling gills using the same data sets as above. As previously mentioned, *ifnγ1-2* transcripts were only increased in the gills of non-mutant sibling fish, with the greatest increase occurring at 8 hpt. Conversely, the *cmyb* mutant gills were not able to induce an *ifnγ1-2* response to R848 at either the early or late timepoints (Fig. 4.10A). It was found that *ifnϕ1* gene transcript levels were increased to the greatest extent at 1 hpt in the gills of non-mutant sibling fish. This increase in transcript levels was reduced by 8 hpt. However, in the *cmyb* mutant gills, *ifnϕ1* appeared to steadily increase over time. By 8 hpt, the *ifnϕ*1 transcript levels in the *cmyb* mutant gills were similar to those in non-mutant sibling

gills (Fig. 4.10B). The pattern of changes in transcript levels of *il1β* appeared to be roughly consistent between *cmyb* mutant fish and non-mutant sibling fish. However, non-mutant sibling fish had produced a much greater increase in *il1β* transcript levels relative to *cmyb* mutant fish. In both instances, *il1β* transcript levels were reduced by 8 hpt (Fig. 4.10C). In the case of *tnfα*, transcripts were detected in *cmyb* mutant fish. However, the response mounted by non-mutant sibling fish was much greater (Fig. 4.10D). Finally, the transcript levels of the neutrophil chemoattractant *cxcl18b* were increased to a greater extent in non-mutant sibling fish, both at 1 and 8 hpt, compared to the *cmyb* mutants. However, it is noteworthy that *cxcl18b* expression levels in *cmyb* mutants at 8 hpt were comparable to the early response in non-mutant sibling fish (Fig. 4.10E). Taken together, it appears that the gills of *cmyb* mutant fish were capable of inducing a dampened antiviral response to R848 treatment by immersion. However, greater sample sizes would be required to determine the significance of these results and enable meaningful statistical analysis. Furthermore, the presence of tlr7 and tl8r receptors in *cmyb* mutants should be confirmed by qRT-PCR or western blot. It may also be interesting to compare tlr7 and tl8r transcript and expression levels between *cmyb* mutant and non-mutant siblings as this may be correlated with the magnitude of the antiviral response.

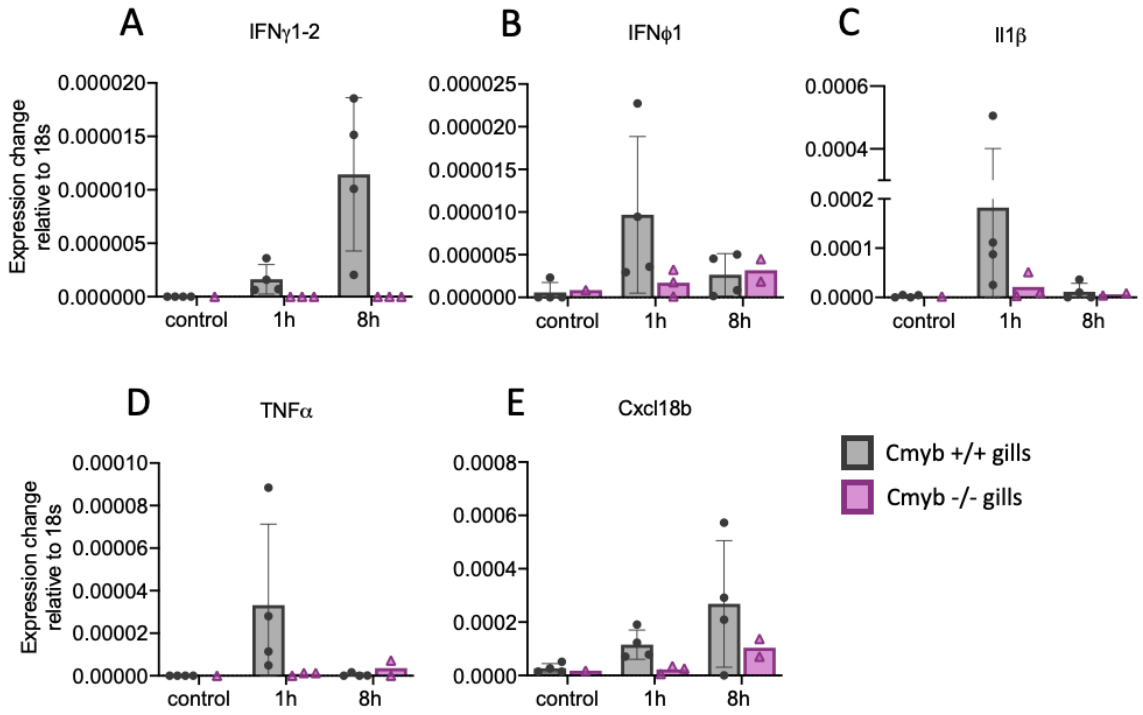

Fig. 4.10 Comparison of the response of *cmyb* mutant and non-mutant gills to R848 immersion.

Pools of 7-8, 5-6 weeks post fertilisation *cmyb* mutant and non-mutant sibling fish were immersed for 10 minutes in 500 µL of 0.5 mg/mL R848 (or 500 µL of E2 for control fish) in the wells of a 24-well plate. The fish were then transferred to E2 medium. The gills were harvested at either 1 or 8 hpt for R848-treated fish (see schematic in Fig.4.8A). Control fish were harvested 8 hpt. Data pooled from 5 independent experiments carried out in collaboration with A. Scemama (MRes. Imperial College London). N=1-4. (**A-E**) qRT-PCR analysis of the gills at 1 and 8 hours post R848 treatment and control. The transcript levels of *ifnγ1-2* (**A**), *ifnϕ1* (**B**), *il1β* (**C**), *tnfα* (**D**) and *cxcl18b* (**E**) are expressed as a ratio relative to 18S levels using formula 2^-(ΔCt). Each dot represents the transcript levels from a pool of 7-8 fish. Mean and SD are shown only where N⩾3.

Due to their small size, it was necessary to pool the gills of *cmyb* mutant fish in order to obtain sufficient quantities of mRNA to carry out gene transcript analysis by qRT-PCR. However, recent studies have demonstrated the presence of tissue-resident immune cells, including metaphocytes found in the skin epidermis and gill mucosa, which are derived of a non-hematopoietic origin (Alemany *et al*., 2018; Lin *et al*., 2019; Lin *et al*., 2020). Therefore, it was hypothesized that the skin and gills of *cmyb* mutant fish may possess such cells and may therefore be capable of mounting an antiviral immune response to immersion in R848. Hence, the decapitated bodies of treated fish were harvested for analysis in addition to their gills. The body samples of control fish were pooled to ensure detection of gene transcripts. However, a high abundance of RNA was isolated from the pooled control sample, such that subsequent samples (including *cmyb* mutant samples) were processed individually. This meant that the response mounted in the body of individual *cmyb* mutant fish could be investigated, thereby increasing the body sample size at 1 and 8-hour timepoints.

Similar to the observations in the gill response, the tissues found in the body of the *cmyb* mutant fish were also unable to produce *ifnγ1-2* transcripts (Fig. 4.11A). All other investigated genes had similar transcript levels in the body as in the pooled gills. *ifnϕ1* exhibited similarly increased transcript level in the body at both 1 and 8 hpt (Fig. 4.11B). *il1β* transcript levels in the body were greatest at 1 hpt and returned to control levels by 8 hpt. Transcript levels in the gills and body were similar at both time points (Fig. 4.11C). Although *il1β* transcript levels in the body were significantly higher at 1 hpt compared to 8 hpt, the transcript levels were low compared to the transcript levels of *il1β* in the gills of non-mutant sibling fish (Fig. 4.10C). The transcript levels of *tnfα* in the body of R848-treated *cmyb* mutant fish were elevated at 1 hpt and exhibited a significant reduction by 8 hpt. The transcript levels measured in the body samples were similar to the pooled gill samples at 1 hpt. At 8 hpt, the two pooled gill samples had very different *tnfα* transcript levels (Fig. 4.11D). Interestingly, there was no obvious outlier among the body samples at 8 hpt that may have correlated to the high *tnfα* transcript level in one of the pooled gill samples. This suggests that increased *tnfα* transcript levels at 8 hpt may be a gill specific response in *cmyb* mutant fish. Comparison between *tnfα* transcript levels in *cmyb* mutant body samples and the pool of non-mutant sibling gills revealed similar trends of high *tnfα* transcript levels at 1 hpt, followed by a reduction at 8 hpt. However, the body samples of *cmyb* mutant fish did not reach the *tnfα* transcript levels observed in the gills of non-mutant sibling fish (Fig. 4.10D). Finally, *cxcl18b* transcript levels in the body and gill samples were similar at both 1 and 8 hpt (Fig. 4.11E) and exhibited the same trend as observed in the gills of non-mutant sibling fish (Fig.4.10E). Overall, the data appears to indicate a reduced ability of *cmyb* mutant fish to mount an antiviral response to R848 treatment when compared to non-mutant sibling fish of a similar age.

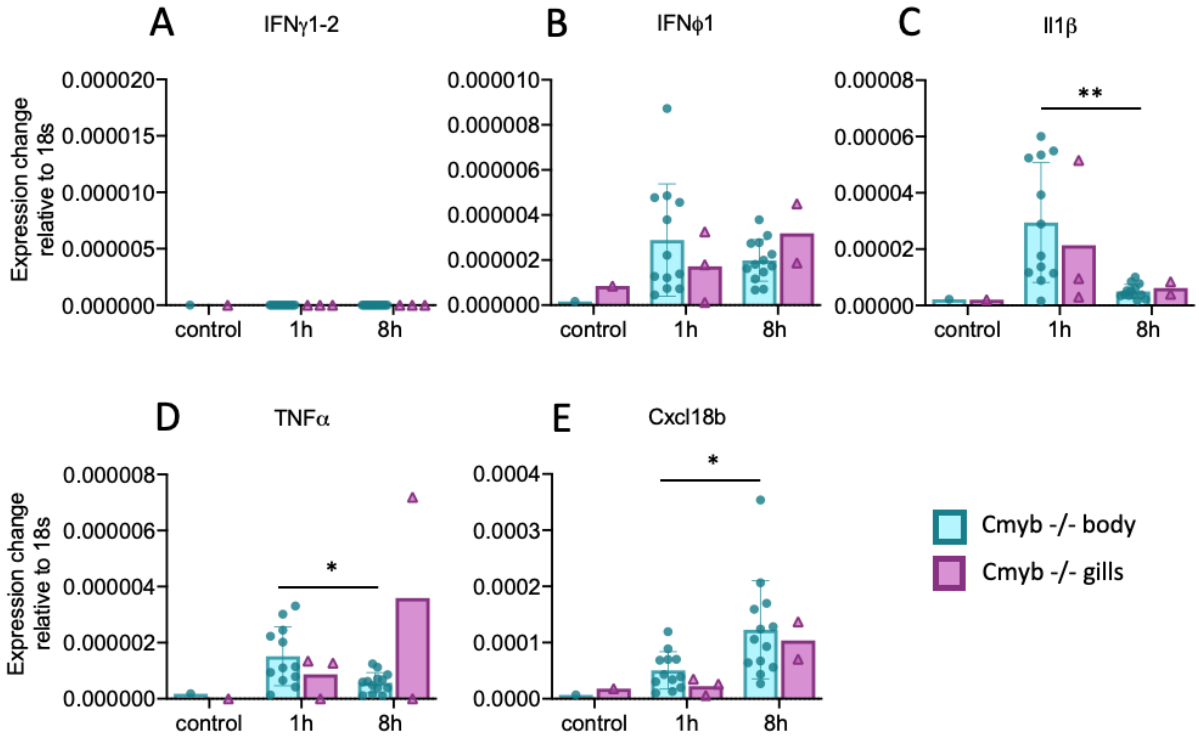

Fig. 4.11 Comparison of the response of *cmyb* mutant gills and body to R848 immersion.

Pools of 7-8, 6 wpf *cmyb* mutant fish were immersed for 10 minutes in 500 µL of 0.5 mg/mL R848 (or 500 µL of E2 for control fish) in the wells of a 24-well plate. The fish were then transferred to E2 medium. The gills and decapitated body were harvested at either 1 or 8 hpt for R848-treated fish (see schematic in Fig.4.8A). Control fish were harvested 8 hpt. Data pooled from 5 independent experiments carried out in collaboration with A. Scemama (MRes. Imperial College London). N=1-12. (**A-E**) qRT-PCR analysis of the pooled gills and individual bodies at 1 and 8 hours post R848 treatment and control (the bodies of control fish were pooled). transcript levels of *ifnγ1-2* (**A**), *ifnϕ1* (**B**), *il1β* (**C**), *tnfα* (**D**) and *cxcl18b* (**E**) are expressed as a ratio relative to 18S levels using formula 2^-(ΔCt). Each dot for the gills and control body sample represents transcript levels from a pool of 7-8 fish. For R848-treated body samples each dot is the transcript level from individual fish. Mean and SD are shown only where N≥3. One-way ANOVA and Tukey's multiple comparisons test *P < 0.05, **P < 0.005. Where P value is not shown, differences were not statistically significant.

Upon establishing that *cmyb* mutants were capable of mounting an attenuated antiviral immune response to R848, the subsequent aim was to investigate the transcript levels of immune cell-lineage genes in *cmyb* mutant and non-mutant sibling fish. To this end, *rag1*, *lyz* and *mpeg* genes were assayed at each time point to detect the presence of lymphocytes, neutrophils and macrophages respectively. The results indicated undetectable levels of *rag1* transcripts in both the gills and body samples of *cmyb* mutant fish (Fig. 4.12A). This was in agreement with previous findings (Soza-Ried *et al.,* 2010). The gill samples of non-mutant sibling fish exhibited highly variable *rag1* transcript levels at 1 hpt, but the data suggests a possible elevation of *rag1* transcripts at this timepoint. This finding would be consistent with the increased number of *lck*:GFP+ cells observed in the filaments of adult fish upon topical R848 gill application by Progatzky *et al.* (2019) at 3 and 8 hpt.

In contrast to *rag1*, both *lyz* and *mpeg* transcripts were detected in *cmyb* mutant fish (Fig. 4.12). As expected, the data indicated reduced *lyz* transcript levels in both the bodies and gills of *cmyb* mutant fish compared to the gills of non-mutant sibling fish. This reduction was greatest in the gill tissue (Fig. 4.12B). This was consistent with observations of adult *Tg(lyz:GFP)* transgenic fish, which had much greater numbers of *lyz*:GFP+ cells in the WKM (located in the body portion of fish) than in their gills, which possessed a much smaller population of *lyz*:GFP+ neutrophils (Chapter 3; Fig. 3.5I).

Finally, transcripts of the macrophage-specific gene *mpeg* were detected both in the gill and body samples of *cmyb* mutant fish. However, transcript levels were lower in the mutant fish at steady-state and 1 hpt compared to non-mutant sibling gill tissue. Interestingly, *mpeg* transcript levels at 8 hpt appeared roughly equivalent between *cmyb* mutant and non-mutant sibling fish in both the pooled gill tissue and body samples (Fig. 4.12C). When gene transcript data of all three cell-specific genes are considered together, there is an indication that a small number of innate immune cells, but not lymphoid cells, may be present in *cmyb* mutant fish at 6 wpf.

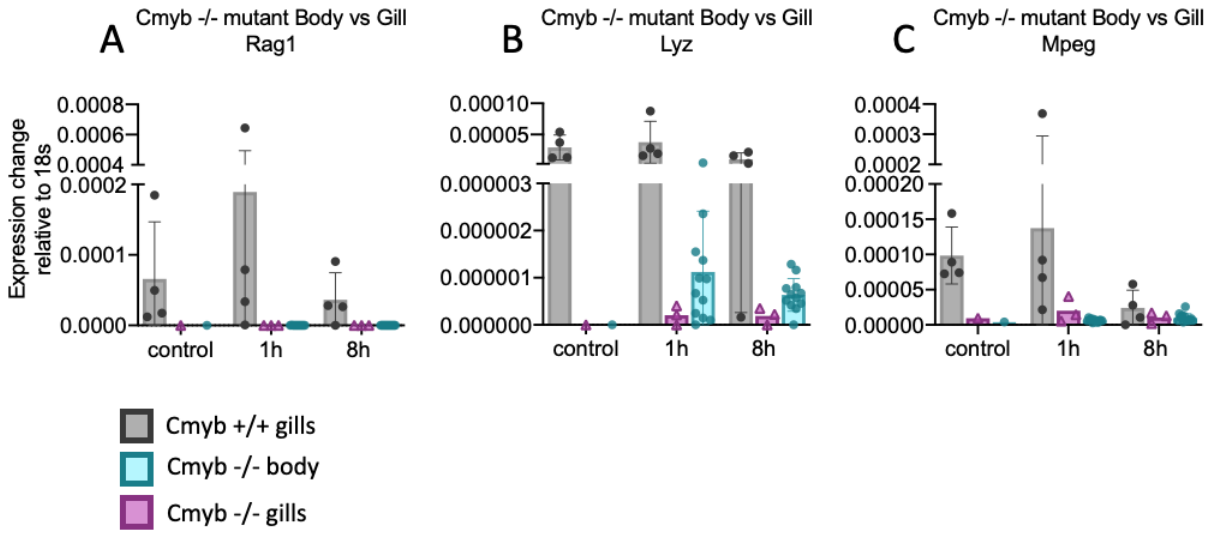

Fig. 4.12 Comparison of cell-lineage gene transcript levels in juvenile *cmyb* mutant and non-mutant sibling gills and bodies in steady-state and in response to R848 immersion.

Pools of 7-8, 5-6 wpf *cmyb* mutant and non-mutant sibling fish were immersed for 10 minutes in 500 µL of 0.5 mg/mL R848 (or 500 µL of E2 for control fish) in the wells of a 24-well plate. The fish were then transferred to E2 medium. The gills of *cmyb* mutant and non-mutant sibling fish, as well as the decapitated bodies of *cmyb* mutant fish, were harvested at either 1 or 8 hpt (see schematic in Fig.4.8A). Control fish were harvested at 8 hpt. Data pooled from 5 independent experiments carried out in collaboration with A. Scemama (MRes. Imperial College London). N=1-12. (**A-C**) qRT-PCR analysis of the pooled gills and individual bodies at 1 and 8 hours post R848 treatment and control (the bodies of control fish were pooled). The transcript levels of *rag1* (**A**), *lyz* (**B**) and *mpeg* (**C**) are expressed as a ratio relative to 18S levels using formula 2^-(ΔCt). Each dot for the gills and control body sample represents transcript levels from a pool of 7-8 fish. For R848-treated body samples each dot is the transcript level from individual fish. Mean and SD are shown only where N≥3.

4.4 Summary

Functional characterisation of *Runx*:mCherry+ cells in the WKM and gills of adult zebrafish has revealed that 10 days of OTC antibiotic treatment by immersion can cause a small reduction in the number of *Runx*:mCherry ^{low} cells in the WKM. This reduction is correlated to 16S bacterial load in the gills of treated fish.

Administration of OTC did not significantly alter the zebrafish cytokine response in the WKM or gill in response to systemic poly I:C treatment. In addition, combination of OCT and poly I:C treatment did not change the abundance of either *lyz*:GFP+ neutrophils or *Runx*:mCherry+ cells in either the WKM or gill.

Topical application of viral mimetic R848 to gills resulted in a small, but not statistically significant, increase in the number of *Runx*:mCherry+ cells in the primary lamellae of the gills at both 3 and 8 hours post treatment, suggesting that *Runx*:mCherry+ cells in the gills may be capable of responding to viral-like stimuli.

The TLR7 agonist R848 can induce a partial and attenuated antiviral cytokine response in the gills and body of juvenile bloodless *cmyb* mutant fish when treated by immersion. Furthermore, *lyz* and *mpeg* expression, but not *rag1* expression, was detected in *cmyb* mutant fish, indicating that some neutrophil and macrophage-like cells may be present at 6 weeks post fertilisation in these mutant fish.

4.5 Discussion

4.5.1 Low-dose PS does not alter hematopoietic output in juvenile or adult zebrafish

Seven-week long low-dose PS treatment did not alter hematopoietic output of major blood cell lineages in juvenile zebrafish that received treatment from 1 wpf. This was evidenced by the abundance of major blood cell populations in the WKM which remained constant (Appendix 1). Furthermore, investigating the abundance of *lck*:GFP+ T cell lymphocytes, *mpx*:GFP+ or *lyz*:GFP+ neutrophils and *Runx*:mCherry+ presumptive HSPCs, revealed that the abundance of these populations was not affected within the WKM (Fig. 4.1C). Similarly, flow cytometry of the WKM revealed that two-week treatment of low-dose PS in adults also did not elicit changes in the abundance of major blood cell populations (Appendix 3), *lyz*:GFP+ cells or *Runx*:mCherry+ cells (Fig. 4.2B). However, functional differences were not investigated in these populations. Differences in the abundance of blood cell populations does not necessarily reveal whether there are functional differences such as a change in HSPC potency, the ability to fight infection or to mount an immune response. Zhou *et al*. found that zebrafish treated with OTC or sulfamethoxazole (SMX) for 6 weeks exhibited changes in gut health and had significantly higher mortality 2-4 days following *Aeromonas hydrophila* exposure (Zhou *et al*., 2018).

As these juvenile fish were not treated with antibiotics until they reached one week of age, it is likely that the microbiome was already colonised and well established. To fully assess the long-term impact of antibiotics, it would be interesting to start treatment with PS on the day of fertilisation as this is more likely to result in changes to the microbial colonization of the embryo.

Due to the use of antibiotics for growth promotion in aquaculture (Butaye *et al*., 2003; He *et al*., 2010; Carvalho *et al*., 2016), the growth rate of zebrafish was also assessed and revealed no difference in weight, length (Appendix 2) or BMI (Fig. 4.1B& D). This is in agreement with data presented by Zhou *et al*. which found that the broad-spectrum antibiotic OTC did not confer growth promotion in zebrafish following 6 weeks of treatment at therapeutic doses. On the other hand, growth promotion was observed in SMX-treated fish (Zhou *et al*., 2018). Furthermore, studies have suggested that low-dose OTC leads to increased cellular oxygen

consumption (Zhou *et al*., 2018; Almeida *et al*., 2019) which could explain why some low-dose antibiotics do not have growth-promoting effects.

4.5.2 Ten-day OTC treatment induced reduction of gill bacterial load is linked to reduced abundance of Runx:mCherry+ cells in the WKM of adult zebrafish

Next, the effect of a more potent antibiotic regimen on the abundance of *lyz*:GFP+ neutrophils and *Runx*:mCherry+ cells in the WKM and gill tissue was investigated. Adult zebrafish were treated with the broad-spectrum antibiotic OTC at 50 mg/L for 10 days. This led to a significant reduction in 16S rRNA levels (Fig. 4.4A), a measure used to estimate bacterial load, in the gills. Furthermore, the results show a significant positive correlation between gill 16S and the abundance of *Runx*:mCherry+ cells in the WKM (Fig.4.4C), indicating that fish that experienced the greatest changes in their gill mucosal microbiome had the most significant reductions in *Runx*:mCherry+ cells in the WKM niche. No changes in the sizes of the *lyz*:GFP+ populations in either the WKM or the gill tissue were observed (Fig. 4.3).

It has previously been found in mouse models that broad-spectrum antibiotic treatment at therapeutic doses led to reduced WBM cellularity, anaemia and leukopenia (Josefsdottir *et al*., 2016). Furthermore, the treatment led to a significant reduction of HSCs and MPPs. The authors report that the changes in hematopoiesis were the result of an altered microbiome, caused by the antibiotic treatment. It was found here, that in the gut, OTC treatment led to increased 16S transcript levels. This is consistent with findings reported by Charlwood (2017), who showed that low-dose PS treatment of embryos led to reduced microbial diversity and altered microbial composition, as identified by Illumina MiSeq sequencing, while simultaneously leading to an increase in the 16S bacterial load in the gut. Therefore, an increase in gut 16S may be indicative of gut dysbiosis. However, to confirm altered gut microbiota following OTC treatment, further metataxonomic analysis would be required. Interestingly, while a reduction in gill 16S rRNA was identified upon OTC treatment here, studies in seabass found that OTC treatment led to a decrease in core diversity in the gill mucosa (Rosado *et al*., 2019). Taken together, the data suggests that a 10-day 50 mg/L OTC treatment may be sufficient to induce microbial dysbiosis in zebrafish, resulting in reduced WKM HSPCs.

Although it is not yet clear which cell type the *Runx*:mCherry^{high} cells in the gill represent, the results in Chapter 3 indicate that these do not correlate with *lck*:GFP+ T cell or *IgM*:GFP+ B cell lymphocytes (Fig. 3.17, 3.16). One hypothesis is that these could be erythroid or thrombocytes-primed cells (Tang *et al*., 2017). The results in Fig. 4.3 indicate that the abundance of *Runx*:mCherry ^{high} cells in the gill remained stable in the presence of OTC. Similarly, Josefsdottir *et al*. found that in mice, platelet count was elevated following antibiotic treatment and granulocyte, megakaryocyte and erythroid progenitors were not affected by the treatment regimen (Josefsdottir *et al*., 2016).

4.5.3 OTC treatment does not alter the antiviral inflammatory response to poly I:C stimulation

OTC did not alter the adult zebrafish basal inflammatory state in the gill or WKM after 10 days of treatment, as shown by unaltered *ifnφ1* and *ifnγ1-2* transcript levels and unchanged *il1β* and *cxcl18b* levels in the presence of OTC (Fig. 4.5). However, it is possible that a short inflammatory burst was missed in these experiments. Rainbow trout immersed in 0.005-50 mg/L OTC for 96 hours exhibited significant gill pathology, whereas fish exposed to 0.31-5 µg/L OTC for 28 days did not show a significant increase in the total gill pathological index (Rodrigues *et al*., 2017). It has also been shown in zebrafish that, following continued exposure to inflammatory insults such as smoke, the initial robust increase in inflammatory cytokine transcript levels by 6 hpt subsided after 6 weeks of continued exposure (Progatzky *et al*., 2016). Therefore, it is possible that a transient inflammatory response to OTC occurred and was resolved by 10 dpt. Earlier time points need to be assayed to determine whether this is the case.

The presence of OTC also did not alter the cytokine response to poly I:C in the WKM or gills of zebrafish following 10 days of OTC treatment, suggesting that OTC does not attenuate the immune response or alter immune cell function. This is in contrast to a study in mice, which showed that antibiotic treatment impaired innate and adaptive antiviral immune responses to influenza virus, delayed viral clearance and increased mortality (Abt *et al*., 2012). Furthermore, OTC and poly I:C did not alter the abundance of *lyz*:GFP+ cells or *Runx*:mCherry+ cells in the gill or WKM while, in germ-free and antibiotic-treated mice, *Listeria monocytogenes* infection caused reduced myelopoiesis, greater pathogen burden and higher mortality relative to WT mice (Khosvari *et al.,* 2014). These results highlight some of

the ways these two model organisms differ, as well as the importance of using a combination of model organisms to study immune responses. It has recently been shown that some zebrafish responses to certain inflammatory stimuli are more similar to humans than the responses of mice to the same stimulant (Progatzky *et al*., 2019).

4.5.4 Topical gill application of R848 may induce a small increase in Runx:mCherry+ cells in the primary lamellae of the gills

To build upon data from the previous chapter investigating properties of *Runx*:mCherry+ cells in the adult zebrafish gill, the ability of these cells to respond to viral stimuli was examined. Topical application of R848 to the gill induces a robust antiviral response in zebrafish with significant increases in transcript levels of type I and type II IFNs (Progatzky *et al*., 2019). Furthermore, this treatment induces a transient increase in neutrophil abundance in the gill, as seen by confocal microscopy. These results were confirmed in these experiments (Fig. 4.6-7). Interestingly, the increase of *lyz*:GFP+ neutrophils in the gills was not detected by flow cytometry. This could be due to incomplete homogenization and extraction of cells from the gill tissue during sample preparation for flow cytometry. Similarly, small differences in the abundance of *Runx*:mCherry+ cells in the gills of R848-treated fish were not detected by flow cytometry. Computational quantification of *Runx*:mCherry+ cells from confocal microscopy images suggest that there may be a small increase in *Runx*:mCherry+ cells in R848-treated gills at 3 and 8 hpt, particularly in the primary lamellae (Fig. 4.6-7). However, these results were not statistically significant, most likely due to the heterogeneity in the abundance of *Runx*:mCherry+ cells in untreated gills (Fig. 3.8E). Thus, further experimental replicates are required to confirm this finding. Power calculations indicate that approximately an additional 15 samples per group are required to achieve 85% power. An increase in *Runx*:mCherry+ cells in the gills upon R848 treatment would suggest that these cells are capable of responding to viral-like stimuli.

As mentioned above, the identity of *Runx*:mCherry+ cells in the gills remains elusive and requires further investigation to determine their ontogeny. One hypothesis is that the +23 enhancer element of the transgene is activated during thrombocyte maturation. If this is the case, progenitor or mature thrombocytes may express the transgene due to transcriptional overlap (Tang *et al.,* 2017; Kobayashi *et al.,* 2019). It has been found in mouse and human

studies that platelets, the mammalian equivalent to thrombocytes, express *TLR7* and are involved in antiviral immune responses, including responses to TLR7 agonists. In both human and mouse samples, platelet TLR7 stimulation led to the formation of large platelet-neutrophil aggregates and systemic thrombocytopenia. Furthermore, neutrophils were found to internalize either fragments or entire CD41+ platelets, as identified through microscopy (Koupenova *et al*., 2014). Neutrophils and platelets have been shown to accumulate in the liver vasculature following poxvirus challenges in mice. This also led to thrombocytopenia and the formation of large, dynamic aggregates between platelets and neutrophils (Jenne *et al*., 2013), indicating that thrombocytes are involved in antiviral immune responses and can be recruited to stimulated sites.

The results presented in this chapter show that the abundance of *lyz*:GFP+ cells increased in the gills following R848 treatment, and indicate that *Runx*:mCherry+ cells may also increase. A greater number of samples would be required to confirm these findings. However, given the involvement of platelets in response to TLR7 stimulation in mammalian systems (Koupenova *et al*., 2014; Jenne *et al*., 2013), the results presented here could indicate that this may also be the case in zebrafish. Ultimately, these experiments would need to be repeated with *Tg(CD41:GFP)* transgenic zebrafish to determine whether thrombocytes are involved with the antiviral response in the gills. Furthermore, crossing *Tg(Runx:mCherry)* and *Tg(CD41:GFP)* fish would provide a definitive answer as to whether there is either overlap or proximity between these fluorescent protein expressing cells in the adult zebrafish gill.

4.5.5 Bloodless cmyb mutant fish can induce type I IFN and inflammatory cytokines in response to R848

The Tlr7 agonist R848 was able to increase transcript levels of type I interferon, *ifnϕ1*, *tnfα*, *cxcl18b* and *il1β* in the gills of *cmyb* mutant fish. However, the increases in transcript levels appeared markedly reduced compared to non-mutant sibling fish (Fig. 4.10). This indicates that immune cells are important in inducing a significant increase in inflammatory cytokine and interferon signalling in response to viral-type stimulation. It is remarkable that the cells present in *cmyb* mutant fish are capable of increasing transcript levels of type I interferon and inflammatory cytokines to the extent that they can. Type II interferon *ifnγ1-2* transcripts were not detected in either the gill or the body of *cmyb* mutants. The discrepancy between the

detection of *ifnγ1-2* and *ifnϕ1* transcripts likely arises from the absence of adaptive immune cells, such as *rag1* and *ikaros*-expressing cells, in the *cmyb* mutants (Fig. 4.12; Soza-Ried *et al*., 2010). Type II interferon *ifnγ1-2* is produced predominantly by adaptive immune cells, such as T cell lymphocytes and NK cells (Lee *et al*., 2017; Schoenborn & Wilson, 2007), which are absent in *cmyb* mutants, whereas type I interferon *ifnϕ1* can be produced by a large array of cell types (Le Page *et al*., 2000).

4.5.6 Lyz and mpeg but no rag1 transcripts detected in six wfp cmyb mutants

As discussed above, type II interferon transcripts were not detected in *cmyb* mutant fish following exposure to R848 treatment. Similarly, transcripts were not detected for the lymphocyte cell marker *rag1*. This is in agreement with previously published data indicating that *rag1*, *T cell receptor b* (*tcrb)* and *ikaros* expression were absent in the thymi of cmyb mutants (Soza-Ried *et al*., 2010). Furthermore, the authors reported detection of *l-plastin* and *spi*+ myelomonocytic cells in the head kidney region by *in situ* hybridisation. Recently, a novel macrophage-like cell type, termed metaphocytes, was identified in the skin and gills of adult zebrafish (Lin *et al*., 2019; Lin *et al*., 2020). These *mpeg1*-expressing cells are derived from non-HSC origin and, therefore, may be present in *cmyb* mutant fish. Indeed, results presented here indicate the presence of *lyz* and *mpeg* transcripts in the body and gill tissue of *cmyb* mutant fish. Unsurprisingly, the transcript levels of *lyz* and *mpeg* are much lower in *cmyb* mutant fish relative to non-mutant sibling fish due to the absence of cells derived from the definitive wave of hematopoiesis. Myeloid cells present could either be remaining long-lived cells from the primitive wave of hematopoiesis, as suggested by Soza-Ried *et al.*, self-renewing cells or, as suggested by Lin *et al.*, macrophage-like metaphocytes of endodermal origin (Lin *et al*., 2019; Lin *et al*., 2020; Tang *et al*., 2017). To confirm the presence of macrophage-like cells at 6 wpf in *cmyb* mutants, these fish were crossed with a reporter line for *mpeg*, *Tg(mpeg1.1:SECFP-YPet)*, to aid in the visualisation of these cells and determine their localisation (see Chapter 5).

Chapter 5

cmyb^{t25127} Characterisation and Refinement of Hematopoietic Stem Cell Transplantation

Chapter 5 | *cmyb*^{t25127} Characterisation and Refinement of Hematopoietic Stem Cell Transplantation

5.1 Introduction

This chapter presents the investigation of *cmyb* mutant fish for their regenerative capacity following fin amputation. Additionally, work was carried out to optimise and refine zebrafish hematopoietic stem and precursor cell transplantation by live, *in vivo* imaging of donor cells and their progeny in the recipient. This builds on previous investigations by Dr. McBrien who carried out work to visualise early post-transplant behaviour of donor cells in order to predict the likelihood of recipient survival and immune reconstitution (McBrien, 2017). Finally, this chapter also sets out to determine the HSC potential of different *Runx*:mCherry+ populations and assess the utility of *cmyb* mutants for transplantation studies.

5.1.1 Bloodless cmyb^{t25127} zebrafish

The bloodless zebrafish *cmyb*^{t25127} mutant line was first described by Soza-Ried *et al.* (2010) and identified initially by its inability to initiate lymphopoiesis in the thymus. *Cmyb* is a gene encoding a highly conserved transcription factor involved in definitive HSC formation, which has been described in Chapter 1 (1.3.5). The single-point mutation in *cmyb*^{t25127} fish is a thymidine to adenine transversion leading to an amino acid change from isoleucine to asparagine at amino acid residue 181. This amino acid change occurs within a highly conserved DNA-binding domain of the transcription factor (Ogata *et al*., 1994) and results in a *cmyb* null mutation, as shown by a lack of DNA-binding activity by the mutant protein *in vitro*. *Cmyb* is an essential gene for definitive hematopoiesis and is involved in HSC budding from the ventral wall of the dorsal aorta during embryogenesis. As a result, zebrafish homozygous for the mutation (hereafter referred to as *cmyb* mutants) will exhaust all circulating blood cells, including erythrocytes, generated during the primitive wave of hematopoiesis by approximately 20 dpf (Soza-Ried *et al.,* 2010). Although these bloodless fish have a high mortality rate relative to their WT counterparts, some can nevertheless survive up until 14 wpf (Hess *et al*., 2013). However, as a result of their severe anaemia, *cmyb* mutant fish exhibit growth retardation, present with cardiac oedema, have a whiteish complexion and do not exhibit signs of sexual dimorphism. Despite reaching over 3 months in age, *cmyb*

mutants do not reach sexual maturity and do not grow larger than approximately 1 cm in length (Hess *et al*., 2013; McBrien, 2017).

5.1.2 Application of cmyb mutant fish in HCT experiments

Cmyb mutant fish offer a valuable model for HCT as they do not require irradiation (IR) preconditioning prior to transplantation due to the absence of erythrocytes and lymphocytes in the adolescent fish. The absence of irradiation or other preconditioning means that the fish are not subjected to an acutely inflammatory milieu which may impact the HCT outcome. In addition, due to the absence of definitive hematopoietic cells, allogenic and indeed xenogenic transplantation has successfully been carried out, leading to long-term engraftment of donor cells (Hess *et al*., 2013; Hess *et al*., 2016). Although unmanipulated *cmyb* mutant fish have not been found to survive past 14 wpf, HCT can rescue the mutant phenotype and increase the life span to over 8 months (this was the last time point in the longitudinal study). Although procedural mortality was high, surviving fish subsequently grew rapidly, regained pinkish complexion, formed circulating erythrocytes and reached sexual maturity, making them phenotypically indistinguishable from WT fish (Hess *et al*., 2013). To further characterise the *Runx*:mCherry+ cell populations described in Chapter 3, HCT assays were carried out to assess the HSC potential of different *Runx*:mCherry+ cell populations using *cmyb* mutant fish. Due to their small size, McBrien found that even in non-transparent *cmyb* mutant fish, transplanted donor cells and any fluorescent protein-expressing progeny can be observed by live *in vivo* microscopy (McBrien, 2017). This enables HSC engraftment and resultant fluorescent protein-expressing progeny to be tracked over time. To improve upon this procedure by enhancing imaging capability, one method was to cross heterozygous *cmyb* mutant fish to *TraNac* mutant fish, thereby establishing a transparent *cmyb* mutant line (White *et al*., 2008). This should allow improved imaging data to be acquired, enabling more accurate tracking of engraftment with a view to developing a scoring system that will allow engraftment outcome to be correlated with survival outcome. If this is achieved, it would be possible to use early post-transplant imaging data to predict the likelihood of long-term survival, which may remove the need for survival data to assess HCT. This would reduce the suffering experienced by individual fish and, consequently, reduce the severity of the HCT protocol by allowing the cull of fish that are predicted not to survive prior to the onset of suffering and eventual death.

5.1.3 The origin of tissue resident macrophages

As described previously in Chapter 1, primitive macrophages can arise from both the rostral blood islands (RBI) and the intermedial cell mass (ICM) in the posterior lateral-plate mesoderm (PLM) during primitive hematopoiesis. Primitive macrophages originating from the RBI give rise to microglia (MG) in zebrafish. Based on mouse lineage tracking studies utilising the CreER-*LoxP* system to track cell fates of *Runx1*+ *Csf1r*+ cells, it was suggested that most adult microglia arise from primitive hematopoiesis (Ginhoux *et al*., 2010; Schulz *et al*., 2012) and are maintained via self-renewal. However, the promoters controlling the CreER-*loxP* system utilised in these studies were not capable of sufficient temporal resolution of *Runx1* and *Csf1r* expression to definitively determine the origin of microglia in the adult animal (Xu *et al*., 2015). Since then, studies in the zebrafish have shown that embryonic and adult microglia arise from distinct locations during zebrafish development. Embryonic microglia arise from RBI-derived macrophages while adult microglia are derived from cells in the ventral wall of the dorsal aorta (VDA), the site of definitive hematopoiesis in both mice and zebrafish (Xu *et al*., 2015). Xu *et al*. used 3 wpf *cmyb* mutant fish to show that microglia derivation from the VDA region is *cmyb*-independent and *runx1*-function dependant. However, it was subsequently shown by Ferrero *et al*. that 75% of microglia in 3 wpf zebrafish were cells remaining from RBI-derived primitive macrophages, which are *cmyb*-independent. Furthermore, they demonstrated that microglia derived from definitive HSCs start to colonize the brain parenchyma at approximately 2 wpf, and fully replace embryonic microglia by 3 months post fertilisation (mpf). Through WKM transplantation studies, they were also able to show that adult (>3 mpf) *cmyb* mutant fish did not possess any host microglia, and that the central nervous system (CNS) was instead colonized entirely by *cmyb*-dependent, donor-derived microglia precursors (Ferrero *et al*., 2018). This challenged the controversial theory of erythroid-myeloid progenitors (EMP) being the origin of adult microglia cells (Perdiguero *et al*., 2015).

Similarly, He *et al*. (2018) used laser-mediated temporal-spatial cell labelling methods in zebrafish to show that tissue resident macrophages in the epidermis, known as Langerhans cells (LCs), originate from different sites in embryos and adults. In the embryo, LCs derive from the RBI, whereas in adults LCs were traced back to the VDA, with only a small number of LCs traced to the posterior blood islands (PBI) which gives rise to EMPs. Just as the

microglia, VDA-derived LCs in the adult were found to be *runx1* and *cmyb*-dependent, suggesting, therefore, that primitive LCs are eventually replaced by definitive cells. Furthermore, Lin *et al*. (2019) identified ectoderm-derived myeloid-like cells in the epidermis of adult zebrafish, which they termed metaphocytes. Metaphocytes were found to be highly similar to LCs in their morphology, transcriptome and localisation. Metaphocytes, like LCs, express fluorescent protein driven by the *mpeg1.1* promoter. However, key differences were identified in the inability of metaphocytes to respond to injury or bacterial infection. Furthermore, it was found that, unlike LCs, which express high levels of chemokine, nucleotide and scavenger receptors, metaphocytes had low expression of these and instead expressed high levels of tight junction genes. These play an important role in enabling metaphocytes to sample soluble antigen from the external environment by transepithelial protrusions (TEPs). Unlike LCs, which can move throughout the epidermis and arrive from the sites of definitive hematopoiesis, metaphocytes were found to be locally restricted, ectoderm-derived cells (Lin *et al*., 2019). These results were further supported by findings in mouse studies which showed that reported LCs and intestinal macrophages were capable of sampling antigen from the environment through TEPs (Kubo *et al*., 2009; Niess *et al*., 2005). In addition, Alemany *et al.* (2018) used single-cell sequencing to show that there are tissue-resident immune cells in the tail fin of adult zebrafish which were found to be clonally distinct from WKM HSCs. These were hypothesized to be derived from either ectodermal ancestors or via epidermal and mesenchymal trans-differentiation. Taken together, it is possible that the metaphocytes identified by Lin *et al*. (2019) correspond to the HSC-independent, epidermal tissue-resident macrophages described by Alemany *et al.* (2018).

5.1.4 Presence of macrophages in cmyb mutant fish

In the initial characterisation of *cmyb* mutants, *l-plastin*- and *spi1*-expressing cells were identified by RNA *in situ* hybridisation in the head kidney region of 7 wpf *cmyb* mutant fish. Furthermore, macrophage-like *ikaros*:eGFP+ cells were observed by fluorescence microscopy. However, the fish were negative for lymphocyte-specific genes such as *tcrb*, *rag1*, the erythrocyte-specific gene *gata1* and the neutrophil-specific gene *mpx* (Soza-Ried *et al.,* 2010). It was hypothesized that macrophage-like cells in adolescent *cmyb* mutants are embryonic-derived tissue-resident cells that differentiated from EMPs in the RBI. Tissue-resident macrophage-like cells such as epidermal LCs, microglia and other tissue-resident

macrophages, were thought to derive from the primitive wave of hematopoiesis and have self-renewal potential (Ginhoux *et al*., 2010). As mentioned earlier, using *cmyb* mutant fish, Xu *et al*. were able to show that RBI-derived embryonic microglia were still present at 3 wpf, suggesting that the cells either have a long lifespan or have self-renewal ability (Xu *et al*., 2015). However, as detailed above, Ferrero *et al*. (2018) later demonstrated that embryonic microglial formation was not impaired in *cmyb* mutants at 4 dpf, and that these cells persisted for over 3 weeks but were eventually replaced by *cmyb*-dependent microglia. In order to confirm the presence of *cmyb*-independent macrophage-like cells, as suggested by *mpeg* mRNA transcripts detected in Chapter 4 (Fig. 4.12C), *cmyb* mutants were crossed to *Tg(mpeg1.1:SECFP-YPet)* zebrafish. This enabled direct *in vivo* visualisation of macrophage-like cells and helped assess their response to injury by tail fin amputation.

5.1.5 Zebrafish regeneration of tail fin tissue

Hess *et al*. reported the significant mortality associated with tail fin amputation in *cmyb* mutants and postulated that this was due to widespread inflammation caused by the injury (Hess *et al*., 2013). However, if primitive macrophages with limited self-renewal potential remain in juvenile *cmyb* mutant fish, as suggested by the detection of *mpeg* transcripts in Chapter 4 (Fig. 4.12C), then these immune cells may have the capacity to respond to injury by neutralising invading pathogens and possibly even coordinating tissue repair.

Neutrophils are the first responders to infection and injury (Martin & Feng, 2009; Tate *et al*., 2008) and are recruited to the site of injury by rapid increase in H_2O_2 levels (Niethammer *et al*., 2009; Pase *et al*., 2012). Neutrophil recruitment to fin fold injury in larval zebrafish peaks at approximately 6 hours post injury and cell numbers largely return to basal levels by 24 hours post injury (Renshaw *et al*., 2006; Bernut-loynes *et al*., 2020). However, in adult tail fin transections neutrophil numbers were found to peak at approximately 3 days post injury (dpi) and returned to pre-amputation levels by 7 dpi (Petrie *et al*., 2015).

Macrophages have been shown to be crucially important in tissue regeneration including in adult heart injury, caudal fin transection, and larval fin fold amputation models (Bevan *et al*., 2020; Petrie *et al*., 2015; Nguyen-Chi *et al*., 2017). Macrophages can be subdivided into classically activated (M1 type) and alternatively activated (M2 type) macrophages. M1 pro-

inflammatory macrophages express *tnfα*, *il6* and *il1β* cytokines and are involved in phagocytosis of dying neutrophils, debris and pathogens, while M2 macrophages are anti-inflammatory and express *tgfβ*. M2 macrophages are involved in resolving inflammation and stimulating tissue repair (Nguyen-Chi *et al*., 2015). In embryonic zebrafish, regeneration following fin fold amputation consists of 3 main stages (Grotek *et al.,* 2013). Firstly, wound healing occurs between 0-1 days post amputation (dpa) and is characterised by an initial wave of robust neutrophil recruitment by H_2O_2 signalling (Niethammer *et al*., 2009) and, subsequently, the recruitment of macrophages, both of which can phagocytose cellular debris and neutralise pathogens. Secondly, the regenerative blastema, a mass of highly proliferative mesenchymal progenitor cells, forms 1-3 dpa. Finally, the regenerative stage, from 3 dpa onwards, involves growth and patterning of new tissue (Petrie *et al*., 2015; Grotek *et al.,* 2013). Nguyen-Chi *et al*. demonstrated that zebrafish *mpeg*:mCherry+ *tnfα*:GFP+ macrophages correspond to M1 macrophages, while *mpeg*:mCherry+ *tnfα*:GFP- macrophages correspond to anti-inflammatory M2 macrophages (Nguyen-Chi *et al*., 2015). The group subsequently showed that *tnfα*+ macrophages are recruited to the injury site in fin fold transection and peak in numbers around 6 (hours post amputation) hpa, followed by a steady decline, and are no longer present by 3 dpa. *tnfα*- macrophages, on the other hand, peak at 6 hpa and are maintained up until 3 dpa when regeneration is complete. Using a combination of genetic approaches, chemical ablation of macrophages, morpholino knockdown models and parabiosis, Nguyen-Chi *et al*. were able to convincingly show that *tnfα/tnfr*-mediated signalling between M1 macrophages and stromal cells is key to ensuring blastemal cells are sufficiently proliferative and lead to successful regeneration of amputated tissue. When macrophages were largely eliminated either by L-clodronate treatment or metronidazole (MTZ) treatment of *Tg(mpeg:Gal4; UAS:NTR-mCherry)* fish, the fin fold regeneration was significantly impaired and the blastema marker *junbl* was reduced, as was proliferation in the blastema at 24 hpa. Regenerative potential was also reduced in late depletion of M2 macrophages (Nguyen-Chi *et al*., 2015). Similar results were obtained using bloodless *cloche* embryos which were found to have limited regenerative capacity due to the reduced proliferation of blastemal cells (Hasegawa *et al*., 2015).

In adult tail fin transection, macrophage numbers were found to peak at approximately 7 dpi and had not quite reached basal levels yet at 14 dpi. Macrophages were found to modulate tail

fin regeneration. When macrophages were depleted in *Tg(mpeg:NTR-eYFP)* zebrafish treated with MTZ, the extent of tail fin regrowth was reduced and the fin tissue that did grow back was disorganized, with both impaired bone ray patterning and bone quality (Petrie *et al*., 2015).

5.1.6 Hematopoietic reconstitution in Zebrafish

The adult zebrafish niche is the WKM, and HSPCs are known to home to this anatomical site following HCT. Homing describes the process by which transplanted HSPCs move via circulation in the vasculature to the recipient niche, and is mediated by chemoattractant signalling. HSPC homing is key for the successful engraftment of donor cells in the recipient. *Stromal-derived factor 1a* (*sdf1a*) is the zebrafish orthologue of the human *CXCL12a* gene and is a key factor involved with HSC homing and engraftment in the zebrafish WKM following HCT (Glass *et al*., 2011). In mammalian systems, *CXCL12a* is associated with HSC maintenance and retention in the niche (Sugiyama *et al*., 2006).

The WKM niche has been subdivided into 3 main sections comprised of the head kidney, which is the most anterior part of the kidney, the mid kidney, located ventral to the swim bladder between the two lobes of the swim bladder, and finally the tail kidney which runs along the swim bladder to the anal pore. There are conflicting data regarding which part of the WKM contains the predominant hematopoietic compartment. The head kidney of teleost is found to be most vascularised and possesses the least renal tubules, while the tail kidney contains more renal tubules and is less vascularised (Zapata *et al*., 1979). As a result, the head kidney, rather than the tail kidney, was hypothesized to be the predominant hematopoietic organ. Several studies have focused on investigating the head kidney (Imagawa *et al*., 1994; Temmink & Bayne, 1987). More recently, however, through the application of HCT assays, Kobayashi *et al.* found that the tail kidney of ginbuna carp contained more HSCs than the head kidney (Kobayashi *et al*., 2006). Subsequently, it was shown that SP cells (used to purify HSCs) were almost exclusively found in the tail kidney region of ginbuna carp, and very few localised to the head kidney (Kobayashi *et al*., 2008). Since then, *Tg(sdf1a:DsRed)* transgenic zebrafish have been generated with the aim of gaining a deeper understanding into the significance of *sdf1/cxcr4* signalling in HSC homing in the zebrafish model. Using this transgenic, it was found that *sdf1* is predominantly expressed in renal tubules in the zebrafish WKM, suggesting that

renal tubules form part of the supportive HSC niche. As renal tubules are most abundant in the tail kidney, this further suggests that the tail kidney may be a major hematopoietic organ of teleost (Glass *et al*., 2011). However, according to HCT research in the Dallman lab, McBrien found that transplanted *CD41*:GFP ^{low} cells colonize the head kidney of zebrafish first (McBrien, 2017). Interestingly, Glass *et al.* also demonstrated that both *sdf1a* and *sdf1b* were upregulated in the skin and the gills of zebrafish in steady-state conditions (Glass *et al*., 2011), suggesting that the gills could constitute an extramedullary site of hematopoiesis or that HSCs may home to the gills. Indeed, in pacific oysters, the major site of hematopoiesis is found in the gills (Jemaa *et al*., 2014). Bivalves evolved over 500 million years ago (Campbel & Reece, 2002), long before the evolution of vertebrates. Therefore, it may be possible that gill hematopoiesis is an evolutionary remnant in zebrafish. However, teleost gills have not been investigated further for hematopoietic activity. Given the abundance of *Runx*:mCherry+ cells (Chapter 3) and high expression of HSC chemoattractant *sdf1a* in the adult zebrafish gill (Glass *et al*., 2011), it is of interest to carry out transplantation of these cells into *cmyb* mutant fish to determine whether they possess hematopoietic activity. Furthermore, it may be interesting to investigate whether transplanted WKM-derived HSPCs home to recipient gills.

Despite significant differences between the mammalian HSC niche in the BM and the WKM niche in teleost, given the high level of evolutionarily conserved mechanisms regulating hematopoiesis, studying HCT in zebrafish provides a unique opportunity to discover new key mechanism of HSC maintenance, self-renewal, homeostasis and differentiation in vertebrates. This, in turn, may help uncover how to improve HSC expansion *ex vivo* for therapeutic applications.

5.2 Aims

The previous chapter examined the response of *Tg(Runx:mCherry; lyz:GFP)* transgenic animals to stimuli such as antibiotic treatment and viral-like stimuli. This was done in order to determine how cells expressing the *Runx*:mCherry transgene may be affected by these stimuli. In addition, it assessed the ability of bloodless *cmyb* mutants to respond to viral-like stimuli. This chapter aims to build on the findings of the previous work by further studying the bloodless *cmyb* mutant fish in steady state, and their ability to respond to damage. Furthermore, this chapter aims to assess the utility of *cmyb* mutant fish for HCT studies and to refine the HCT procedure.

More specifically, the aims of this chapter are to:

1. Determine whether *cmyb* mutant fish possess *mpeg*+ cells, and how their abundance may change over time.
2. Assess the regenerative capacity of juvenile *cmyb* mutant fish following tail fin amputation and compare it to the regenerative capacity of *cmyb* mutant embryos.
3. Develop non-invasive refinements for hematopoietic cell transplantation to reduce the severity of the protocol and the number of fish used.
4. Utilise the *cmyb* mutants in the hematopoietic cell transplantation model to gain further functional insights into the *Runx*:mCherry+ populations identified in Chapter 3.

5.3 Results

5.3.1 Six weeks post fertilisation cmyb mutant fish have a small number of mpeg+ cells

When investigating the ability of *cmyb* mutant fish to respond to viral mimetic R848, transcripts of the macrophage-specific gene *mpeg* were detected by qRT-PCR (Chapter 4; Fig. 4.12C). Furthermore, it was found in the work of Alemany *et al*. (2018) and Lin *et al*. (2019) that HSC-independent resident immune cells, such as *mpeg*+ metaphocytes, are present in the epidermis of zebrafish. To confirm whether this HSC-independent cell type was present in *cmyb* mutants, *Tg(mpeg1.1:SECFP-YPet)* fish (Andrews, 2016), which express CFP and YFP fluorescent proteins under the *mpeg1.1* promoter, were crossed to adult heterozygous *cmyb* mutant fish. Heterozygous fish were utilised for the crosses because homozygous mutants do not reach sexual maturity and therefore cannot reproduce, whereas heterozygous mutant fish are phenotypically WT and do not exhibit growth or hematopoietic defects (Soza-Ried *et al*., 2010). A mix of male fish heterozygous and homozygous for the *mpeg1.1*:SECFP-YPet transgene were crossed to female *cmyb* heterozygous mutants. According to Mendelian genetics, 50% of the offspring from this cross should be heterozygous for the *cmyb*^{t25127} gene and the *mpeg1.1*:SECFP-YPet transgene. Zebrafish do not have sex-determining chromosomes in the way mammalian species do, and sex determination is highly complex (von Hofsten, 2005). Sex determination, particularly in laboratory lines, is at least in part governed by environmental factors such as temperature, dissolved oxygen content and food availability (Kossack & Draper, 2019). Neither the *cmyb* nor *mpeg1.1* genes are located on chromosomes associated with sex determination regions (Liew *et al*., 2012; Liew & Orbán, 2014). However, the location of the *mpeg1.1*:SECFP-YPet transgene has not been mapped in the zebrafish genome. Consequently, equal distribution of male and female offspring may be expected in laboratory conditions. However, in this experiment, all fish that were heterozygous for both the *cmyb*^{t25127} mutation and the *mpeg1.1*:SECFP-YPet transgene were female. As a result, it was not possible to cross these fish to each other. Hence, *cmyb*+/- *mpeg1.1*:SECFP-YPet+/- fish were crossed to *cmyb*+/- males that did not possess the *mpeg1.1*:SECFP-YPet transgene (Fig. 5.1A). This meant that the *cmyb* mutation was incrossed while the transgene was outcrossed. According to Mendelian genetics, if there was no associated embryonic lethality, 12.5 % of the resultant embryos should be homozygous for the *cmyb* mutation and contain at least 1 copy of the *mpeg1.1*:SECFP-YPet transgene (Fig. 5.1A). The phenotype of *cmyb* mutant fish cannot be readily identified until approximately 4

wpf. Therefore, for the purpose of this experiment, all *mpeg1.1*:SECFP-YPet+ transgenic embryos were raised. However, due to mortality associated with homozygosity of the *cmyb* mutant gene, as well as the low number of offspring produced from the crosses, only one *cmyb* mutant was identified that was positive for the *mpeg1.1*:SECFP-YPet transgene at 6 wpf. This time point was chosen as *mpeg* transcripts were previously detected in 6 wpf *cmyb* mutant fish treated by R848 immersion (Fig. 4.12C).

The results show that *mpeg1.1*:SECFP-YPet+ cells were abundant throughout non-mutant sibling fish, including in the epidermal layer of the ventral fin (Fig. 5.1C). *mpeg1.1*:SECFP-YPet+ cells exhibited a highly dendritic morphology, commonly associated with macrophages and the recently discovered metaphocytes (Lin *et al*., 2019). Although there was only an n of 1 for this experiment, *mpeg1.1*:SECFP-YPet+ dendritic cells were identified in the *mpeg1.1*:SECFP-YPet+ *cmyb* mutant fish (Fig. 5.1D). However, no cells with dendritic shape were identified in the *mpeg1.1*:SECFP-YPet- *cmyb* mutant fish (Fig. 5.1E). This suggests that the cells identified in the *mpeg1.1*:SECFP-YPet+ *cmyb* mutant fish were indeed cells expressing the transgene and were not auto-fluorescent cells. This is consistent with the data from section 4.3.4 of Chapter 4, which showed that *mpeg* gene transcripts were detected in *cmyb* mutant fish (Fig. 4.12C). Interestingly, when fish were imaged at 15 dpf, qualitatively similar abundances of *mpeg1.1*:SECFP-YPet+ cells were observed in both the *cmyb* mutant fish and non-mutant sibling fish (Fig. 5.2, cell numbers were not quantified). However, due to the small number of fish in this study, definitive conclusions cannot be made about the longevity of these cells or the timeline in which *mpeg1.1*:SECFP-YPet+ cell numbers may start to diminish in *cmyb* mutant fish compared to non-mutant siblings. Indeed, a greater number of fish would be required to determine the size of the *mpeg1.1*:SECFP-YPet+ population in *cmyb* mutant fish relative to non-mutant siblings at various timepoints throughout their development.

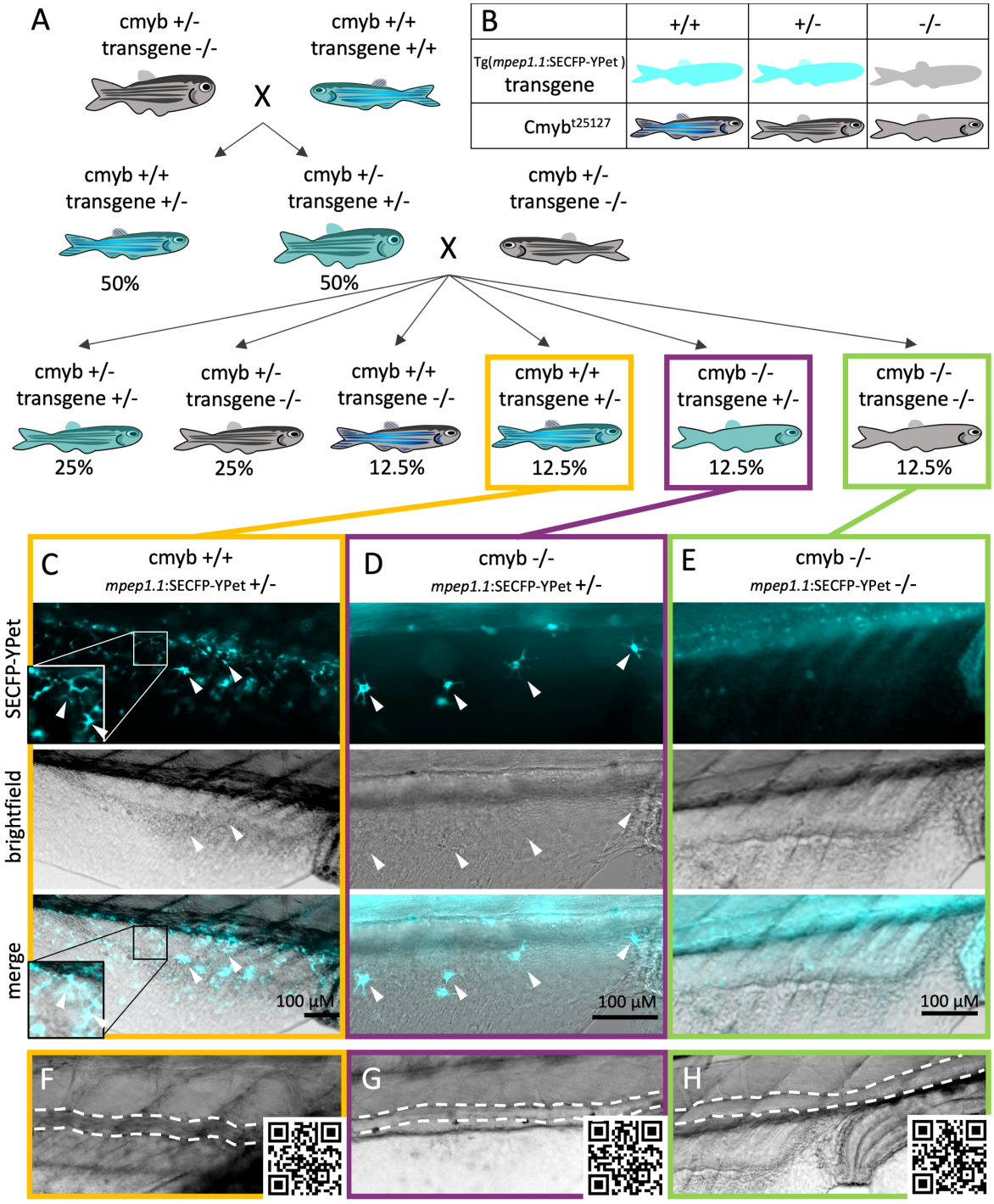

Fig. 5.1 Presence of *mpeg1.1*:SECFP-YPet+ cells in 6 wpf *cmyb* mutant zebrafish.

(**A**) Depiction of the cross carried out to between *cmyb* heterozygous mutant fish with *Tg(mpeg1.1*:SECFP-YPet*)* transgenic fish. Ratio of offspring expected for each genotype is denoted beneath fish of each genotype. (**B**) A key indicating how fish of each genotype are depicted. (**C-E**) Widefield live intravital microscopy of 6 wpf fish at 100X magnification. Top panel shows YPet fluorescence in cyan, middle panel shows brightfield (BF) image of ventral fin region of the fish and lower panel shows the merge of the YPet and BF images. Scale bars represent 100 µm. White arrow heads indicate locations of *mpeg1.1*:SECFP-YPet+ dendritic cells. (**C**) Representative image of *cmyb*+/+ *mpeg1.1*:SECFP-YPet+ fish (yellow box, n=5). (**D**) *cmyb* mutant *mpeg1.1*:SECFP-YPet+ fish (purple box, n=1). (**E**) Representative image of *cmyb* mutant *mpeg1.1*:SECFP-YPet- fish (green box, n=4). (**F-H**) BF images of ventral vein correlated with the fish in **C-E**. The outline is shown with white dashed lines. Videos were taken at a single z slice and can be viewed by using the adjacent QR code or these links (**F**) qrgo.page.link/UYRgS, (**G**) qrgo.page.link/8PGQx, (**H**) qrgo.page.link/YV8qh.

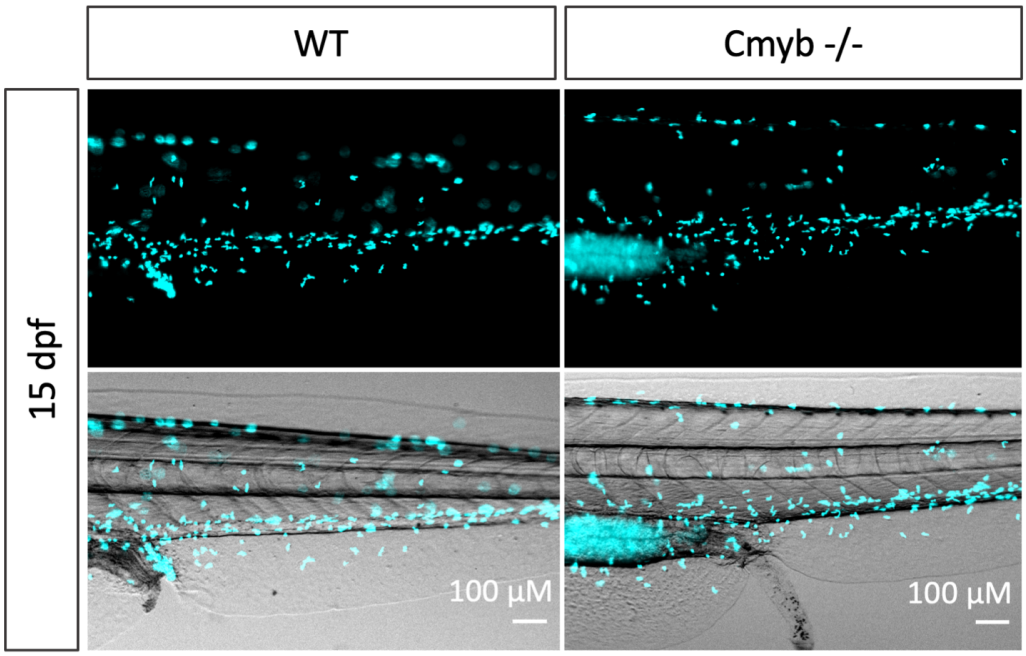

Fig. 5.2 Similar abundance of *mpeg1.1*:SECFP-YPet+ cells in 15 dpf *cmyb* mutant and non-mutant sibling fish.

Widefield live intravital microscopy of the ventral fin region in 15 dpf *Tg(mpeg1.1*:SECFP-YPet) (left, n=10) and *cmyb* mutant *Tg(mpeg1.1*:SECFP-YPet*)* fish (right, n=1). Top panel shows YPet fluorescence in cyan and lower panel shows a merge of the YPet and BF images. Scale bars represent 100 µm.

5.3.2 Six weeks post fertilisation cmyb mutant fish can regenerate following tail fin amputation

Following the observation that 6 wpf *cmyb* mutant fish possess *mpeg*+ cells and are capable of mounting an antiviral response to R848 (Chapter 4; Fig. 4.11), the next aim was to determine their regenerative capacity following damage such as tail fin amputation. It was reported by Hess *et al*. (2013) that *cmyb* mutants do not survive more than 2-3 days following tail fin amputation due to resultant widespread infection. However, I found that *cmyb* mutant fish were able to survive wound damage when maintained in E2 containing penicillin and streptomycin (PS) antibiotics. Therefore, for the purpose of regeneration studies, the fish were maintained in E2 + PS medium which was replaced daily 20 minutes after feeding to ensure food and waste debris was removed. Short-term survival of *cmyb* mutant fish following tail transection was not significantly different compared to control *cmyb* mutant fish, which were not manipulated (P=0.14, Fig. 5.3C). However, unsurprisingly, the survival of non-mutant sibling fish following tail transection was significantly higher than either that of the control *cmyb* mutant fish (P=0.0002) or amputated *cmyb* mutant fish (P= 0.002). The findings show that *cmyb* mutant fish are capable of tail fin regeneration following amputation (Fig. 5. 3B). When *cmyb* mutant fish are compared to their heterozygous and WT siblings, (referred to collectively as non-mutant siblings), it is evident that the regeneration of *cmyb* mutant fish is

impaired. The structure and organization of the regenerating tail fin tissue appeared impaired in *cmyb* mutant fish relative to non-mutant sibling fish (Fig. 5.3A& B, 5 dpa). In addition, there appeared to be greater variability in the extent of regeneration in mutant fish (data not shown).

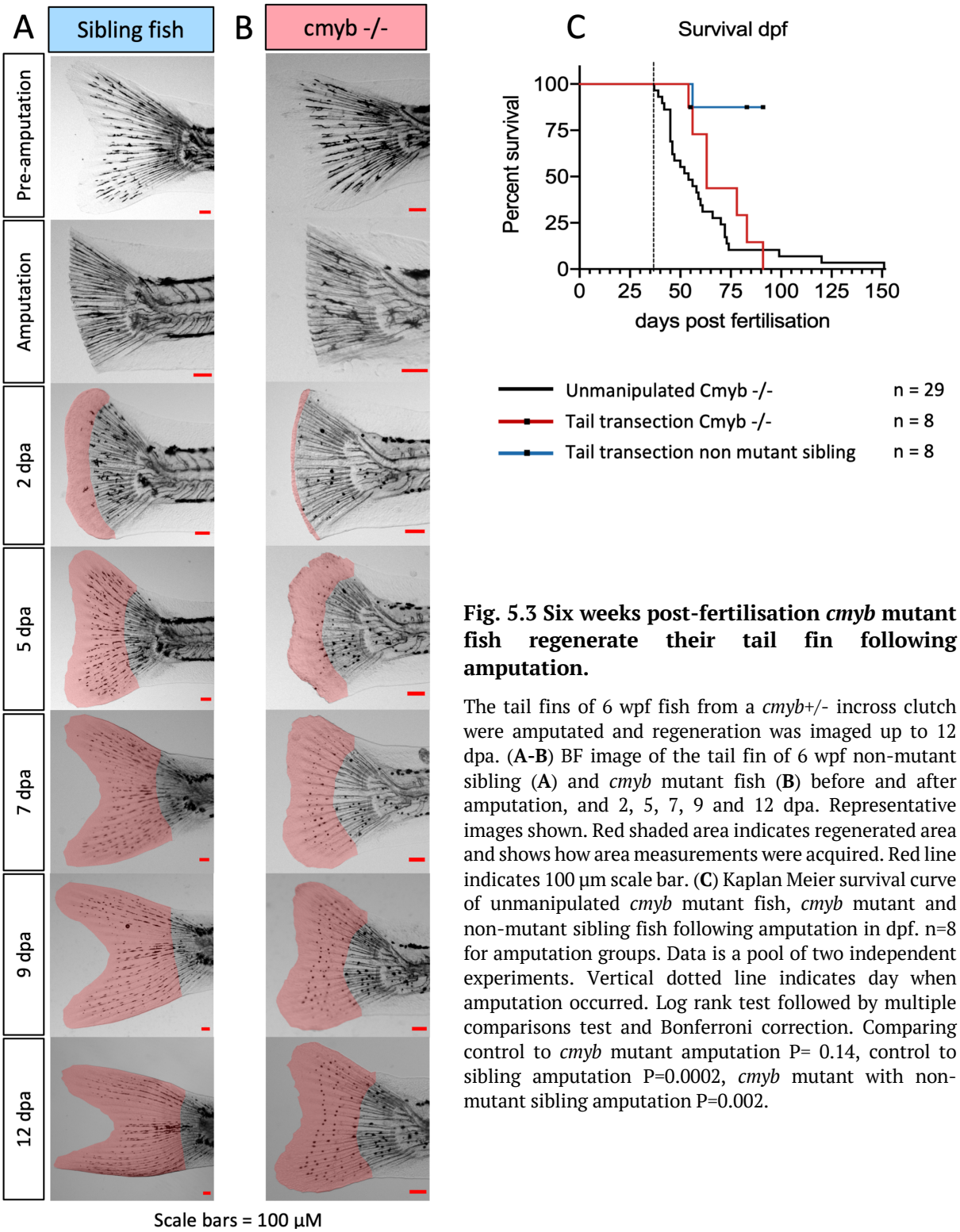

Fig. 5.3 Six weeks post-fertilisation *cmyb* mutant fish regenerate their tail fin following amputation.

The tail fins of 6 wpf fish from a *cmyb*+/- incross clutch were amputated and regeneration was imaged up to 12 dpa. (**A-B**) BF image of the tail fin of 6 wpf non-mutant sibling (**A**) and *cmyb* mutant fish (**B**) before and after amputation, and 2, 5, 7, 9 and 12 dpa. Representative images shown. Red shaded area indicates regenerated area and shows how area measurements were acquired. Red line indicates 100 µm scale bar. (**C**) Kaplan Meier survival curve of unmanipulated *cmyb* mutant fish, *cmyb* mutant and non-mutant sibling fish following amputation in dpf. n=8 for amputation groups. Data is a pool of two independent experiments. Vertical dotted line indicates day when amputation occurred. Log rank test followed by multiple comparisons test and Bonferroni correction. Comparing control to *cmyb* mutant amputation P= 0.14, control to sibling amputation P=0.0002, *cmyb* mutant with non-mutant sibling amputation P=0.002.

Quantification of the regenerated area revealed that most non-mutant sibling fish regenerated a significantly larger area of the tail fin than *cmyb* mutants (Fig. 5.4A). This also corresponded with a significantly reduced average rate of regeneration in *cmyb* mutant fish at 9 dpa as calculated by rate in μm^2 per day (Fig. 5.4B). Interestingly, some non-mutant sibling fish exhibited a similar area and rate of regeneration as the *cmyb* mutant fish, indicating high variability in the rate of regeneration among non-mutant sibling fish. However, this may be attributed to differences between WT and *cmyb* heterozygous fish. The initial area of tail fins was measured for one of two independent experiments. This was due to a change in imaging technique by using of an agar plate with a thin layer of water as a substrate on which to place the fish. This technique enabled the tail fin to spread out and the fin area to be measured. Therefore, the percentage of the original area that had regenerated could be calculated for these fish in order to determine the timepoint at which the full amputated area had grown back. This measure also indicated a significant difference between *cmyb* mutant and non-mutant sibling fish (Fig. 5.4C). However, investigating the percentage area regenerated revealed that, by 14 dpa, 2 out of 3 *cmyb* mutant fish were able to fully grow back the area of fin that had been amputated. However, it is worth noting that, at 6 wpf, juvenile fish are still growing, and it is therefore likely that the full area of the tail fin increases during the 2-week regeneration period. Indeed, sibling fish grew up to 500% of their original tail fin area during this time (Fig. 5.4C). Finally, the percentage of fin length regenerated was also measured in these experiments. As the percentage area regenerated could not be determined for every fish (due to the change in image acquisition protocol described above), length was utilised as this could be measured even when the tail fin was not splayed out. The length was always measured from the injury site to the most distal part of the tail fin (Fig. 5.4F). These data are in agreement with the trend seen in the percentage of area regenerated and shows that, by 9dpa, all non-mutant sibling fish were able to fully regenerate the length of tail fin tissue that had been removed. However, less than half of *cmyb* mutant fish had grown back the full length of their original fins by the same time. Overall, the data indicates that *cmyb* mutant fish were capable of regeneration following tail fin amputation, and this did not negatively impact their short-term survival. However, regeneration was impaired and occurred at a slower rate compared to non-mutant sibling fish.

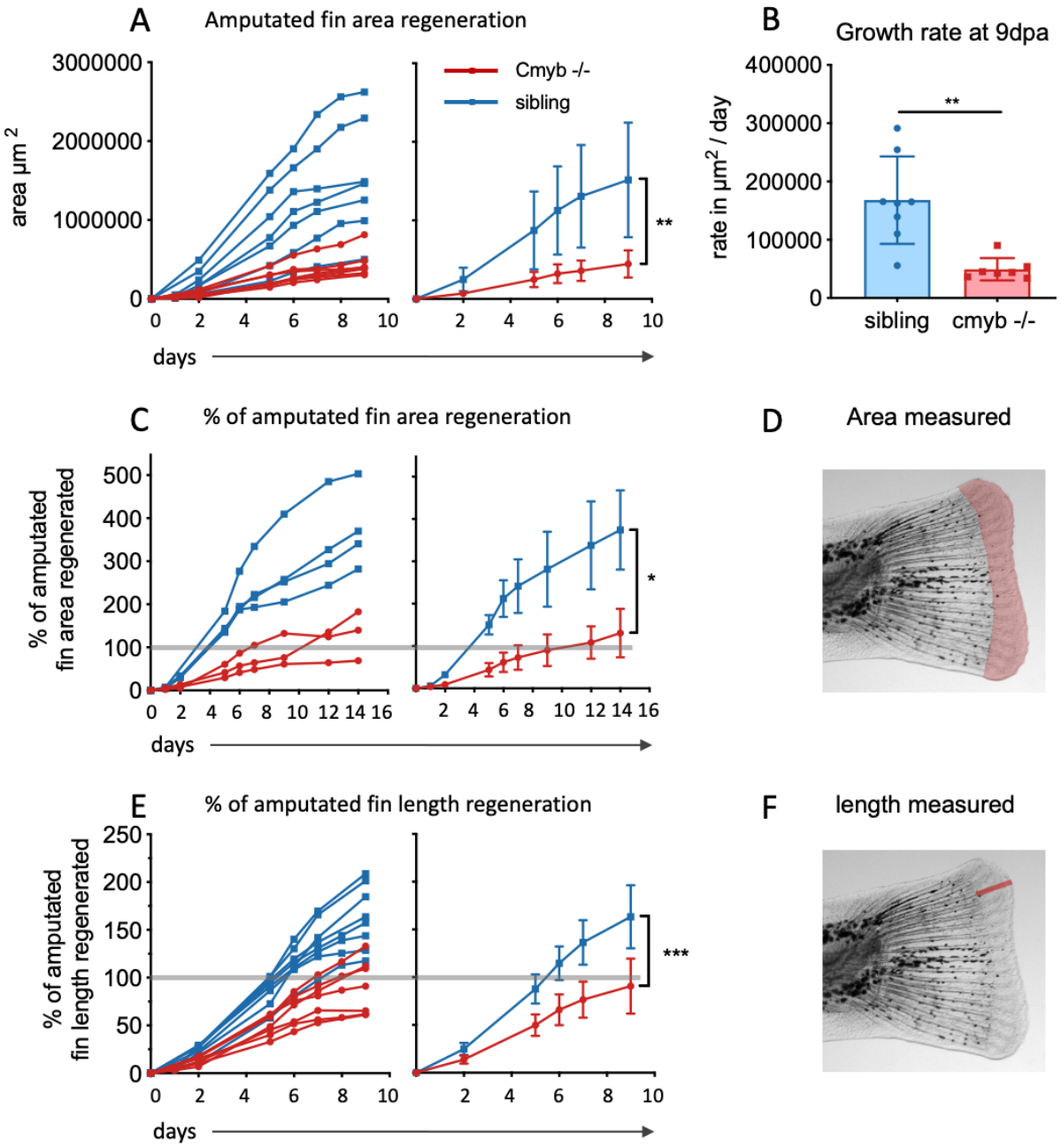

Fig. 5.4 Six weeks post-fertilisation *cmyb* mutants take longer to fully recover tail fin area and length following amputation compared to WT and heterozygous sibling fish.

The tail fins of 6 wpf fish from a *cmyb*+/- incross clutch were amputated and regeneration was imaged. Area and length were measured up to 14 dpa. n=3-8. Data is a pool of two independent experiments. (**A**) Area measurement of tail fin post-amputation in µm^2 up to 9 dpa for each individual fish (left) and as a pooled average (right). Mean and SD shown. Area was measured from amputation site, as shown in **D**. (**B**) Average growth rate at 9 dpa in µm^2 for non-mutant sibling and *cmyb* mutant fish. Each dot indicates measurements from one individual fish. Mean and SD are shown. (**C**) Percentage of amputated fin area regenerated over time from individual fish (left) and as a pooled average (right). Mean and SD are shown. n=3-4. Data from one experiment. Grey line indicates when 100% of amputated area had regenerated. (**D & F**) Representative BF images of regenerating tail fin. (**D**) Red shaded area indicates regeneration area and how area measurements were acquired. (**F**) Red line shows how length measurements were carried out. (**E**) Percentage of amputated fin length regenerated over time from individual fish (left) and as a pooled average (right). Mean and SD are shown. n=7-8. Data from two independent experiments. Grey line indicates when 100% of amputated length had grown back. Unpaired, two tailed t-test, * P<0.05, ** P<0.005, *** P<0.0005.

5.3.3 Three days post fertilisation cmyb mutant embryos effectively regenerate their fin fold following transection

Following the observation that juvenile *cmyb* mutant fish can carry out impaired regeneration of their tail fins following amputation, without adversely affecting their short-term survival, the next aim was to assess the regeneration in *cmyb* mutant embryos. *cmyb* mutants go through the first wave of hematopoiesis successfully and produce blood cells normally until approximately 3 dpf, when definitive hematopoiesis starts and takes over blood- and immune-cell production (Jing & Zon, 2011). At this stage, cells are no longer produced from the primitive wave's cells. Therefore, in *cmyb* mutant fish, which cannot initiate the definitive wave of hematopoiesis, blood and immune cell numbers begin to decline (Soza-Ried *et al*., 2010). It was hypothesized that until cell numbers from the primitive wave start to reduce, the *cmyb* mutant embryos may have regenerative abilities similar to WT fish. To determine whether the *cmyb*^{t25127} mutation could impact the regenerative capacity of 3 dpf embryos, fin fold amputations were carried out in collaboration with Yuan Sun (MRes. Imperial College London). The regeneration area, as well as the neutrophil count therein, were investigated. To ensure consistent measurements of the regeneration area (taking into account variability of the fin fold transections), the first 200µm were measured from the posterior end of the notochord toward the anterior part of the fish. The area was then measured from that point, as depicted in Fig. 5.5A. To determine the regenerative capacity, the regrown area and neutrophil cell numbers were quantified at 6 and 24 hpa for *cmyb* mutants, heterozygotes and WT fish. These time points were chosen because it has been shown that neutrophil infiltration to the wound site peaks at approximately 6 hpa and is reduced by 24 hpa (Renshaw *et al*., 2006; Bernut & loynes *et al*., 2020). Statistically significant differences between the three genotypes of fish were not identified in either neutrophil infiltration (Fig. 5.5B-C) or area regrown within 24 hours (Fig. 5.5D-E), suggesting that the *cmyb* mutation in either heterozygous or homozygous fish does not diminish regenerative capacity of 3 dpf embryos relative to WT embryos.

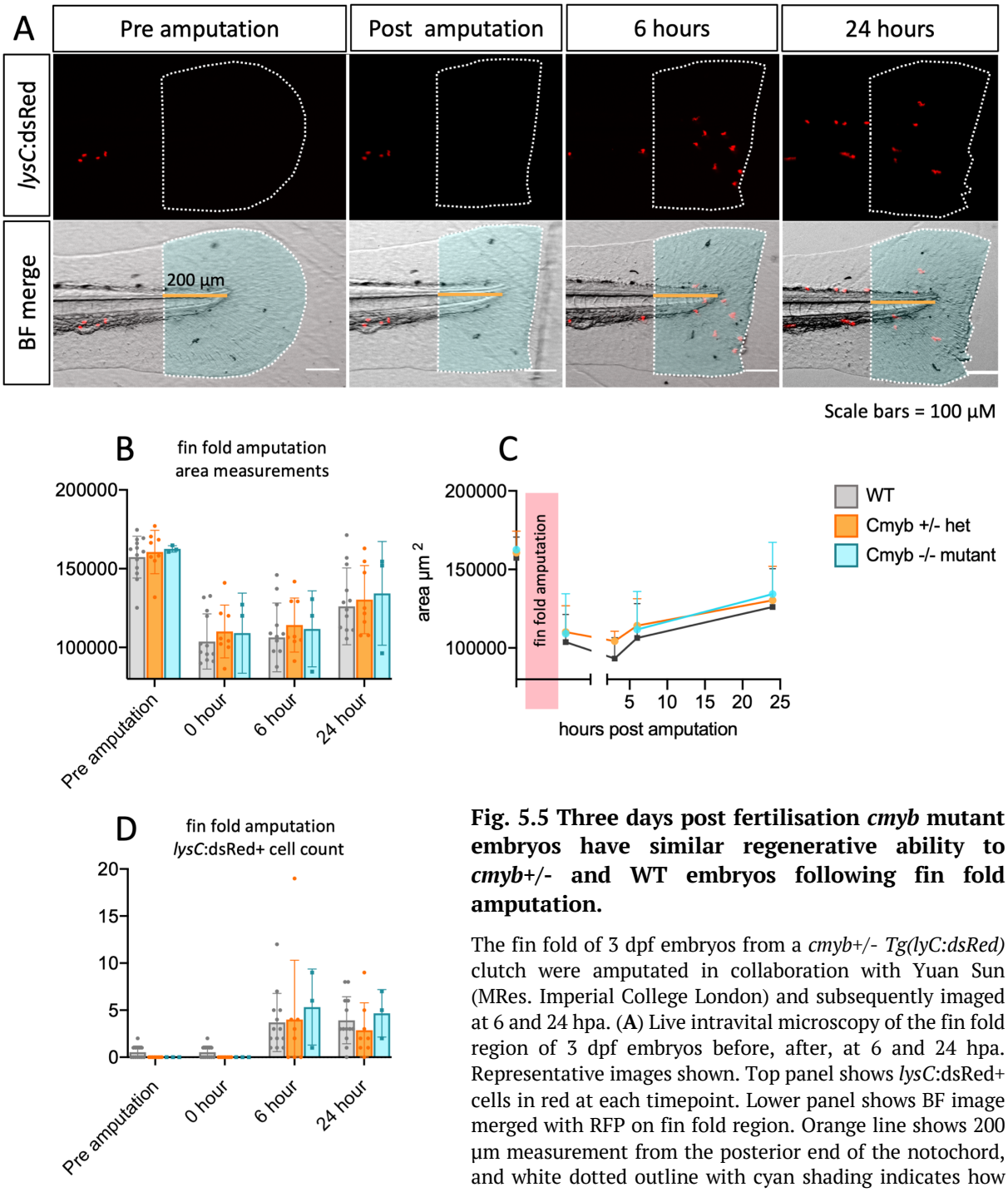

Fig. 5.5 Three days post fertilisation *cmyb* mutant embryos have similar regenerative ability to *cmyb*+/- and WT embryos following fin fold amputation.

The fin fold of 3 dpf embryos from a *cmyb*+/- *Tg(lyC:dsRed)* clutch were amputated in collaboration with Yuan Sun (MRes. Imperial College London) and subsequently imaged at 6 and 24 hpa. (**A**) Live intravital microscopy of the fin fold region of 3 dpf embryos before, after, at 6 and 24 hpa. Representative images shown. Top panel shows *lysC*:dsRed+ cells in red at each timepoint. Lower panel shows BF image merged with RFP on fin fold region. Orange line shows 200 µm measurement from the posterior end of the notochord, and white dotted outline with cyan shading indicates how area measurements were acquired and within which which *lysC*:dsRed+ cells were quantified. White line indicates 100 µm scale bar. (**B**) Area measurement in µm^2 of fin fold region pre amputation, post-amputation (0 hours), 6 and 24 hpa of each genotype (WT, *cmyb*+/- and *cmyb* mutants). Each individual dot represents the area measurement from an individual fish. (**C**) Mean average of area for each genotype over time. Red shaded area indicates when amputation occurred. (**D**) Cell count of *lysC*:dsRed+ cells in the fin fold region pre amputation, post-amputation (0 hours), 6 and 24 hpa of each genotype (WT, *cmyb*+/- and *cmyb* mutants). Each individual dot represents the area measurement from an individual fish. (**B & D**) Mean and SD shown. N=3-13. Data pooled from 3 independent experimental repeats.

5.3.4 Non-invasive identification of cmyb mutant fish reduces transplant numbers

cmyb mutant fish have been used in HCT models to assess various aspects of HSC biology. They are valuable as recipients in HCT experiments as they do not require IR preconditioning prior to allogenic transplantation to ablate host HSCs and immune cells. They cannot go through the definitive wave of hematopoiesis, which produces the HSCs that maintain hematopoiesis into adulthood. Therefore, their hematopoietic niche is effectively empty and can be colonised by donor cells. In previous work by McBrien (2017), transplantation was carried out on fish that were screened for the *cmyb*^{t25127} mutation by assessing complexion, as it was reported that *cmyb* mutant fish cannot survive tail fin transection (Hess *et al*., 2013). This meant that fish that were paler were selected for transplantation and fish were only assessed for their genotype when the animals were harvested post-transplant. However, there are non-mutant sibling fish that may exhibit growth retardation or have a paler complexion regardless of their heterozygous or WT genotype (data not shown). As a result, a number of non-mutant sibling fish can inadvertently be subjected to the HCT procedure. Thus, one aim of this study was to determine whether *cmyb* mutant fish could be screened and identified with greater accuracy in order to eliminate the transplantation of non-mutant sibling fish. It was hypothesized that this would be possible without fin clipping, which can induce inflammation and would increase suffering experienced by transplant recipients. It was demonstrated by Soza-Ried *et al*. (2010) that *cmyb* mutant fish are almost completely depleted of erythrocytes by approximately 3 wpf. Hence, it was hypothesized that circulating cells could be assessed in 6 wpf fish prior to transplantation using a dissection microscope. This would eliminate the transplantation of small and pale non-mutant sibling fish. BF microscopy with the same dissection microscope as would be utilised during micro-injection for HCT at (10X magnification), was sufficient to detect the presence or absence of circulating cells in the ventral vein of fish. It was found that *cmyb* mutant fish could be readily distinguished from non-mutant sibling clutch mates using this method (Fig. 5.6). Furthermore, it was found that *cmyb* mutant fish were fully anaesthetised within 1-2 minutes of being placed in 4.2 % tricaine solution. In combination with the short duration of time required to identify *cmyb* mutant fish, it was possible to assess their vasculature directly prior to retroorbital injection for HCT. This meant that fish were only anaesthetised once to carry out both the assessment of their vasculature and HCT procedures.

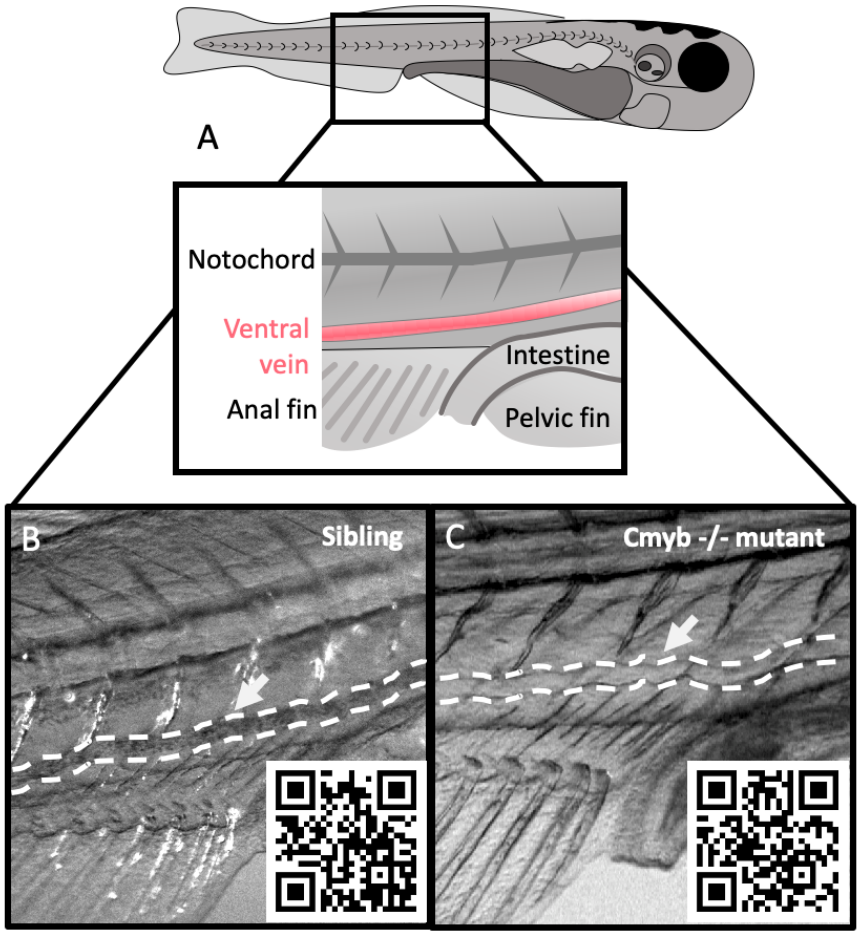

Fig. 5.6 Homozygous *cmyb* mutant fish can be identified by assessing the abundance of circulating cells in the ventral vein.

6 wpf *cmyb* mutants and non-mutant sibling fish were anaesthetised in 4.2 % tricaine in E2. BF imaging at 12.5X magnification was used to screen for circulating cells in the ventral vein. (**A**) Diagram depicting the area of the fish imaged, highlighting the location of the notochord, ventral vein (pink), anal fin, pelvic fin and intestine. (**B-C**) Single BF images from videos of non-mutant sibling (**B**) and *cmyb* mutant (**C**) fish from the same clutch. White arrow points to, and dashed lines outline, the ventral vein where the presence (**B**) or absence (**C**) of circulating cells was visible. Videos were taken at a single z slice and can be viewed by using the adjacent QR code the following links (**B**) qrgo.page.link/cdyir, (**C**) qrgo.page.link/n43x4.

In experiments carried out for the purpose of this thesis, fish were first pre-screened and selected based on size and complexion. Selected fish were subsequently assessed for cells in circulation using the method shown in Fig. 5.6. It is approximated that roughly 25 % of fish were mistakenly identified as *cmyb* mutants based on size and complexion alone. For comparison, this figure was closer to 3% after assessing the vasculature using the method shown in Fig. 5.6. A total of 126 fish underwent the HCT procedure after their vasculature was assessed, meaning that roughly 28 non-mutant sibling fish might have been unnecessarily subjected to the HCT procedure if assessment for circulating cells had not been carried out.

However, these numbers are approximations based on observation and experience. Unfortunately, this data was not consistently recorded throughout the duration of the project.

5.3.5 Development of a scoring system for hematopoietic transplant recipients

Once it had been identified that *cmyb* mutant fish could be accurately identified using a bright field microscopy assessment method, the next aim was to develop a post-transplant scoring system to track the progress of HCT engraftment in *cmyb* mutant zebrafish. This scoring system would subsequently be utilised for HCT experiments to determine which factor, or combination of factors, constituted the strongest predictors of successful transplantation and long-term survival.

Factor 1: Cells in circulation

Given that *cmyb* mutants can be identified by the very characteristic that there are no circulating cells in their vasculature, it was reasoned that an engrafting fish that received multilineage reconstituting HSPCs would show a steady increase in circulating cells until WT levels were reached. Unfortunately, quantification of circulating cells in the vasculature can be challenging for several reasons. Firstly, due to the speed at which cells travel through the blood vessels, it can be difficult to see each individual cell in a single image or frame. Therefore, videos are required to detect the movement of cells and give a better impression of the number of cells present. However, for cells to be enumerated, either a specific length of a blood vessel would need to be consistently quantified, or a representative segment if the size of fish varies. Secondly, it would require the same length of exposure for image acquisition, and this can vary depending on the brightness of bulbs on different microscopes. Thirdly, due to the speed at which individual cells move through the vasculature, videos must be acquired in a single z plane. This means that some out of focus cells may be missed. In addition, as the number of circulating cells increases, it becomes difficult to resolve individual cells for quantification both due to cell density and due to cells obstructing each other. Therefore, a qualitative measure was devised instead. When no or very few cells were observed throughout the acquisition of 300 frames that were 20-30 ms apart (totalling ~6-9 seconds), a score of 0 was given. Sparsely populated blood vessels that exhibited a constant flow of a low number of cells received a score of 1. A consistent flow of a higher number of individually resolved cells was given a score of 2 and, finally, blood vessels with circulation akin to that

found in WT blood vessels were given a score of 3 (Fig. 5.7). When scoring transplant recipients, mid-integer scores were also assigned to fish that exhibited an abundance of cells in circulation (or fluorescent cells in the WKM and gill) that was between the integer scores defined below.

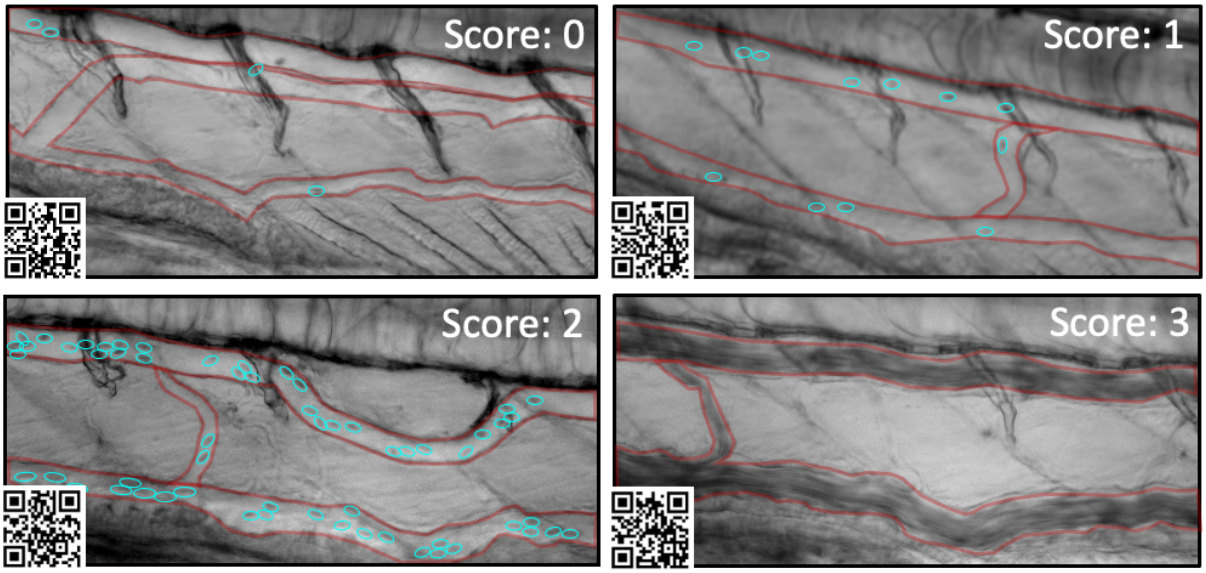

Fig. 5.7 Post-transplant scoring of cells in circulation

Scoring of the abundance of cells in circulation of *cmyb* mutant fish following HCT. BF imaging at 10X magnification was used to capture videos of circulating cells in the vasculature. Blood vessels are outlined in red and, where individual blood cells could be resolved, these are circled in cyan. Individual cells were identified from corresponding videos as cells can be difficult to identify from a single frame. Videos were taken at a single z slice and can be viewed by using the adjacent QR code or these links (**score 0**) qrgo.page.link/xDG7j, (**score 1**) qrgo.page.link/ymxrT, (**score 2**) qrgo.page.link/r4h4Z, (**score 3**) qrgo.page.link/iEXJM. Representative images are shown for each score.

Factor 2: Runx:mCherry+ cells in the head kidney marrow

It was shown by McBrien (2017) that *lysC*:dsRed+ cells derived from *CD41*:GFP ^{low} donor cells first populate the head kidney region of the WKM, suggesting that this may be the area of the kidney first populated by HSPCs. Furthermore, in juvenile 21 dpf donor *Tg(Runx:mCherry; lyz:GFP)* fish, the head kidney region exhibited the greatest population of *Runx*:mCherry+ cells compared to the mid or tail regions of the WKM (Fig. 5.8A). Hence, it was hypothesized that successfully reconstituted *cmyb* mutant fish would also exhibit well populated head kidneys, and this was indeed found to be the case (Fig. 5.8B). Based on qualitative comparison, it was found that successfully-reconstituted *cmyb* mutant fish had a similarly populated WKM at 21 dpt as juvenile donor fish of the same age (Fig. 5.8).

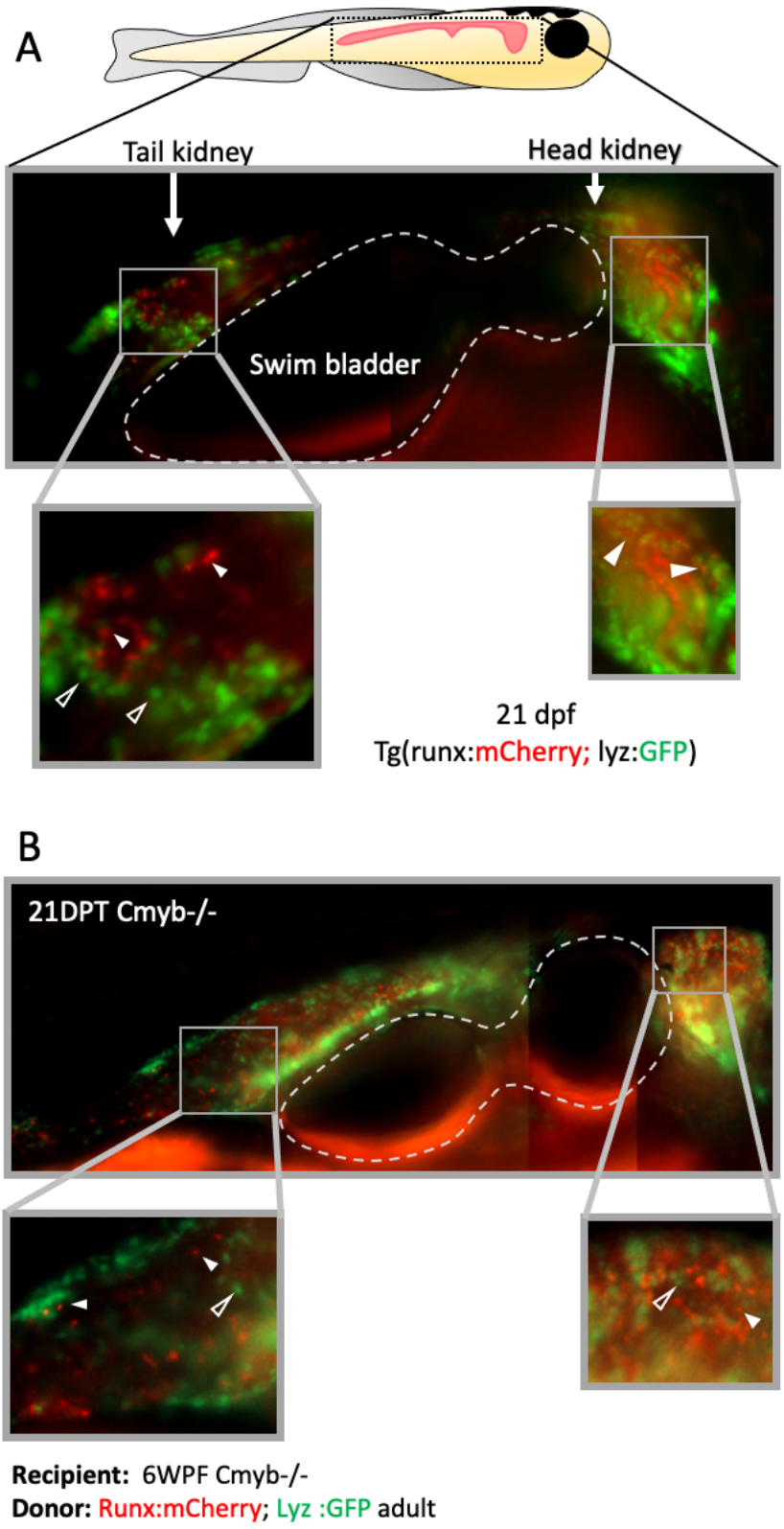

Fig. 5.8 The population of *Runx*:mCherry+ cells in the WKM of 21 dpt *cmyb* mutant fish is similar to the WKM of 21 dpf *Tg(Runx:mCherry; lyz:GFP)* donor fish.

A 21 dpt transplanted *cmyb* mutant fish and a representative 21 dpf juvenile transgenic fish were anaesthetised in 4.2 % tricaine for imaging. Live intravital fluorescence imagines of WKM were acquired using 20X objective. Images were acquired either at a single z slice or represent the maximum projection of 3-5 z slices. Diagram of juvenile fish indicates the imaged area of the WKM. Enlarged are regions of the head and tail kidney marrow where individual fluorescent *Runx*+ cells are indicated with a filled arrowhead. *lyz*:GFP+ myeloid cells are in green and shown with arrow head outline. (**A**) juvenile *Tg(Runx:mCherry; lyz:GFP)* fish 21 dpf. (**B**) 21 dpt *cmyb* mutant fish. Fish received *Runx*:mCherry+ cells from *Tg(Runx:mCherry; lyz:GFP)* adult WKM.

The next factor investigated was the abundance *Runx*:mCherry+ HSPCs in the head kidney of transplanted fish. Owing to the difficulty of quantifying individual cells in the WKM of larger fish due to the optical depth of the tissue and the low fluorescence intensity of *Runx*:mCherry+ cells, a qualitative scoring matrix was developed. When 0-5 *Runx*:mCherry+ cells were observed throughout the entire WKM, a score of 0 was given. When approximately than 5-15 cells were observed throughout the WKM and some of these were in the head kidney, this was given a score of 1. An intermediate number of *Runx*:mCherry+ cells in the head kidney was scored 2, while a dense population of *Runx*:mCherry+ cells, akin to that seen in juvenile donor fish, was awarded a score of 3 (Fig. 5.8; Fig. 5.9). At this stage, if donor fish also possessed transgenes for *ubi*:GFP or *lyz*:GFP, these would also be expected to densely populate the head kidney if successful long-term multilineage reconstitution had occurred.

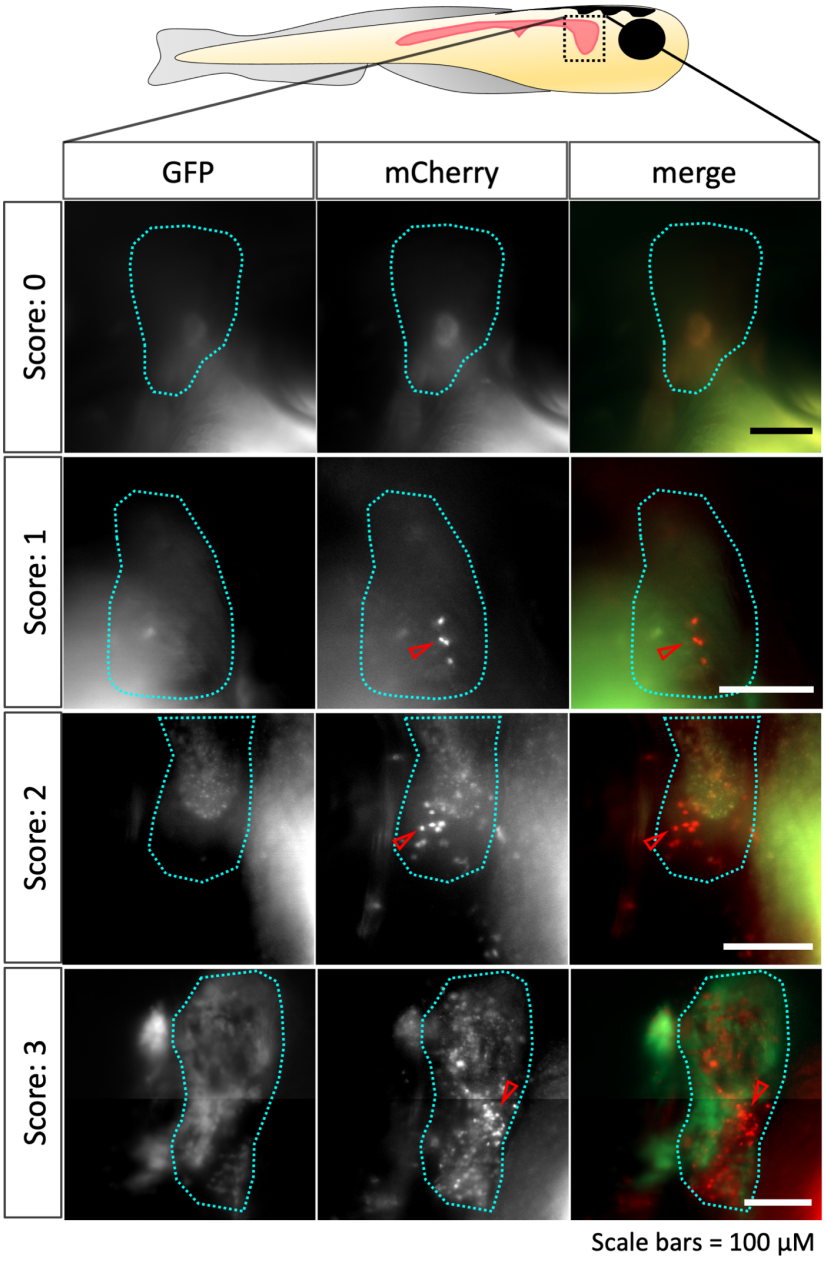

Fig. 5.9 Post-transplant scoring of *Runx*:mCherry+ cells in the head kidney.

Transplanted *cmyb* mutant fish were anaesthetised in 4.2 % tricaine in E2 for imaging. Live intravital fluorescence imaging at 10X magnification was carried out to capture images of the head kidney of transplanted fish. Images were acquired either at a single z slice or represent the maximum projection of 3-5 z slices. The head kidney regions are outlined with cyan dotted lines and red arrow heads point to the location of individual *Runx*:mCherry+ cells. Left column indicates GFP fluorescence (*ubi*:GFP or *lyz*:GFP), middle column mCherry fluorescence (*Runx*:mCherry) and the right column is the merge of the two. Some autofluorescence visible in kidney tubules. Scale bars represent 100 µm. Representative images are shown for each score.

Factor 3: Runx:mCherry + cells in the gills

Finally, although it has not yet been fully elucidated what cell type *Runx*:mCherry+ cells in the gills represent, it has been shown in *Chapter 3* of this thesis that these cells were highly abundant in adult *Tg(Runx:mCherry)* zebrafish. Thus, it was hypothesized that in long-term reconstituted *cmyb* mutant fish, *Runx*:mCherry+ cells would populate the gills. This was indeed the case and *Runx*:mCherry+ cells were observed within the gills of transplanted *cmyb* mutant fish. Hence, this was incorporated into the scoring of transplanted fish. Once again, it was not practical to quantify individual cells, and a qualitative scoring system was devised instead. When no or very few *Runx*:mCherry+ cells were present in the gills, a score of 0 was

awarded. Identification of a small number of positive cells throughout the kidney was scored as 1. An intermediate number of cells, with some in circulation, was given a score of 2. When a high number of *Runx*:mCherry+ cells were present in the filaments and seen in circulation (as was observed in *Tg(Runx:mCherry)* fish characterised in Chapter 3), this was scored as 3 (Fig. 5.10).

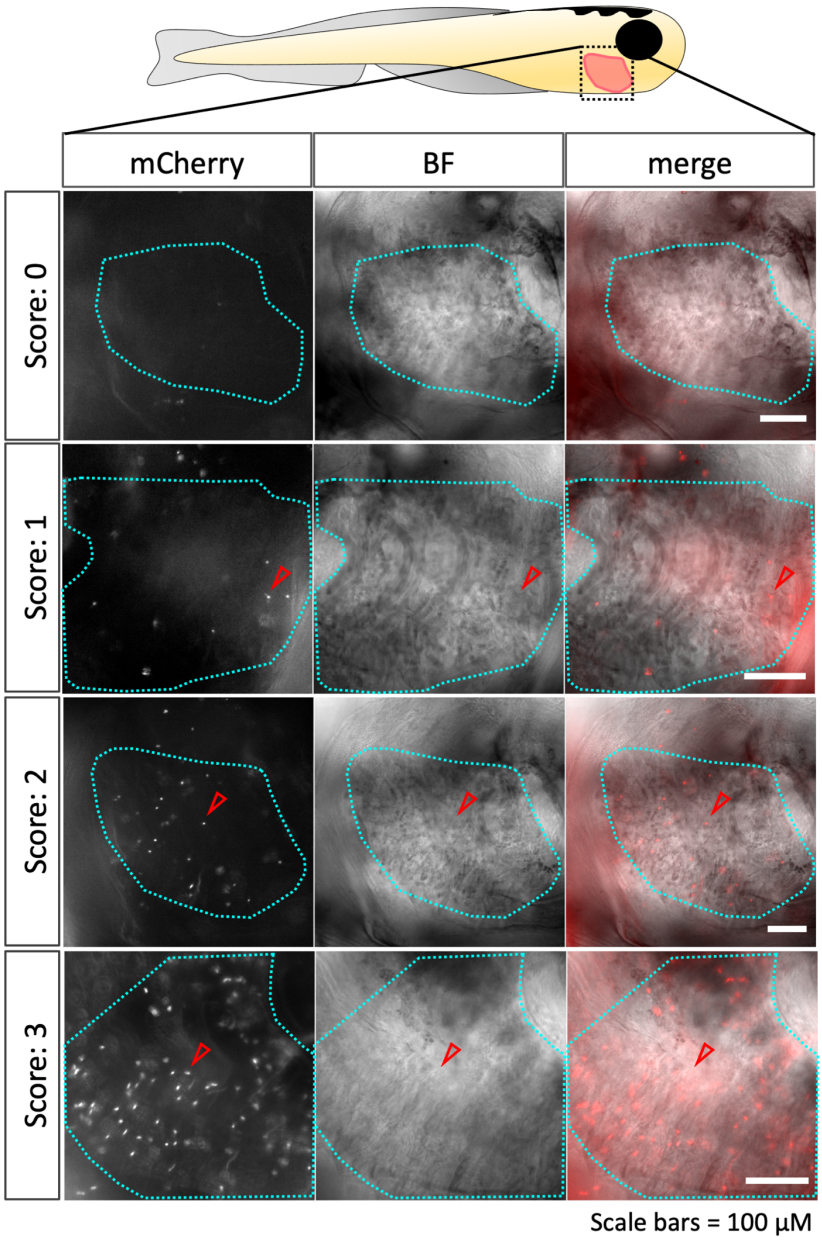

Fig. 5.10 Post-transplant scoring of *Runx*:mCherry+ cells in the gills.

Transplanted *cmyb* mutant fish were anaesthetised in 4.2 % tricaine in E2 for imaging. Live intravital fluorescence imaging at 10X magnification was carried out to capture images of the gills of transplanted fish. Images were acquired at a single z slice. The gill regions are outlined with cyan dotted lines and red arrow heads point to the locations of individual *Runx*:mCherry+ cells. Left column indicates mCherry fluorescence, middle column indicates BF (used to identify the lamellae in the gills), and the right column shows the merge of the two. Scale bars represent 100 µm. Representative images are shown for each score.

The scoring of each factor was developed following observations in fully reconstituted *cmyb* mutant fish which made it possible to determine what a score of 3 would look like for each factor. Imaging of transplanted fish occurred at 3, 6, 8, 10, 15, 22 and 29 dpt and all images were blinded before assigning scores for each factor. However, throughout the time course of

the experiment, individual fish did not generally transit through every score in the matrix. Therefore, examples of representative scores were collected from a number of individuals at various timepoints for Figures 5.7, 5.9 & 5.10. In practice, when the scoring system was applied, it was sometimes found that, in transplanted fish that were engrafting donor cells successfully, the scores across each factor rapidly reached 3 and were maintained at that level. As an example, a *cmyb* mutant fish that was transplanted with 2000 *Runx*:mCherry ^{low} donor cells from the WKM of adult *Tg(Runx:mCherry; lyz:GFP)* zebrafish already scored a 2 on circulation by 3 dpt, which increased to 2.5 at 6 dpt and a score of 3 by 8 dpt. This score was achieved at each subsequent timepoint until the final imaging timepoint at 29 dpt (Fig. 5.11). Similarly, the scoring for *Runx*:mCherry cells in the head kidney of the same fish reached a score of 2 by 3 dpt, and consistently scored 3 at subsequent imaging timepoints (Fig. 5.12). In the gills, this fish had a score of 1 at 3 dpt but reached a score of 3 by 6 dpt, maintaining that score at all subsequent imaging timepoints (Fig. 5.13). The fact that each factor reached a score of 3 by 8 dpt, as well as the fact that the scores remained at 3 for all subsequent time points, suggested that successful reconstitution had occurred.

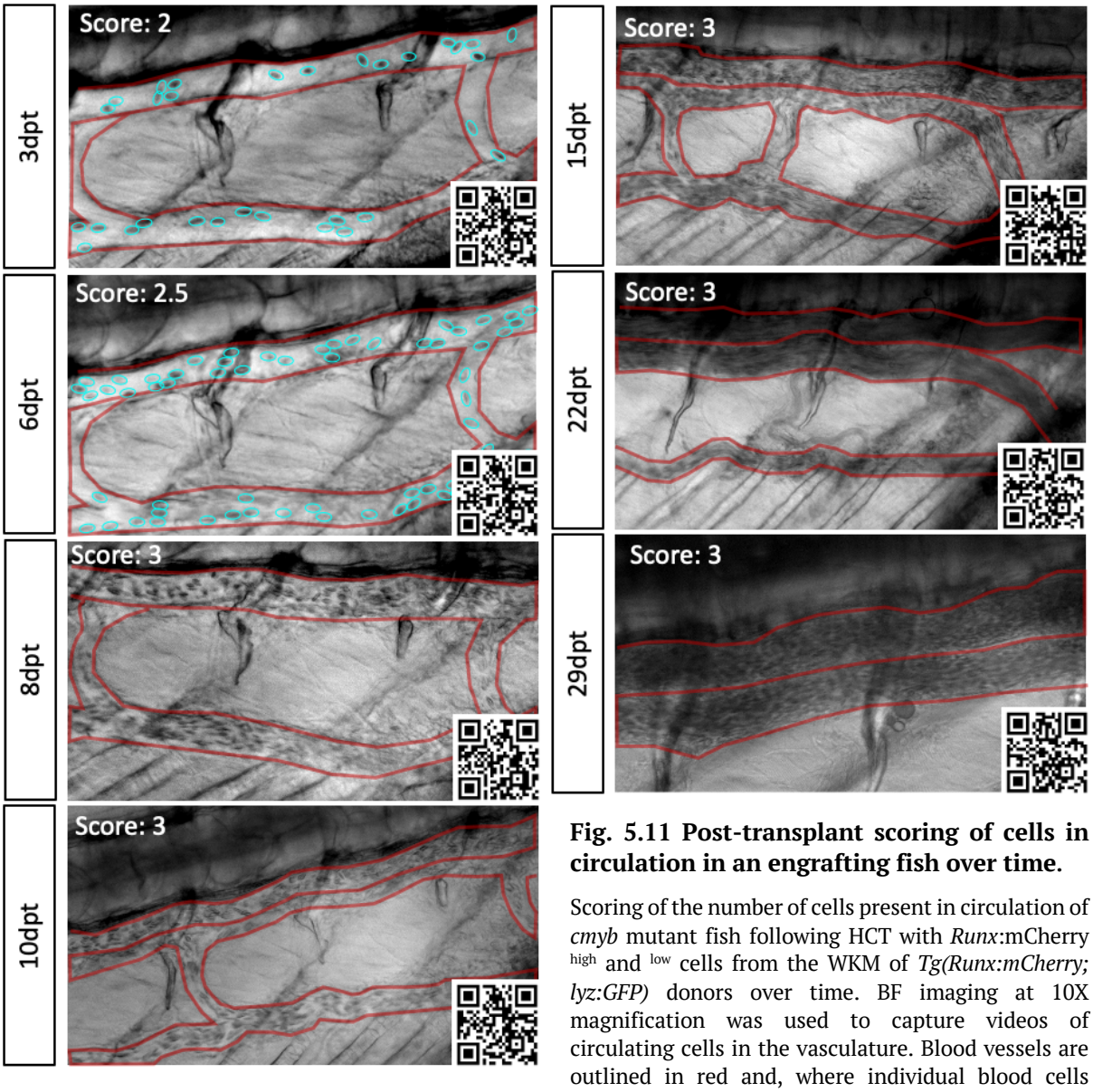

Fig. 5.11 Post-transplant scoring of cells in circulation in an engrafting fish over time.

Scoring of the number of cells present in circulation of *cmyb* mutant fish following HCT with *Runx*:mCherry ^{high} and ^{low} cells from the WKM of *Tg(Runx:mCherry; lyz:GFP)* donors over time. BF imaging at 10X magnification was used to capture videos of circulating cells in the vasculature. Blood vessels are outlined in red and, where individual blood cells can be resolved, these are circled in cyan. Individual cells were identified from corresponding videos as cells can be difficult to identify in a single frame. Videos were taken at a single z slice and can be viewed by using the adjacent QR code or the following links (**3 dpt**) qrgo.page.link/iGqDo, (**6 dpt**) qrgo.page.link/vx8G6, (**8 dpt**) qrgo.page.link/9A9Gt, (**10 dpt**) qrgo.page.link/6t6U2, (**15 dpt**) qrgo.page.link/a3uLX, (**22 dpt**) qrgo.page.link/SmWBU, (**29 dpt**) qrgo.page.link/bZkgH. The time points and corresponding scores assigned to each video are indicated.

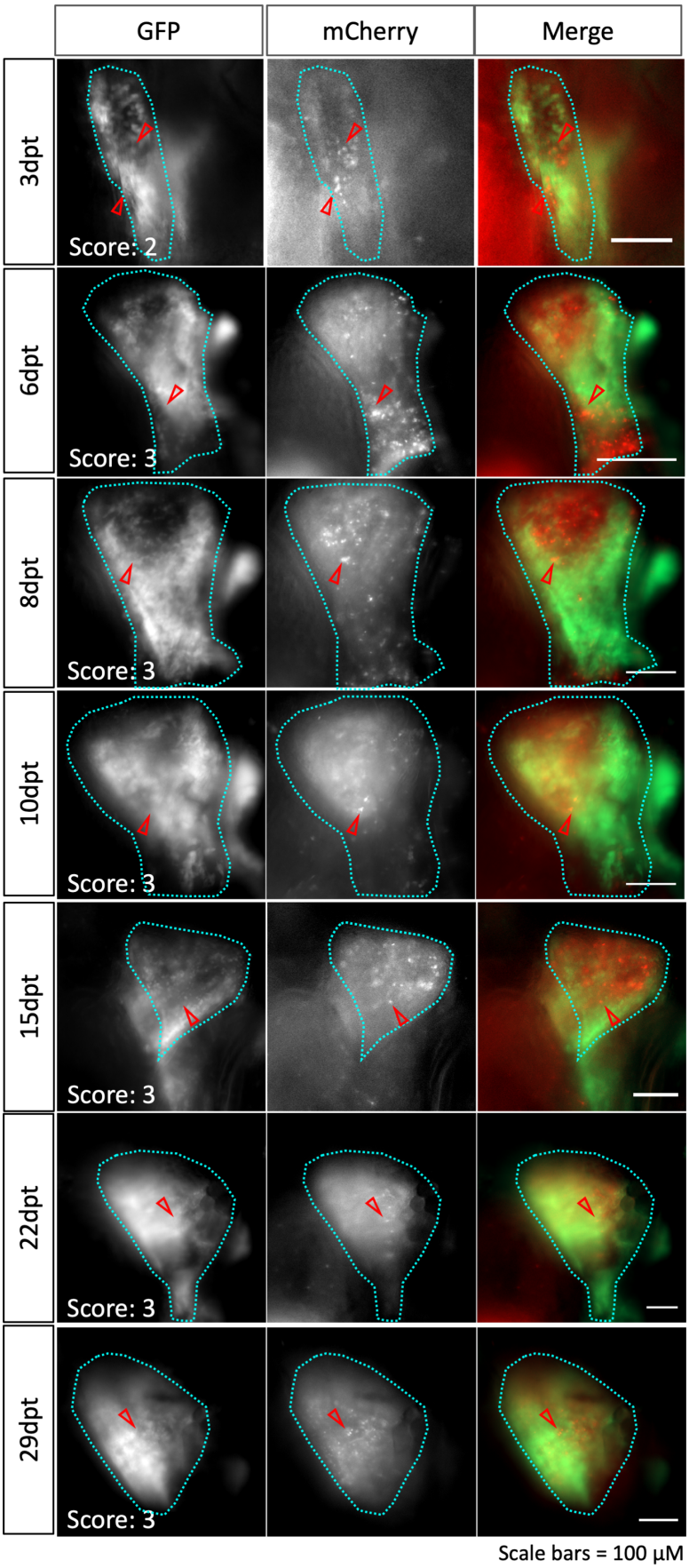

Fig. 5.12 Post-transplant scoring of *Runx*:mCherry+ cells in the head kidney in an engrafting fish over time.

Scoring of the number of *Runx*:mCherry+ cells present in the head kidney of *cmyb* mutant fish following HCT with *Runx*:mCherry ^{high} and ^{low} cells from the WKM of *Tg(Runx:mCherry; lyz:GFP)* donors over time. Fluorescence imaging at 10X magnification was used to capture images of cells in the head kidney. Images were acquired either at a single z slice or represent the maximum projection of 3-5 z slices. The head kidney regions are outlined with a cyan dotted line and red arrow heads point to the locations of individual *Runx*:mCherry+ cells. Left column indicates GFP fluorescence, middle mCherry fluorescence and the right column is the merge of the two. Scale bars represent 100 µm. Imaging time points and corresponding scores assigned to each are indicated.

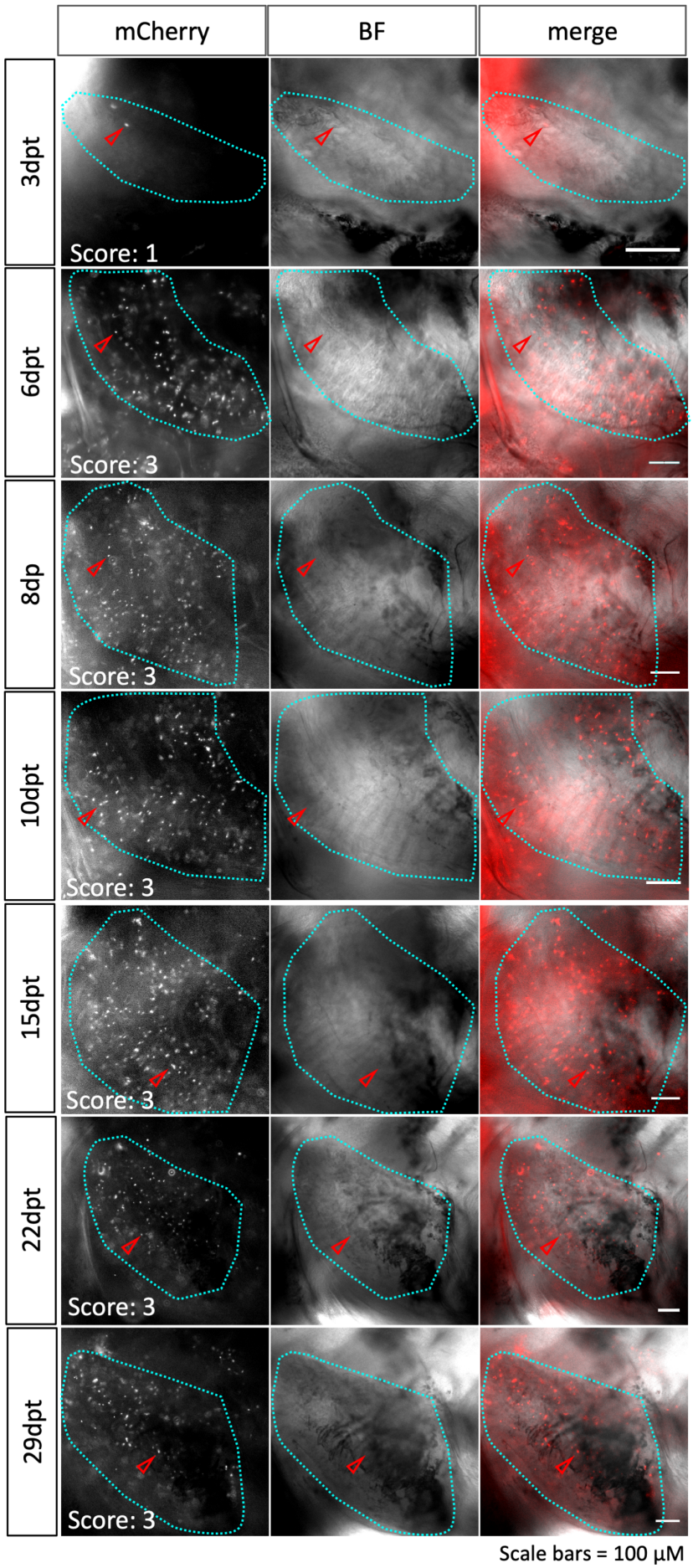

Fig. 5.13 Post-transplant scoring of *Runx*:mCherry+ cells in the gills of an engrafting fish over time.

Scoring of the number of *Runx*:mCherry+ cells present in the gills of *cmyb* mutant fish following HCT with *Runx*:mCherry ^{high} and ^{low} cells from the WKM of *Tg(Runx:mCherry; lyz:GFP)* donors over time. BF and fluorescence imaging was used at 10X magnification to capture images of *Runx*+ cells in the gills. Images were acquired at a single z slice. The gills are outlined with a cyan dotted line and red arrow heads point to the locations of individual *Runx*:mCherry+ cells. Left column indicates mCherry fluorescence, middle is BF and the right column is the merge of the two. Scale bars represent 100 µm. Imaging time points and corresponding scores assigned to each are indicated.

5.3.6 WKM Runx:mCherry low cells are capable of more robust reconstitution than Runx:mCherry high cells

Once the scoring system for transplantation had been established, thus enabling the progress of engraftment to be tracked, the next aim was to apply the scoring system in order to assess the stem cell potential of the various *Runx*:mCherry+ populations identified in adult transgenic fish, as described in Chapter 3. Subsequently, it should be possible to utilise the scoring data to determine which factor or combination of factors is the most effective predictor of long-term engraftment and survival.

In Chapter 3 of this thesis, it was demonstrated that the *Runx*:mCherry ^{high} population significantly overlapped with the *Runx*:GFP+ population (Fig. 3.12), which has been shown by Tamplin *et al.* (2015) to have a high HSPC purity. However, there were also indications that the *Runx*:mCherry ^{high} populations in the WKM and gill may correlate to *CD41*:GFP ^{high} thrombocytes, as described by Lin *et al.* (2005) (Fig. 3.18-3.20). Gene transcript analysis by qRT-PCR revealed that the *Runx*:mCherry ^{low}, FSC $^{med-high}$ population had greater *cmyb* and *ckit* transcript levels, indicating HSPCs may reside in this population. On the other hand, *rag1* and *IgM* transcripts were also detected in this population but not in the *Runx*:mCherry ^{high}, FSC ^{low} population in the WKM or gill. Furthermore, *runx1* transcript levels were higher in the *Runx*:mCherry ^{high} populations (Fig. 3.25-26). Therefore, it remained unclear whether *Runx*:mCherry ^{high} or ^{low} populations in the WKM contained long-term multilineage-reconstituting HSCs. To assess this, HCTs were carried out with each population, the survival recorded and engraftment tracked. Furthermore, the functional characteristics of *Runx*:mCherry+ cells in the gill remained elusive, with high levels of *ckit* and *runx1* transcripts, which are associated with HPSCs, having been detected (Fig. 3.25-26). Therefore, to definitively assess whether gill *Runx*:mCherry+ cells are capable of hematopoietic reconstitution, transplantation assays were carried out.

Six wpf *cmyb* mutant fish were transplanted with 2000 FACS sorted *Runx*:mCherry+ cells and 10^5 peripheral blood (PB) carrier cells. *cmyb* mutant fish were transplanted at this age because growth retardation means that they are too small at earlier stages. By 6 wpf, they reached a size that allowed for experimental manipulation and retro-orbital injection using the refinement methods described by McBrien (2017), specifically by use of a micromanipulator

and glass-pulled needle to reduce the insertion site of the injection. The transplanted *Runx*:mCherry+ cell populations were either FACS sorted *Runx*:mCherry ^{low}, FSC $^{med-high}$ cells from the WKM or *Runx*:mCherry ^{high}, FSC ^{low} cells from either the WKM (Fig. 5.14) or the gills. When cells were isolated from the gills, the same FACS gating strategy was applied to isolate *Runx*:mCherry ^{high}, FSC ^{low} cells as was used for the WKM (Fig. 5.14A-D). Transplanted fish were then imaged at 3, 6, 8, 10, 15, 22 and 29 dpt. Imaging data was used to score and track engraftment using the scoring factors described in section 5.3.5 of this chapter.

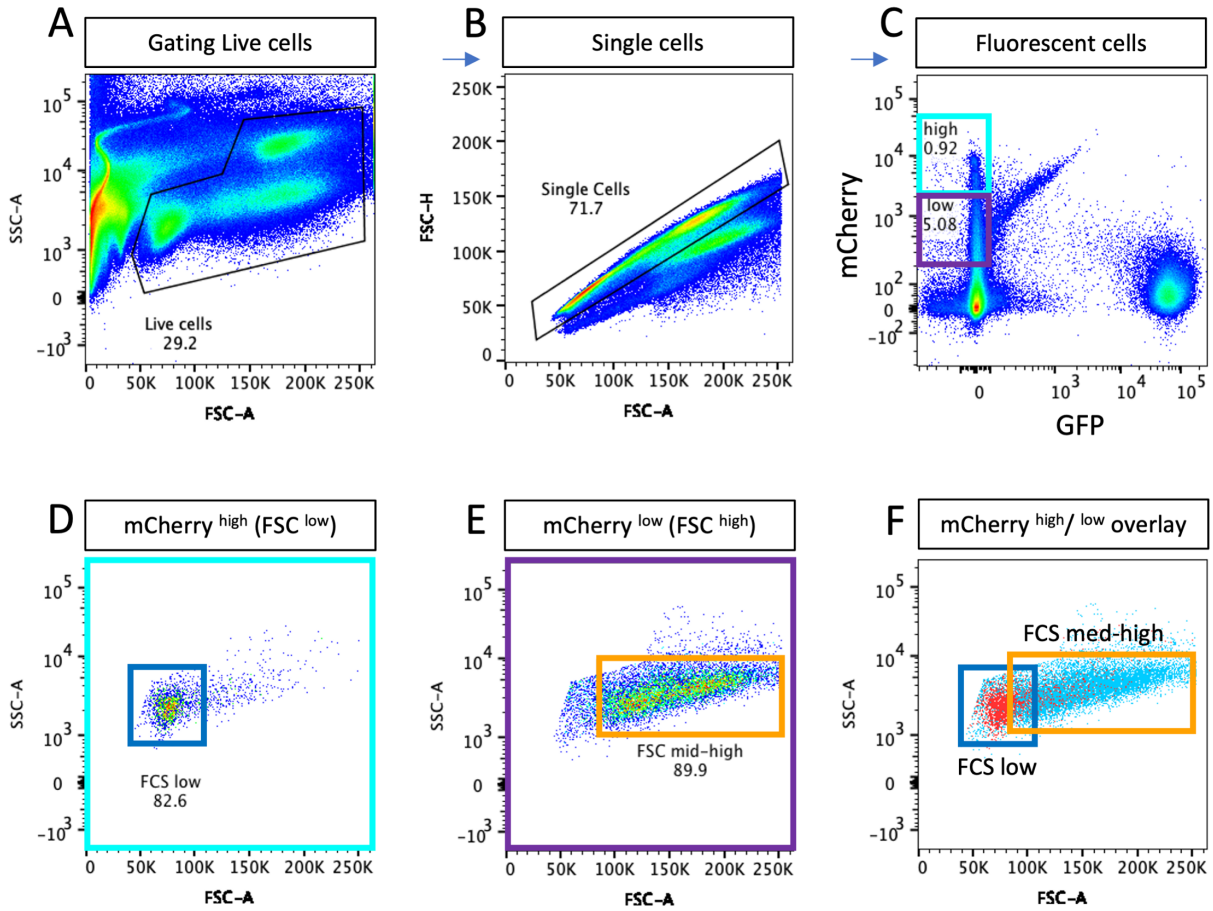

Fig. 5.14 FACS gating strategy to sort *Runx*:mCherry ^{high} and ^{low} populations for HCT.

Single-cell suspension of WKM tissue pooled from 4 *Tg(Runx:mCherry; lyz:GFP)* fish. (**A**) Representative FSC-A/SSC-A profile. Black lines indicate gating for live cells. (**B**) Gating to exclude doublet cells. (**C**) mCherry/ GFP plot with gating of *Runx*:mCherry ^{high} and ^{low} populations. Cyan box outline represents gating for *Runx*:mCherry ^{high} cells, purple box outline represents gating for *Runx*:mCherry ^{low} cells. (**D**) FSC/SSC plot of *Runx*:mCherry ^{high} cells. Dark blue box outline represents gating for FSC ^{low} cells which are sorted as HCT donor cells. (**E**) FSC/SSC plot of *Runx*:mCherry ^{low} cells. Orange box outline represents gating for FSC $^{med-high}$ cells which are sorted as HCT donor cells. Values adjacent to gates reflect the percentage of events within each gate compared to total events in the whole plot. (**F**) Overlap of **D** and **E** to show relationship of *Runx*:mCherry ^{high} and ^{low} cells on FSC/SSC.

Comparing the average scores across all three factors (cells in circulation, *Runx*:mCherry cells in the WKM and in the gill) between the three different *Runx*:mCherry+ donor cell populations, it was found that *Runx*:mCherry ^{low}, FSC $^{med-high}$ donor cells gave rise to the most effective reconstitution and resulted in scores of 3/3 for each factor at 22 dpt (Fig. 5.15A). *Runx*:mCherry ^{high}, FSC ^{low} cells were also capable of reconstituting cells in circulation, as well as fluorescent cells in the WKM and gills. However, this population appeared to increase cells in circulation more effectively than the *Runx*+ cells in the WKM or gills, suggesting a possible lineage bias, or late engraftment and increased time for reconstitution (Fig. 5.15B). Finally, the *Runx*:mCherry+ population isolated from the gills appeared to increase cells in circulation transiently before reducing again, and very few *Runx*+ cells were present either in the WKM or the gills throughout subsequent imaging timepoints (Fig. 5.15C).

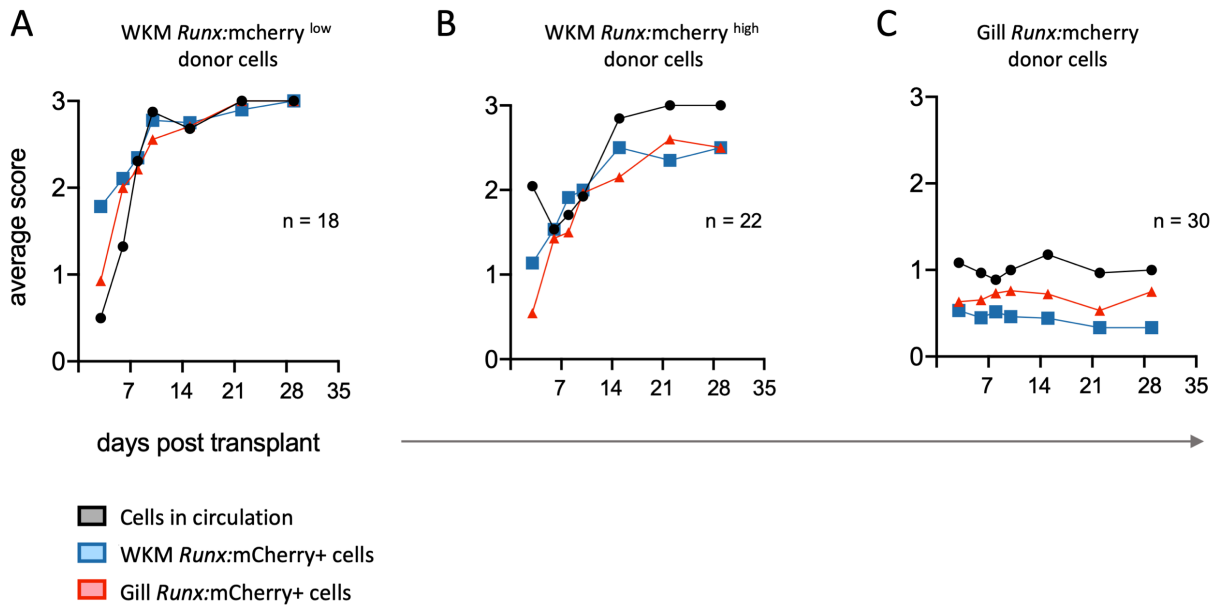

Fig. 5.15 Comparison of the post-transplant engraftment scores arising form from different *Runx*:mCherry+ donor populations.

Transplanted *cmyb* mutant fish received 2000 *Runx*:mCherry+ cells from either the gill (n=30) or WKM *Runx*:mCherry ^{high} (n=22) or *Runx*:mCherry ^{low} (n=18), in addition to 10^5 PB carrier cells. Data pooled from 22 experiments. Recipients were imaged at 3, 6, 8,10, 15, 22 and 29 dpt. Scores for the reconstitution of the cells in circulation, *Runx*:mCherry+ cells in the WKM and gill were determined according to the scoring matrix devised in section 5.3.5. Mean averages of scores for each factor over time in recipients of *Runx*:mCherry ^{low} cells (**A**), *Runx*:mCherry ^{high} cells from the WKM (**B**) and *Runx*:mCherry ^{high} cells isolated from gills (**C**).

Comparing post-transplant scoring of the cells in circulation between different donor cells revealed that *Runx*:mCherry ^{high} or ^{low} donor cells isolated from the WKM were the most effective at increasing the abundance of cells in circulation in the vasculature of *cmyb* mutant

fish (Fig. 5.16A). On average, *Runx*:mCherry ^{low} donor cells resulted in a steady increase in circulating cells between 3-10 dpt, at which point most fish had a score of 3 which persisted until 29 dpt (Fig. 5.16A). Conversely, *cmyb* mutant fish transplanted with *Runx*:mCherry ^{high} cells from the WKM had a greater number of cells in circulation at 3 dpt. However, this decreased before increasing again and reaching a score of 3 at 15 dpt, indicating that erythrocytes can be produced by WKM-derived *Runx*:mCherry ^{high} donor cells with a slight delay when compared to *Runx*:mCherry ^{low} cells. Transplantation of *cmyb* mutant fish with PB carrier cells but no donor cells revealed that injected carrier blood cells in circulation are depleted by approximately 15 dpt. Therefore, cells in circulation after this time have likely come from differentiated cells arising from donor cells. Interestingly, gill-derived *Runx*:mCherry ^{high} cells were also capable of erythroid output and increased the number of cells in circulation. However, this was highly variable between fish. Over 50 % of fish received a circulation score of 0-1 at all timepoints, while the remaining fish had scores ranging from 0-3, suggesting that in some cases gill-derived *Runx*:mCherry+ cells were capable of erythroid output (Fig. 5.16A).

The average WKM and gill scores of transplanted fish show that WKM-derived *Runx*:mCherry ^{low} cells were most effective at reconstituting the population of *Runx*:mCherry cells in transplanted *cmyb* mutant fish. Investigating the head kidney, it was found that *Runx*:mCherry ^{low} donor cells on average reached a score of 2.5 by 8 dpt and, by 10 dpt, 100 % of transplanted fish scored between 2 and 3 (Fig. 5.16B). Similarly, in the gills, scores steadily increased from 1 at 3 dpt to 75% of fish scoring 3 at 15 dpt (Fig. 5.16C). Fish receiving *Runx*:mCherry ^{high} cells from the WKM showed engraftment scores which were on average approximately ½ a score below those that received *Runx*:mCherry ^{low} cells for both WKM and gill reconstitution. However, WKM scores of these fish were highly variable and thus differences were not found to be statistically significant at individual time points (Fig. 5.16B). Gill and circulation scores, on the other hand, increased much more reliably in recipients of *Runx*:mCherry ^{high} cells. On the whole, recipients of gill donor cells were not able to reconstitute either the WKM or the gill *Runx*:mCherry+ cells, although it appears as if transplanted cells may have preferentially homed to the gill as opposed to the WKM as scores in the gill were consistently slightly higher than in the WKM (Fig. 5.16B-C). Ultimately, limiting dilution transplant assays or competitive repopulation assays would give more

accurate measures of stem cell fitness between these 3 populations (Kwarteng & Heinonen, 2016). While these experiments were planned, this type of quantification was not possible within the scope of this thesis due to time constraints.

Next, it was investigated how full reconstitution across all three factors combined could best be represented. Two approaches were utilised for this. One was to add the scores from each factor together and create a combined score out of 9 (Fig. 5.16D). This would reflect the extent of engraftment observed overall, across each of the anatomical locations, and would also report on partial or lineage-biased engraftment. The other approach was to multiply scores together to generate a combined engraftment score out of 27 (Fig. 5.16E). To differentiate between them, the latter is termed the '*engraftment score*'. The rational for this was that if any individual factor, whether it be the cell circulation, cells in the gill or WKM, exhibited a score of 0, then successful multilineage reconstitution cannot have occurred. Thus, multiplying scores together would give the best indication of whether successful multilineage engraftment had occurred. Therefore, this could give a clearer indication of which *Runx*+ population had the greatest HSC potential. It was found in these experiments that out of the three transplanted *Runx*+ populations, *Runx*:mCherry ^{low}, FSC $^{med\text{-}high}$ cells from the kidney had the greatest ability for long-term reconstitution, followed by *Runx*:mCherry ^{high}, FSC ^{low} cells isolated from the kidney (Fig. 5.16D). On the other hand, the addition of scores can provide information on whether lineage-biased reconstitution may have occurred, as appeared to be the case when gill *Runx*:mCherry+ cells were transplanted (Fig. 5.16D).

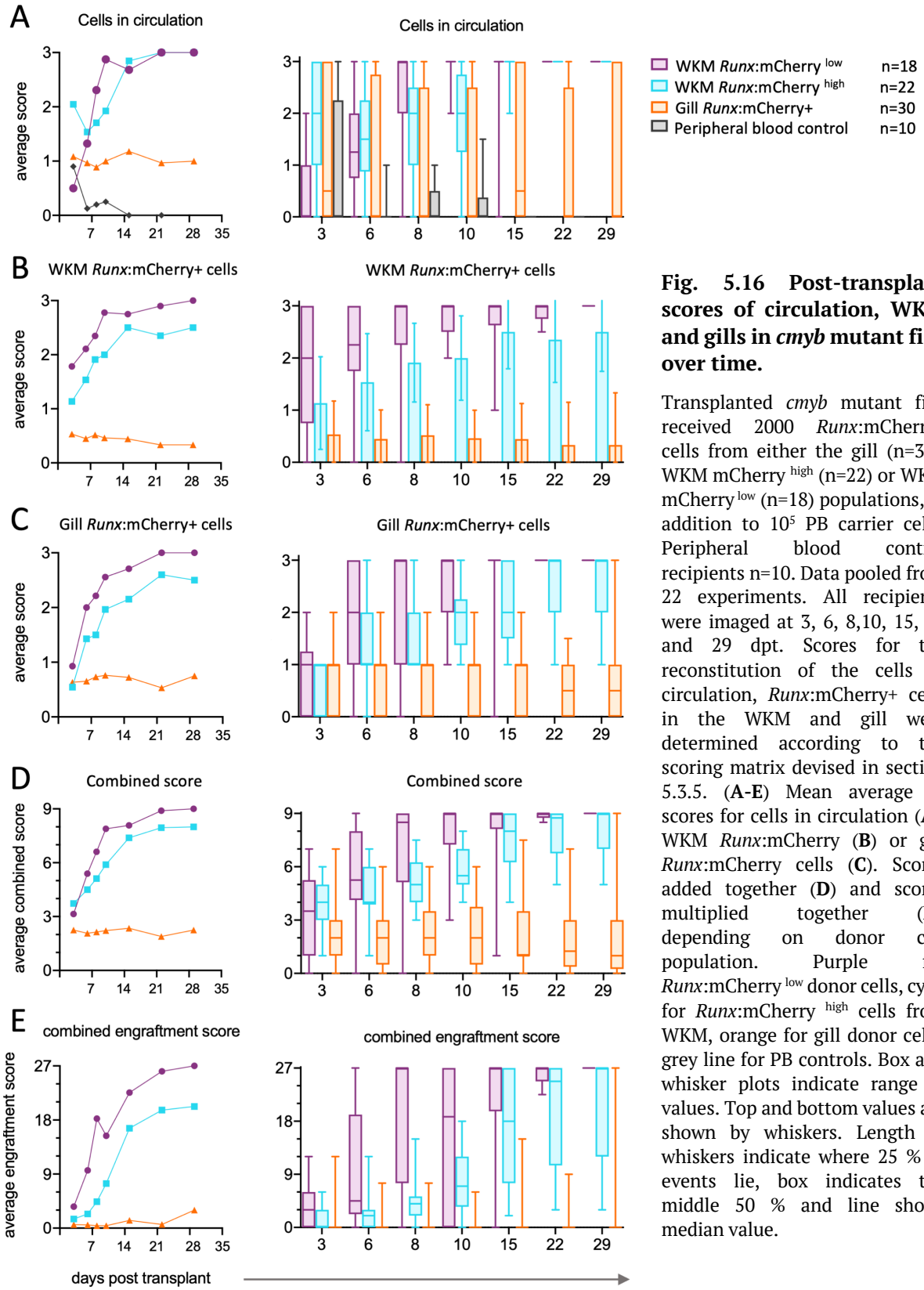

Fig. 5.16 Post-transplant scores of circulation, WKM and gills in *cmyb* mutant fish over time.

Transplanted *cmyb* mutant fish received 2000 *Runx*:mCherry+ cells from either the gill (n=30), WKM mCherry ^{high} (n=22) or WKM mCherry ^{low} (n=18) populations, in addition to 10^5 PB carrier cells. Peripheral blood control recipients n=10. Data pooled from 22 experiments. All recipients were imaged at 3, 6, 8,10, 15, 22 and 29 dpt. Scores for the reconstitution of the cells in circulation, *Runx*:mCherry+ cells in the WKM and gill were determined according to the scoring matrix devised in section 5.3.5. (**A-E**) Mean average of scores for cells in circulation (**A**), WKM *Runx*:mCherry (**B**) or gill *Runx*:mCherry cells (**C**). Scores added together (**D**) and scores multiplied together (**E**), depending on donor cell population. Purple for *Runx*:mCherry ^{low} donor cells, cyan for *Runx*:mCherry ^{high} cells from WKM, orange for gill donor cells, grey line for PB controls. Box and whisker plots indicate range of values. Top and bottom values are shown by whiskers. Length of whiskers indicate where 25 % of events lie, box indicates the middle 50 % and line shows median value.

In addition to tracking the success of engraftment in transplanted *cmyb* mutant fish via scoring of cells in circulation, WKM and gills, the long-term survival of transplanted fish was also assessed both in terms of dpt and dpf. This was done to enable a comparison between the survival of transplanted and unmanipulated *cmyb* mutants. Statistically significant differences were identified using multiple log rank tests with Bonferonni multiple comparisons correction to the significance values. It was found that the difference in survival (measured in dpt) between control PB recipients and recipients of *Runx*:mCherry ^{low} donor cells was statistically significant (P= 0.0003), as was the difference in survival between recipients of *Runx*:mCherry ^{high} donor cells compared *Runx*:mCherry ^{low} cells (P= 0.0016, Fig. 5.17A). When survival was investigated as a measure in dpf, it was found that there was no statistical difference in survival between control PB recipients and unmanipulated *cmyb* mutants. Interestingly, the highest survival of unmanipulated *cmyb* mutants in this study was up to 151 dpf (21.6 weeks). This was higher than the 14-week survival previously published by Hess *et al*. (2013). However, 90 % of unmanipulated mutant fish did not survive past 75 dpf. Due to the long survival observed in unmanipulated fish, it was difficult to assess the extent to which transplantation enhanced the survival of *cmyb* mutant fish. The data shows that transplantation of *Runx*:mCherry ^{high} cells, either from the WKM or gill, did not result in a statistically significant increase in the survival of *cmyb* mutant fish. However, *Runx*:mCherry ^{low} cells were able to rescue some fish and increase the survival of many. This increase in survival was statistically significant and fell below the Bonferonni-adjusted significance threshold for multiple comparisons of 0.0125 (P= 0.0007; Fig. 5.17B).

The percentage of surviving fish from each donor cell group that had shown signs of successful engraftment (engraftment scores ≥ 8/27) was also investigated. Of the surviving *cmyb* mutant fish that received *Runx*:mCherry ^{low} cells from the WKM, 92 % had an engraftment score of 8 or higher at 15 dpt (n=11), and by 22 and 29 dpt, 100% of surviving fish had an engraftment score of 8 or higher (n=6; Fig. 5.17C). Indeed, at 29 dpt, all surviving fish that received *Runx*:mCherry ^{low} cells had an engraftment score of 27/27 (n=6; Fig. 5.16E). Of the surviving fish that received *Runx*:mCherry ^{high} cells from the WKM, 77 % had an engraftment score over 8 (n= 10), which rose to 80 % at 22 dpt and 88 % at 29 dpt (n=7). Interestingly, there was also 1 fish (out of 20) from the gill *Runx*:mCherry donor group that also exhibited features of reconstitution with an engraftment score greater than 8 (Fig. 5.17C). Next, the percentage of

all transplanted fish for each donor cell type that held engraftment scores greater than 8 was investigated. This provided information on the likelihood of each donor cell population to engraft. Of the *cmyb* mutant fish injected with *Runx*:mCherry ^{low} donor cells, 79 % were found to have had an engraftment score ⩾ 8 at 15 dpt (n= 11). This was reduced to 67 % at 22 and 29 dpt (n=6; Fig. 5.17D) because some fish were harvested for flow cytometry analysis to assess multilineage reconstitution. These fish were included in survival analysis as right-censored values, meaning that their removal from the experiment before death had occurred was accounted for in the statistical analysis (Fig. 5.18). Of the fish transplanted with WKM-derived *Runx*:mCherry ^{high} cells, 45 % had engraftment scores over 8 at 15 dpt (n=10). This reduced to 36 % at 22dpt and 32% at 29dpt, suggesting that *Runx*:mCherry ^{high} cells were not as likely to lead to successful reconstitution of transplanted fish (Fig. 5.17D). Taken together, these data suggest that the *Runx*:mCherry ^{low}, FSC $^{med-high}$ population from the WKM had greater stem cell potential than the *Runx*:mCherry ^{high}, FSC ^{low} population. Furthermore, *cmyb* mutant fish transplanted with *Runx*:mCherry ^{low}, FSC $^{med-high}$ cells also exhibited significantly improved survival, indicating that engrafting fish are more likely to survive longer than fish that do not engraft donor cells.

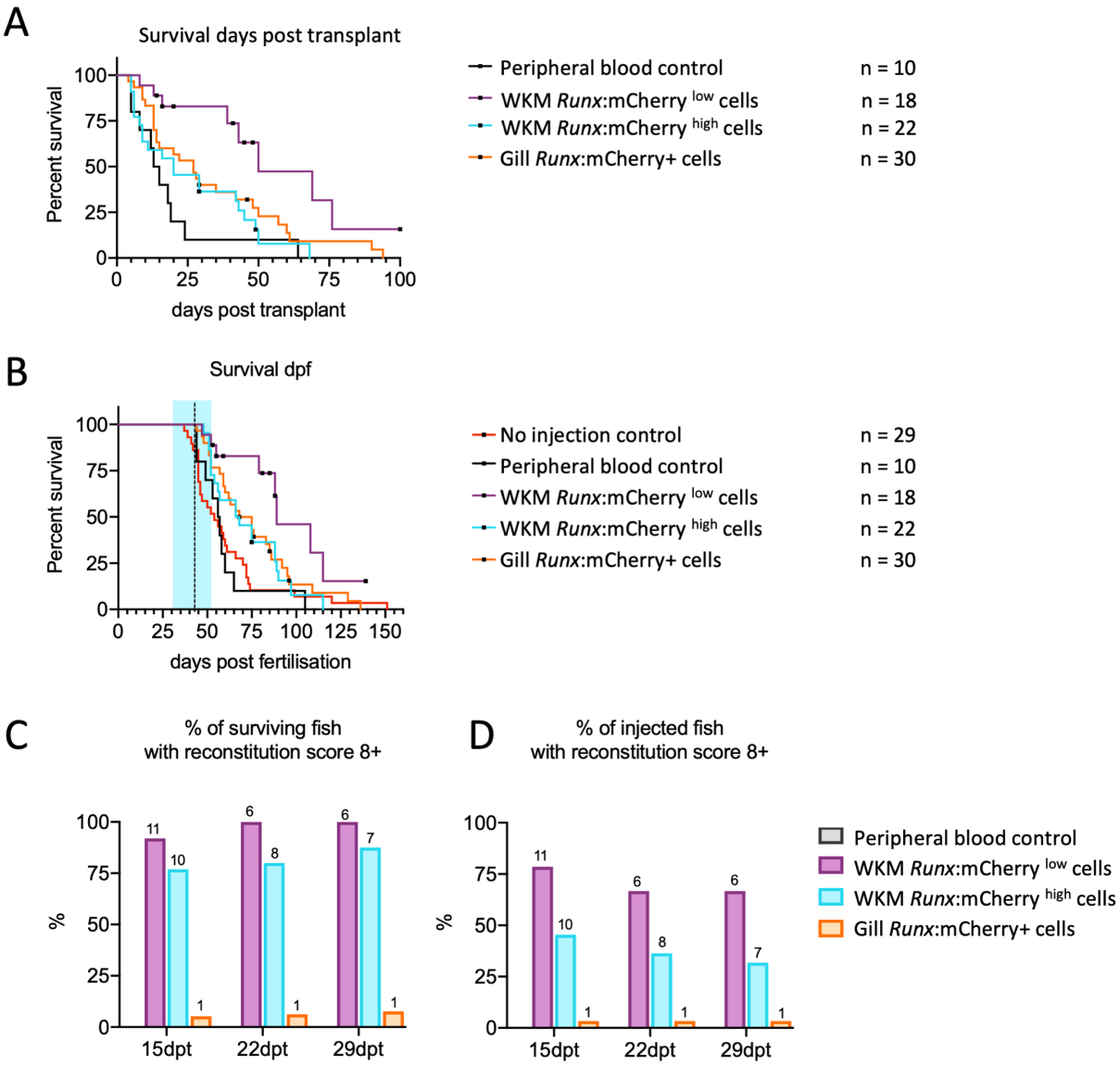

Fig. 5.17 Survival of HCT-recipient *cmyb* mutant fish.

Transplanted *cmyb* mutant fish received 2000 *Runx*:mCherry+ cells either from the gill (n=30), WKM *Runx*:mCherry ^{low} (n=18) or ^{high} populations (n=22), in addition to 10^5 PB carrier cells (n=10) at 6 wpf. Data pooled from 22 experiments. PB controls did not receive *Runx*:mCherry+ donor cells. Long-term survival of HCT recipients was assessed in dpa (**A**) and dpf where unmanipulated *cmyb* mutant fish were included (n=29) (**B**). (**B**) Vertical dotted line indicates median transplant timepoint, blue shaded area indicates minimum and maximum range of transplant days. Statistically significant differences were determined by multiple log rank tests. Significance threshold was determined using Bonferroni-corrected values. (**A**) Statistically significant differences were identified between PB control and *Runx*:mCherry ^{low} donor cells (P= 0.0003), and between *Runx*:mCherry ^{high} and ^{low} donor cells from the WKM (P=0.0016). (**B**) A statistically significant difference was identified between survival of unmanipulated *cmyb* mutant fish and *Runx*:mCherry ^{low} donor cell recipients (P= 0.0007). (**C**) The percentage of surviving fish that presented with a combined engraftment score ⩾ 8 at 15, 22 and 29 dpt. (**D**) The percentage of injected fish that presented with a combined engraftment score ⩾ 8 at 15, 22 and 29 dpt.

In addition to tracking engraftment of transplanted *cmyb* mutant fish using factors such as the abundance of cells in circulation or *Runx*:mCherry+ cells in the WKM and gill to determine the extent of hematopoietic reconstitution, multilineage reconstitution was also assessed by

flow cytometry. According to the data, recipients of *Runx*:mCherry ^{low}, FSC $^{med-high}$ cells engrafted to the greatest extent (Fig. 5.16). Therefore, recipients of these cells were harvested at 21 dpt and assessed for multilineage reconstitution in the WKM, gills and blood. Due to the small size of recipient fish, dissection was challenging. As a result, there is a possibility that tissues were contaminated with cells flowing out of the kidney or blood. Nevertheless, flow cytometry confirmed that multilineage reconstitution had occurred and all major blood cell lineages were present in the tissues of 21 dpt recipient fish, as determined by SSC/FSC plots (Fig. 5.18A) (Traver *et al*., 2003). In addition, the *Runx*:mCherry+ and *lyz*:GFP+ populations were also assessed. Interestingly, it was found that the pattern of *Runx*:mCherry expression in the WKM, gill and blood of engrafted fish was akin to that found in the adult *Tg(Runx:mCherry)* transgenic fish (Chapter 3; section 3.3.3). The WKM possessed both *Runx*:mCherry ^{high} and ^{low} cells but both the gills and blood contained predominantly *Runx*:mCherry ^{high} cells, with only a small population of *Runx*:mCherry ^{low} cells (Fig. 5.18B). Given that *Runx*:mCherry ^{low} cells were transplanted, this suggests that this population gave rise to *Runx*:mCherry ^{high} cells in recipient fish, further indicating that HSPCs may reside among this population. *lyz*:GFP+ neutrophils derived from donor cells were also detected. The distribution in the abundance of *lyz*:GFP+ cells also resembled that seen in adult transgenic fish. The WKM of recipients had a large population of *lyz*:GFP+ cells, but the abundance in the gills and the blood was lower (Fig. 5.18B).

The abundance of *Runx*:mCherry+ cells and *lyz*:GFP+ cells in 21 dpt *cmyb* mutant recipients was compared to adult *Tg(Runx:mCherry; lyz:GFP)* transgenic fish. This revealed that the percentage of *Runx*:mCherry+ cells and *lyz*:GFP+ cells in the WKM of *cmyb* mutant recipients was significantly lower than in transgenic adult fish (Fig. 5.18C & F). However, this may in part be accounted for by the considerable difference in size between adult fish and 21 dpt *cmyb* mutant recipient fish which are much smaller (approximately 1 cm in length compared to ~4-5 cm). Interestingly, the abundance of *Runx*:mCherry+ and *lyz*:GFP+ cells in the gills and blood of 21 dpt recipient fish was similar to the abundance of these cells found in adult donor fish (Fig. 5.18D, E & G). Taken together, the data suggests that the transplantation of 2000 *Runx*:mCherry ^{low} cells into *cmyb* mutant fish at 6 wpf is sufficient to lead to successful engraftment and multilineage reconstitution by 21 dpt.

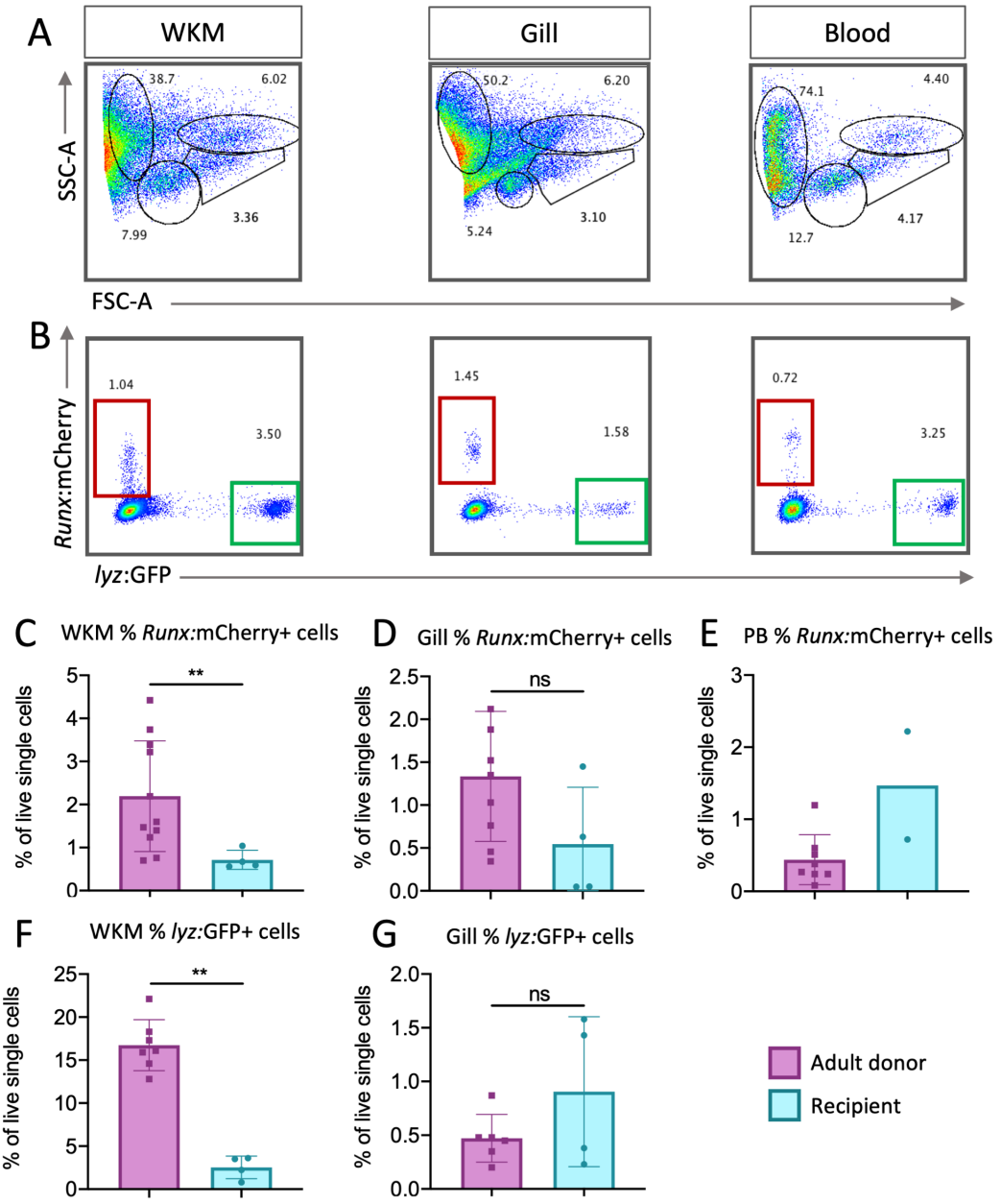

Fig. 5.18 Partial multilineage reconstitution of *cmyb* mutant fish at 21 dpt, transplanted with *Runx*:mCherry ^{low} cells isolated from the WKM of adult *Tg(Runx:mCherry; lyz:GFP)* transgenic donor zebrafish.

Four *cmyb* mutant fish transplanted with *Runx*:mCherry ^{low} cells from the WKM of adult *Tg(Runx:mCherry; lyz:GFP)* transgenic donor zebrafish were harvested at 21 dpt to assess, via flow cytometry, whether multilineage reconstitution had occurred. The WKM and gills were harvested from all 4 HCT recipients and PB samples were harvested from 2 recipients. The WKM, gills and blood were also harvested from *Tg(Runx:mCherry; lyz:GFP)* transgenic fish. (**A**) Representative FSC vs SSC plots of the WKM (left), gill (middle) and blood (right) of transplant *cmyb* mutant recipient fish, with gating of major blood cell populations as described by Traver *et al.* (2003). (**B**) mCherry/GFP plots of live single-cell populations, with gating of fluorescent populations. Red box outline indicates gating for *Runx*:mCherry+ cells, green box outline for *lyz*:GFP+ cells. Values above gates reflect the percentage of events within each gate compared to total events in the plot. (**C-E**) Comparison of *Runx*:mCherry+ cells as a proportion of the WKM (**C**), gill (**D**) and PB (**E**) between adult donor fish and engrafting recipient fish at 21 dpt. (**F-G**) Comparison *lyz*:GFP+ cells as a proportion of the WKM (**F**) and gill (**G**) between adult donor fish and engrafting recipient fish at 21 dpt. Each dot represents values from individual fish. N=4 for recipients and n=6-11 for adult transgenic donors. Data pooled from 2 experiments. Mean and SD are shown. Student's t-tests, ns: non-significant and ** P <0.01.

5.3.7 Utility of early post-transplant scoring data to predict successful engraftment and survival

Having established that engraftment of *cmyb* mutant fish can be accurately tracked utilising the scoring system described, the next aim was to model and determine whether a particular factor or combination of factors could be utilised to predict either the survival of recipient fish or the extent of engraftment that will be achieved. The importance in this lies in refinement of the HCT protocol. If engraftment and long-term survival of recipient fish can be predicted using early imaging data, this would enable fish that are not expected to survive or engraft in the long term to be humanely culled before the onset of suffering leading to the death of the individual fish. Thus, the severity of the protocol could be reduced from severe to moderate.

To determine whether post-transplant scores could predict survival of recipient fish, linear regression models were utilised. Initially, the scores from every transplant recipient, regardless of the donor cells received, were plotted against their survival in dpt. Post-transplant scoring of each factor was plotted separately. However, all imaging time points were plotted on each graph (Fig. 5.19). When fish were harvested for flow cytometry analysis, meaning long-term survival could not be assessed, their scores were not included in the linear regression. The linear regressions revealed that the scores for the cells in circulation at 8 and 10 dpt had the strongest positive correlation with survival (Fig. 5.19A). The Pearson's correlation coefficient was statistically significant at 8 and 10 dpt (P= 0.042). However, the R^2 value (indicating goodness of fit) was greater at 10 dpt (0.104) than at 8 dpt (0.086) (Fig. 5.20A-B). Interestingly, the scores relating to the abundance of *Runx*:mCherry+ cells in the WKM and gills did not have a strong correlation with the survival outcome (Fig. 5.19B-C). The only statistically significant non-zero slope identified from WKM and gill scores was at 3 dpt in the gill with a P value of 0.042 and R^2 of 0.071 (Fig. 5.20D). The correlation between the engraftment score (derived from multiplying each individual factor score together) and survival was also assessed. The engraftment score correlated well with survival and the gradients of the lines of best fit at 6, 8 and 10 dpt were found to be significantly non-zero (Fig. 5.19D). Of these, the strongest correlation was identified at 6 dpt (P=0.006, R^2 = 0.138, Fig. 5.20C).

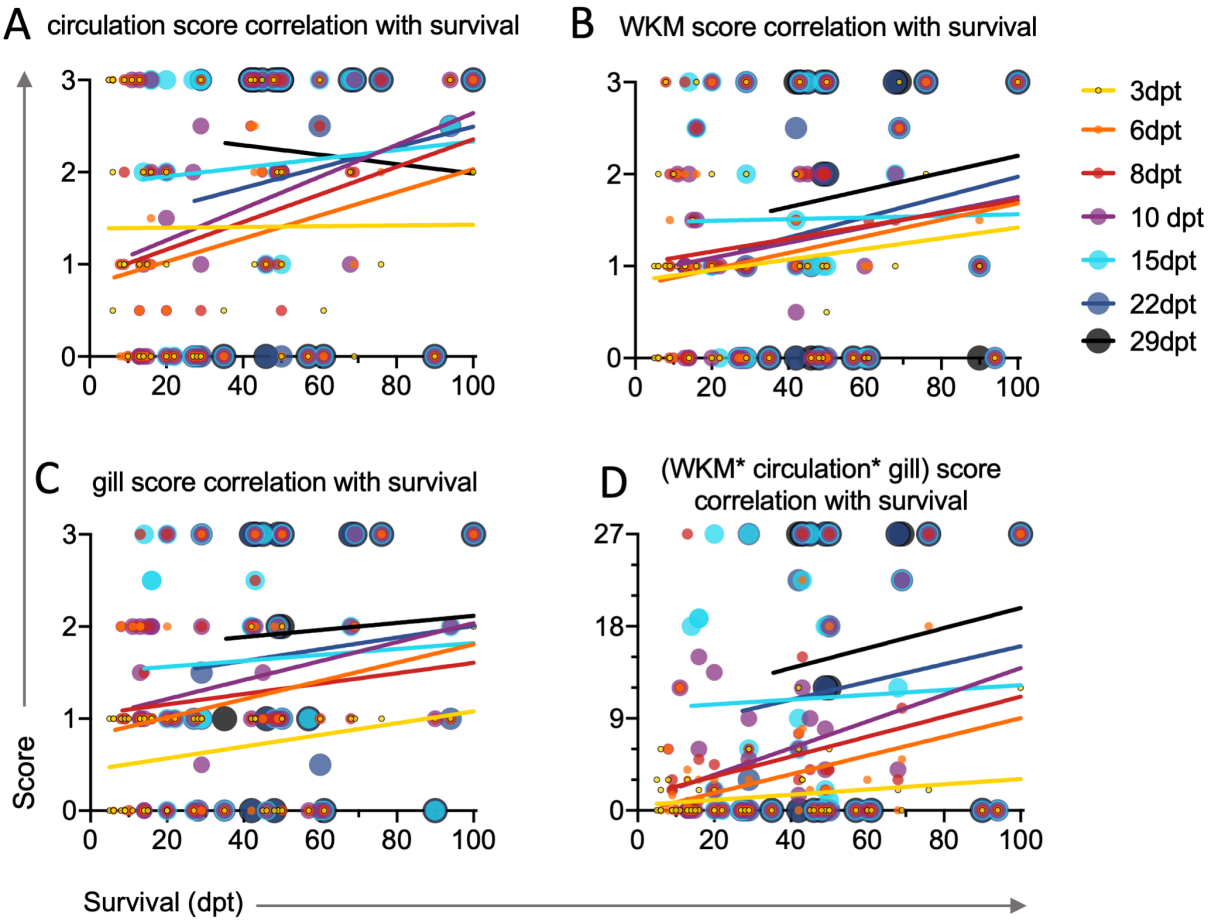

Fig. 5.19 Correlation of imaging-derived post-transplant scores from *cmyb* mutant recipients with their survival.

cmyb mutant fish were transplanted with 2000 *Runx*:mCherry+ cells from WKM *Runx*:mCherry ^{high} or ^{low} populations, or with *Runx*:mCherry+ cells from the gill of *Tg(Runx:mCherry; lyz:GFP)* donors, along with 10^5 carrier PB cells from WT fish. Recipients were imaged at 3, 6, 8, 10, 15, 22 and 29 dpt, and scored for the abundance of circulating cells in their vasculature, *Runx*:mCherry+ cells in the WKM and *Runx*:mCherry+ cells in the gills. (**A-C**) Scores for each recipient at each timepoint are correlated with the survival of that recipient. Simple linear regression has been applied for each timepoint. Each individual dot represents one fish. Data pooled from 22 experiments. Survival is plotted on the *x* axis and post-transplant scores are plotted on the *y* axis. (**A**) Correlation between circulation score and survival of recipients. (**B**) Correlation between WKM score and survival. (**C**) Correlation between gill score and survival at each timepoint. (**D**) Scores for cells in circulation, WKM and gills are multiplied together to get an overall score for engraftment. This score out of 27 is plotted against survival at each time point.

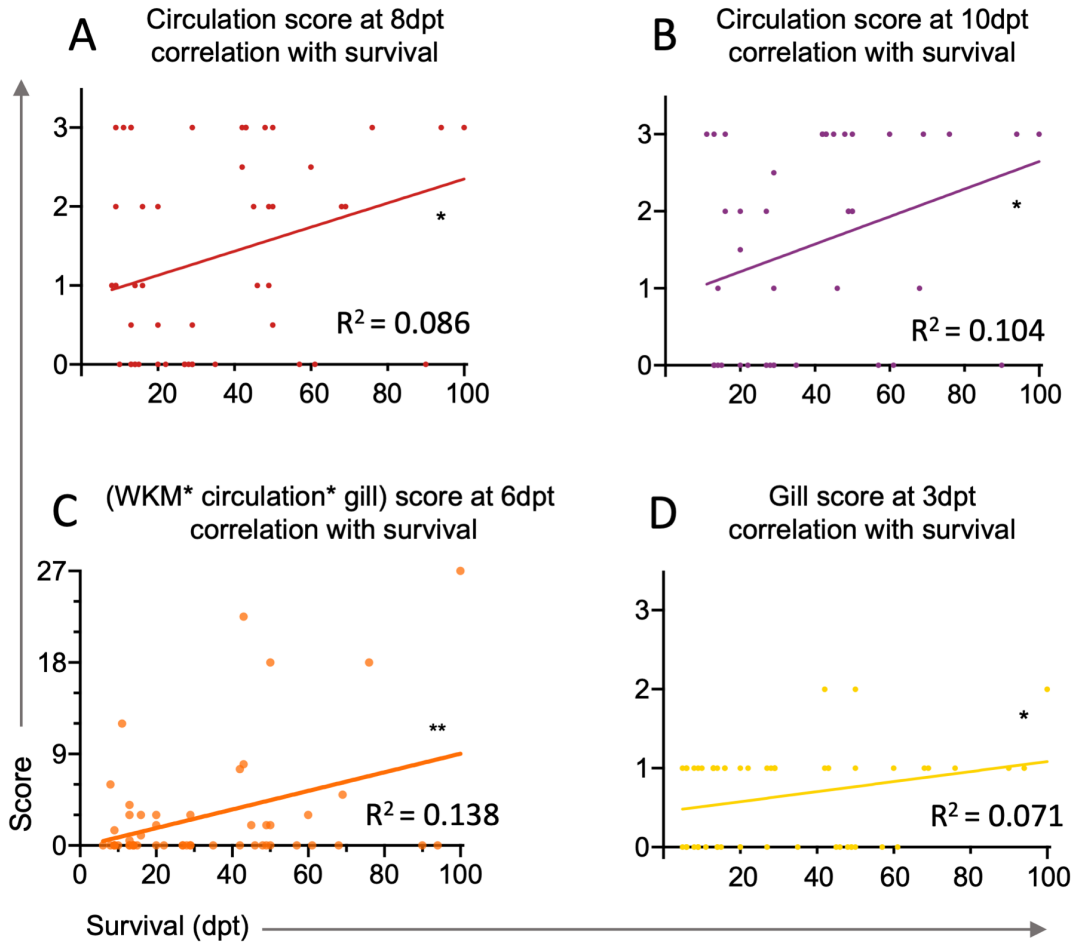

Fig. 5.20 Imaging-derived post-transplant scores from *cmyb* mutant recipients correlate with survival outcome at different timepoints for different factors.

cmyb mutant fish were transplanted with 2000 *Runx*:mCherry+ cells from WKM *Runx*:mCherry ^{high} or ^{low} populations or with *Runx*:mCherry+ cells from the gill of *Tg(Runx:mCherry; lyz:GFP)* donors, along with 10^5 PB cells from WT fish. Recipients were imaged at 3, 6, 8, 10, 15, 22 and 29 dpt, and scored for the abundance of circulating cells in their vasculature, *Runx*:mCherry+ cells in the WKM and *Runx*:mCherry+ cells in the gills. Scores for each recipient at each timepoint were correlated with the survival of that recipient (Fig. 5.19). Pearson's correlation coefficient was calculated for each timepoint and statistically significant correlations are shown. Each individual dot represents one fish. Data pooled from 22 experiments. Survival is plotted on the *x* axis and post-transplant scores are plotted on the *y* axis. (**A**-**B**) Correlation between survival and circulation score at 8 dpt (**A**) and 10 dpt (**B**). (**C**) Scores for cells in circulation, WKM and gill are multiplied together to get an overall score for engraftment. This score is plotted against survival at 6 dpt. (**D**) Correlation between gill score at 3 dpt and survival. Pearson's correlation coefficient, *P <0.05, **P< 0.01.

Next, the correlation between survival and both the sum of scores and the engraftment score was assessed for HCT recipients of WKM-derived cells specifically. This analysis, focusing specifically on recipients of WKM-derived cells which are capable of multilineage reconstitution, was carried out to determine whether the predictive capacity of the scoring system was greater when non-HSC containing donor populations were excluded. This is particularly beneficial because unmanipulated *cmyb* mutant fish can exhibit long survival (Fig. 5.17B), thus making it more difficult to assess the contribution of HCT to survival. In addition,

cells from the gills were able to increase the cells in circulation and the number of *Runx*:mCherry+ cells in the gills to a limited extent but failed to recapitulate multilineage reconstitution. Therefore, scores for these recipients may not correlate well with survival. Furthermore, as seen in Fig. 5.17B, the survival of gill *Runx*:mCherry recipient fish was similar to unmanipulated *cmyb* mutant fish.

The scores of WKM cell recipients were either added together in order to model factors that can change independent of each other or multiplied to model factors that are dependant or linked to one another. It was hypothesized that, if multilineage reconstitution occurred, the scores for each factor would be linked and interdependent. For example, if a successfully reconstituting fish had an increasing population of *Runx*:mCherry+ cells in the WKM, it was hypothesized that the abundance of *Runx*:mCherry+ cells in the gill and cells in circulation would therefore also increase. However, if the abundance of cells in circulation increases independently of cells in the gill or WKM, this may suggest lineage-biased reconstitution. It was found that scores from both the independent model (scores added together) and the dependent model (scores multiplied) had statistically significant correlation with survival at 3, 6, 8 and 10 dpt (Fig. 5.21A-B). The greatest statistical significance was at 6 dpt, suggesting that this is a key timepoint for predictions of the long-term survival outcome. These scores showed a statistically significant correlation with survival in both the independent (P=0.0074; R^2 value of 0.307; Fig. 5.21C) and dependent (P= 0.0062 and an R^2 value of 0.283 Fig. 5.21C) models. Therefore, either the addition or multiplication of the scores for circulation, *Runx*:mCherry cells in the WKM and gill at 6 dpt can be utilised as an indication for the likelihood of long-term survival.

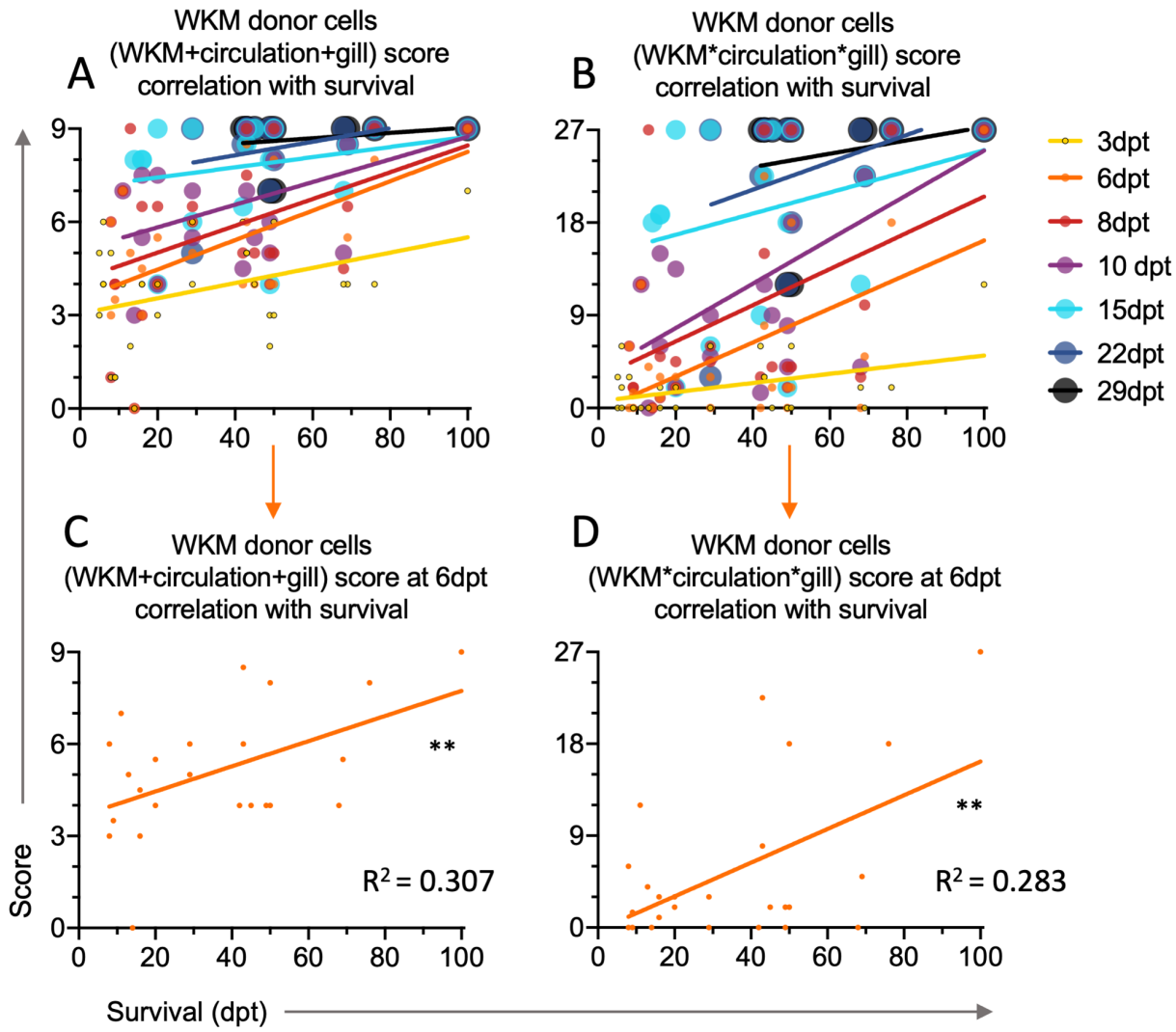

Fig. 5.21 Both dependent and independent models of interaction between post-transplant imaging factors indicate a significant correlation between extent engraftment at 6 dpt and survival outcome for recipients of WKM-derived *Runx*:mCherry+ cells.

cmyb mutant fish were transplanted with 2000 *Runx*:mCherry+ cells from WKM *Runx*:mCherry ^{high} or ^{low} populations of *Tg(Runx:mCherry; lyz:GFP)* donors along with 10^5 PB cells from WT fish. Recipients were imaged at 3, 6, 8, 10, 15, 22 and 29 dpt, and scored for the abundance of circulating cells in their vasculature, *Runx*:mCherry+ cells in the WKM and *Runx*:mCherry+ cells in the gills. Scores from each factor were either added together (**A & C**) or multiplied (**B & D**) to model independent factors as well as interactions between factors. Each individual dot represents one fish. Data pooled from 22 experiments. Survival is plotted on the *x* axis and post-transplant scores are plotted on the *y* axis. Pearson's correlation coefficient was calculated for each timepoint and statistically significant correlations were found at 6 dpt in each case (**C, D**). Pearson's correlation coefficient **P< 0.01.

Having assessed the correlation between transplant scoring and survival of *cmyb* mutant fish, the correlation between early and late engraftment scores was investigated next. This was done to determine whether initial improvements in engraftment could predict long-term engraftment of recipients. Although the final imaging time point was at 29 dpt, the 22 dpt timepoint was used for correlation with early engraftment scores to increase sample size, as

a number of recipients were harvested for flow cytometry analysis after 22 dpt. In addition, it was found that engraftment scores frequently plateaued by 22 dpt and did not increase further. Scores from *cmyb* mutant recipients of each cell type (WKM *Runx*:mCherry ^{high}, ^{low} and *Runx*:mCherry+ cells from the gills) were all included in the analysis.

Based on the results of the linear regression models comparing survival with imaging scores, the early imaging timepoints at 6, 8 and 10 dpt were selected. Correlation between the scores at these time points and the engraftment score (scores multiplied) at 22 dpt was assessed. The data revealed significant correlation between circulation scores at 8 dpt (P=0.0042, R^2=0.26) and 10 dpt (P=0.0061, R^2=0.24) with the engraftment score at 22 dpt (Fig. 5.22A). This data is consistent with the data shown in Fig. 5.20A & B, which showed that the circulation score at 8 and 10 dpt had significant correlation with survival. Indeed, the abundance of cells in circulation was one of the best predictors of survival. Interestingly, when investigating the correlation of early imaging scores with engraftment at 22 dpt, WKM and gill scores were more significant. In the WKM, scores at all three (6, 8 and 10 dpt) timepoints had a strong correlation with engraftment achieved by 22 dpt (P<0.0001 for each timepoint; R^2 =0.56-0.64; Fig. 5.22B). Similarly, the correlation of engraftment at 22 dpt with gill scores at 6, 8 and 10 dpt was also significant (P<0.0002 for each; R^2=0.41- 0.49; Fig. 5.22C). Finally, the correlation between early post-transplant engraftment scores and engraftment scores at 22 dpt was assessed. This was also found to be statistically significant with P values less than 0.0001 at 8 and 10 dpt, and P= 0.0016 at 6 dpt. The goodness of fit was greatest at 10 dpt (R^2=0.55) compared to R^2=0.3 at 6 dpt and R^2=0.46 at 8 dpt (Fig. 5.22D). Taken together, the linear regression models indicate that early post-transplant imaging scores, particularly in the WKM, can be predictive of engraftment at later timepoints.

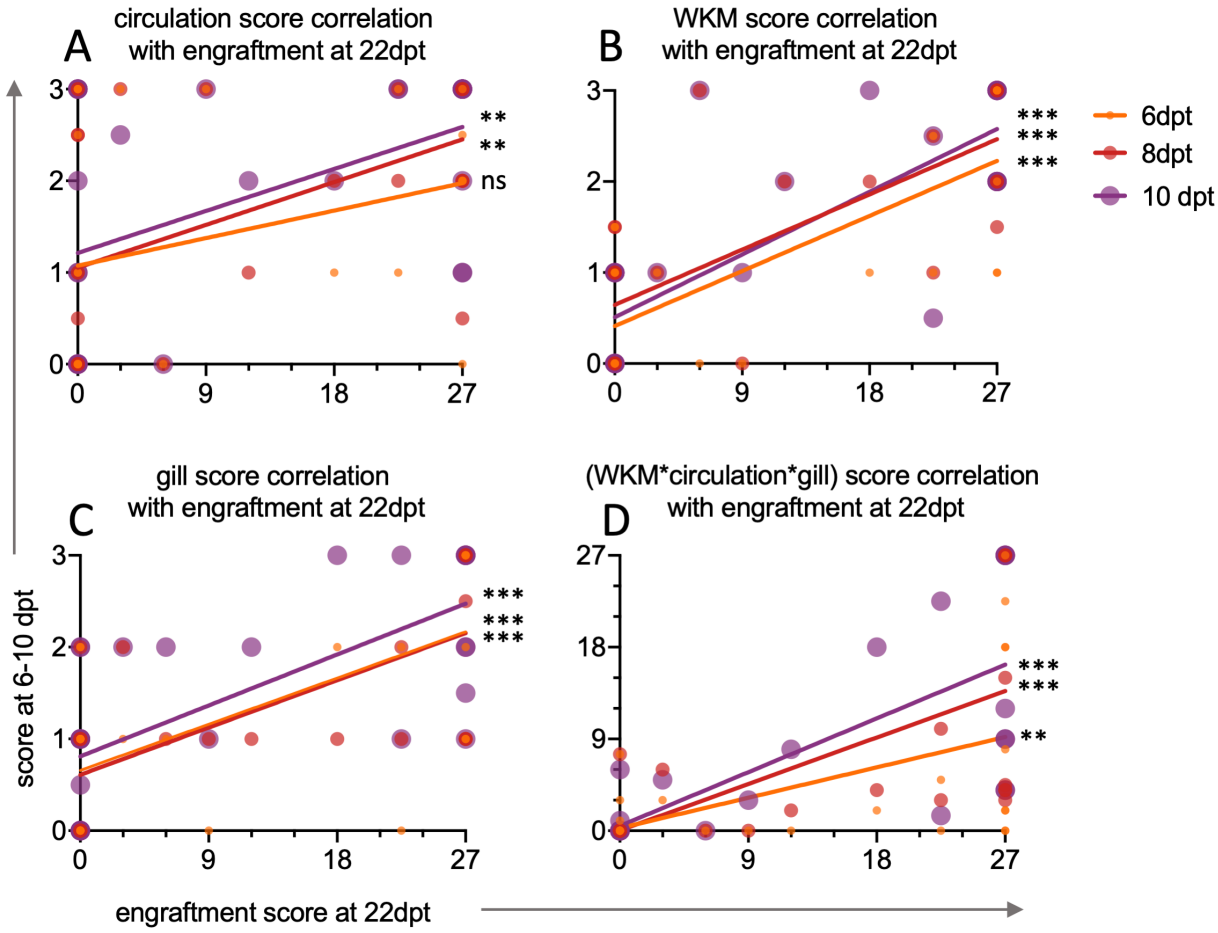

Fig. 5.22 Early post-transplant scores correlate with engraftment score at 22 dpt in *cmyb* mutant recipients.

cmyb mutant fish were transplanted with 2000 *Runx*:mCherry+ cells from the WKM *Runx*:mCherry ^{high} or ^{low} populations or with *Runx*:mCherry+ cells from the gill of *Tg(Runx:mCherry; lyz:GFP)* donors along with 10^5 PB cells from WT fish. Recipients were imaged at 3, 6, 8, 10, 15, 22 and 29 dpt, and scored for the abundance of circulating cells in their vasculature, *Runx*:mCherry+ cells in the WKM and the gills. (**A-C**) Scores from each factor (circulation (**A**), WKM (**B**) and gill (**C**)) at 6, 8 and 10 dpt were assessed for correlation with engraftment score (scores from all 3 factors multiplied together) at 22 dpt. Each individual dot represents one fish. Data pooled from 22 experiments. Engraftment score at 22 dpt is plotted on the *x* axis and scores for each factor individually are plotted on the *y* axis. (**D**) Correlation of engraftment score at 6, 8 and 10 dpt with engraftment score at 22 dpt. Pearson's correlation coefficient *P < 0.05, **P< 0.01, ***P,0.001.

5.4 Summary

One *cmyb* mutant fish positive for *mpeg1.1*:SECFP-YPet transgene was found to possess similar numbers of *mpeg1.1*:SECFP-YPet+ cells as non-mutant sibling fish at 15 dpf. However, by 6 wpf, the mutant fish had severely reduced abundance of *mpeg1.1*:SECFP-YPet+ cells compared to non-mutant sibling fish.

Six wpf *cmyb* mutant fish were capable of regeneration following tail fin amputation. Furthermore, their short-term survival was not reduced compared to control *cmyb* mutants that were not subjected to amputation. However, the regeneration of *cmyb* mutant fish was impaired compared to their non-mutant siblings.
On the other hand, following fin fold amputation of *cmyb* mutant fish at 3 dpf, no difference in neutrophil recruitment or regeneration was detected at 6 or 24 hpa compared to non-mutant sibling fish.

By assessing circulating cells in the ventral vein, *cmyb* mutant fish can be identified accurately at 6 wpf. Assessing the abundance of circulating cells prior to HCT can reduce the number of non-mutant fish transplanted inadvertently. In addition, post-transplant scoring of the cells in circulation, abundance of *Runx*:mCherry+ cells in the WKM and gill can be used to track engraftment. Furthermore, multiplying together scores from each factor can be predictive of survival at 6 dpt. However, the best predictor for long-term engraftment was found the be the score for *Runx*:mCherry+ cells in the WKM at 6 dpt.

The *Runx*:mCherry ^{low}, FSC $^{med\text{-}high}$ population in the WKM of *Tg(Runx:mCherry)* transgenic zebrafish was found to be the most effective at hematopoietic reconstitution and survival rescue of 6 wpf *cmyb* mutant fish following HCT. Furthermore, *Runx*:mCherry ^{low} donor cells from the WKM gave rise to *Runx*:mCherry ^{high} cells in the recipient fish. *cmyb* mutant fish transplanted with WKM *Runx*:mCherry ^{high} cells were capable of delayed reconstitution. However, survival outcome was not improved. Finally, gill-derived *Runx*:mCherry+ donor cells were capable of increasing cells in circulation but did not lead to full reconstitution or survival rescue.

5.5 Discussion

The aim of this chapter was to further characterise *cmyb* mutant fish and ascertain whether the *mpeg*+ macrophage-like cells can be observed after hematopoietic cells from the primitive wave of hematopoiesis are exhausted around 20 dpf. This was done with the aim of using *cmyb* mutant *Tg(mpeg1.1:SECFP-YPet)* zebrafish to study the response of *mpeg*+ cells to tail fin transection. Although this was not possible due to limited success in establishing a line of transgenic *cmyb* mutant fish, the regenerative capacity of *cmyb* mutant fish following tail fin transection was investigated.

Another section of this chapter focused on the refinement of HCT studies using *cmyb* mutant fish with the aim of reducing the number of fish transplanted as a result of error-prone screening based on macroscopic observations, which can lead to the transplantation of non-mutant fish that have not received myeloablative preconditioning. Furthermore, a qualitative scoring of post-transplant engraftment was designed to help determine the extent of donor cell engraftment in transparent *cmyb* mutant recipients. Using this scoring system, the long-term engraftment potential of different *Runx*:mCherry+ populations identified in Chapter 3 was assessed and the resulting data was used to determine whether early post-transplant scoring could be used to predict long-term survival and engraftment.

5.5.1 Presence of mpeg+ cells in cmyb mutant fish

Soza-Ried *et al.* (2010) has previously shown that reduced numbers of *l-plastin* and *spi1* expressing cells, which likely correspond to macrophages, are present in the head kidney region of *cmyb* mutant fish at 7 wpf. In agreement with Soza-Ried *et al.*, *mpeg*+ cells were identified in 15 dpf and 6 wpf *cmyb* mutants by microscopy (Fig. 5.1, 5.2). The abundance of *mpeg*+ cells in the 15 dpf *cmyb* mutant fish was qualitatively similar to the abundance of *mpeg*+ cells observed in non-mutant transgenic fish (Fig. 5.2). This suggests that at this stage, all *mpeg*+ cells present are derived from the primitive wave of hematopoiesis. Soza-Ried *et al.* described leukocytes from the primitive wave as being exhausted by 20 dpf. Therefore, it was hypothesized that *mpeg*+ cells at 15 dpf may be fewer in number in the *cmyb* mutant compared to non-mutant transgenic fish. Although, there was only one *cmyb* mutant fish positive for the *mpeg1.1*:SECFP-YPet transgene, the fact that there were similar numbers of *mpeg*+ cells in mutant and non-mutant fish suggests that these cells have a long half-life. Indeed, Xu *et*

al. previously showed in *cmyb*^{hkz3} mutant fish that at 3 wpf, embryonic microglia, derived from the primitive wave of hematopoiesis from the RBI, were still present (Xu *et al*., 2015). This was also in agreement with results from Ferrero *et al*., which found that the microglia in *cmyb* mutant fish were still RBI-derived at 21 dpf. However, Ferrero *et al*. then described the way in which adult microglia were subsequently replaced by cells derived from definitive HSCs by 3 mpf (Ferrero *et al*., 2018). This may suggest that most, if not all, macrophage-like cells in older *cmyb* mutant fish may eventually be depleted. Therefore, it was interesting to find *mpeg*+ cells in 6 wpf *cmyb* mutants. However, the significantly reduced numbers of these cells in *cmyb* mutants compared to non-mutant transgenic fish was in agreement with the findings of Ferrero *et al*. (2018), indicating that tissue-resident macrophages are replaced as zebrafish mature. It is, however, interesting to speculate whether the *mpeg*+ cells observed in 6 wpf *cmyb* mutants may correspond to the ectoderm-derived metaphocytes described by Lin *et al*. (2019). Indeed, the *mpeg*+ cells observed were likely located in the epidermis of mutant fish, as indicated by the presence of these cells in the ventral fin. If this was the case, these cells may be expected to remain in *cmyb* mutant fish long term by self-renewal mechanisms. Although Ferrero *et al*. described the replacement of microglial cells post-transplant in *cmyb* mutant fish by 3 mpf, the metaphocytes identified by Lin *et al*. appeared to have a different ectodermal origin and were found to comprise just 30% of epidermis-resident *mpeg*+ cells. Therefore, the reduction in *mpeg*+ cells in the *cmyb* mutant between 15 dpf to 6 wpf may be the result of the exhaustion of RBI-derived primitive macrophages, while ectoderm-derived metaphocytes may remain. It would be interesting to investigate this further and ascertain whether *mpeg*+ cells derived from *cmyb* mutant fish are maintained long term in HCT-rescued fish. To further investigate the composition of *mpeg*+ cells in HCT-rescued *cmyb* mutants, *mpeg1.1*:SECFP-YPet+ *cmyb* mutants could be used as recipients, and *Tg(Runx:mChery; mpeg:mCherry)* zebrafish could be used as donors. This would enable donor HSPCs to be isolated and transplanted based on their mCherry expression and FSC/SSC profiles. Subsequently, *mpeg*+ cells derived from donor *Runx*:mCherry+ HSPCs could be identified by morphology with microscopy, in addition to their FSC/SSC profile in flow cytometry (Traver *et al*., 2003).

5.5.2 Regeneration of cmyb mutant tail fin following transection

Previous research indicates that *cmyb* mutant fish cannot survive past 2-3 dpa following tail fin transection (Hess *et al*., 2013). In contrast, the results in this chapter have shown that when *cmyb* mutant fish are maintained in E2 medium with PS, tail transection does not impact the short-term survival of *cmyb* mutant fish compared to un-manipulated *cmyb* mutants (Fig. 5.3C). In addition, maintaining *cmyb* mutants in this medium, regularly replacing the medium approximately 20 minutes after feeding and regularly cleaning the tanks also appears to have increased their maximum survival from the previously reported 14 wpf (Hess *et al*., 2013) to over 21 wpf (Fig. 5.3C). This suggests that, with a more intensive care routine and the use of E2 medium with antibiotics, it is possible to maintain a healthier population of *cmyb* mutants. This is likely to improve the outcome of any intervention for these highly susceptible bloodless fish and, therefore, this refinement in care routine could also reduce the suffering experienced by *cmyb* mutants.

In addition to improved survival, it was also found that *cmyb* mutant fish were capable of regenerating their tail fin tissue following amputation at 6 wpf (Fig. 5.3B). At this stage, *cmyb* mutants are depleted of circulating erythrocytes, monocytes and neutrophils in their vasculature (Soza- Ried *et al*., 2010). However, as discussed earlier, they have a small population of remaining *mpeg*+ cells in the head kidney, thymus (Soza- Ried *et al*., 2010) and skin (Fig. 5.1). Despite the absence of neutrophils in these mutants, they appeared capable of responding to injury and initiating regeneration. This finding is in agreement with data from Li *et al*. which evidenced that neutrophils are dispensable in zebrafish fin fold regeneration, whereas macrophages play a key role and accelerate epimorphic regeneration (Li *et al*., 2012). In the scope of this thesis, it could not be determined whether the *mpeg*+ cells that reside in 6 wpf *cmyb* mutants were remaining long-lived cells or self-renewing macrophage-like cells that either arose during primitive hematopoiesis or were ectoderm-derived methaphocytes (Lin *et al*., 2012). However, remaining *mpeg*+ cells may be involved in the process of tissue regeneration. It is possible that those *mpeg*+ cells that are present in these fish may be recruited to the amputation site by DAMPs, such as hydrogen peroxide, released at the site of injury (Niethammer *et al*., 2009). Although *cmyb* mutant fish were capable of partial regeneration, it is clear that both the rate of tissue regeneration and the total area of regeneration was significantly reduced in *cmyb* mutant fish compared to their non-mutant

siblings (Fig. 5.4). Li *et al*. also found that fin fold regeneration in embryos can occur with delayed dynamics and impaired regeneration in the absence of macrophages, as shown through the use of *irf8* morphants to knockdown macrophages (Li *et al*., 2012). The reduced rate of regeneration is likely related to the absence of hematopoietic cells, including M1- and M2-type macrophages, which are involved in the removal of debris and pathogens (M1) and the stimulation of blastemal cell proliferation (M2) (Nguyen-Chi *et al*., 2015). In agreement with the results obtained by Nguyen-Chi *et al.* following M2 macrophage depletion, *cmyb* mutant fish also exhibited impaired fin fold regeneration. The phenotype of disorganised tail fin regeneration was also reported by Petrie *et al*. following tail fin amputation of adult *Tg(mpeg:NTR-eYGP)* transgenic zebrafish treated with MTZ to deplete macrophages (Petrie *et al*., 2015). To further investigate regeneration in *cmyb* mutant fish, it would be interesting to carry out tail fin injury assays in *cmyb* mutants carrying an *mpeg1.1*:SECFP-YPet transgene. This would enable the visualisation of the response of *mpeg*+ cells to injury *in vivo*. Furthermore, it is not known what type of *mpeg*+ cells are present in *cmyb* mutants, whether they are external antigen-sensing methaphocytes, tissue-resident Langerhans cells, classically-activated M1 macrophages or anti-inflammatory M2 macrophages. Crossing *Tg(mpeg1:mCherry-F; tnfα:eGFP-F)* zebrafish to *cmyb* mutants would allow an investigation of whether M1- and M2-type macrophages can be identified in *cmyb* mutants (Nguyen-Chi *et al*., 2015).

In contrast to the observations made about tail fin regeneration in 6 wpf *cmyb* mutants, embryonic mutants at 3 dpf were capable of full fin fold regeneration that was indistinguishable from non-mutant sibling fish both in terms of area regenerated and neutrophil infiltration to the injury site. This was expected because the *cmyb* mutation inhibits the initiation of the definitive wave of hematopoiesis when HSCs are formed, while the primitive wave of hematopoiesis is unaffected by the mutation (Soza-Ried *et al*., 2010). As such, 3 dpf *cmyb* mutant embryos are indistinguishable from their non-mutant siblings until the cells of the primitive wave are depleted. Hence, it was hypothesized that their response to injury and regenerative capacity would remain un-impaired at this stage. This is in contrast to observations made in *cloche* mutants which have a primitive hematopoietic defect. In *cloche* mutants, partial regeneration does still occur but is impaired, as evidenced by a significant

reduction in the total area regenerated (Hasegawa *et al*., 2015). This reduction in regeneration was linked to increased cell death in the tail and reduced blastema proliferation.

5.5.3 Refined identification of cmyb mutants

As tail fin transection for *cmyb* mutant fish was reportedly lethal (Hess *et al*., 2013), this method was not utilised to obtain genetic material to carry out genotyping of mutant fish. Instead, phenotypic identification was most commonly carried out to identify *cmyb* mutants for use in experiments, including HCT. Subsequently, once the experiments were concluded, tail fin tissue was utilised to confirm the genotype of fish (McBrien, 2017). This method led to a number of WT or heterozygous animals being subjected to HCT in the absence of myeloablative preconditioning. The number of non-mutant fish transplanted, or being used for studies of *cmyb* mutant phenotype, can be reduced by carrying out BF microscopy to assess circulating cells in the vasculature. This method was found to be highly reliable and time efficient as it was possible to carry out screening in a matter of seconds, directly before commencing with the HCT procedure (Fig. 5.6), thus negating the need for additional anaesthesia. If applied more widely by the laboratories interested in studying *cmyb* mutants, particularly if this were to expand, it could be very beneficial to new researchers to ensure that *cmyb* mutants are correctly identified prior to their utilisation in experiments. Throughout the course of this thesis, it is estimated that approximately 28 non-mutant fish were removed from *cmyb* mutant experimental groups as a result of this assessment method. Given the intensive nature of these experiments for both the recipient fish and the experimenter, I believe this is a significant refinement to the procedure.

5.5.4 cmyb HCT refinements and scoring

Upon refining the identification of *cmyb* mutant fish at 6 wpf, the next aim was to develop a post-transplant scoring system based on a combination of donor-derived fluorescent cells and the presence of cells in circulation. Classically, tetramethylrhodamine (TRITC)-conjugated dextran has been utilised to assess the success of the transplantation procedure. Conjugated fluorescent dextran labels the vasculature by binding endothelial cells and erythrocytes. Therefore, when it enters circulation (along with donor cells) following a successful injection, the entire vasculature becomes visible when viewed under a fluorescent microscope (Pugach *et al*., 2010). However, due to the long half-life of TRITC-conjugated dextran, it was found to

interfere with imaging of fluorescent cells in transparent HCT recipients (McBrien, 2017). Therefore, dextran-TRITC was not applied in HCT experiments. However, as part of the HCT protocol, the FACS-isolated cells are transplanted with PB carrier cells (LeBlanc *et al*., 2007). For the experiments presented in this thesis, 10^5 PB cells were injected along with donor cells in each HCT. Due to the small size of recipient *cmyb* mutant fish (maximum 1 cm in length), and the complete absence of circulating cells prior to transplantation, this quantity of PB cells is visible in the vasculature of recipient fish immediately following injection. This provided the opportunity to assess the success of the injection procedure based on the presence or absence of circulating cells. This could be assessed directly following injection and without taking the fish out of anaesthesia, making it minimally disruptive to the fish. Furthermore, it was possible to utilise the abundance of circulating cells as a readout for engraftment by longitudinal imaging of the same fish (Fig. 5.11). Any detectable increase in the abundance of circulating cells over time indicated the engraftment of cells and subsequent proliferation and differentiation into erythrocytes. Despite challenges in quantitative enumeration of circulating cells, the qualitative scoring has made it possible to determine the extent to which the vasculature is populated by circulating cells over time (Fig. 5.7, 5.11). However, utilisation of cells in circulation alone as a score for engraftment could be misleading as it could falsely indicate engraftment of cells that do not have long-term multilineage reconstitution ability. For example, erythroid-primed HSPCs found among the *Runx*:GFP+ population may increase cells in circulation but not lead to successful multilineage reconstitution (Tang *et al*., 2017). As such, other readouts for engraftment, such as qualitative assessments of abundance of *Runx*:mCherry+ cells in the head kidney and gill, were also applied. The head kidney was chosen as this was one of the early sites in which engrafting HSPCs were found (McBrien, 2017). Furthermore, based on experience, it was found that successfully engrafted HCT-recipient fish consistently had *Runx*:mCherry+ cells in the head kidney. In addition, the head kidney provided a practical location for imaging and the majority of the head kidney was in view within a single image acquisition (Fig. 5.9), thereby minimising the size of data accumulated. The abundance of *Runx*:mCherry+ cells in the gill was also utilised for scoring due to the high number of *Runx*:mCherry+ cells seen during steady-state conditions in *Tg(Runx:mCherry)* transgenic gills (Chapter 3). The results from this suggested that if *Runx*:mCherry+ cells in the gills were HSC-derived, they would also appear in the gill post-

transplant. This was indeed found to be the case and the first *Runx*:mCherry+ cells were frequently observed in the gills by 6 dpt (Fig. 5.13).

In terms of post-transplant sequence of events, it appears that in fish exhibiting successful reconstitution, the head kidney and vasculature were the first to be populated, by 3 dpt, with *Runx*:mCherry+ cells and circulating cells respectively. This suggests that engraftment of *Runx*:mCherry+ cells, differentiation and proliferation of HSPCs occurs before 3 dpt. However, the increase in *Runx*:mCherry+ cells in the gill took longer to manifest. This suggests that the cells in the gill were derived from WKM *Runx*:mCherry+ cells, but may represent a different cell type which takes longer to reconstitute post-transplant.

5.5.5 Identifying the Runx:mCherry+ cell population capable of long-term multilineage reconstitution

By applying the post-transplant scoring system described above and investigating how cells in circulation and *Runx*:mCherry+ cells in the WKM and gill change over time, it was found that WKM-derived *Runx*:mCherry ^{low}, FSC $^{mid\text{-}high}$ cells possessed the greatest long-term multilineage reconstituting potential in *cmyb* mutants imaged until 29 dpt. This was determined by the observation that this population of cells was capable of rapidly increasing cell abundance in all three scored locations in *cmyb* mutant recipients and consistently maintained high scores in each until the final imaging time point at 29 dpt (Fig. 5.15). Recipients of *Runx*:mCherry ^{low}, FSC $^{mid\text{-}high}$ cells had achieved multilineage reconstitution, as assessed by flow cytometry, at 21 dpt. These recipients possessed cells from each of the major blood cell populations in the WKM, gill and PB, in addition to the presence of *Runx*:mCherry ^{high}, *Runx*:mCherry ^{low} and *lyz:*GFP+ cells (Fig.5.18). Additionally, long-term survival was only increased significantly when transplanting this donor cell population (Fig. 5.17). When WKM-derived *Runx*:mCherry ^{high}, FSC ^{low} cells were transplanted, the average post-transplant scores for cells in circulation reached a score of 3 by 15 dpt, compared to 10 dpt with *Runx*:mCherry ^{low}, FSC $^{mid\text{-}high}$ cells. Although the initial score at 3 dpt was, on average, greater in recipients of *Runx*:mCherry ^{high}, FSC ^{low} cells, this may have been a reflection of the number of cells that entered circulation directly from the injection of donor- and PB-carrier cells. It is possible that a lower cell dose may have been injected in recipients of *Runx*:mCherry ^{low}, FSC $^{mid\text{-}high}$ cells. If this was the case, it would indicate that this population of cells had even greater

reconstituting potential. In addition, transplanted *Runx*:mCherry ^{high}, FSC ^{low} cells were not able to increase the abundance of *Runx*:mCherry+ cells in the WKM or gills to the same extent as *Runx*:mCherry ^{low}, FSC $^{mid-high}$ donor cells (Fig. 5.15). This further supports the hypothesis that *Runx*:mCherry ^{low}, FSC $^{mid-high}$ cells have greater HSC purity. The qRT-PCR data from Chapter 3 also showed that *Runx*:mCherry ^{low}, FSC $^{mid-high}$ cells had higher transcript levels of the key HSC-associated genes *cmyb* and *ckit*.

Furthermore, following the conclusion of all experiments reported in this thesis, it was reported by Kobayashi *et al*. that the combination of 2 transgenic markers, *Runx*:mCherry and *Gata2a*:GFP in *Tg(Runx:mCherry; Gata2a:GFP)* transgenic zebrafish, to sort HSCs significantly increased long-term multilineage reconstitution potential compared to the isolation of single-positive *Runx*:mCherry+ cells (Kobayashi *et al*., 2019). Interestingly, *Runx*:mCherry+ *Gata2a*:GFP+ double-positive cells were also SSC ^{low}, FSC ^{med}, similar to the *Runx*:mCherry ^{low}, FSC $^{med-high}$ population identified in this thesis. Therefore, it is possible that *Runx*:mCherry ^{low}, FSC $^{med-high}$ cells have an increased HSC purity. However, the *Runx*:mCherry ^{low} population identified in this thesis cannot be considered directly equivalent to *Runx*:mCherry+ *Gata2a*:GFP+ double-positive cells as the selection parameters are not equivalent. Furthermore, there are *Runx*:mCherry ^{high} cells that fall within the FSC ^{med} precursor gate. The finding that HSC-enriched *Runx*:mCherry+ *Gata2a*:GFP+ double-positive cells were found within the SSC ^{low}, FSC ^{med} gate is in contrast to the earlier, and widely accepted, hypothesis that zebrafish HSCs reside in the SSC ^{low}, FSC ^{low} lymphocyte compartment, as reported by Traver *et al.* (2003). Furthermore, the data in this chapter indicates that *Runx*:mCherry ^{high}, FSC ^{low} cells may have lower reconstitution potential than the *Runx*:mCherry ^{low}, FSC $^{med-high}$ population of cells when transplanted into *cmyb* mutant fish. This is further supported by results from Kobayashi *et al*. which demonstrated a complete absence of long-term reconstitution potential by *Runx*:mCherry+ *Gata2a*:GFP- cells at 16 wpt. The work by Kobayashi *et al.* also indicated that the *Runx*:mCherry+ *Gata2a*:GFP- population is biased towards erythroid, myeloid and thrombocyte lineages. This may explain why the *Runx*:mCherry ^{high}, FSC ^{low} population was capable of reconstitution, with delayed dynamics, and why cells in circulation may have transiently increased when gill-derived *Runx*:mCherry ^{high} cells were transplanted. Further support for this hypothesis comes from the identification of erythroid-primed HSPCs among *Runx*:GFP+ cells (Tang *et al*., 2017) and, as demonstrated

in Chapter 3, there is almost 100 % overlap between *Runx*:GFP+ and *Runx*:mCherry ^{high} cells in adult zebrafish. Finally, when discussing engraftment and reconstitution from *Runx*:mCherry ^{high} cells sorted from gill tissue, it must be noted that cells in circulation cannot be eliminated from the gill tissue, which is by its nature highly vascularised. Therefore, any engraftment or resultant proliferation could also have come from *Runx*:mCherry ^{high} cells in circulation. This may explain the single *cmyb* mutant recipient that exhibited signs of successful reconstitution following HCT of gill-derived donor cells (Fig. 5.17C).

Furthermore, the results of this chapter support the use of an engraftment score, calculated either by addition or multiplication of scores together from each of the categories of cells in circulation, *Runx*:mCherry+ cells in the head WKM and in the gill, to provide a valuable readout for overall engraftment.

5.5.6 Application of early post-transplant scoring data to predict engraftment and survival

One of the aims of this chapter was to assess whether imaging data could be utilised to accurately predict long-term survival and engraftment. This section builds upon work by McBrien (2017) who identified 6 dpt as an important post-transplant time point to assess the extent of engraftment. In her work, McBrien was not able to identify a statistically significant correlation between survival and either the number of *CD41*:GFP+ or *lyz*:dsRed+ cells in the head kidney. However, the author described a trend suggesting that the number of each cell type in the head kidney at 6 dpt may correlate with survival. The HCT experiments presented by McBrien were of non-mutant fish that received sub-lethal IR preconditioning. Therefore, it is possible that host immune reconstitution contributed to survival, even when only a small number of *CD41*:GFP+ cells appeared to have engrafted in the head kidney. Furthermore, donors and recipients were not immune-matched. Therefore, immune rejection by the host cells was also a potential confounding factor.

In contrast, the work presented in this thesis was carried out using *cmyb* mutant fish, incapable of initiating definitive hematopoiesis (Soza-Ried *et al*., 2010). Consequently, host cell reconstitution cannot occur, and steady-state survival is limited to approximately 14 wpf (Hess *et al*., 2013). Therefore, the effect of donor cells on survival could be measured more accurately as donor cells are required for long-term survival of *cmyb* mutant fish. A positive

correlation between the number of engrafted cells and survival of recipient fish is expected. To investigate this, the score from each factor was correlated with survival, as was a combined engraftment score derived by multiplying together the scores from each individual factor. The overall engraftment score was determined in this way because if any factor scored 0, then successful multilineage reconstitution could not have occurred.

In agreement with the data reported by McBrien (2017), the results of this chapter also suggest that 6 dpt is an important time point to predict survival of HCT recipients. When considering every HCT carried out, regardless of the donor cell population, the most significant correlation was found at 6 dpt using the engraftment score (WKM*circulation*gill; Fig. 5.20). However, when gill-derived donor cell HCT recipients were excluded from the linear regression models, on the basis that these did not lead to multilineage engraftment, it was found that both addition of each score and multiplication of scores lead to statistically significant correlation with survival at 6 dpt (Fig. 5.21). Importantly, the early post-transplant scores correlated not only with survival but also with engraftment at later time points, indicating that early signs of engraftment can be predictive of longer-term engraftment and survival. In this regard, the score for *Runx*:mCherry+ cells in the head kidney between 6-10 dpt was particularly informative and exhibited the most significant correlation with the engraftment score at 22 dpt. Having identified 6 dpt as a key timepoint both in terms of predicting survival and engraftment, all subsequent imaging time points could potentially be eliminated in future studies. This would further refine the procedure as imaging is conducted under anaesthesia and is therefore associated with additional stress and potential suffering for the fish. By imaging at 6 dpt and investigating each factor individually, survival and long-term engraftment can be predicted. Therefore, fish without engraftment may be removed from experimental groups using a humane end point, thus reducing the severity of the protocol from severe to moderate.

Chapter 6

Final Discussion

Chapter 6 | Final Discussion

6.1 Significance and key findings

Zebrafish provide a novel opportunity to investigate factors that impact HCT outcome and HSC biology. Despite significant differences in the HSC niche between the WKM in teleost and BM in mammals, there are many similarities among the factors that govern hematopoiesis between teleost and mammals. Studying the WKM and HSCs in an HCT setting provides a unique opportunity to uncover universal and conserved factors regulating HSC maintenance, self-renewal, homeostasis and differentiation in vertebrates. The accurate and reliable identification of HSCs is key to enable the study of their properties. In this thesis, I sought to further characterise, evaluate and refine the HCT model to enable the study of the WKM niche and HSCs in the zebrafish. To this end, I dissected and investigated the fluorescent cell populations identified in *Tg(Runx:mCherry)* transgenic donors, assessed their functional responses to immune stimuli and their ability to reconstitute bloodless recipients. The utility of *cmyb* mutant fish to investigate non cell-autonomous factors of HSC engraftment was also assessed by evaluating steady-state conditions and response to injury and inflammation.

In **Chapter 3**, a combination of microscopy, flow cytometry and gene transcription analysis techniques were applied to investigate the fluorescent protein-expressing cells in the *Tg(Runx:mCherry)* transgenic line and, subsequently, also in the *Tg(Runx:GFP)* line. Microscopy revealed that *Runx*+ cells arise in the gill around 21 dpf and that the distribution of these cells is similar to that of *CD41*:GFP+ cells. Flow cytometry revealed that, in the WKM, *runx*:mCherry+ cells can be subdivided into *Runx*:mCherry ^{high} and *Runx*:mCherry ^{low} populations, and that these possess differential FSC/SSC properties. Furthermore, it was found that *Runx*:GFP+ cells overlap almost entirely and exclusively with *Runx*:mCherry ^{high} but not *Runx*:mCherry ^{low} cells. Finally, gene transcription analysis indicated that the *Runx*:mCherry ^{low}, FSC $^{med-high}$ population had higher transcript levels of the HSC markers *cmyb* and *ckit* than *Runx*:mCherry ^{high}, FSC ^{low} cells, which were previously described as the HSPC-containing compartment (Tamplin *et al*., 2015).

In **Chapter 4**, the functional characteristics of *Runx*:mCherry+ populations were assessed through antibiotic treatment and immune stimulation with the viral mimetics poly I:C and

R848. As a result of OTC antibiotic treatment, a small reduction in the abundance of *Runx*:mCherry ^{low} cells was detected in the WKM. The cytokine response to poly I:C was not attenuated by the antibiotic treatment. On the other hand, topical application of R848 to the gills may lead to a small increase in the abundance of *Runx*:mCherry+ cells in the gills at both 3 and 8 hpt. However, as this small change in *Runx*:mCherry+ cells in the gills was detected by confocal microscopy following immune-staining, it was not possible to determine the native fluorescence intensity of the cells. Therefore, it is unknown whether *Runx*:mCherry ^{high} or *Runx*:mCherry ^{low} cells increased in the gills. Finally, R848 treatment increased transcript levels of type I IFNs in *cmyb* mutant fish, which also possessed detectable levels of *mpeg* and *lyz* transcripts.

In **Chapter 5**, the *cmyb* mutant fish were further characterised and utilised for regenerative and HCT studies. Microscopy of transgenic mutant fish revealed that a small number of *mpeg*+ macrophage-like cells were present in 6 wpf *cmyb* mutant fish. This is in agreement with previous work indicating the presence of myeloid but not lymphoid cells in *cmyb* mutant fish (Soza-ried *et al*.,2010). Interestingly, it was found that, in contrast to previous studies (Hess *et al*., 2013), 6 wpf *cmyb* mutant fish were capable of tail fin regeneration following amputation, and their short term survival was not adversely affected by amputation. HCT studies revealed that *Runx*:mCherry ^{low}, FSC ^{high} cells have the greatest multilineage reconstitution potential and improved the survival outcome of *cmyb* mutant transplant recipients. Finally, this chapter built on the work of McBrien (2017) to develop post-transplant scoring to enable the prediction of survival outcome and the extent of engraftment. It was found that multiplication of the scores for the cells in circulation, fluorescent cells in the WKM and in the gills resulted in the most accurate early predictor of survival outcome. However, for longer term engraftment, the most accurate early predictor was found to be the score for *Runx*:mCherry+ cells in the WKM.

6.2 Conclusions and future work

6.2.1 Identification of the cell populations present within the Runx:mCherry+ fraction in the adult zebrafish

Taking together flow cytometry data, transcription analysis and HCT assays, the results in this thesis indicate that isolation of *Runx*:mCherry ^{low}, FSC ^{high} cells from the WKM results in a

population of cells with significant hematopoietic reconstitution potential. Isolating these cells from the total *Runx*:mCherry+ population appears to lead to a greater purity of HSCs, at least in terms of their ability to reconstitute *cmyb*$^{-/-}$ mutants. This is beneficial as it does not require an additional transgenic marker to increase HSC concentration (Kobayashi *et al*., 2019). However, the stem cell purity of the *Runx*:mCherry ^{low}, FSC $^{med-high}$ population has not been quantitatively assessed by either competitive transplantation or limiting dilution assays and, therefore, cannot be directly compared to either the *Runx*+ *gata2a*+ cell population described by Kobayashi *et al.* (2019) or the whole *Runx*:mCherry+ population as assessed by Tamplin *et al.* (2015). Nevertheless, this work has shown that in the *cmyb* mutant recipient transplant model, the *Runx*:mCherry ^{high} FSC ^{low} population was less efficient at achieving multilineage reconstitution and increasing survival of *cmyb* mutant fish. Furthermore, the *Runx*:GFP+ population overlapped almost entirely with the *Runx*:mCherry ^{high} population. Taken together, this suggests that *Runx*:GFP+ FSC ^{low} cells may also possess reduced capability of multilineage reconstitution in *cmyb* mutant recipients, compared to the *Runx*:mCherry ^{low}, FSC ^{high} population. However, this does not exclude the ability of *Runx*:GFP+ cells to reconstitute *cmyb* mutant fish, as WKM-derived *Runx*:mCherry ^{high} donor cells were able to contribute to hematopoiesis in the recipients (Fig.5.16). In addition, Tamplin *et al.* (2015) also demonstrated the long-term multilineage reconstitution potential present within the *Runx*:GFP+ population when transplanted into embryos. This may indicate that the reconstitution potential of the populations identified in this project differ depending on the recipients. For example, transplantation into *cmyb*$^{-/-}$ mutant fish may have different engraftment dynamics compared to transplantation into embryos or irradiated WT adult fish. Nevertheless, the ability of WKM-derived *Runx*:mCherry ^{high} donor cells and, hence, most likely also *Runx*:GFP+ cells, to contribute to multilineage reconstitution in *cmyb* mutant recipients suggests that these equivalent populations could be used for competitive transplant assays as previously suggested by McBrien (2017). This would make it possible to investigate the effect of immune stimulation or antibiotic treatment on HSC stem cell fitness with an internal control. As a result, fewer animals would be used in HCT assays, and simultaneously the statistical power of experiments would be greater. Indeed, similar experiments have been carried out in zebrafish using WKM from *Tg(β-actin:GFP)* and *RedGlo(DsRed2)* donors (Li *et al.,* 2015).

6.2.2 Identification of Runx:mCherry ^{high} cells in the gills of adult zebrafish

The identification of *Runx*:mCherry+ cells in the gills is a particularly interesting and unexpected finding. Tamplin *et al.* describe *Runx*:mCherry+ cells as a population specifically enriched for HSPCs. As such, it was expected that fluorescent *Runx*:mCherry+ cells would reside predominantly in the WKM of adult zebrafish, in addition to a population in circulation. Therefore, the finding that a significant population of *Runx*:mCherry+ cells reside within the adult gill was unexpected. One possibility is that *Runx*:mCherry+ cells label terminally differentiated cells of hematopoietic lineage in the gills. Alternatively, HSPCs may be recruited to the gill tissue specifically. If this is the case, this would indicate that there is an extramedullary HSPC niche in the adult zebrafish gill. Recently, it has been shown that mouse lungs host extramedullary hematopoiesis (EMH) in the lung during steady state conditions (Lefrançais *et al.,* 2017). The authors found that 50% of platelet production occurred in the lung. Thus, the lungs appear to be a site for lineage-biased EMH. Indeed, lineage-biased HSPCs appear to be regulated by distinct niches (Pinho *et al.,* 2018). Extraordinarily, Lefrançais *et al.* also found that the lung maintained a reservoir of HSPCs. These HSPCs from the mouse lung were capable of migrating out of the lung to reconstitute multilineage hematopoiesis in the BM under conditions of thrombocytopenia and stem cell deficiency (Lefrançais *et al.*, 2017). The possibility that there may be evolutionary conservation between the function of the lung and the gill with regards to hematopoietic potential merits further investigation. It is unlikely that the *Runx*:mCherry+ cells in the gill are of a non-hematopoietic lineage as WKM-derived *Runx*:mCherry+ cells gave rise to *Runx*:mCherry+ cells in the gill post-transplant (Fig. 5.15A & B). While HSPCs isolated from the lung were capable of reconstituting the hematopoietic system in mice (Lefrançais *et al.,* 2017), this study found that *Runx*:mCherry+ cells isolated from the gill were not capable of long-term multilineage reconstitution of hematopoiesis in the *cmyb*$^{-/-}$ transplant model. However, there did appear to be a short-term increase in the abundance of cells in circulation, at least in some transplants (Fig. 5.16A). This may indicate that the *Runx*:mCherry+ cells present in the gill are lineage-biased HSPCs. This would be consistent with previous reports which identified erythroid-primed HSPCs among the *Runx*:GFP+ population (Tang *et al.,* 2017). Given the closely related transcriptional regulation of *Runx*:mCherry+ and *CD41*:GFP+ cells (Tang *et al.,* 2017; Kobayashi *et al.,* 2019), it is possible that gill-derived *Runx*:mCherry+ HSPCs also have a thrombocyte lineage bias, similar to the platelet biogenesis in the mouse lung. Indeed, *runx1*

is involved in zebrafish thrombocyte development (Sood *et al.,* 2010; Michaud *et al.,* 2002; Antony-Debré *et al.,* 2012). This may also explain the similar distributions of *Runx*:mCherry+ and *CD41*:GFP+ cells identified in the adult zebrafish gill (Fig. 3.18), and would be consistent with the findings of Pinho *et al.* which indicate that lineage-biased HSPCs have distinct niches within mammalian BM. It may be that the distinct niche for erythroid and thrombocyte-biased HSPCs is located within the gill tissue in zebrafish and other teleost.

On the other hand, if the *Runx*:mCherry+ cells in the gill represent terminally differentiated hematopoietic cells, it is possible that they may be of thrombocyte lineage due to the transcriptional overlap identified between the *Runx*:mCherry+ and *CD41*:GFP+ populations (Tang *et al.,* 2017; Kobayashi *et al.,* 2019). In future work, crossing of *Tg(CD41:GFP)* and *Tg(Runx:mCherry)* transgenic zebrafish would reveal the extent of overlap or proximity between these cell populations in the adult zebrafish, particularly in the gills. If there is overlap between *CD41*:GFP+ and *Runx*:mCherry+ cells in the gills of adult zebrafish, it would be interesting to determine which cells overlap by flow cytometry, and whether there is a clear distinction between *Runx*:mCherry ^{high} and *Runx*:mCherry ^{low} cells overlapping with *CD41*:GFP+ cells. Alternatively, *Runx*:mCherry+ cells, which arrive and embed in the developing gill to coincide approximately with the development of adaptive immunity in the zebrafish (Lam et al., 2004; Page et al., 2013; Chi et al., 2018; Trede et al., 2001; Hu et al., 2010), may represent cells of the adaptive immune system, such as *IgZ*+ B cells. However, data presented by Kobayashi *et al.* (2019) indicates that *Runx*+ *gata2a*- cells are enriched for thrombocyte, myeloid and erythroid marker genes, but not lymphoid marker genes.

The delayed dynamics with which *Runx*:mCherry ^{high} cells embed in the gill tissue during development bring into question whether the *Runx*:mCherry ^{high} cells in the WKM and in the gill are equivalent. It was also found that the *Runx*:mCherry+ cells may arrive in the gill with slightly delayed dynamics compared to their arrival in the WKM following HCT (section 5.3.6; Fig. 5.15). This would suggest that those cells which embed in the gill tissue are differentiated cells derived from *Runx*:mCherry HSPCs in the WKM.

6.2.3 The immune-modulatory effects of antibiotics

Although no differences were observed in the abundance of *Runx:*mCherry+ cells, *lyz:*GFP+ or other hematopoietic cells in the WKM following either longer term or shorter term PS treatment of juvenile and adult fish, functional differences in the hematopoietic compartment were not investigated following antibiotic treatment. Similarly, following 10 days of high dose OTC treatment, only a small change in the abundance of *Runx:*mCherry+ cells was observed. However, the changes in the abundance of cells cannot give an indication regarding either their ability to fight infection, or the stem cell fitness of HSPCs. The former could be investigated by assessing the cytokine response to inflammatory challenges such as application of R848 or poly I:C, or exposure to an infectious agent. It has previously been shown that zebrafish exposed to OTC or SMX for 6 weeks exhibited a significantly higher mortality 2-4 days following *Aeromonas hydrophila* exposure (Zhou *et al.*, 2018). Similarly, mouse studies found that commensal bacteria were important in ensuring sufficient TLR stimulation for effective antiviral responses (Abt *et al.,* 2012; Ichinohe *et al.*, 2011). Abt *et al.* showed that antibiotic treatment resulted in delayed viral clearance, increased mortality and impaired immune response to the influenza virus, which was improved by administration of poly I:C prior to influenza exposure. In Chapter 4, the response to poly I:C was investigated in the presence and absence of OTC pre-treatment. The results indicated that 10 days of 50 mg/L OTC treatment did not alter the cytokine response to poly I:C. This may suggest that a 10-day treatment duration is too short, or the dose too low, to elicit an altered immune response. Zhou *et al.* (2018) also describe a reduction in gut health and a significant decrease in the intestinal microbial richness following OTC treatment. Reduced microbial richness and diversity have been linked to impaired hematopoiesis in mice (Josefsdottir *et al.,* 2016; Abt *et al.,* 2012).

This project found a positive correlation between the abundance of *Runx:*mCherry+ HSPCs in the WKM and bacterial load in the gill, as measured by 16S rRNA. This suggests that the dose and regime with which the fish were treated is sufficient to alter the microbial community and affect hematopoiesis in the WKM of adult zebrafish, similarly to results in mice (Josefsdottir *et al.,* 2016). However, it did not result in an altered immune response to poly I:C. This may indicate that zebrafish have mechanisms to compensate for the impact that reduced microbial

load may have on hematopoiesis. Alternatively, it may indicate that there is redundant and sufficient TLR stimulation despite OTC treatment of the water.

Another factor to take into consideration when discussing the results observed in Chapter 4 is the anti-inflammatory effect that some antibiotics can have. Anti-inflammatory effects of antibiotics have been observed in mammalian cells (Voils *et al.,* 2005; Yamamoto *et al.*, 2016; Speer *et al.,* 2018) as well as in fish (Li *et al.,* 2019). For example, in rainbow trout, two-week OTC treatment was sufficient to reduce plasma immunoglobulin levels and result in a reduction in immune function (Yonar *et al.,*2012). However, there have been conflicting results regarding the immune-modulatory effects of OTC in fish. In contrast to the anti-inflammatory effect observed in rainbow trout, OTC treatment alone of larval zebrafish led to significant increases of neutrophils and increased *il1b* and *mpx* transcript levels after just 48 hours of high-dose treatment (Barros-Becker *et al.,* 2012). In adult zebrafish, 10 days of 50 mg/L OTC pre-treatment moderately enhanced the *ifnphi1* transcriptional response of the WKM and the gill to topical gill application of R848 (Wane, 2021). In gilthead sea bream, OTC treatment led to a transient increase in the abundance of blood leukocytes including neutrophils (Serezlí, 2005). In Nile tilapia, OTC treatment resulted in an increase in cytokine transcripts in the gut and liver (Limbu *et al.,* 2018). Given the varied responses that have been detected following OTC treatment, as well as the range of species and experimental conditions, it is difficult to make comparisons between studies. The aim of this work was to investigate the effect that antibiotic treatment has on zebrafish hematopoiesis in steady state and to investigate the impact this may have on stem cell fitness of HSCs. In future, studies could explore this further by carrying out competitive HCT assays using un-manipulated and antibiotic-treated donors and assessing chimerism in the recipient.

6.2.4 Investigating the role of thrombocytes in antiviral immune responses

Given the interactions identified between neutrophils and megakaryocytes in response to TLR7 agonists in mouse and human samples (Koupenova *et al.*, 2014; Jenne *et al.*, 2013), it would be interesting to investigate whether the same is true in zebrafish. *lysC*:DsRed and *CD41*:GFP-expressing transgenic zebrafish could be used to investigate, using confocal microscopy, the interactions between neutrophils and thrombocytes following R848 application to the gills. Utilising a model developed by the Dallman lab to challenge the gill

mucosa with R848 (Progatzky *et al*., 2019), it would be possible to further investigate the involvement of thrombocytes in the antiviral immune response and probe the factors contributed by these cells to the immune response.

6.2.5 Investigating the impact of immune signalling on HSC engraftment and reconstitution

Although carrying out transplantation experiments with a range of inflammatory settings was beyond the scope of this thesis, there are many interesting questions regarding the impact of inflammation on transplantation outcome and HSC behaviour. Previously, McBrien (2017) investigated the effect of chronic systemic inflammation induced by repeated poly I:C treatment in the donor and recipient on HCT outcome and found that chronic stimulation of the donor led to an increased rate of HSPC engraftment in the recipient. In contrast to immune stimulation, the OTC treatment regimen described in Chapter 4 could be utilised to investigate the engraftment capability of donor cells exposed to OTC. These donors likely experience reduced immune signalling as a result of reduced microbial diversity (Josefsdottir *et al*., 2016; Rosado *et al*., 2019). The finding that *Runx:*mCherry ^{high} cells overlap almost entirely with *Runx:*GFP+ cells makes it possible to utilise these populations for competitive HCT assays either in irradiated recipients or in *cmyb* mutants. The benefit of utilising *cmyb* mutants for the purpose of investigating the effect of inflammation on stem cell fitness is that *cmyb* mutants do not require irradiation or other myeloablative pre-conditioning prior to allogenic or xenogeneic HCT (Hess *et al.,* 2013; Hess *et al.,* 2016). Thus, HCT assays into *cmyb* mutants are not compromised by the inflammation induced by myeloablative pre-conditioning. Further investigation of the interplay between immune signalling and stem cell fitness would improve therapeutic application of HSCs by elucidating how the immune environment impacts HCT outcome.

6.2.6 Utilising cmyb mutant fish regeneration studies

The ability of *cmyb* mutant fish to regenerate their tail fin following amputation with no noticeable negative impact on survival, provides a unique opportunity to investigate the non-hematopoietic factors involved in the coordination of limb regeneration. It may also be interesting to investigate the role of the remaining *mpeg*+ cells in these mutant fish upon tail fin amputation. These cells may correspond to metaphocytes, involved in the sampling of soluble antigen (Lin *et al*., 2019), or other long-lived macrophage-like cells derived from

primitive hematopoiesis. If the latter is the case, it would be interesting to assess whether they are involved in the response to injury.

6.2.7 Utilising bloodless and immune deficient mutant fish for transplantation studies

As discussed above, *cmyb* mutant fish do not require IR preconditioning prior to HCT. This gives them immense potential for further xenogeneic transplant studies such as those carried out by Hess *et al*. (2016). Through further development of this model, *cmyb* mutants could be utilised in personalised medicine by transplantation of patient cells in order to investigate cell abnormalities and responses to therapeutics *in vivo*. Furthermore, xenograft studies where human cells are transplanted into zebrafish (Lee *et al*., 2005; Rajan *et al.,* 2019), could help to obtain a deeper understanding of the similarities and differences between niche factors that regulate human and teleost HSCs. A similar model has also been developed by generating T cell deficient, transparent zebrafish (Lv *et al.,* 2020). In this model, zebrafish are homozygous mutants for *Forkhead box N1 (foxn1)* as well as *mitfa* and *roy*. The former makes the zebrafish T cell deficient, which means that irradiation and other myeloablative pre-conditioning is not required for HCT, and the latter eliminates pigment cells, thereby making the fish transparent. A similar approach was pursued in this project by crossing immune deficient *cmyb* mutant fish onto the *tra*$^{-/-}$/*nacre*$^{-/-}$ background, ensuring that transplanted cells can be visualised *in vivo*. Transparent zebrafish have been utilised for HCT studies for this reason for over a decade (White *et al.,* 2008). However, their use in combination with immune deficient mutant lines is more recent. In the case of *cmyb*/ *tra*/ *nacre* mutants, there is unfortunately a small trade off. The transparency of these small mutants makes visualisation of transplanted cells and their progeny readily accessible. However, there is a fitness cost associated with the *tra* mutation in these already vulnerable fish which cannot survive without HCT for more than a few months (Soza-Ried *et al.,* 2010). In contrast, the mutant line generated by Lv *et al*. (2020) has a significantly higher survival rate of 86 % when maintained under antibiotic-supplemented conditions. This increased survival is undoubtedly very beneficial. However, in their model, transplanted donor cells are still in competition with host HSCs for niche spaces, while the *cmyb* mutants do not possess HSCs or any hematopoietic cells. This means that when *cmyb* mutants undergo HCT, the donor cell contribution to hematopoiesis is expected to be 100 %, whereas chimerism is expected in *foxn1*/*capser* recipients.

In another zebrafish model, *runx1*^{w84x} mutants are utilised for conditioning-free HCT (Fraint *et al.,* 2020). Here, the authors rely on the mutant line first described by Sood *et al.* (2010). These mutants are also unable to initiate the definitive wave of hematopoiesis, rendering them blood cell free by approximately 8-12 dpf. Similarly to the *cmyb* mutant line, *runx1* mutant bloodless fish have empty HSC niches. However, in contrast to *cmyb* mutants, bloodless *runx1* mutants do not survive this bloodless phase. As a result, adult bloodless *runx1* mutants cannot be transplanted. Instead, Fraint *et al.* transplanted *runx1* mutants at 2 dpf. However, at this early stage, it is impossible to distinguish mutants that will remain bloodless from the 20 % of fish which will recover. Thus, in this model, some fish may have chimerism between donor and recipient cells as well. Indeed, ⩾5 % donor-derived myeloid chimerism was considered a successful engraftment (Fraint *et al.,* 2020). Furthermore, the recovery phenotype seen in 20 % of mutants means that non-transplanted, sham injected controls are required for each experiment. As a result, this significantly increases the number of animals undergoing HCT procedures. As the homozygous *cmyb* mutation is fatal to fish before sexual maturity is reached, heterozygous mutant fish must be inbred in order to generate homozygous individuals. Therefore, substantial numbers of animals are required for breeding purposes to generate homozygous mutants, as is addressed by the authors in their discussion. While this issue leads to excessive fish being culled, it may be overcome by breeding HCT-rescued individuals. Other limitations, such as the need to carry out tail fin amputation for genotyping of *cmyb* mutant fish prior to HCT, can also be overcome. Genotyping may be carried out at the end point of an experiment (McBrien, 2017) or by identifying *cmyb* mutant fish through assessment of their vasculature, which is minimally invasive and can be carried out directly prior to HCT (Fig. 5.6).

The zebrafish HCT models described above each have benefits and limitations, making each differentially suited for addressing different types of research questions. *runx1* mutants are ideal for high throughput HCT in embryos, while *foxn1/casper* fish are well suited for investigations of normal and malignant hematopoiesis, as well as xenogeneic HCT in adults. *cmyb* mutants are ideal for HCT studies in the absence of host hematopoietic cells. Furthermore, the absence of host cells in *cmyb* mutants makes it possible to track HCT by more readily imaging the abundance of cells in circulation, as well as the abundance of

fluorescent progeny in the WKM and gill. This makes the *cmyb* mutants more suitable to study early post-transplant behaviours of HSC in adult fish.

The scoring system developed in Chapter 5 may provide a valuable opportunity to reduce the severity of HCT protocols by eliminating death as a readout and utilising the scoring system to track the success or failure of transplantation in *cmyb* mutant fish. This will allow us to intervene and reduce the suffering of fish that will not survive long term. It was found that a snapshot of the of engraftment score at 6 dpt correlated well with the extent of engraftment at later timepoints. Thus, in future, fewer imaging time points may be required, reducing the need for repeated anaesthesia which is stressful to the fish. Furthermore, the scoring system could be applied to investigate the impact of different treatments and immune stimuli on HSC reconstitution potential. As a proof of principle experiment, HCT could be carried out ± prostaglandin E2 treatment to assess whether early post-transplant scores are significantly improved when this treatment is administered, compared to sham-treated controls (North *et al.*, 2007).

6.2.8 Limitations and technical challenges when using cmyb mutant fish and impacts on the 3Rs

When choosing an appropriate model for animal research, it is important to consider the limitations of that model as well the impact on animal welfare. Therefore, this next section will discuss specific limitations of using *cmyb* mutant zebrafish, as well as refinements developed in this project and their impact on reduction, replacement, and refinement (the 3Rs) of animal research. Due to the inability of *cmyb* mutant fish to reach sexual maturity, it is necessary to breed heterozygous mutants to obtain 25 % homozygous mutant clutch. This means that there is an excess of at least 75 % of fish within each clutch. In addition, it is not possible to screen for mutant fish until at least 4 wpf when their vasculature has lost all primitive blood cells. While genotyping by fin clipping is possible, and has been shown here not to adversely affect the short-term survival of mutant fish, it does add additional stress to these vulnerable fish which may therefore impact experimental outcomes. This limitation can be overcome by genotyping before 5 dpf. By genotyping at this early stage, heterozygous or non-mutant siblings can be humanely culled before the onset of independent feeding and, hence, before they are protected under ASPA (1986). Furthermore, as shown in this thesis, fin clipping of *cmyb* mutants at early stages in the presence of primitive hematopoietic cells does

not adversely affect regeneration of fin fold tissue. Alternatively, DNA sample collection could be carried out using more refined techniques such as skin swabbing, which does not require amputation or anaesthesia (Tilley *et al.,* 2020).

In this thesis, *cmyb* mutants were first identified at 6 wpf by macroscopic differences such as their small size and pale complexion compared to heterozygous and non-mutant siblings. Subsequently, the vasculature of selected fish was assessed by microscopy using a simple dissection light microscope when fish were already under anaesthesia for the HCT procedure. This was a refinement as it eliminated the requirement for additional anaesthesia prior to HCT. Subsequently, genotyping was completed at the end point of an experiment. Using this method, it is estimated that approximately 28 heterozygous and non-mutant fish were removed from HCT groups prior to transplantation. This was considered a significant improvement due to the intensive nature of HCT experiments both for the fish and the experimenter.

Another limitation when using *cmyb* mutant fish for HCT is the difficulty of manipulation due to their small size. A refinement developed by McBrien (2017) was the use of glass pulled needles, a microinjector and micromanipulator instead of a Hamilton syringe to reduce the injury site to *cmyb* mutant fish. However, this HCT method is technically challenging. Therefore, it is important to carefully consider whether the use of *cmyb* mutant fish is the most appropriate model for any given experiment.

An important aspect of this project was to refine HCT procedure in *cmyb* mutant. This has been achieved in a number of ways. For example, refined rearing methods have increased the maximum survival of unmanipulated *cmyb* mutant fish from 14 wpf to 21 wpf. This was achieved by rearing fish in static tanks supplemented with antibiotics, as well as a weekly cleaning routine. The screening methods described above are a refinement as they reduce the number of procedures fish are subjected to. Finally, the post-transplant scoring system developed in this study has made it possible to track engraftment in individual fish over time. This also eliminated the requirement to harvest animals in order to assess the extent of engraftment. Using this method, it is expected that fewer animals will be required in order to obtain meaningful data.

6.3 Wider implications

Ultimately, zebrafish hematopoiesis is studied with the aim of gaining a better understanding of HSC ontogeny and of human hematopoiesis. This is possible due to a large number of evolutionarily conserved factors that regulate hematopoiesis in teleost and mammals. Therefore, there should be an emphasis on the study of evolutionarily conserved mechanisms of HSC maintenance, as opposed to species-specific mechanisms. On the other hand, studying species-specific mechanisms could help identify genes or gene products involved in improved HSC maintenance in zebrafish. Studying these could help in the further development of HSC therapies in humans. By improving the tools available to study HSCs in zebrafish, for example by increasing HSC purity within a donor cell population, it will be possible to investigate factors influencing interactions between HSCs and their respective niches more specifically. This will also help shed light on factors altering HSC biology. Further elucidation of the factors that govern HSC maintenance and reconstitution potential will improve our ability to expand HSCs *ex vivo* for therapeutic purposes, thereby reducing the requirement for donor-derived HSCs. Ultimately, a better understanding of HSC biology will improve therapeutic uses of HSCs in humans.

References

Abbott, J.D., Huang, Y., Liu, D., Hickey, R., Krause, D.S., and Giordano, F.J. (2004). Stromal cell-derived factor-1α plays a critical role in stem cell recruitment to the heart after myocardial infarction but is not sufficient to induce homing in the absence of injury. Circulation 110, 3300–3305.

Abt, M.C., Osborne, L.C., Monticelli, L.A., Doering, T.A., Alenghat, T., Sonnenberg, G.F., Paley, M.A., Antenus, M., Williams, K.L., Erikson, J., et al. (2012). Commensal Bacteria Calibrate the Activation Threshold of Innate Antiviral Immunity. Immunity *37*, 158–170.

Akashi, K., Traver, D., Miyamoto, T., and Weissman, I.L. (2000). A clonogenic common myeloid progenitor that gives rise to all myeloid lineages. Nature *404*, 193–197.

Alemany, A., Florescu, M., Baron, C.S., Peterson-Maduro, J., and Van Oudenaarden, A. (2018). Whole-organism clone tracing using single-cell sequencing. Nature *556*, 108–112.

Almeida, A.R., Alves, M., Domingues, I., and Henriques, I. (2019). The impact of antibiotic exposure in water and zebrafish gut microbiomes: A 16S rRNA gene-based metagenomic analysis. Ecotoxicol. Environ. Saf. *186*, 109771.

Almeida, A.R., Tacão, M., Machado, A.L., Golovko, O., Zlabek, V., Domingues, I., and Henriques, I. (2019). Long-term effects of oxytetracycline exposure in zebrafish: A multi-level perspective. Chemosphere *222*, 333–344.

Andrews, N. (2016). Spatio-temporal Mapping of Protein Activity in Live Zebrafish using FRET FLIM OPT.

Andrews, N., Ramel, M.-C., Kumar, S., Alexandrov, Y., Kelly, D.J., Warren, S.C., Kerry, L., Lockwood, N., Frolov, A., Frankel, P., et al. (2016). Visualising apoptosis in live zebrafish using fluorescence lifetime imaging with optical projection tomography to map FRET biosensor activity in space and time. J. Biophotonics *9*, 414–424.

Antony-Debré, I., Bluteau, D., Itzykson, R., Baccini, V., Renneville, A., Boehlen, F., Morabito, M., Droin, N., Deswarte, C., Chang, Y., et al. (2012). MYH10 protein expression in platelets as a biomarker of RUNX1 and FLI1 alterations. Blood *120*, 2719–2722.

Arora, N., Wenzel, P.L., McKinney-Freeman, S.L., Ross, S.J., Kim, P.G., Chou, S.S., Yoshimoto, M., Yoder, M.C., and Daley, G.Q. (2014). Effect of developmental stage of HSC and recipient on transplant outcomes. Dev. Cell 29, 621–628.

Asakura, S., and Colby, T. V. (1994). Agnogenic myeloid metaplasia with extramedullary hematopoiesis and fibrosis in the lung: Report of two cases. Chest *105*, 1866–1868.

Baldridge, M.T., King, K.Y., Boles, N.C., Weksberg, D.C., and Goodell, M.A. (2010). Quiescent haematopoietic stem cells are activated by IFN-γ in response to chronic infection. Nature *465*, 793–797.

Baldridge, M.T., King, K.Y., Boles, N.C., Weksberg, D.C., and Goodell, M.A. (2010). Response To Chronic Infection. Nature *465*, 793–797.

Balmer, M.L., Schürch, C.M., Saito, Y., Geuking, M.B., Li, H., Cuenca, M., Kovtonyuk, L. V., McCoy, K.D., Hapfelmeier, S., Ochsenbein, A.F., et al. (2014). Microbiota-Derived Compounds Drive Steady-State Granulopoiesis via MyD88/TICAM Signaling. J. Immunol. *193*, 5273–5283.

Barros-Becker, F., Romero, J., Pulgar, A., and Feijóo, C.G. (2012). Persistent oxytetracycline exposure induces an inflammatory process that improves regenerative capacity in zebrafish larvae. PLoS One *7*, 1–9.

Batsivari, A., Haltalli, M.L.R., Passaro, D., Pospori, C., Lo Celso, C., and Bonnet, D. (2020). Dynamic responses of the haematopoietic stem cell niche to diverse stresses. Nat. Cell Biol. *22*, 7–17.

Baum, C.M., Weissman, I.L., Tsukamoto, A.S., Buckle, A.M., and Peault, B. (1992). Isolation of a candidate human hematopoietic stem-cell population. Proc. Natl. Acad. Sci. U. S. A. *89*, 2804–2808.

Bee, T., Ashley, E.L.K., Bickley, S.R.B., Jarratt, A., Li, P.S., Sloane-Stanley, J., Göttgens, B., and De Bruijn, M.F.T.R. (2009). The mouse Runx1 +23 hematopoietic stem cell enhancer confers hematopoietic specificity to both Runx1 promoters. Blood *113*, 5121–5214.

Bennett, C.M., Kanki, J.P., Rhodes, J., Liu, T.X., Paw, B.H., Kieran, M.W., Langenau, D.M., Delahaye-Brown, A., Zon, L.I., Fleming, M.D., et al. (2001). Myelopoiesis in the zebrafish, Danio rerio. Blood *98*, 643–651.

Bernard, J.J., Cowing-Zitron, C., Nakatsuji, T., Muehleisen, B., Muto, J., Borkowski, A.W., Martinez, L., Greidinger, E.L., Yu, B.D., and Gallo, R.L. (2012). Ultraviolet radiation damages self noncoding RNA and is detected by TLR3. Nat. Med. *18*, 1286–1290.

Bernut, A., Loynes, C.A., Floto, R.A., and Renshaw, S.A. (2020). Deletion of cftr Leads to an Excessive Neutrophilic Response and Defective Tissue Repair in a Zebrafish Model of Sterile Inflammation. Front. Immunol. *11*, 1733.

Bertrand, J.Y., Chi, N.C., Santoso, B., Teng, S., Stainier, D.Y.R., and Traver, D. (2010). Haematopoietic stem cells derive directly from aortic endothelium during development. Nature *464*, 108–111.

Bertrand, J.Y., Cisson, J.L., Stachura, D.L., and Traver, D. (2010). Notch signaling distinguishes 2 waves of definitive hematopoiesis in the zebrafish embryo. Blood *115*, 2777–2783.

Bertrand, J.Y., Kim, A.D., Teng, S., and Traver, D. (2008). CD41+ cmyb+ precursors colonize the zebrafish pronephros by a novel migration route to initiate adult hematopoiesis. Development 135, 1853–1862.

Bertrand, J.Y., Kim, A.D., Violette, E.P., Stachura, D.L., Cisson, J.L., and Traver, D. (2007). Definitive hematopoiesis initiates through a committed erythromyeloid progenitor in the zebrafish embryo. Development *134*, 4147–4156.

Bevan, L., Lim, Z.W., Venkatesh, B., Riley, P.R., Martin, P., and Richardson, R.J. (2020). Specific macrophage populations promote both cardiac scar deposition and subsequent resolution in adult zebrafish. Cardiovasc. Res. *116*, 1357–1371.

Bhattacharya, D., Rossi, D.J., Bryder, D., and Weissman, I.L. (2006). Purified hematopoietic stem cell engraftment of rare niches corrects severe lymphoid deficiencies without host conditioning. J. Exp. Med. 203, 73–85.

Boettcher, S., and Manz, M.G. (2017). Regulation of Inflammation- and Infection-Driven Hematopoiesis. Trends Immunol. *38*, 345–357.

Bonkhofer, F., Rispoli, R., Pinheiro, P., Krecsmarik, M., Schneider-Swales, J., Ho Ching Tsang, I., De Bruijn, M., Monteiro, R., Peterkin, T., and Patient, R. (2019). Blood stem cell-forming haemogenic endothelium derives from arterial endothelium. Nat Commun *10*.

Boula, A., Mantadakis, E., Xilouri, I., Foudoulakis, A., and Samonis, G. (2005). Agnogenic myeloid metaplasia with pulmonary hematopoiesis. Hematology 10, 501–503.

Bowie, M.B., Kent, D.G., Dykstra, B., McKnight, K.D., McCaffrey, L., Hoodless, P.A., and Eaves, C.J. (2007). Identification of a new intrinsically timed developmental checkpoint that reprograms key hematopoietic stem cell properties. Proc. Natl. Acad. Sci. U. S. A. 104, 5878–5882.

Brandt, J., Lu, L., Walker, E.B., and Hoffman, R. (1988). Detection of a human hematopoietic progenitor cell capable of forming blast cell containing colonies in vitro. Adv. Exp. Med. Biol. *241*, 165–173.

Bresciani, E., Carrington, B., Wincovitch, S., Jones, M., Gore, A. V., Weinstein, B.M., Sood, R., and Liu, P.P. (2014). CBFβ and RUNX1 are required at 2 different steps during the development of hematopoietic stem cells in zebrafish. Blood *124*, 70–78.

Brownlie, A., Hersey, C., Oates, A.C., Paw, B.H., Falick, A.M., Witkowska, H.E., Flint, J., Higgs, D., Jessen, J., Bahary, N., et al. (2003). Characterization of embryonic globin genes of the zebrafish. Dev. Biol. *255*, 48–61.

Bu, Q., Wang, B., Huang, J., Deng, S., and Yu, G. (2013). Pharmaceuticals and personal care products in the aquatic environment in China: A review. J. Hazard. Mater. *262*, 189–211.

Burberry, A., Zeng, M.Y., Ding, L., Wicks, I., Inohara, N., Morrison, S.J., and Núnez, G. (2014). Infection mobilizes hematopoietic stem cells through cooperative NOD-like receptor and toll-like receptor signaling. Cell Host Microbe *15*, 779–791.

Burket, C.T., Montgomery, J.E., Thummel, R., Kassen, S.C., LaFave, M.C., Langenau, D.M., Zon, L.I., and Hyde, D.R. (2008). Generation and characterization of transgenic zebrafish lines using different ubiquitous promoters. Transgenic Res. *17*, 265–279.

Burns, C.E., DeBlasio, T., Zhou, Y., Zhang, J., Zon, L., and Nimer, S.D. (2002). Isolation and characterization of runxa and runxb, zebrafish members of the runt family of transcriptional regulators. Exp. Hematol. *30*, 1381–1389.

Burns, C.E., Traver, D., Mayhall, E., Shepard, J.L., and Zon, L.I. (2005). Hematopoietic stem cell fate is established by the Notch-Runx pathway. Genes Dev. *19*, 2331–2342.

Busch, K., Klapproth, K., Barile, M., Flossdorf, M., Holland-Letz, T., Schlenner, S.M., Reth, M., Höfer, T., and Rodewald, H.R. (2015). Fundamental properties of unperturbed haematopoiesis from stem cells in vivo. Nature 518, 542–546.

Butaye, P., Devriese, L.A., and Haesebrouck, F. (2003). Antimicrobial growth promoters used in animal feed: Effects of less well known antibiotics on gram-positive bacteria. Clin. Microbiol. Rev. *16*, 175–188.

Butko, E., Distel, M., Pouget, C., Weijts, B., Kobayashi, I., Ng, K., Mosimann, C., Poulain, F.E., McPherson, A., Ni, C.W., et al. (2015). Gata2b is a restricted early regulator of hemogenic endothelium in the zebrafish embryo. Dev. *142*, 1050–1061.

Campbell, and Reece (2002). Biology (Pearson).Carvalho, I.T., and Santos, L. (2016). Antibiotics in the aquatic environments: A review of the European scenario. Environ. Int. *94*, 736–757.

Casanova-Acebes, M., Pitaval, C., Weiss, L.A., Nombela-Arrieta, C., Chèvre, R., A-González, N., Kunisaki, Y., Zhang, D., Van Rooijen, N., Silberstein, L.E., et al. (2013). Rhythmic modulation of the hematopoietic niche through neutrophil clearance. Cell *153*, 1025.

Challen, G.A., Boles, N., Lin, K.K.Y., and Goodell, M.A. (2009). Mouse hematopoietic stem cell identification and analysis. Cytom. Part A *75*, 14–24.

Charlwood, K. (2017). Investigating the effect of dietary cholesterol on the intestine in zebrafish larvae.

Chen, M.J., Yokomizo, T., Zeigler, B., Dzierzak, E., and Speck, a (2009). Transition But Not Thereafter. Nature *457*, 887–891.

Cheng, H., Zheng, Z., and Cheng, T. (2019). New paradigms on hematopoietic stem cell differentiation. Protein Cell.

Chi, Y., Huang, Z., Chen, Q., Xiong, X., Chen, K., Xu, J., Zhang, Y., and Zhang, W. (2018). Loss of RUNX1 function results in B cell immunodeficiency but not T cell in adult Zebrafish. R. Soc. Open Sci. *8*.

Chou, D.B., Sworder, B., Bouladoux, N., Roy, C.N., Uchida, A.M., Grigg, M., Robey, P.G., and Belkaid, Y. Stromal-derived IL-6 alters the balance of myeloerythroid progenitors during Toxoplasma gondii infection.

Crane, G.M., Jeffery, E., and Morrison, S.J. (2017). Adult haematopoietic stem cell niches. Nat. Rev. Immunol. 17, 573–590.

Czechowicz, A., Kraft, D., Weissman, I.L., and Bhattacharya, D. (2007). Efficient transplantation via antibody-based clearance of hematopoietic stem cell niches. Science (80-.). 318, 1296–1299.

D'Agati, G., Beltre, R., Sessa, A., Burger, A., Zhou, Y., Mosimann, C., and White, R.M. (2017). A defect in the mitochondrial protein Mpv17 underlies the transparent casper zebrafish. Dev. Biol. *430*, 11–17.

Dancey, J.T., Deubelbeiss, K.A., and Harker andFinch, L.A.C.A. (1976). Neutrophil kinetics in man. J. Clin. Invest. *58*, 705–715.

De Bruin, A.M., Demirel, Ö., Hooibrink, B., Brandts, C.H., and Nolte, M.A. (2013). Interferon-γ impairs proliferation of hematopoietic stem cells in mice. Blood *121*, 3578–3585.

De Chaumont, F., Dallongeville, S., Chenouard, N., Hervé, N., Pop, S., Provoost, T., Meas-Yedid, V., Pankajakshan, P., Lecomte, T., Le Montagner, Y., et al. (2012). Icy: An open bioimage informatics platform for extended reproducible research. Nat. Methods *9*, 690–696.

De Jong, J.L.O., Burns, C.E., Chen, A.T., Pugach, E., Mayhall, E.A., Smith, A.C.H., Feldman, H.A., Zhou, Y., and Zon, L.I. (2011). Characterization of immune-matched hematopoietic transplantation in zebrafish. Blood *117*, 4234–4242.

De Jong, J.L.O., and Zon, L.I. (2012). Histocompatibility and hematopoietic transplantation in the zebrafish. Adv. Hematol. *2012*.

De Luca, K., Frances-Duvert, V., Asensio, M.J., Ihsani, R., Debien, E., Taillardet, M., Verhoeyen, E., Bella, C., Lantheaume, S., Genestier, L., et al. (2009). The TLR1/2 agonist PAM3CSK4 instructs commitment of human hematopoietic stem cells to a myeloid cell fate. Leukemia *23*, 2063–2074.

Dee, C.T., Nagaraju, R.T., Athanasiadis, E.I., Gray, C., Fernandez del Ama, L., Johnston, S.A., Secombes, C.J., Cvejic, A., and Hurlstone, A.F.L. (2016). CD4-Transgenic Zebrafish Reveal Tissue-

Resident Th2- and Regulatory T Cell–like Populations and Diverse Mononuclear Phagocytes. J. Immunol. *197*, 3520–3530.

Dominici, M., Rasini, V., Bussolari, R., Chen, X., Hofmann, T.J., Spano, C., Bernabei, D., Veronesi, E., Bertoni, F., Paolucci, P., et al. (2009). Restoration and reversible expansion of the osteoblastic hematopoietic stem cell niche after marrow radioablation. Blood 114, 2333–2343.

Ellett, F., Pase, L., Hayman, J.W., Andrianopoulos, A., and Lieschke, G.J. (2011). mpeg1 promoter transgenes direct macrophage-lineage expression in zebrafish. Blood *117*, e49.

Essers, M.A.G.G., Offner, S., Blanco-Bose, W.E., Waibler, Z., Kalinke, U., Duchosal, M.A., and Trumpp, A. (2009). IFNα activates dormant haematopoietic stem cells in vivo. Nature *458*, 904–908.

Evans, D.H., Piermarini, P.M., and Choe, K.P. (2005). The multifunctional fish gill: Dominant site of gas exchange, osmoregulation, acid-base regulation, and excretion of nitrogenous waste. Physiol. Rev. 85, 97–177.

Fantin, A., Vieira, J.M., Gestri, G., Denti, L., Schwarz, Q., Prykhozhij, S., Peri, F., Wilson, S.W., and Ruhrberg, C. (2010). Tissue macrophages act as cellular chaperones for vascular anastomosis downstream of VEGF-mediated endothelial tip cell induction. Blood *116*, 829–840.

Ferrero, G., Gomez, E., Lyer, S., Rovira, M., Miserocchi, M., Langenau, D.M., Bertrand, J.Y., and Wittamer, V. (2020). The macrophage-expressed gene (mpeg) 1 identifies a subpopulation of B cells in the adult zebrafish. J. Leukoc. Biol. *107*, 431–443.

Ferrero, G., Mahony, C.B., Dupuis, E., Yvernogeau, L., Di Ruggiero, E., Miserocchi, M., Caron, M., Robin, C., Traver, D., Bertrand, J.Y., et al. (2018). Embryonic Microglia Derive from Primitive Macrophages and Are Replaced by cmyb-Dependent Definitive Microglia in Zebrafish. Cell Rep. *24*, 130–141.

Finlay, A.C., Hobby, G.L., P'An, S.Y., Regna, P.P., Routien, J.B., Seeley, D.B., Shull, G.M., Sobin, B.A., Solomons, I.A., Vinson, J.W., et al. (1950). Terramycin, a new antibiotic. Science (80-.). *111*, 85.

Foudi, A., and Hochedlinger, K. (2009). Defining Hematopoietic Stem and Progenitor Cell Turnover by Analysis of Histone 2B-GFP Dilution. Nat. Biotechnol. *27*, 84–90.

Fraint, E., Norberto, M.F., and Bowman, T. V. (2020). A novel conditioning-free hematopoietic stem cell transplantation model in zebrafish. Blood Adv. 4, 6189–6198.

Galloway, J.L., Wingert, R.A., Thisse, C., Thisse, B., and Zon, L.I. (2005). Loss of Gata1 but not Gata2 converts erythropoiesis to myelopoiesis in zebrafish embryos. Dev. Cell *8*, 109–116.

Ganis, J.J., Hsia, N., Trompouki, E., de Jong, J.L.O., DiBiase, A., Lambert, J.S., Jia, Z., Sabo, P.J., Weaver, M., Sandstrom, R., et al. (2012). Zebrafish globin switching occurs in two developmental stages and is controlled by the LCR. Dev. Biol. *366*, 185–194.

Gering, M., Rodaway, A.R.F., Göttgens, B., Patient, R.K., and Green, A.R. (1998). The SCL gene specifies haemangioblast development from early mesoderm. EMBO J. *17*, 4029–4045.Gerlach,

G.F., Schrader, L.N., and Wingert, R.A. (2011). Dissection of the adult zebrafish kidney. J. Vis. Exp. e2839–e2839.

Ginhoux, F., and Merad, M. (2010). Ontogeny and homeostasis of Langerhans cells. Immunol. Cell Biol. *88*, 387–392.

Glass, T.J., Lund, T.C., Patrinostro, X., Tolar, J., Bowman, T. V., Zon, L.I., and Blazar, B.R. (2011). Stromal cell-derived factor-1 and hematopoietic cell homing in an adult zebrafish model of hematopoietic cell transplantation. Blood *118*, 766–774.

Glenn, N.O., Schumacher, J.A., Kim, H.J., Zhao, E.J., Skerniskyte, J., and Sumanas, S. (2014). Distinct regulation of the anterior and posterior myeloperoxidase expression by Etv2 and Gata1 during primitive Granulopoiesis in zebrafish. Dev. Biol. *393*, 149–159.

Gomez Perdiguero, E., Klapproth, K., Schulz, C., Busch, K., Azzoni, E., Crozet, L., Garner, H., Trouillet, C., De Bruijn, M.F., Geissmann, F., et al. (2015). Tissue-resident macrophages originate from yolk-sac-derived erythro-myeloid progenitors. Nature *518*, 547–551.

Gomez Perdiguero, E., Klapproth, K., Schulz, C., Busch, K., de Bruijn, M., Rodewald, H.R., and Geissmann, F. (2015). The Origin of Tissue-Resident Macrophages: When an Erythro-myeloid Progenitor Is an Erythro-myeloid Progenitor. Immunity *43*, 1023–1024.

Gómez, G.D., and Balcázar, J.L. (2008). A review on the interactions between gut microbiota and innate immunity of fish. FEMS Immunol. Med. Microbiol. *52*, 145–154.

Goodell, M.A., Brose, K., Paradis, G., Conner, A.S., and Mulligan, R.C. (1996). Isolation and functional properties of murine hematopoietic stem cells that are replicating in vivo. J. Exp. Med. *183*, 1797–1806.

Gordon, M.Y., Lewis, J.L., and Marley, S.B. (2002). Of mice and men . . . and elephants [3]. Blood *100*, 4679–4680.

Gore, A. V., Athans, B., Iben, J.R., Johnson, K., Russanova, V., Castranova, D., Pham, V.N., Butler, M.G., Williams-Simons, L., Nichols, J.T., et al. (2016). Epigenetic regulation of hematopoiesis by DNA methylation. Elife *5*, 1–25.

Gray, C., Loynes, C.A., Whyte, M.K.B., Crossman, D.C., Renshaw, S.A., and Chico, T.J.A. (2011). Simultaneous intravital imaging of macrophage and neutrophil behaviour during inflammation using a novel transgenic zebrafish. Thromb. Haemost. *105*, 811–819.

Griffith, M.B. (2017). Toxicological perspective on the osmoregulation and ionoregulation physiology of major ions by freshwater animals: Teleost fish, crustacea, aquatic insects, and Mollusca. Environ. Toxicol. Chem. 36, 576–600.

Grunewald, M., Avraham, I., Dor, Y., Bachar-Lustig, E., Itin, A., Yung, S., Chimenti, S., Landsman, L., Abramovitch, R., and Keshet, E. (2006). VEGF-induced adult neovascularization: Recruitment, retention, and role of accessory cells. Cell 124, 175–189.

Gupta, V., and Poss, K.D. (2012). Clonally dominant cardiomyocytes direct heart morphogenesis. Nature *484*, 479–484.

Gyurkocza, B., Rezvani, A., and Storb, R.F. (2010). Allogeneic hematopoietic cell transplantation: The state of the art. Expert Rev. Hematol. *3*, 285–299.

Hall, C., Flores, M., Storm, T., Crosier, K., and Crosier, P. (2007). The zebrafish lysozyme C promoter drives myeloid-specific expression in transgenic fish. BMC Dev. Biol. *7*.

Hall, C.J., Flores, M.V., Oehlers, S.H., Sanderson, L.E., Lam, E.Y., Crosier, K.E., and Crosier, P.S. (2012). Infection-responsive expansion of the hematopoietic stem and progenitor cell compartment in zebrafish is dependent upon inducible nitric oxide. Cell Stem Cell *10*, 198–209.

Hasegawa, T., Nakajima, T., Ishida, T., Kudo, A., and Kawakami, A. (2015). A diffusible signal derived from hematopoietic cells supports the survival and proliferation of regenerative cells during zebrafish fin fold regeneration. Dev. Biol. *399*, 80–90.

He, S., Chen, J., Jiang, Y., Wu, Y., Zhu, L., Jin, W., Zhao, C., Yu, T., Wang, T., Wu, S., et al. (2018). Adult zebrafish langerhans cells arise from hematopoietic stem/progenitor cells. Elife *7*.

He, S., Zhou, Z., Liu, Y., Cao, Y., Meng, K., Shi, P., Yao, B., and Ringø, E. (2010). Effects of the antibiotic growth promoters flavomycin and florfenicol on the autochthonous intestinal microbiota of hybrid tilapia (Oreochromis niloticus ♀ × O. aureus ♂). Arch. Microbiol. *192*, 985–994.

Hemmi, H., Kaisho, T., Takeuchi, O., Sato, S., Sanjo, H., Hoshino, K., Horiuchi, T., Tomizawa, H., Takeda, K., and Akira, S. (2002). Small-antiviral compounds activate immune cells via the TLR7 MyD88-dependent signaling pathway. Nat. Immunol. *3*, 196–200.

Henninger, J., Santoso, B., Hans, S., Durand, E., Moore, J., Mosimann, C., Brand, M., Traver, D., and Zon, L. (2017). Clonal fate mapping quantifies the number of haematopoietic stem cells that arise during development. Nat. Cell Biol. 1.

Hénon, P., Sovalat, H., Becker, M., Arkam, Y., Ojeda-Uribe, M., Raidot, J.P., Hesseini, F., Wunder, E., Bouderont, D., and Audhuy, B. (1998). Primordial role of CD34+38- cells in early and late trilineage haemopoietic engraftment after autologous blood cell transplantation. Br. J. Haematol. *103*, 568–581.

Hérault, A., Binnewies, M., Leong, S., Calero-Nieto, F.J., Zhang, S.Y., Kang, Y.A., Wang, X., Pietras, E.M., Chu, S.H., Barry-Holson, K., et al. (2017). Myeloid progenitor cluster formation drives emergency and leukaemic myelopoiesis. Nature *544*, 53–58.

Herbomel, P., Thisse, B., and Thisse, C. (2001). Zebrafish early macrophages colonize cephalic mesenchyme and developing brain, retina, and epidermis through a M-CSF receptor-dependent invasive process. Dev. Biol. *238*, 274–288.

Herbomel, P., Thisse, B., and Thisse, C. (1999). Ontogeny and behaviour of early macrophages in the zebrafish embryo. Development *126*, 3735–3745.Hess, I., and Boehm, T. (2016). Stable multilineage xenogeneic replacement of definitive hematopoiesis in adult zebrafish. Sci. Rep. *6*, 19634.

Hess, I., Iwanami, N., Schorpp, M., and Boehm, T. (2013). Zebrafish model for allogeneic hematopoietic cell transplantation not requiring preconditioning. Proc. Natl. Acad. Sci. U. S. A. *110*, 4327–4332.

Hess, I., and Boehm, T. (2016). Stable multilineage xenogeneic replacement of definitive hematopoiesis in adult zebrafish. Sci. Rep. 6, 19634.

Hoshino, K., Takeuchi, O., Kawai, T., Sanjo, H., Ogawa, T., Takeda, Y., Takeda, K., and Akira, S. (2016). Pillars Article: Cutting Edge: Toll-Like Receptor 4 (TLR4)-Deficient Mice Are Hyporesponsive to Lipopolysaccharide: Evidence for TLR4 as the Lps Gene Product. J. Immunol. 1999. 162: 3749-3752. J. Immunol. *197*, 2563–2566.

Howell, W.H., and Donahue, D.D. (1937). The production of blood platelets in the lungs. J. Exp. Med. 65, 177–204.

Hu, Y.L., Xiang, L.X., and Shao, J.Z. (2010). Identification and characterization of a novel immunoglobulin Z isotype in zebrafish: Implications for a distinct B cell receptor in lower vertebrates. Mol. Immunol. *47*, 738–746.

Ichinohe, T., Pang, I.K., Kumamoto, Y., Peaper, D.R., Ho, J.H., Murray, T.S., and Iwasaki, A. (2011). Microbiota regulates immune defense against respiratory tract influenza a virus infection. Proc. Natl. Acad. Sci. U. S. A. *108*, 5354–5359.

Imagawa, T., Kitagawa, H., and Uehara, M. (1994). Ultrastructure of blood vessels in the head kidney of the carp, Cyprinus carpio. J. Anat. *185*, 521–521.Ingersoll, M.A., Kline, K.A., Nielsen, H.

V., and Hultgren, S.J. (2008). G-CSF induction early in uropathogenic Escherichia coli infection of the urinary tract modulates host immunity. Cell. Microbiol. *10*, 2568–2578.

Itkin, T., Ludin, A., Gradus, B., Gur-Cohen, S., Kalinkovich, A., Schajnovitz, A., Ovadya, Y., Kollet, O., Canaani, J., Shezen, E., et al. (2012). FGF-2 expands murine hematopoietic stem and progenitor cells via proliferation of stromal cells, c-Kit activation, and CXCL12 down-regulation. Blood *120*, 1843–1855.

Iwasaki-Arai, J., Iwasaki, H., Miyamoto, T., Watanabe, S., and Akashi, K. (2003). Enforced Granulocyte/Macrophage Colony-stimulating Factor Signals Do Not Support Lymphopoiesis, but Instruct Lymphoid to Myelomonocytic Lineage Conversion. J. Exp. Med. J. Exp. Med. ⊠ *197*, 1311–1322.

Janeway, C.A., and Medzhitov, R. (2002). Innate immune recognition. Annu. Rev. Immunol. *20*, 197–216.Jemaa, M., Morin, N., Cavelier, P., Cau, J., Strub, J.M., and Delsert, C. (2014). Adult somatic progenitor cells and hematopoiesis in oysters. J. Exp. Biol. *217*, 3067–3077.

Jenne, C.N., Wong, C.H.Y., Zemp, F.J., McDonald, B., Rahman, M.M., Forsyth, P.A., McFadden, G., and Kubes, P. (2013). Neutrophils recruited to sites of infection protect from virus challenge by releasing neutrophil extracellular traps. Cell Host Microbe *13*, 169–180.

Jin, H., Huang, Z., Chi, Y., Wu, M., Zhou, R., Zhao, L., Xu, J., Zhen, F., Lan, Y., Li, L., et al. (2016). c-Myb acts in parallel and cooperatively with Cebp1 to regulate neutrophil maturation in zebrafish. Blood *128*, 415–426.

Jin, H., Li, L., Xu, J., Zhen, F., Zhu, L., Liu, P.P., Zhang, M., Zhang, W., and Wen, Z. (2012). Runx1 regulates embryonic myeloid fate choice in zebrafish through a negative feedback loop inhibiting Pu.1 expression. Blood *119*, 5239–5249.

Jin, H., Sood, R., Xu, J., Zhen, F., English, M.A., Liu, P.P., and Wen, Z. (2009). Erratum: Definitive hematopoietic stem/progenitor cells manifest distinct differentiation output in the zebrafish VDA and PBI (Development vol. 136 (647-654)). Development *136*, 1397.

Jin, H., Xu, J., and Wen, Z. (2007). Migratory path of definitive hematopoietic stem/progenitor cells during zebrafish development. Blood *109*, 5208–5214.Jing, L., Tamplin, O.J., Chen, M.J., Deng, Q., Patterson, S., Kim, P.G., Durand, E.M., McNeil, A., Green, J.M., Matsuura, S., et al. (2015). Adenosine signaling promotes hematopoietic stem and progenitor cell emergence. J. Exp. Med. *212*, 649–663.

Jing, L., and Zon, L.I. (2011). Zebrafish as a model for normal and malignant hematopoiesis. DMM Dis. Model. Mech. *4*, 433–438.

Josefsdottir, K.S., Baldridge, M.T., Kadmon, C.S., and King, K.Y. (2016). Antibiotics impair murine hematopoiesis by depleting intestinal microbiota. Blood *3996*, 729–740.

Kalev-Zylinska, M.L., Horsfield, J.A., Flores, M.V.C., Postlethwait, J.H., Vitas, M.R., Baas, A.M., Crosier, P.S., and Crosier, K.E. (2002). Runx1 is required for zebrafish blood and vessel development and expression of a human RUNX-1-CBF2T1 transgene advances a model for studies of leukemogenesis. Development *129*, 2015–2030.

Karamitros, D., Stoilova, B., Aboukhalil, Z., Hamey, F., Reinisch, A., Samitsch, M., Quek, L., Otto, G., Repapi, E., Doondeea, J., et al. (2018). Single-cell analysis reveals the continuum of human lympho-myeloid progenitor cells article. Nat. Immunol. 19, 85–97.

Kawai, T., and Akira, S. (2010). The role of pattern-recognition receptors in innate immunity: Update on toll-like receptors. Nat. Immunol. *11*, 373–384.Kelly, C., and Salinas, I. (2017). Under pressure: Interactions between commensal microbiota and the teleost immune system. Front. Immunol. *8*.

Khosravi, A., Yáñez, A., Price, J.G., Chow, A., Merad, M., Goodridge, H.S., and Mazmanian, S.K. (2014). Gut microbiota promote hematopoiesis to control bacterial infection. Cell Host Microbe *15*, 374–381.

Kiel, M.J., He, S., Ashkenazi, R., Gentry, S.N., Teta, M., Kushner, J.A., Jackson, T.L., and Morrison, S.J. (2007). Haematopoietic stem cells do not asymmetrically segregate chromosomes or retain BrdU. Nature *449*, 238–242.

Kiel, M.J., Yilmaz, Ö.H., Iwashita, T., Yilmaz, O.H., Terhorst, C., and Morrison, S.J. (2005). SLAM family receptors distinguish hematopoietic stem and progenitor cells and reveal endothelial niches for stem cells. Cell *121*, 1109–1121.

Kim, A.D., Melick, C.H., Clements, W.K., Stachura, D.L., Distel, M., Panáková, D., MacRae, C., Mork, L.A., Crump, J.G., and Traver, D. (2014). Discrete Notch signaling requirements in the specification of hematopoietic stem cells. EMBO J. *33*, 2363–2373.

Kim, M., Turnquist, H., Sgagias, M., Yan, Y., Cowan, K., Jackson, J., Sharp, J.G., Gong, M., and Dean, M. (2002). The multidrug resistance transporter ABCG2 (breast cancer resistance protein 1) effluxes Hoechst 33342 and is overexpressed in hematopoietic stem cells. Clin. Cancer Res. *8*, 22–28.

King, K.Y., and Goodell, M.A. (2011). Inflammatory modulation of HSCs: Viewing the HSC as a foundation for the immune response. Nat. Rev. Immunol. *11*, 685–692.

Kissa, K., and Herbomel, P. (2010). Blood stem cells emerge from aortic endothelium by a novel type of cell transition. Nature *464*, 112–115.

Kissa, K., Murayama, E., Zapata, A., Cortés, A., Perret, E., Machu, C., and Herbomel, P. (2008). Live imaging of emerging hematopoietic stem cells and early thymus colonization. Blood *111*, 1147–1156.

Kobayashi, I., Kobayashi-Sun, J., Kim, A.D., Pouget, C., Fujita, N., Suda, T., and Traver, D. (2014). Jam1a-Jam2a interactions regulate haematopoietic stem cell fate through Notch signalling. Nature *512*, 319–323.

Kobayashi, I., Kondo, M., Yamamori, S., Kobayashi-Sun, J., Taniguchi, M., Kanemaru, K., Katakura, F., and Traver, D. (2019). Enrichment of hematopoietic stem/progenitor cells in the zebrafish kidney. Sci. Rep. *9*, 1–11.

Kobayashi, I., Ono, H., Moritomo, T., Kano, K., Nakanishi, T., and Suda, T. (2010). Comparative gene expression analysis of zebrafish and mammals identifies common regulators in hematopoietic stem cells. Blood *115*, 1–9.

Kobayashi, I., Saito, K., Moritomo, T., Araki, K., Takizawa, F., and Nakanishi, T. (2008). Characterization and localization of side population (SP) cells in zebrafish kidney hematopoietic tissue. Blood *111*, 1131–1137.

Kobayashi, I., Sekiya, M., Moritomo, T., Ototake, M., and Nakanishi, T. (2006). Demonstration of hematopoietic stem cells in ginbuna carp (Carassius auratus langsdorfii) kidney. Dev. Comp. Immunol. *30*, 1034–1046.

Koch, C.A., Li, C.Y., Mesa, R.A., and Tefferi, A. (2003). Nonhepatosplenic extramedullary hematopoiesis: Associated diseases, pathology, clinical course, and treatment. Mayo Clin. Proc. 78, 1223–1233.

Kondo, M., Scherer, D.C., Miyamoto, T., King, A.G., Akashi, K., Sugamura[2], K., and Weissman, I.L. (2000). Cell-fate conversion of lymphoid-committed progenitors by instructive actions of cytokines.

Kossack, M.E., and Draper, B.W. (2019). Genetic regulation of sex determination and maintenance in zebrafish (Danio rerio). In Current Topics in Developmental Biology, (Academic Press Inc.), pp. 119–149.

Koth, J., Wang, X., Killen, A.C., Stockdale, W.T., Potts, H.G., Jefferson, A., Bonkhofer, F., Riley, P.R., Patient, R.K., Göttgens, B., et al. (2020). Runx1 promotes scar deposition and inhibits myocardial proliferation and survival during zebrafish heart regeneration. Dev. *147*.

Koupenova, M., Vitseva, O., MacKay, C.R., Beaulieu, L.M., Benjamin, E.J., Mick, E., Kurt-Jones, E.A., Ravid, K., and Freedman, J.E. (2014). Platelet-TLR7 mediates host survival and platelet count during viral infection in the absence of platelet-dependent thrombosis. Blood *124*, 791–802.

Krauss, J., Astrinides, P., Frohnhöfer, H.G., Walderich, B., and Nüsslein-Volhard, C. (2013). Transparent, a gene affecting stripe formation in Zebrafish, encodes the mitochondrial protein Mpv17 that is required for iridophore survival. Biol. Open *2*, 703–710.

Kubo, A., Nagao, K., Yokouchi, M., Sasaki, H., and Amagai, M. (2009). External antigen uptake by Langerhans cells with reorganization of epidermal tight junction barriers. J. Exp. Med. *206*, 2937–2946.

Kwarteng, E.O., and Heinonen, K.M. (2016). Competitive transplants to evaluate hematopoietic stem cell fitness. J. Vis. Exp. 2016, 54345.

Lacombe, J., Herblot, S., Rojas-Sutterlin, S., Haman, A., Barakat, S., Iscove, N.N., Sauvageau, G., and Hoang, T. (2010). Scl regulates the quiescence and the long-term competence of hematopoietic stem cells. Blood *115*, 792–803.

Lam, E.Y.N., Chau, J.Y.M., Kalev-Zylinska, M.L., Fountaine, T.M., Mead, R.S., Hall, C.J., Crosier, P.S., Crosier, K.E., and Flores, M.V. (2009). Zebrafish runx1 promoter-EGFP transgenics mark discrete sites of definitive blood progenitors. Blood *113*, 1241–1249.

Lam, E.Y.N., Hall, C.J., Crosier, P.S., Crosier, K.E., and Flores, M.V. (2010). Live imaging of Runx1 expression in the dorsal aorta tracks the emergence of blood progenitors from endothelial cells. Blood *116*, 909–914.

Lam, S.H., Chua, H.L., Gong, Z., Lam, T.J., and Sin, Y.M. (2004). Development and maturation of the immune system in zebrafish, Danio rerio: A gene expression profiling, in situ hybridization and immunological study. Dev. Comp. Immunol. *28*, 9–28.

Langenau, D.M., and Zon, L.I. (2005). The zebrafish: A new model of T-cell and thymic development. Nat. Rev. Immunol. *5*, 307–317.

Langenau, D.M., Ferrando, A.A., Traver, D., Kutok, J.L., Hezel, J.P.D.J.-P.D., Kanki, J.P., Zon, L.I., Look, A.T., Trede, N.S., Thomas Look, A., et al. (2004). In vivo tracking of T cell development, ablation, and engraftment in transgenic zebrafish. Proc. Natl. Acad. Sci. *101*, 7369–7374.

Langenau, D.M., Traver, D., Ferrando, A.A., Kutok, J.L., Aster, J.C., Kanki, J.P., Lin, S., Prochownik, E., Trede, N.S., Zon, L.I., et al. (2003). Myc-induced T cell leukemia in transgenic zebrafish. Science (80-.). *299*, 887–890.

Lawson, N.D., and Weinstein, B.M. (2002). In vivo imaging of embryonic vascular development using transgenic zebrafish. Dev. Biol. *248*, 307–318.Le Page, C., Génin, P., Baines, M.G., and Hiscott, J. (2000). Interferon activation and innate immunity. Rev. Immunogenet. *2*, 374–386.

LeBlanc, J., Bowman, T.V., and Zon, L. (2006). Transplantation of whole kidney marrow in adult zebrafish. J. Vis. Exp. 159.

Lee, A.J., Chen, B., Chew, M. V., Barra, N.G., Shenouda, M.M., Nham, T., van Rooijen, N., Jordana, M., Mossman, K.L., Schreiber, R.D., et al. (2017). Inflammatory monocytes require type I interferon receptor signaling to activate NK cells via IL-18 during a mucosal viral infection. J. Exp. Med. *214*, 1153–1167.

Lee, L.M.J., Seftor, E.A., Bonde, G., Cornell, R.A., and Hendrix, M.J.C. (2005). The fate of human malignant melanoma cells transplanted into zebrafish embryos: Assessment of migration and cell division in the absence of tumor formation. Dev. Dyn. *233*, 1560–1570.

Lefrançais, E., Ortiz-Muñoz, G., Caudrillier, A., Mallavia, B., Liu, F., Sayah, D.M., Thornton, E.E., Headley, M.B., David, T., Coughlin, S.R., et al. (2017). The lung is a site of platelet biogenesis and a reservoir for haematopoietic progenitors. Nature 544, 105–109.

Levanon, D., and Groner, Y. (2004). Structure and regulated expression of mammalian RUNX genes. Oncogene *23*, 4211–4219.

Li, J., Dong, T., Keerthisinghe, T.P., Chen, H., Li, M., Chu, W., Yang, J., Hu, Z., Snyder, S.A., Dong, W., et al. (2020). Long-term oxytetracycline exposure potentially alters brain thyroid hormone and serotonin homeostasis in zebrafish. J. Hazard. Mater. *399*, 123061.

Li, L., Jin, H., Xu, J., Shi, Y., and Wen, Z. (2011). Irf8 regulates macrophage versus neutrophil fate during zebrafish primitive myelopoiesis. Blood *117*, 1359–1369.

Li, L., Yan, B., Shi, Y.Q., Zhang, W.Q., and Wen, Z.L. (2012). Live imaging reveals differing roles of macrophages and neutrophils during zebrafish tail fin regeneration. J. Biol. Chem. *287*, 25353–25360.

Li, P., Ye, J., Zeng, S., and Yang, C. (2019). Florfenicol alleviated lipopolysaccharide (LPS)-induced inflammatory responses in Ctenopharyngodon idella through inhibiting toll / NF-κB signaling pathways. Fish Shellfish Immunol. 94, 479–484.

Li, P., Lahvic, J.L., Binder, V., Pugach, E.K., Riley, E.B., Tamplin, O.J., Panigrahy, D., Bowman, T. V, Barrett, F.G., Heffner, G.C., et al. (2015). Epoxyeicosatrienoic acids enhance embryonic haematopoiesis and adult marrow engraftment. Nature *523*, 468–471.

Li, Y., Li, Y., Cao, X., Jin, X., and Jin, T. (2017). Pattern recognition receptors in zebrafish provide functional and evolutionary insight into innate immune signaling pathways. Cell. Mol. Immunol. *14*, 80–89.

Li, Y., Song, X., Wang, W., Wang, L., Yi, Q., Jiang, S., Jia, Z., Du, X., Qiu, L., and Song, L. (2017). The hematopoiesis in gill and its role in the immune response of Pacific oyster Crassostrea gigas against secondary challenge with Vibrio splendidus. Dev. Comp. Immunol. 71, 59–69.

Liao, W., Bisgrove, B.W., Sawyer, H., Hug, B., Bell, B., Peters, K., Grunwald, D.J., and Stainier, D.Y.R. (1997). The zebrafish gene cloche acts upstream of a flk-1 homologue to regulate endothelial cell differentiation. Development *124*, 381–389.

Lieschke, G.J., Grail, D., Hodgson, G., Metcalf, D., Stanley, E., Cheers, C., Fowler, K.J., Basu, S., Zhan, Y.F., and Dunn, A.R. (1994). Mice lacking granulocyte colony-stimulating factor have chronic neutropenia, granulocyte and macrophage progenitor cell deficiency, and impaired neutrophil mobilization. Blood *84*, 1737–1746.

Lieschke, G.J., Oates, A.C., Paw, B.H., Thompson, M.A., Hall, N.E., Ward, A.C., Ho, R.K., Zon, L.I., and Layton, J.E. (2002). Zebrafish SPI-1 (PU.1) marks a site of myeloid development independent of primitive erythropoiesis: Implications for axial patterning. Dev. Biol. *246*, 274–295.

Liew, W.C., Bartfai, R., Lim, Z., Sreenivasan, R., Siegfried, K.R., and Orban, L. (2012). Polygenic sex determination system in zebrafish. PLoS One *7*.

Liew, W.C., and Orbán, L. (2014). Zebrafish sex: A complicated affair. Brief. Funct. Genomics *13*, 172–187.

Limbu, S.M., Zhou, L., Sun, S.X., Zhang, M.L., and Du, Z.Y. (2018). Chronic exposure to low environmental concentrations and legal aquaculture doses of antibiotics cause systemic adverse effects in Nile tilapia and provoke differential human health risk. Environ. Int. 115, 205–219.

Lin, H.F., Traver, D., Zhu, H., Dooley, K., Paw, B.H., Zon, L.I., and Handin, R.I. (2005). Analysis of thrombocyte development in CD41-GFP transgenic zebrafish. Blood *106*, 3803–3810.

Lin, X., Zhou, Q., Lin, G., Zhao, C., and Wen, Z. (2020). Endoderm-Derived Myeloid-like Metaphocytes in Zebrafish Gill Mediate Soluble Antigen-Induced Immunity. Cell Rep. *33*, 108227.

Lin, X., Zhou, Q., Zhao, C., Lin, G., Xu, J., and Wen, Z. (2019). An Ectoderm-Derived Myeloid-like Cell Population Functions as Antigen Transporters for Langerhans Cells in Zebrafish Epidermis. Dev. Cell *49*, 605-617.e5.

Liongue, C., Hall, C.J., O'Connell, B.A., Crosier, P., and Ward, A.C. (2009). Zebrafish granulocyte colony-stimulating factor receptor signaling promotes myelopoiesis and myeloid cell migration. Blood *113*, 2535–2546.

Lister, J.A., Robertson, C.P., Lepage, T., Johnson, S.L., and Raible, D.W. (1999). Nacre Encodes a Zebrafish Microphthalmia-Related Protein That Regulates Neural-Crest-Derived Pigment Cell Fate. Development *126*, 3757–3767.

Liu, F., and Wen, Z. (2002). Cloning and expression pattern of the lysozyme C gene in zebrafish. Mech. Dev. *113*, 69–72.

Liu, X., Li, Y.-S., Shinton, S.A., Rhodes, J., Tang, L., Feng, H., Jette, C.A., Look, A.T., Hayakawa, K., and Hardy, R.R. (2017). Zebrafish B Cell Development without a Pre–B Cell Stage, Revealed by CD79 Fluorescence Reporter Transgenes. J. Immunol. *199*, 1706–1715.

Livak, K.J., and Schmittgen, T.D. (2001). Analysis of relative gene expression data using real-time quantitative PCR and the 2-ΔΔCT method. Methods *25*, 402–408.

Lo Celso, C., Fleming, H.E., Wu, J.W., Zhao, C.X., Miake-Lye, S., Fujisaki, J., Côté, D., Rowe, D.W., Lin, C.P., and Scadden, D.T. (2009). Live-animal tracking of individual haematopoietic stem/progenitor cells in their niche. Nature *457*, 92–96.

Lobov, I.B., Rao, S., Carroll, T.J., Vallance, J.E., Ito, M., Ondr, J.K., Kurup, S., Glass, D.A., Patel, M.S., Shu, W., et al. (2005). WNT7b mediates macrophage-induced programmed cell death in patterning of the vasculature. Nature *437*, 417–421.

Long, Q., Meng, A., Wang, M., Jessen, J.R., Farrell, M.J., and Lin, S. (1997). GATA-1 expression pattern can be recapitulated in living transgenic zebrafish using GFP reporter gene. Development *124*, 4105–4111.

Lunde, T., and Bylund, G. (2000). The influence of in vitro and in vivo exposure to antibiotics on mitogen-induced proliferation of lymphoid cells in rainbow trout (Oncorhynchus mykiss). Fish Shellfish Immunol. *10*, 395–404.

Lundén, T., Miettinen, S., Lönnström, L.G., Lllius, E.M., and Bylund, G. (1998). Influence of oxytetracycline and oxolinic acid on the immune response of rainbow trout (Oncorhynchus mykiss). Fish Shellfish Immunol. *8*, 217–230.

Lv, P., Ma, D., Gao, S., Zhang, Y., Bae, Y.K., Liang, G., Gao, S., Choi, J.H., Kim, C.H., Wang, L., et al. (2020). Generation of foxn1/Casper Mutant Zebrafish for Allograft and Xenograft of Normal and Malignant Cells. Stem Cell Reports 15, 749–760.

Ma, D., Zhang, J., Lin, H., Italiano, J., and Handin, R.I. (2011). The identification and characterization of zebrafish hematopoietic stem cells. Blood *118*, 289–297.

Macaulay, I.C., Svensson, V., Labalette, C., Ferreira, L., Hamey, F., Voet, T., Teichmann, S.A., and Cvejic, A. (2016). Single-Cell RNA-Sequencing Reveals a Continuous Spectrum of Differentiation in Hematopoietic Cells. Cell Rep. *14*, 966–977.

Manz, M.G., and Boettcher, S. (2014). Emergency granulopoiesis. Nat. Rev. Immunol. *14*, 302–314.

Marjoram, L., Alvers, A., Deerhake, M.E., Bagwell, J., Mankiewicz, J., Cocchiaro, J.L., Beerman, R.W., Willer, J., Sumigray, K.D., Katsanis, N., et al. (2015). Epigenetic control of intestinal barrier function and inflammation in zebrafish. Proc. Natl. Acad. Sci. U. S. A. *112*, 2770–2775.

Martin, P., and Feng, Y. (2009). Inflammation: Wound healing in zebrafish. Nature *459*, 921–923.

Massberg, S., Schaerli, P., Knezevic-Maramica, I., Köllnberger, M., Tubo, N., Moseman, E.A., Huff, I. V, Junt, T., Wagers, A.J., Mazo, I.B., et al. (2007). Immunosurveillance by hematopoietic progenitor cells trafficking through blood, lymph, and peripheral tissues. Cell *131*, 994–1008.

Matsuo, A., Oshiumi, H., Tsujita, T., Mitani, H., Kasai, H., Yoshimizu, M., Matsumoto, M., and Seya, T. (2008). Teleost TLR22 Recognizes RNA Duplex to Induce IFN and Protect Cells from Birnaviruses. J. Immunol. *181*, 3474–3485.

McBrien, M. (2017). The effect of Poly I:C induced inflammation on hematopoietic stem and progenitor cell behavior in the zebrafish hematopoietic transplant model. Imperial College London.

McCabe, A., Zhang, Y., Thai, V., Jones, M., Jordan, M.B., and MacNamara, K.C. (2015). Macrophage-lineage cells negatively regulate the hematopoietic stem cell pool in response to interferon gamma at steady state and during infection. Stem Cells *33*, 2294–2305.

McGrath, K.E., Frame, J.M., Fegan, K.H., Bowen, J.R., Conway, S.J., Catherman, S.C., Kingsley, P.D., Koniski, A.D., and Palis, J. (2015). Distinct Sources of Hematopoietic Progenitors Emerge before HSCs and Provide Functional Blood Cells in the Mammalian Embryo. Cell Rep. *11*, 1892–1904.

McKenna, A., Findlay, G.M., Gagnon, J.A., Horwitz, M.S., Schier, A.F., and Shendure, J. (2016). Whole-organism lineage tracing by combinatorial and cumulative genome editing. Science (80-.). *353*, 9071–11.

Meeker, N.D., and Trede, N.S. (2008). Immunology and zebrafish: Spawning new models of human disease. Dev. Comp. Immunol. *32*, 745–757.

Megías, J., Yáñez, A., Moriano, S., O'Connor, J.E., Gozalbo, D., and Gil, M.L. (2012). Direct toll-like receptor-mediated stimulation of hematopoietic stem and progenitor cells occurs in vivo and promotes differentiation toward macrophages. Stem Cells *30*, 1486–1495.

Mendt, M., and Cardier, J.E. (2015). Role of SDF-1 (CXCL12) in regulating hematopoietic stem and progenitor cells traffic into the liver during extramedullary hematopoiesis induced by G-CSF, AMD3100 and PHZ. Cytokine 76, 214–221.

Metcalf, D., and Moore, M. (1971). Haemopoietic Cells. Front. Biol. 24, 550.

Michaud, J., Wu, F., Osato, M., Cottles, G.M., Yanagida, M., Asou, N., Shigesada, K., Ito, Y., Benson, K.F., Raskind, W.H., et al. (2002). In vitro analyses of known and novel RUNX1/AML1 mutations in dominant familial platelet disorder with predisposition to acute myelogenous leukemia: Implications for mechanisms of pathogenesis. Blood *99*, 1364–1372.

Mizgireuv, I. V, and Revskoy, S.Y. (2006). Transplantable tumor lines generated in clonal zebrafish. Cancer Res. *66*, 3120–3125.

Mohammed, H.H., and Arias, C.R. (2015). Potassium permanganate elicits a shift of the external fish microbiome and increases host susceptibility to columnaris disease. Vet. Res. *46*.

Morrison, S.J., and Weissman, I.L. (1994). The long-term repopulating subset of hematopoietic stem cells is deterministic and isolatable by phenotype. Immunity *1*, 661–673.

Mosimann, C., Kaufman, C.K., Li, P., Pugach, E.K., Tamplin, O.J., and Zon, L.I. (2011). Ubiquitous transgene expression and Cre-based recombination driven by the ubiquitin promoter in zebrafish. Development *138*, 169–177.

Moss, L.D., Monette, M.M., Jaso-Friedmann, L., Leary, J.H., Dougan, S.T., Krunkosky, T., and Evans, D.L. (2009). Identification of phagocytic cells, NK-like cytotoxic cell activity and the production of cellular exudates in the coelomic cavity of adult zebrafish. Dev. Comp. Immunol. *33*, 1077–1087.

Murayama, E., Kissa, K., Zapata, A., Mordelet, E., Briolat, V., Lin, H.F., Handin, R.I., and Herbomel, P. (2006). Tracing Hematopoietic Precursor Migration to Successive Hematopoietic Organs during Zebrafish Development. Immunity *25*, 963–975.

Nagai, Y., Garrett, K.P., Ohta, S., Bahrun, U., Kouro, T., Akira, S., Takatsu, K., and Kincade, P.W. (2006). Toll-like Receptors on Hematopoietic Progenitor Cells Stimulate Innate Immune System Replenishment. Immunity *24*, 801–812.

Nefedochkina, A. V., Petrova, N. V., Ioudinkova, E.S., Kovina, A.P., Iarovaia, O. V., and Razin, S. V. (2016). Characterization of the enhancer element of the Danio rerio minor globin gene locus. Histochem. Cell Biol. *145*, 463–473.

Neftel, K.A., Hauser, S.P., and Muller, M.R. (1985). Inhibition of granulopoiesis in vivo and in vitro by β-lactam antibiotics. J. Infect. Dis. *152*, 90–98.

Ng, A.P., and Alexander, W.S. (2017). Haematopoietic stem cells: past, present and future. Cell Death Discov. *3*, 17002.

Ng, C.E.L., Yokomizo, T., Yamashita, N., Cirovic, B., Jin, H., Wen, Z., Ito, Y., and Osato, M. (2010). A Runx1 Intronic Enhancer Marks Hemogenic Endothelial Cells and Hematopoietic Stem Cells. Stem Cells *28*, 1869–1881.

Nguyen-Chi, M., Laplace-Builhé, B., Travnickova, J., Luz-Crawford, P., Tejedor, G., Lutfalla, G., Kissa, K., Jorgensen, C., and Djouad, F. (2017). TNF signaling and macrophages govern fin regeneration in zebrafish larvae. Cell Death Dis. *8*, e2979.

Nguyen-Chi, M., Laplace-Builhe, B., Travnickova, J., Luz-Crawford, P., Tejedor, G., Phan, Q.T., Duroux-Richard, I., Levraud, J.P., Kissa, K., Lutfalla, G., et al. (2015). Identification of polarized macrophage subsets in zebrafish. Elife *4*, 1–14.

Niebuhr, B., Kriebitzsch, N., Fischer, M., Behrens, K., Günther, T., Alawi, M., Bergholz, U., Müller, U., Roscher, S., Ziegler, M., et al. (2013). Runx1 is essential at two stages of early murine B cell development. Blood *122*, 413–423.

Niess, J.H., Brand, S., Gu, X., Landsman, L., Jung, S., McCormick, B.A., Vyas, J.M., Boes, M., Ploegh, H.L., Fox, J.G., et al. (2005). CX3CR1-mediated dendritic cell access to the intestinal lumen and bacterial clearance. Science (80-.). *307*, 254–258.

Niethammer, P., Grabher, C., Look, A.T., and Mitchison, T.J. (2009). A tissue-scale gradient of hydrogen peroxide mediates rapid wound detection in zebrafish. Nature *459*, 996–999.

North, T.E., Goessling, W., Walkley, C.R., Lengerke, C., Kopani, K.R., Lord, A.M., Weber, G.J., Bowman, T. V, Jang, I.-H., Grosser, T., et al. (2007). Prostaglandin E2 regulates vertebrate haematopoietic stem cell homeostasis. Nature *447*, 1007–1011.

Notta, F., Doulatov, S., Laurenti, E., Poeppl, A., Jurisica, I., and Dick, J.E. (2011). Isolation of Single Human Hematopoietic. Science (80-.). *333*, 218–222.

Nottingham, W.T., Jarratt, A., Burgess, M., Speck, C.L., Cheng, J.F., Prabhakar, S., Rubin, E.M., Li, P.S., Sloane-Stanley, J., Kong-A-San, J., et al. (2007). Runx1-mediated hematopoietic stem-cell emergence is controlled by a Gata/Ets/SCL-regulated enhancer. Blood *110*, 4188–4197.

Ogata, K., Morikawa, S., Nakamura, H., Sekikawa, A., Inoue, T., Kanai, H., Sarai, A., Ishii, S., and Nishimura, Y. (1994). Solution structure of a specific DNA complex of the Myb DNA-binding domain with cooperative recognition helices. Cell *79*, 639–648.

Olaison, L., Belin, L., Hogevik, H., and Alestig, K. (1999). Incidence of β-lactam-induced delayed hypersensitivity and neutropenia during treatment of infective endocarditis. Arch. Intern. Med. *159*, 607–615.

Oliveira, R., McDonough, S., Ladewig, J.C.L., Soares, A.M.V.M., Nogueira, A.J.A., and Domingues, I. (2013). Effects of oxytetracycline and amoxicillin on development and biomarkers activities of zebrafish (Danio rerio). Environ. Toxicol. Pharmacol. *36*, 903–912.

Olivo-Marin, J.C. (2002). Extraction of spots in biological images using multiscale products. Pattern Recognit. *35*, 1989–1996.

Olson, K.R. (2002). Vascular anatomy of the fish gill. In Journal of Experimental Zoology, (John Wiley & Sons, Ltd), pp. 214–231.

Osawa, M., Hanada, K.I., Hamada, H., and Nakauchi, H. (1996). Long-term lymphohematopoietic reconstitution by a single CD34- low/negative hematopoietic stem cell. Science (80-.). *273*, 242–245.

Page, D.M., Wittamer, V., Bertrand, J.Y., Lewis, K.L., Pratt, D.N., Delgado, N., Schale, S.E., McGue, C., Jacobsen, B.H., Doty, A., et al. (2013). An evolutionarily conserved program of B-cell development and activation in zebrafish. Blood *122*, 1–12.

Palti, Y., Gahr, S.A., Purcell, M.K., Hadidi, S., Rexroad, C.E., and Wiens, G.D. (2010). Identification, characterization and genetic mapping of TLR7, TLR8a1 and TLR8a2 genes in rainbow trout (Oncorhynchus mykiss). Dev. Comp. Immunol. *34*, 219–233.

Pan, Y.A., Freundlich, T., Weissman, T. a, Schoppik, D., Wang, X.C., Zimmerman, S., Ciruna, B., Sanes, J.R., Lichtman, J.W., and Schier, A.F. (2013). Zebrabow: multispectral cell labeling for cell tracing and lineage analysis in zebrafish. Development *140*, 2835–2846.

Pase, L., Layton, J.E., Wittmann, C., Ellett, F., Nowell, C.J., Reyes-Aldasoro, C.C., Varma, S., Rogers, K.L., Hall, C.J., Keightley, M.C., et al. (2012). Neutrophil-delivered myeloperoxidase dampens the hydrogen peroxide burst after tissue wounding in zebrafish. Curr. Biol. *22*, 1818–1824.

Passegué, E., Wagers, A.J., Giuriato, S., Anderson, W.C., and Weissman, I.L. (2005). Global analysis of proliferation and cell cycle gene expression in the regulation of hematopoietic stem and progenitor cell fates. J. Exp. Med. *202*, 1599–1611.

Patterson, L.J., Gering, M., Eckfeldt, C.E., Green, A.R., Verfaillie, C.M., Ekker, S.C., and Patient, R. (2007). The transcription factors Scl and Lmo2 act together during development of the hemangioblast in zebrafish. Blood *109*, 2389–2398.

Pei, W., Feyerabend, T.B., Rössler, J., Wang, X., Postrach, D., Busch, K., Rode, I., Klapproth, K., Dietlein, N., Quedenau, C., et al. (2017). Polylox barcoding reveals haematopoietic stem cell fates realized in vivo. Nature 548, 456–460.

Pellin, D., Loperfido, M., Baricordi, C., Wolock, S.L., Montepeloso, A., Weinberg, O.K., Biffi, A., Klein, A.M., and Biasco, L. (2019). A comprehensive single cell transcriptional landscape of human hematopoietic progenitors. Nat. Commun. *10*.

Pereiro, P., Varela, M., Diaz-Rosales, P., Romero, A., Dios, S., Figueras, A., and Novoa, B. (2015). Zebrafish Nk-lysins: First insights about their cellular and functional diversification. Dev. Comp. Immunol. *51*, 148–159.

Petit, I., Ponomaryov, T., Zipori, D., and Tsvee, L. (2002). G-CSF induces stem cell mobilization by decreasing bone marrow SDF-1 and up-regulating CXCR4. Nat. Immunol. *3*, 687–694.

Petrie, T.A., Strand, N.S., Yang, C.-T., Rabinowitz, J.S., and Moon, R.T. (2015). Macrophages modulate adult zebrafish tail fin regeneration. Development *142*, 406–406.

Pietras, E.M., Lakshminarasimhan, R., Techner, J.M., Fong, S., Flach, J., Binnewies, M., and Passegué, E. (2014). Re-entry into quiescence protects hematopoietic stem cells from the killing effect of chronic exposure to type I interferons. J. Exp. Med. *211*, 245–262.

Pietras, E.M., Mirantes-Barbeito, C., Fong, S., Loeffler, D., Kovtonyuk, L. V., Zhang, S., Lakshminarasimhan, R., Chin, C.P., Techner, J.-M., Will, B., et al. (2016). Chronic interleukin-1 exposure drives haematopoietic stem cells towards precocious myeloid differentiation at the expense of self-renewal. Nat. Cell Biol. *18*, 607–618.

Pinho, S., Marchand, T., Yang, E., Wei, Q., Nerlov, C., and Frenette, P.S. (2018). Lineage-Biased Hematopoietic Stem Cells Are Regulated by Distinct Niches. Dev. Cell *44*, 634-641.e4.

Ponomaryov, T., Peled, A., Petit, I., Taichman, R.S., Habler, L., Sandbank, J., Arenzana-Seisdedos, F., Magerus, A., Caruz, A., Fujii, N., et al. (2000). Induction of the chemokine stromal-derived factor-1 following DNA damage improves human stem cell function. J. Clin. Invest. *106*, 1331–1339.

Prise, K.M., Schettino, G., Folkard, M., and Held, K.D. (2005). New insights on cell death from radiation exposure. Lancet Oncol. *6*, 520–528.

Progatzky, F., Jha, A., Wane, M., Thwaites, R.S., Makris, S., Shattock, R.J., Johansson, C., Openshaw, P.J., Bugeon, L., Hansel, T.T., et al. (2019). Induction of innate cytokine responses by respiratory mucosal challenge with R848 in zebrafish, mice, and humans. J. Allergy Clin. Immunol. *144*, 342-345.e7.

Progatzky, F., Sangha, N.J., Yoshida, N., McBrien, M., Cheung, J., Shia, A., Scott, J., Marchesi, J.R., Lamb, J.R., Bugeon, L., et al. (2014). Dietary cholesterol directly induces acute inflammasome-dependent intestinal inflammation. Nat. Commun. *5*, 5864.

Progatzky, F., Terence Cook, H., Lamb, J.R., Bugeon, L., and Dallman, M.J. (2016). Mucosal inflammation at the respiratory interface: A zebrafish model. Am. J. Physiol. - Lung Cell. Mol. Physiol. *310*, L551–L561.

Pugach, E.K., Li, P., White, R., and Zon, L. (2010). Retro-orbital injection in adult zebrafish. J. Vis. Exp. e1645–e1645.

Purcell, M.K., Smith, K.D., Aderem, A., Hood, L., Winton, J.R., and Roach, J.C. (2006). Conservation of Toll-like receptor signaling pathways in teleost fish. Comp. Biochem. Physiol. - Part D Genomics Proteomics *1*, 77–88.

Qi, W. (2002). Social and economic impacts of aquatic animal health problems in aquaculture in China. FAO Fish. Tech. Pap. *2*, 55–61.

Qin, Y., Fang, K., Lu, N., Hu, Y., Tian, Z., and Zhang, C. (2019). Interferon gamma inhibits the differentiation of mouse adult liver and bone marrow hematopoietic stem cells by inhibiting the activation of notch signaling. Stem Cell Res. Ther. *10*, 1–16.

Quesenberry, P.J., Goldberg, L., Aliotta, J., and Dooner, M. (2014). Marrow hematopoietic stem cells revisited: They exist in a continuum and are not defined by standard purification approaches; then there are the microvesicles. Front. Oncol. *4 APR*.

Qureshi, S.T., Larivière, L., Leveque, G., Clermont, S., Moore, K.J., Gros, P., and Malo, D. (1999). Endotoxin-tolerant mice have mutations in toll-like receptor 4 (Tlr4). J. Exp. Med. *189*, 615–625.

Rajan, V., Melong, N., Wong, W.H., King, B., Tong, R.S., Mahajan, N., Gaston, D., Lund, T., Rittenberg, D., Dellaire, G., et al. (2019). Humanized zebrafish enhance human hematopoietic stem cell survival and promote acute myeloid leukemia clonal diversity. Haematologica haematol.2019.223040.

Ransom, D.G., Haffter, P., Odenthal, J., Brownlie, A., Vogelsang, E., Kelsh, R.N., Brand, M., Van Eeden, F.J.M., Furutani-Seiki, M., Granato, M., et al. (1996). Characterization of zebrafish mutants with defects in embryonic hematopoiesis. Development *123*, 311–319.

Reid, K.M., Patel, S., Robinson, A.J., Bu, L., Jarungsriapisit, J., Moore, L.J., and Salinas, I. (2017). Salmonid alphavirus infection causes skin dysbiosis in Atlantic salmon (Salmo salar L.) post-smolts. PLoS One *12*.

Reischauer, S., Stone, O.A., Villasenor, A., Chi, N., Jin, S.-W., Martin, M., Lee, M.T., Fukuda, N., Marass, M., Witty, A., et al. (2016). Cloche is a bHLH-PAS transcription factor that drives haemato-vascular specification. Nature *535*, 294–298.

Renshaw, S.A., Loynes, C.A., Trushell, D.M.I., Elworthy, S., Ingham, P.W., and Whyte, M.K.B. (2006). A transgenic zebrafish model of neutrophilic inflammation. Blood *108*, 3976–3978.

Renshaw, S.A., and Trede, N.S. (2012). A model 450 million years in the making: Zebrafish and vertebrate immunity. DMM Dis. Model. Mech. *5*, 38–47.

Rgen Adolfsson, J., Borge, O.J., Bryder, D., Theilgaard-Mö, K., Strand-Grundströ, I.A.˚, Sitnicka, E., Sasaki, Y., and Jacobsen, S.E.W. (2001). Sweden 2 The Granulocyte Research Laboratory Dao et al (Miller and Eaves).

Rhodes, J., Hagen, A., Hsu, K., Deng, M., Liu, T.X., Look, A.T., and Kanki, J.P. (2005). Interplay of pu.1 and Gata1 determines myelo-erythroid progenitor cell fate in zebrafish. Dev. Cell *8*, 97–108.

Rodrigues, S., Antunes, S.C.C., Nunes, B., and Correia, A.T.T. (2017). Histological alterations in gills and liver of rainbow trout (Oncorhynchus mykiss) after exposure to the antibiotic oxytetracycline. Environ. Toxicol. Pharmacol. *53*, 164–176.

Rodrigues, S., Antunes, S.C., Nunes, B., and Correia, A.T. (2019). Histopathological effects of the antibiotic erythromycin on the freshwater fish species Oncorhynchus mykiss. Ecotoxicol. Environ. Saf. *181*, 1–10.

Rombough, P. (2007). The functional ontogeny of the teleost gill: Which comes first, gas or ion exchange? Comp. Biochem. Physiol. - A Mol. Integr. Physiol. 148, 732–742.

Rosado, D., Xavier, R., Severino, R., Tavares, F., Cable, J., and Pérez-Losada, M. (2019). Effects of disease, antibiotic treatment and recovery trajectory on the microbiome of farmed seabass (Dicentrarchus labrax). Sci. Rep. *9*, 1–11.

Rossi, L., Manfredini, R., Bertolini, F., Ferrari, D., Fogli, M., Zini, R., Salati, S., Salvestrini, V., Gulinelli, S., Adinolfi, E., et al. (2007). The extracellular nucleotide UTP is a potent inducer of hematopoietic stem cell migration. Blood *109*, 533–542.Round, J.L., and Mazmanian, S.K. (2009). The gut microbiota shapes intestinal immune responses during health and disease. Nat. Rev. Immunol. *9*, 313–323.

Rueden, C.T., Schindelin, J., Hiner, M.C., DeZonia, B.E., Walter, A.E., Arena, E.T., and Eliceiri, K.W. (2017). ImageJ2: ImageJ for the next generation of scientific image data. BMC Bioinformatics *18*.

Ryo, S., Wijdeven, R.H.M., Tyagi, A., Hermsen, T., Kono, T., Karunasagar, I., Rombout, J.H.W.M., Sakai, M., Kemenade, B.M.L.V. van, and Savan, R. (2010). Common carp have two subclasses of bonyfish specific antibody IgZ showing differential expression in response to infection. Dev. Comp. Immunol. *34*, 1183–1190.

Santos, L., and Ramos, F. (2018). Antimicrobial resistance in aquaculture: Current knowledge and alternatives to tackle the problem. Int. J. Antimicrob. Agents *52*, 135–143.

Sato, T., Onai, N., Yoshihara, H., Arai, F., Suda, T., and Ohteki, T. (2009). Interferon regulatory factor-2 protects quiescent hematopoietic stem cells from type i interferon-dependent exhaustion. Nat. Med. *15*, 696–700.

Schajnovitz, A., Itkin, T., D'Uva, G., Kalinkovich, A., Golan, K., Ludin, A., Cohen, D., Shulman, Z., Avigdor, A., Nagler, A., et al. (2011). CXCL12 secretion by bone marrow stromal cells is dependent on cell contact and mediated by connexin-43 and connexin-45 gap junctions. Nat. Immunol. *12*, 391–398.

Scharenberg, C.W., Harkey, M.A., and Torok-Storb, B. (2002). The ABCG2 transporter is an efficient Hoechst 33342 efflux pump and is preferentially expressed by immature human hematopoietic progenitors. Blood *99*, 507–512.

Schindelin, J., Arganda-Carreras, I., Frise, E., Kaynig, V., Longair, M., Pietzsch, T., Preibisch, S., Rueden, C., Saalfeld, S., Schmid, B., et al. (2012). Fiji: An open-source platform for biological-image analysis. Nat. Methods *9*, 676–682.

Schoenborn, J.R., and Wilson, C.B. (2007). Regulation of Interferon-γ During Innate and Adaptive Immune Responses. Adv. Immunol. *96*, 41–101.

Schroder, K., Hertzog, P.J., Ravasi, T., and Hume, D.A. (2004). Interferon-γ: an overview of signals, mechanisms and functions. J. Leukoc. Biol. *75*, 163–189.

Schuettpelz, L.G., Borgerding, J.N., Christopher, M.J., Gopalan, P.K., Romine, M.P., Herman, A.C., Woloszynek, J.R., Greenbaum, A.M., and Link, D.C. (2014). G-CSF regulates hematopoietic stem cell activity, in part, through activation of Toll-like receptor signaling. Leukemia *28*, 1851–1860.

Schulz, C., Perdiguero, E.G., Chorro, L., Szabo-Rogers, H., Cagnard, N., Kierdorf, K., Prinz, M., Wu, B., Jacobsen, S.E.W., Pollard, J.W., et al. (2012). A lineage of myeloid cells independent of myb and hematopoietic stem cells. Science (80-.). *335*, 86–90.

Schürch, C.M., Riether, C., and Ochsenbein, A.F. (2014). Cytotoxic CD8+ T cells stimulate hematopoietic progenitors by promoting cytokine release from bone marrow mesenchymal stromal cells. Cell Stem Cell *14*, 460–472.

Serezli, R., Çağirgan, H., Okumuş, I., Akhan, S., and Balta, F. (2005). The effect of oxytetracycline on non-specific immune response in sea bream (Sparus aurata L. 1758). Turkish J. Vet. Anim. Sci. 29, 31–35.

Shimazaki, C., Sumikuma, T., and Inaba, T. (2004). CD34+ CD90+ cells and late hematopoietic reconstitution after autologous peripheral blood stem cell transplantation. Leuk. Lymphoma *45*, 661–668.

Shimoto, M., Sugiyama, T., and Nagasawa, T. (2017). Numerous niches for hematopoietic stem cells remain empty during homeostasis. Blood 129, 2124–2131.

Shin, J.Y., Hu, W., Naramura, M., and Park, C.Y. (2014). High c-Kit expression identifies hematopoietic stem cells with impaired self-renewal and megakaryocytic bias. J. Exp. Med. *211*, 217–231.

Sioud, M., Fløisand, Y., Forfang, L., and Lund-Johansen, F. (2006). Signaling through Toll-like Receptor 7/8 Induces the Differentiation of Human Bone Marrow CD34+ Progenitor Cells along the Myeloid Lineage. J. Mol. Biol. *364*, 945–954.

Smith, A.C.H., Raimondi, A.R., Salthouse, C.D., Ignatius, M.S., Blackburn, J.S., Mizgirev, I. V., Storer, N.Y., De Jong, J.L.O., Chen, A.T., Zhou, Y., et al. (2010). High-throughput cell

transplantation establishes that tumor-initiating cells are abundant in zebrafish T-cell acute lymphoblastic leukemia. Blood *115*, 3296–3303.

Snoeck, H.W., Bockstaele, D.R.V., Nys, G., Lenjou, M., Lardon, F., Haenen, L., Odrigus, I.R., Peetermans, M.E., and Berneman, Z.N. (1994). Interferon γ selectively inhibits very primitive CD342+ CD38− and not more mature CD34+ CD38+ human hematopoietic progenitor cells. J. Exp. Med. *180*, 1177–1182.

Song, X., Song, Y., Dong, M., Liu, Z., Wang, W., Wang, L., and Song, L. (2019). A new member of the runt domain family from Pacific oyster Crassostrea gigas (CgRunx) potentially involved in immune response and larvae hematopoiesis. Fish Shellfish Immunol. 89, 228–236.

Sood, R., English, M.A., Belele, C.L., Jin, H., Bishop, K., Haskins, R., McKinney, M.C., Chahal, J., Weinstein, B.M., Wen, Z., et al. (2010). Development of multilineage adult hematopoiesis in the zebrafish with a runx1 truncation mutation. Blood *115*, 2806–2809.

Soza-ried, C., Hess, I., Netuschil, N., Schorpp, M., and Boehm, T. (2010). Essential role of c-myb in de fi nitive hematopoiesis is evolutionarily conserved. Pnas *107*, 17304–17308.

Spangrude, G.J., Heimfeld, S., and Weissman, I.L. (1988). Hematopoietic Stem. Science (80-.). 58–62.Speck, N.A., and Gilliland, D.G. (2002). Core-binding factors in haematopoiesis and leukaemia. Nat. Rev. Cancer *2*, 502–513.

Speck, N.A., and Gilliland, D.G. (2002). Core-binding factors in haematopoiesis and leukaemia. Nat. Rev. Cancer 2, 502–513.

Speer, E.M., Dowling, D.J., Xu, J., Ozog, L.S., Mathew, J.A., Chander, A., Yin, D., and Levy, O. (2018). Pentoxifylline, dexamethasone and azithromycin demonstrate distinct age-dependent and synergistic inhibition of TLR- and inflammasome-mediated cytokine production in human newborn and adult blood in vitro. PLoS One 13.

Stachura, D.L., Svoboda, O., Campbell, C.A., Espín-Palazón, R., Lau, R.P., Zon, L.I., Bartůněk, P., and Traver, D. (2013). The zebrafish granulocyte colony-stimulating factors (Gcsfs): 2 Paralogous cytokines and their roles in hematopoietic development and maintenance. Blood *122*, 3918–3928.

Stainier, D.Y.R., Weinstein, B.M., Detrich, H.W., Zon, L.I., and Fishman, M.C. (1995). Cloche, an Early Acting Zebrafish Gene, Is Required by Both the Endothelial and Hematopoietic Lineages. Development *121*, 3141–3150.

Sugiyama, T., Kohara, H., Noda, M., and Nagasawa, T. (2006). Maintenance of the Hematopoietic Stem Cell Pool by CXCL12-CXCR4 Chemokine Signalling in Bone Marrow Stromal Cell Niches. Immunity *25*, 977–988.Sültmann, H., Mayer, W.E., Figueroa, F., O'Huigin, C., and Klein, J. (1994). Organization of mhc class ii b genes in the zebrafish (brachydanio rerio). Genomics *23*, 1–14.

Sültmann, H., Mayer, W.E., Figueroa, F., O'Huigin, C., and Klein, J. (1994). Organization of mhc class ii b genes in the zebrafish (brachydanio rerio). Genomics 23, 1–14.

Sun, J., Ramos, A., Chapman, B., Johnnidis, J.B., Le, L., Ho, Y.J., Klein, A., Hofmann, O., and Camargo, F.D. (2014). Clonal dynamics of native haematopoiesis. Nature 514, 322–327.

Svingerud, T., Solstad, T., Sun, B., Nyrud, M.L.J., Kileng, Ø., Greiner-Tollersrud, L., and Robertsen, B. (2012). Atlantic Salmon Type I IFN Subtypes Show Differences in Antiviral Activity and Cell-Dependent Expression: Evidence for High IFNb/IFNc–Producing Cells in Fish Lymphoid Tissues. J. Immunol. *189*, 5912–5923.

Takeuchi, O., Hoshino, K., Kawai, T., Sanjo, H., Takada, H., Ogawa, T., Takeda, K., and Akira, S. (1999). Differential roles of TLR2 and TLR4 in recognition of gram-negative and gram-positive bacterial cell wall components. Immunity *11*, 443–451.

Takizawa, H., Boettcher, S., and Manz, M.G. (2012). Demand-adapted regulation of early hematopoiesis in infection and inflammation. Blood *119*, 2991–3002.

Takizawa, H., Fritsch, K., Kovtonyuk, L. V., Saito, Y., Yakkala, C., Jacobs, K., Ahuja, A.K., Lopes, M., Hausmann, A., Hardt, W.D., et al. (2017). Pathogen-Induced TLR4-TRIF Innate Immune Signaling in Hematopoietic Stem Cells Promotes Proliferation but Reduces Competitive Fitness. Cell Stem Cell *21*, 225-240.e5.

Takizawa, H., and Manz, M.G. (2017). Impact of inflammation on early hematopoiesis and the microenvironment. Int. J. Hematol.

Takizawa, H., Regoes, R.R., Boddupalli, C.S., Bonhoeffer, S., and Manz, M.G. (2011). Dynamic variation in cycling of hematopoietic stem cells in steady state and inflammation. J. Exp. Med. *208*, 273–284.

Tamplin, O.J., Durand, E.M., Carr, L.A., Childs, S.J., Hagedorn, E.J., Li, P., Yzaguirre, A.D., Speck, N.A., and Zon, L.I. (2015). Hematopoietic stem cell arrival triggers dynamic remodeling of the perivascular niche. Cell *160*, 241–252.

Tang, Q., Iyer, S., Lobbardi, R., Moore, J.C., Chen, H., Lareau, C., Hebert, C., Shaw, M.L., Neftel, C., Suva, M.L., et al. (2017). Dissecting hematopoietic and renal cell heterogeneity in adult zebrafish at single-cell resolution using RNA sequencing. J. Exp. Med. *214*, 2875–2887.

Tate, M.D., Brooks, A.G., and Reading, P.C. (2008). The role of neutrophils in the upper and lower respiratory tract during influenza virus infection of mice. Respir. Res. *9*.

Taur, Y., Jenq, R.R., Perales, M.A., Littmann, E.R., Morjaria, S., Ling, L., No, D., Gobourne, A., Viale, A., Dahi, P.B., et al. (2014). The effects of intestinal tract bacterial diversity on mortality following allogeneic hematopoietic stem cell transplantation. Blood *124*, 1174–1182.

Temmink, J.H.M., and Bayne, C.J. (1987). Ultrastructural characterization of leucocytes in the pronephros of carp (Cyprinus carpio, L.). Dev. Comp. Immunol. *11*, 125–137.

Terstappen, L., Huang, S., Safford, M., Lansdorp, P., and Loken, M. (1991). Sequential generations of hematopoietic colonies derived from single nonlineage-committed CD34+CD38- progenitor cells. Blood *77*, 1218–1227.

Thorén, L.A., Liuba, K., Bryder, D., Nygren, J.M., Jensen, C.T., Qian, H., Antonchuk, J., and Jacobsen, S.-E.W. (2008). Kit Regulates Maintenance of Quiescent Hematopoietic Stem Cells. J. Immunol. *180*, 2045–2053.

Tiedke, J., Gerlach, F., Mitz, S.A., Hankeln, T., and Burmester, T. (2011). Ontogeny of globin expression in zebrafish (Danio rerio). J. Comp. Physiol. B Biochem. Syst. Environ. Physiol. *181*, 1011–1021.

Till, J.E., and McCulloch, E.A. (1961). A direct measurement of the radiation sensitivity of normal mouse bone marrow cells. Radiat. Res. *14*, 213–222.

Tilley, C.A., Carreño Gutierrez, H., Sebire, M., Obasaju, O., Reichmann, F., Katsiadaki, I., Barber, I., and Norton, W.H.J. (2020). Skin swabbing is a refined technique to collect DNA from model fish species. Sci. Reports 2020 101 10, 1–17.

Tinevez, J.Y., Perry, N., Schindelin, J., Hoopes, G.M., Reynolds, G.D., Laplantine, E., Bednarek, S.Y., Shorte, S.L., and Eliceiri, K.W. (2017). TrackMate: An open and extensible platform for single-particle tracking. Methods *115*, 80–90.

Traver, D., Paw, B.H., Poss, K.D., Penberthy, W.T., Lin, S., and Zon, L.I. (2003). Transplantation and in vivo imaging of multilineage engraftment in zebrafish bloodless mutants. Nat. Immunol. *4*, 1238–1246.

Traver, D., Winzeler, A., Stern, H.M., Mayhall, E.A., Langenau, D.M., Kutok, J.L., Look, A.T., and Zon, L.I. (2004). Effects of lethal irradiation in zebrafish and rescue by hematopoietic cell transplantation. Blood *104*, 1298–1305.

Trede, N.S., Zapata, A., and Zon, L.I. (2001). Fishing for lymphoid genes. Trends Immunol. *22*, 302–307.

Tsinkalovsky, O., Vik-Mo, A.O., Ferreira, S., Laerum, O.D., and Fjose, A. (2007). Zebrafish kidney marrow contains ABCG2-dependent side population cells exhibiting hematopoietic stem cell properties. Differentiation *75*, 175–183.

Van Rooijen, E., Voest, E.E., Logister, I., Korving, J., Schwerte, T., Schulte-Merker, S., Giles, R.H., and Van Eeden, F.J. (2009). Zebrafish mutants in the von Hippel-Lindau tumor suppressor display a hypoxic response and recapitulate key aspects of Chuvash polycythemia. Blood 113, 6449–6460.

Velten, L., Haas, S.F., Raffel, S., Blaszkiewicz, S., Islam, S., Hennig, B.P., Hirche, C., Lutz, C., Buss, E.C., Nowak, D., et al. (2017). Human haematopoietic stem cell lineage commitment is a continuous process. Nat. Cell Biol. *19*, 271–281.

Verfaillie, C., Blakolmer, K., and McGlave, P. (1990). Purified primitive human hematopoietic progenitor cells with longterm in vitro repopulating capacity adhere selectively to irradiated bone marrow stroma. J. Exp. Med. *172*, 509–520.

Vogeli, K.M., Jin, S.W., Martin, G.R., and Stainier, D.Y.R. (2006). A common progenitor for haematopoietic and endothelial lineages in the zebrafish gastrula. Nature *443*, 337–339.

Voils, S.A., Evans, M.E., Lane, M.T., Schosser, R.H., and Rapp, R.P. (2005). Use of macrolides and tetracyclines for chronic inflammatory diseases. Ann. Pharmacother. 39, 86–94.

von Hofsten, J., and Olsson, P.E. (2005). Zebrafish sex determination and differentiation: Involvement of FTZ-F1 genes. Reprod. Biol. Endocrinol. *3*, 63.

Walker, C., Walsh, G.S., and Moens, C. (2009). Making gynogenetic diploid zebrafish by early pressure. J. Vis. Exp. 1396.

Walton, E.M., Cronan, M.R., Beerman, R.W., and Tobin, D.M. (2015). The macrophage-specific promoter mfap4 allows live, long-term analysis of macrophage behavior during mycobacterial infection in zebrafish. PLoS One *10*.

Wane, M. (2021). Investigation of zebrafish gills as a model to study respiratory immunology. Imperial College London.

Wang, H., Wang, N., Wang, B., Fang, H., Fu, C., Tang, C., Jiang, F., Zhou, Y., He, G., Zhao, Q., et al. (2016). Antibiotics detected in urines and adipogenesis in school children. Environ. Int. *89–90*, 204–211.

Wang, X., Dong, F., Zhang, S., Yang, W., Yu, W., Wang, Z., Zhang, S., Wang, J., Ma, S., Wu, P., et al. (2018). TGF-β1 Negatively Regulates the Number and Function of Hematopoietic Stem Cells. Stem Cell Reports *11*, 274–287.

Warga, R.M., Kane, D.A., and Ho, R.K. (2009). Fate Mapping Embryonic Blood in Zebrafish: Multi- and Unipotential Lineages Are Segregated at Gastrulation. Dev. Cell *16*, 744–755.

Weidinger, G., Grotek, B., and Wehner, D. (2013). Notch signaling coordinates cellular proliferation with differentiation during zebrafish fin regeneration. Dev. *140*, 1412–1423.

Weinstein, B.M., Schier, A.F., Abdelilah, S., Malicki, J., Solnica-Krezel, L., Stemple, D.L., Stainier, D.Y.R., Zwartkruis, F., Driever, W., and Fishman, M.C. (1996). Hematopoietic mutations in the zebrafish. Development *123*, 303–309.

Wenz, R., Conibear, E., Bugeon, L., and Dallman, M. (2020). Fast, easy and early (larval) identification of transparent mutant zebrafish using standard fluorescence microscopy. F1000Research *9*, 963.

White, R.M., Sessa, A., Burke, C., Bowman, T., LeBlanc, J., Ceol, C., Bourque, C., Dovey, M., Goessling, W., Burns, C.E., et al. (2008). Transparent Adult Zebrafish as a Tool for In Vivo Transplantation Analysis. Cell Stem Cell *2*, 183–189.

Willis, A.R., Torraca, V., Gomes, M.C., Shelley, J., Mazon-Moya, M., Filloux, A., Lo Celso, C., and Mostowy, S. (2018). Shigella-induced emergency granulopoiesis protects Zebrafish Larvae from secondary infection. MBio *9*, 1–10.

Wilson, A., Laurenti, E., Oser, G., Wath, R.C. Van Der, Blanco-Bose, W., Jaworski, M., Macdonald, H.R., Offner, S., Dunant, C.F., Eshkind, L., et al. (2008). Hematopoietic Stem Cells Reversibly Switch from Dormancy to Self-Renewal during Homeostasis and Repair. Cell *135*, 1118–1129.

Wilson, A., Oser, G.M., Jaworski, M., Blanco-Bose, W.E., Laurenti, E., Adolphe, C., Essers, M.A., Macdonald, H.R., and Trumpp, A. (2007). Dormant and self-renewing hematopoietic stem cells and their niches. Ann. N. Y. Acad. Sci. *1106*, 64–75.

Wittamer, V., Bertrand, J.Y., Gutschow, P.W., and Traver, D. (2011). Characterization of the mononuclear phagocyte system in zebrafish. Blood *117*, 7126–7135.

Xie, H., Ye, M., Feng, R., and Graf, T. (2004). Stepwise reprogramming of B cells into macrophages. Cell *117*, 663–676.

Xu, J., Wang, T., Wu, Y., Jin, W., and Wen, Z. (2016). Microglia Colonization of Developing Zebrafish Midbrain Is Promoted by Apoptotic Neuron and Lysophosphatidylcholine. Dev. Cell *38*, 214–222.

Xu, J., Zhu, L., He, S., Wu, Y., Jin, W., Yu, T., Qu, J.Y., and Wen, Z. (2015). Temporal-Spatial Resolution Fate Mapping Reveals Distinct Origins for Embryonic and Adult Microglia in Zebrafish. Dev. Cell *34*, 632–641.

Xu, P., Zhang, X., Wang, X., Li, J., Liu, G., Kuang, Y., Xu, J., Zheng, X., Ren, L., Wang, G., et al. (2014). Genome sequence and genetic diversity of the common carp, Cyprinus carpio. Nat. Genet. *46*, 1212–1219.

Xue, Y., Lv, J., Zhang, C., Wang, L., Ma, D., and Liu, F. (2017). The Vascular Niche Regulates Hematopoietic Stem and Progenitor Cell Lodgment and Expansion via klf6a-ccl25b. Dev. Cell *42*, 349-362.e4.

Yamamoto, K., Yamamoto, S., Ogasawara, N., Takano, K., Shiraishi, T., Sato, T., Miyata, R., Kakuki, T., Kamekura, R., Kojima, T., et al. (2016). Clarithromycin prevents human respiratory syncytial virus-induced airway epithelial responses by modulating activation of interferon regulatory factor-3. Pharmacol. Res. 111, 804–814.

Yamane, T. (2018). Mouse yolk sac hematopoiesis. Front. Cell Dev. Biol. 6, 80.

Yamazaki, S., Ema, H., Karlsson, G., Yamaguchi, T., Miyoshi, H., Shioda, S., Taketo, M.M., Karlsson, S., Iwama, A., and Nakauchi, H. (2011). Nonmyelinating schwann cells maintain hematopoietic stem cell hibernation in the bone marrow niche. Cell *147*, 1146–1158.

Yang, L., Bryder, D., Adolfsson, J., Nygren, J., Månsson, R., Sigvardsson, M., and Jacobsen, S.E.W. (2005). Identification of Lin-Sca1+kit+CD34 +Flt3- short-term hematopoietic stem cells capable of rapidly reconstituting and rescuing myeloablated transplant recipients. Blood *105*, 2717–2723.

Yonar, M.E. (2012). The effect of lycopene on oxytetracycline-induced oxidative stress and immunosuppression in rainbow trout (Oncorhynchus mykiss, W.). Fish Shellfish Immunol. *32*, 994–1001.

Yu, K., Li, X., Qiu, Y., Zeng, X., Yu, X., Wang, W., Yi, X., and Huang, L. (2020). Low-dose effects on thyroid disruption in zebrafish by long-term exposure to oxytetracycline. Aquat. Toxicol. *227*, 105608.

Zakrzewska, A., Cui, C., Stockhammer, O.W., Benard, E.L., Spaink, H.P., and Meijer, A.H. (2010). Macrophage-specific gene functions in Spi1-directed innate immunity. Blood *116*, e1–e11.

Zapata, A. (1979). Ultrastructural study of the teleost fish kidney. Dev. Comp. Immunol. *3*, 55–65.

Zhang, Q., Cheng, J., and Xin, Q. (2015). Effects of tetracycline on developmental toxicity and molecular responses in zebrafish (Danio rerio) embryos. Ecotoxicology *24*, 707–719.

Zhang, T., Qiu, L., Sun, Z., Wang, L., Zhou, Z., Liu, R., Yue, F., Sun, R., and Song, L. (2014). The specifically enhanced cellular immune responses in Pacific oyster (Crassostrea gigas) against secondary challenge with Vibrio splendidus. Dev. Comp. Immunol. 45, 141–150.

Zhang, X.Y., and Rodaway, A.R.F. (2007). SCL-GFP transgenic zebrafish: In vivo imaging of blood and endothelial development and identification of the initial site of definitive hematopoiesis. Dev. Biol. 307, 179–194.

Zhang, Y.A., Salinas, I., Li, J., Parra, D., Bjork, S., Xu, Z., Lapatra, S.E., Bartholomew, J., and Sunyer, J.O. (2010). IgT, a primitive immunoglobulin class specialized in mucosal immunity. Nat. Immunol. *11*, 827–835.

Zhao, M., Perry, J.M., Marshall, H., Venkatraman, A., Qian, P., He, X.C., Ahamed, J., and Li, L. (2014). Megakaryocytes maintain homeostatic quiescence and promote post-injury regeneration of hematopoietic stem cells. Nat. Med. *20*, 1321–1326.

Zhen, F., Lan, Y., Yan, B., Zhang, W., and Wen, Z. (2013). Hemogenic endothelium specification and hematopoietic stem cell maintenance employ distinct Scl isoforms. Dev. *140*, 3977–3985.

Zheng, S., Papalexi, E., Butler, A., Stephenson, W., and Satija, R. (2018). Molecular transitions in early progenitors during human cord blood hematopoiesis. Mol. Syst. Biol. *14*, 8041.

Zhou, L., Limbu, S.M., Qiao, F., Du, Z.-Y., and Zhang, M. (2018). Influence of Long-Term Feeding Antibiotics on the Gut Health of Zebrafish. Zebrafish zeb.2017.1526.

Zhou, S., Schuetz, J.D., Bunting, K.D., Colapietro, A.M., Sampath, J., Morris, J.J., Lagutina, I., Grosveld, G.C., Osawa, M., Nakauchi, H., et al. (2001). The ABC transporter Bcrp1/ABCG2 is expressed in a wide variety of stem cells and is a molecular determinant of the side-population phenotype. Nat. Med. *7*, 1028–1034.

Zhou, Z. xia, and Sun, L. (2015). Immune effects of R848: Evidences that suggest an essential role of TLR7/8-induced, Myd88- and NF-κB-dependent signaling in the antiviral immunity of Japanese flounder (Paralichthys olivaceus). Dev. Comp. Immunol. *49*, 113–120.

Zhu, H., Kwak, H.-J., Liu, P., Bajrami, B., Xu, Y., Park, S.-Y., Nombela-Arrieta, C., Mondal, S., Kambara, H., Yu, H., et al. (2017). Reactive Oxygen Species–Producing Myeloid Cells Act as a Bone Marrow Niche for Sterile Inflammation–Induced Reactive Granulopoiesis. J. Immunol. *198*, 2854–2864.

Appendices

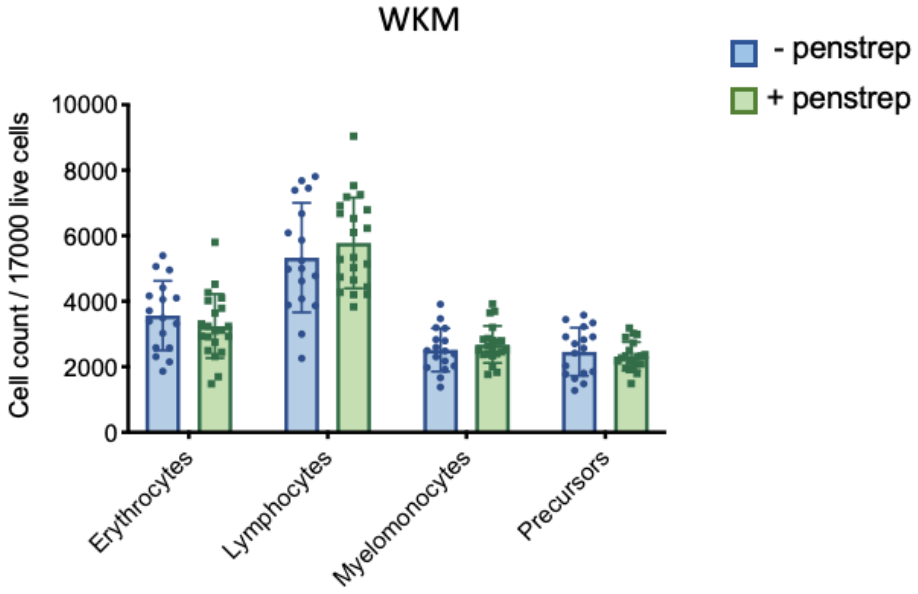

Appendix 1 Seven weeks of low dose PS treatment does not alter major blood cell populations in the WKM of juvenile fish.

Six dpf, transgenic *Tg(Runx:mCherry; lyz:GFP), Tg(lck:GFP)* and *Tg(mpx:GFP)* fish were placed into E2 medium ± PS (10 U/mL penicillin and 10 µg/mL of streptomycin) and reared in benchtop tanks for 7 weeks. Treatment was administered through the addition of 200 mL E2± PS each day, in addition to a weekly change of tanks. For schematic representation of experimental set up see Fig. 4.1. Single cell suspensions of WKM were subjected to flow cytometry and cell counts/ 17000 live cells were analysed for major blood cell population. Each dot indicates 1 fish. N= 17-20. Mean and SD shown.

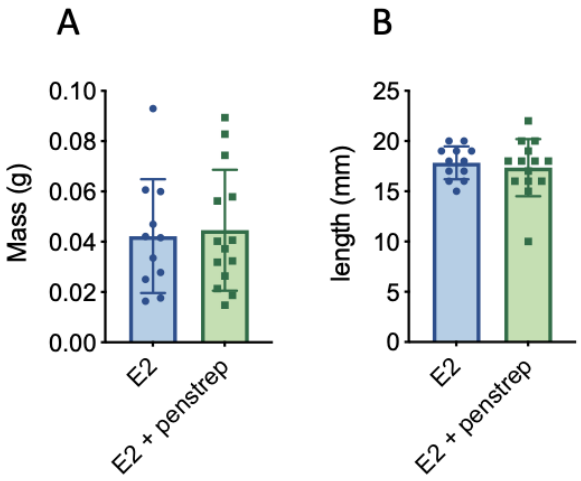

Appendix 2 Seven weeks of low dose PS treatment does not alter length or mass of juvenile fish.

Six dpf, transgenic *Tg(Runx:mCherry; lyz:GFP), Tg(lck:GFP)* and *Tg(mpx:GFP)* fish were placed into E2 medium ± PS (10 U/mL penicillin and 10 µg/mL of streptomycin) and reared in benchtop tanks for 7 weeks. Treatment was administered through the addition of 200 mL E2± PS each day, in addition to a weekly change of tanks. For schematic representation of experimental set up see Fig. 4.1. (**A**) Mass in grams and (**B**) length in mm, of zebrafish reared on E2± PS. Each dot indicates 1 fish. N= 11-14. Mean and SD shown.

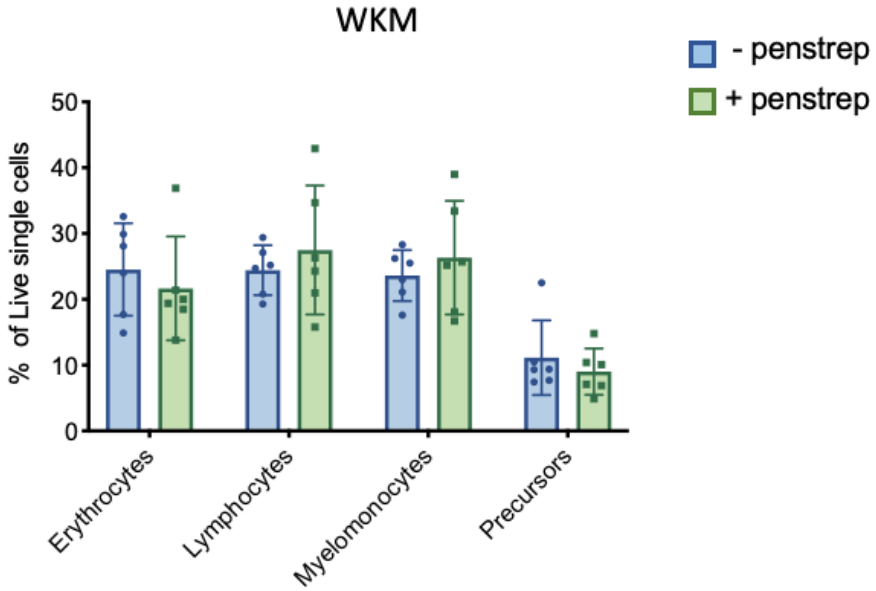

Appendix 3 Two weeks of low-dose PS treatment does not alter major blood cell populations in the WKM of adult *Tg(Runx:mCherry; lyz:GFP)* zebrafish.

Adult transgenic *Tg(Runx:mCherry; lyz:GFP)* fish were treated in system water ± PS (10 U/mL penicillin and 10 µg/mL of streptomycin) for 2 weeks. Treatment was administered through the addition of system water ± PS each day with 10 % exchange. For schematic representation of experimental set up see Fig. 4.2. Single cell suspensions of WKM were subjected to flow cytometry. Major blood cell lineages were analysed as a percentage of live cells. Each dot indicates 1 fish. N= 6. Mean and SD are shown.

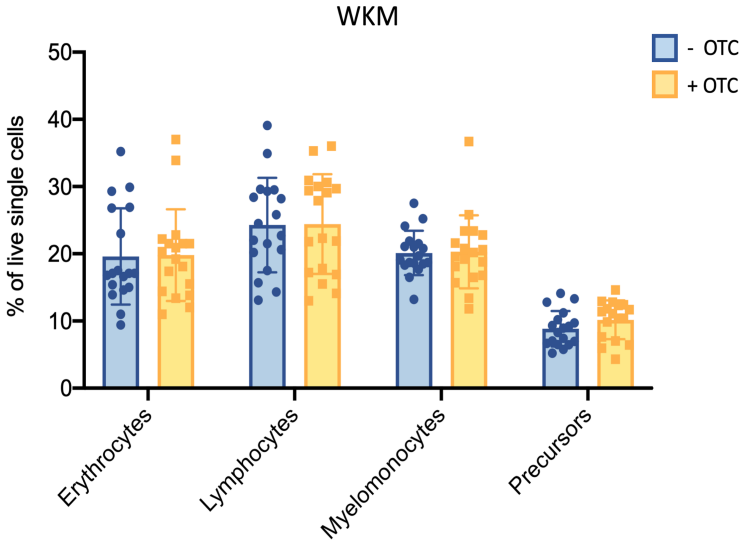

Appendix 4 Ten days of OTC treatment does not alter major blood cell populations in the WKM of adult *Tg(Runx:mCherry; lyz:GFP)* zebrafish.

Adult transgenic *Tg(Runx:mCherry; lyz:GFP)* fish were treated in system water ± OTC (50 mg/L) for 10 days. Treatment was administered via the daily replacement of all water ± OTC to ensure OTC remained bioactive. For schematic representation of experimental set up see Fig. 4.3. Single cell suspensions of WKM were subjected to flow cytometry. Major blood cell lineages were analysed as a percentage of live cells. Each dot indicates 1 fish. N= 16-18. Mean and SD are shown. Data is pooled from 3 independent experimental repeats.